Republic of Iraq
Ministry of Higher Education
and Scientific Research
University of Babylon
College of Engineering

Simulation and Evaluation of Digital Video Broadcasting Terrestrial 2nd Standard Using Different Scenarios

A Thesis

Submitted to the Department of Electrical Engineering / College of Engineering / University of Babylon in Partial Fulfillment of the Requirements for the Degree of Doctor of Philosophy in Engineering / Electrical Engineering / Electronics and Communications

By

Hamzah Sabr Ghayyib Krafa

(B.Sc. 2014)

(M.Sc. 2017)

Supervised by

Prof.

Dr. Samir Jasim Mohammed

2022 A.D **1443 A.H**

بِسْمِ اللَّهِ الرَّحْمَنِ الرَّحِيمِ

﴿ نَرْفَعُ دَرَجَاتٍ مَنْ نَشَاءُ وَفَوْقَ كُلِّ ذِي عِلْمٍ عَلِيمٌ ﴾

صَدَقَ اللَّهُ الْعَلِيّ الْعَظِيم

يوسف(76)

To the leader “Imam Mahdi”

To my beloved family

Acknowledgments

In the name of Allah, Most Gracious, Most Merciful

First and above all, I praise ALLAH, the almighty for providing me this opportunity and granting the capability to proceed this thesis.

I submit my highest appreciation to my advisor, Prof. Dr. Samir Jasim M. AL-Muraab, for his help, encouragement, guidance, patience and support through this research.

I would like to thank my friends and colleagues for their assistance, collaboration and friendship. I also thank the faculty and staff of the Department of Electrical Engineering for their kind support. Also, I thank the doctors whom I consulted for their cooperation and advices.

I offer my thanks to all people who have stood beside me during my studying in University of Babylon, but I cannot mention their names here one by one.

I would like to thank my parents who gave me the ambition and the opportunity to finish my study and I also thank all my beloved family, for encouraging and supporting me along the studying and research time.

Abstract

Digital Video Broadcasting Terrestrial Second-Generation (DVB-T2) technology is the world's most advanced Digital Terrestrial Television (DTT) system, offering a high-performance terrestrial transmission system with a good broadcasting reliability. DVB-T2 has the ability to expand channel capacity in a variety of terrestrial environments, which is a significant improvement for the DVB-T2 standard. In terms of Forward Error Correction (FEC) coding, modulation approaches, Fast Fourier Transform (FFT) sizes, new pilot patterns, multiple antenna technologies, constellation rotation, and cyclic delay techniques, DVB-T2 introduces several enhancements over first-generation.

In this thesis, the work is divided into four main objectives including different modulation mode, coding rates, and multipath channel models. All parts are simulated and evaluated by using MATLAB program version R2020b. The first objective performs the evaluation of DVB-T2 system before and after employing constellation rotation technique. The constellation rotation technique results in additional diversity to enhance the Bit Interleaved Coding and Modulation (BICM) module in different fading environments and improve the overall DVB-T2 performance.

The second objective evaluates the DVB-T2 system when applying the Multiple-Input Single-Output (MISO) technique based on a modified Alamouti coding scheme in the condition of single frequency networks areas (SFNs). The DVB-T2 MISO mode is compared with the traditional Single-Input Single-Output (SISO) SFNs based on the resulting MISO diversity gain. The achieved gain shows the benefit of using MISO mode, which improves the signal reception quality in SFN areas.

The T2-Lite profile was simulated and evaluated in the third objective. Also, the performance of the T2-Lite is compared before and after utilizing

constellation rotation and cyclic Quadrature (Q) delay schemes. Finally, in the fourth objective, the advanced BICM module from Digital Video Broadcasting next-generation handheld (DVB-NGH) is proposed to be adopted inside the T2-Lite profile rather than its original module. Two types of rotation techniques have been used with this module, two and four-dimensional constellations rotation, based on the selected modulation mode and coding rates.

The results achieved from the first objective shows that the maximum gain is 3.6dB can be obtained over 0dB Echo channel with QPSK and 5/6 coding rate. The second objective results illustrated that the maximum MISO gains are 3.3dB accomplished with QPSK and a high coding rate of 5/6 over the Rayleigh MISO channel and 4.3dB when adopting both MISO and constellation rotation. Furthermore, in the third objective, the maximum gain is 2.2dB can be obtained from using QPSK and 11/15 coding rate over 0dB echo channel. Finally, The proposed BICM module can provide a maximum gain of 3.5 dB over 0dB echo channel from employing QPSK and 11/15 high coding rate.

Table of Contents

List of Abbreviations

Abbreviation	Definition
2D	Two-dimensions
3D	Three-Dimension
4D	Four-dimensions
16-QAM	16-ary Quadrature Amplitude Modulation
64-QAM	64-ary Quadrature Amplitude Modulation
256-QAM	256-ary Quadrature Amplitude Modulation
ACE	Active Constellation Extension
ATSC	Advanced Television Systems Committee standards (American)
AWGN	Additive White Gaussian Noise
BB	BaseBand
BCH	Bose Chaudhuri Hocquengham
BER	Bit Error Rate
BICM	Bit-Interleaved Coded and Modulation
CBR	Constant Bit Rate
CI	Cell Interleaver
CIR	Channel Impulse Response
COFDM	Coded Orthogonal Frequency Division Multiplexing
COST207	European Cooperation in the fields of Scientific and Technical Research
CP	Continual Pilot
CRC	Cyclic Redundancy Check
DAB	Digital Audio Broadcasting
DAC	Digital to Analogue Conversion
DFL	Data Field Length
DNP	Deleted Null Packets
DTG	Digital Television Group
DTMB	Digital Terrestrial Multimedia Broadcast (China)
DTT	Digital Terrestrial Television
DVB	Digital Video Broadcasting
DVB-H	Digital Video Broadcasting–Handheld
DVB-NGH	Digital Video Broadcasting Next-Generation Handheld
DVB-S2	Digital Video Broadcasting Satellite Second- Generation
DVB-SH	Digital Video Broadcasting-Satellite to Handheld

DVB-T	Digital Video Broadcasting Terrestrial
DVB-T2	Digital Video Broadcasting Terrestrial Second-Generation
eSFN	enhanced Single-Frequency Networks
ESM-MIMO	Enhanced Spatial Multiplexing Multiple-Input Multiple-Output
FC	Frame-Closing Symbols
FEC	Forward Error Correction
FEF	Future Extension Frames
FFT	Fast Fourier Transform
GCS	Generic Continuous Stream
GFPS	Generic Fixed-length Packetized Stream
GI	Guard Interval
GSE	Generic Encapsulated Stream
GSM	Global System for Mobile Communications
HD	High Definition
ICI	Inter-Carrier Interference
IF	Interleaving Frame
IFFT	Inverse Fast Fourier Transform
IP	Internet Protocol
ISDB-T	Integrated Services Digital Broadcasting-Terrestrial (Japan)
ISSY	Input Stream Synchronizer
LDPC	Low-Density Parity-Check
LLR	Log-likelihood Ratio
MFNs	Multi-Frequency Networks
MIMO	Multiple-Input Multiple-Output
MISO	Multiple-Input Single-Output
MMSE	Minimum Mean Squared Error
MSB	Most Significant Bit
NPD	Null Packet Deletion
PAPR	Peak-to-Average Power Ratio
PLP	Physical Layer Pipe
PN	Pseudorandom
PRBS	Pseudo-Random Binary Sequence
Q delay	Quadrature delay
QPSK	Quaternary Phase Shift Keying
RS	Reed Solomon codes
SFBC	Space-Frequency Block Code
SFNs	Single Frequency Networks

SISO	Single-input single-output
SNR	Signal-to-Noise Ratio
SP	Scattered Pilots
SSD	Signal Space Diversity
SVC	Scalable Video Coding
TFS	Time-Frequency Slicing
TI	Time Interleaver
TR	Tone Reservation
TS	Transport Stream
TU6	Typical Urban Channel
UHF	Ultra-High Frequency
UP	User Packets
XOR	Exclusive Or
ZF	Zero Forcing
TFS	Time-Frequency Slicing

List of Symbols

Symbol	Description
a_i	LDPC codeword bits
$a_{m,l,p}$	Frequency-Interleaved cell value, cell index p of symbol l of T2-frame m
A_{sp}	Amplitude of the scattered pilot cells
b	Output sub-streams of the de-multiplexer
C/N	Carrier-to-noise ratio
C_{data}	Number of active cells in one normal symbol
C_{FC}	Number of active cells in one frame closing symbol
C_{P2}	Number of active cells in one P2 symbol
div	Integer division operator
$d_{r,q}$	Cell interleaver output for cell q of FEC block r
D_X	Difference in carrier index between adjacent scattered-pilot-bearing carriers
D_Y	Difference in symbol number between successive scattered pilots on a given carrier
E_b/N_0	Energy per bit to noise power ratio
F_q	Constellation point normalized to mean energy of 1
g(x)	BCH generator polynomial
G_q	OFDM cell value after constellation rotation and cyclic Q delay
H(p)	Frequency interleaver permutation function, element p
$H_0(p)$	Frequency interleaver permutation function, element p, for even symbols
$H_1(p)$	Frequency interleaver permutation function, element p, for odd symbols
I_{JUMP}	Frame interval: difference in frame index between successive T2-frames to which a particular PLP is mapped
I_{JUMP}	Frame interval: difference in frame index between successive T2-frames to which a particular PLP is mapped (for PLP i)
j	$\sqrt{-1}$
k	OFDM carrier index
K_{bch}	Number of bits of BCH un-coded Block
K_{ldpc}	Number of bits of LDPC un-coded Block
K_{max}	Carrier index of last (highest frequency) active carrier

K_{min}	Carrier index of first (lowest frequency) active carrier
K_{total}	Number of OFDM carriers
l	Index of OFDM symbol within the T2-frame
L_{data}	Number of data symbols per T2-frame including any frame closing symbol but excluding P1 and P2
L_F	Number of OFDM symbols per T2-frame excluding P1
$L_r(q)$	Cell interleaver permutation function for FEC block r of the TI-block
mod	Modulo operator
M_{TI}	Maximum number of cells required in the TI memory
n	Interleaving Frame index within the super-frame
N_{bch}	Number of bits of BCH coded Block
$N_{BLOCK\_IF}(n)$	Number of FEC blocks in Interleaving Frame n (for PLP i)
$N_{BLOCKS\_IF\_MAX}$	Maximum value of $N_{BLOCK\_IF}(n)$
N_{cells}	Number of OFDM cells per FEC Block (for PLP i)
N_D	Number of rotation dimensions
N_{data}	Number of data cells in an OFDM symbol (including any un-modulated data cells in the frame closing symbol)
$N_{FEC\_TI\_MAX}$	Maximum Number of FEC blocks in TI-block
$N_{FEC\text{-}TI}(n,s)$	Number of FEC blocks in TI-block s of Interleaving Frame n
N_{FEF}	Number of FEF parts in one super-frame
N_{FFT}	FFT size
N_{IU}	Number of interleaver units
N_{ldpc}	Number of bits of LDPC coded Block
n_{MOD}	Number of transmitted bits per constellation symbol (for PLP i)
N_{P2}	Number of P2 symbols per T2-frame
$N_{substreams}$	Number of substreams produced by the bit-to-sub-stream demultiplexer
N_{T2}	Number of T2-frames in a super-frame
N_{TI}	Number of TI-blocks in an Interleaving Frame
N_{TI}	Number of TI-blocks in an Interleaving Frame
N_{TI}	Number of TI-blocks in an Interleaving Frame
N_{TR}	Number of TR cells in each symbol
P(r)	Cyclic shift value for cell interleaver in FEC block r of the TI-block
P_I	Number of T2-frames to which each Interleaving Frame is mapped

P_I	Number of T2-frames to which each Interleaving Frame is mapped (for PLP i)
p_{nl}	Frame level PN sequence value for symbol l
Q_{ldpc}	Code-rate dependent LDPC constant
r	FEC block index
R'_i	Value of element i of the frequency interleaver sequence prior to bit permutations
$r_{l,k}$	Pilot reference sequence value for carrier k in symbol l
R_{RQD}	Complex phasor representing constellation rotation angle
s	Index of TI-block within the Interleaving Frame
t	BCH error correction capability
T	Elementary time period for the bandwidth in use
t_c	Column-twist value for column c
T_F	Duration of one T2-frame
T_{FEF}	Duration of one FEF part
T_{P1}	Duration of the P1 symbol
T_s	Total OFDM symbol duration
T_{SF}	Duration of one super-frame
T_U	Active OFDM symbol duration
Tx1	Transmitter 1 belong to MISO group 1
Tx2	Transmitter 2 belong to MISO group 2
u_i	Parity-interleaver output bits
v_i	Column-twist-interleaver output bits
v_i	Streams of input bits applied to the de-multiplexer
$x_{m,l,p}$	Complex cell modulation value for cell index p of OFDM symbol l of T2-frame m
z_q	Constellation point prior to normalization
σ^2	Channel noise variance
$\oplus$	Exclusive OR / modulo-2 addition operation
Δ	Guard interval duration

List of Tables

List of Figures

List of Publications

1. Published:- H. S. Ghayyib and S. J. Mohammed, “Performance enhancement of FEC Code For DVB-T2 system by using rotated constellations,” *2021 1st Babylon International Conference on Information Technology and Science (BICITS)*, pp. 234-238, 2021, doi: 10.1109/BICITS51482.2021.9509871.

2. Published:- H. S. Ghayyib, and S. J. Mohammed, “Improving BICM efficiency for DVB-T2 system using rotated constellations and cyclic Q delay,” *Technology Reports of Kansai University*, vol. 63, no. 2, pp. 7271- 7281, 2021.

3. Published:- H. S. Ghayyib, and S. J. Mohammed, “BICM module of next generation handheld broadcasting for system diversity development in multipath fading channels,” *International Journal of Engineering Trends and Technology*, vol. 69, no. 8, pp. 96-101, 2021.

4. Published:- H. S. Ghayyib and S. J. Mohammed, "Next Generation Mobile Broadcasting BICM Module to Improve T2-Lite System Robustness," *2021 International Conference on Advanced Computer Applications (ACA)*, 2021, pp. 193-198, doi: 10.1109/ACA52198.2021.9626794.

5. Accepted:- H. S. Ghayyib, and S. J. Mohammed, “Performance Improvement of DVB-T2 SFNS By Using MISO Transmission Scheme,” *AIP Conference Proceedings*.

6. Accepted:- H. S. Ghayyib, and S. J. Mohammed, “Improvement of Terrestrial Broadcasting Second-Generation Performance using MISO Mode,” *International Journal of Electrical and Computer Engineering (IJECE)*.

Chapter One

Introduction

1.1 Background

Significant advancements in television broadcasting systems have been noticed due to fast technological progress. Modern technologies enable broadcasting in High Definition (HD) and three-Dimension (3D) and viewing of material from fixed or mobile positions. In addition, advancements in wireless communications impact terrestrial broadcasting, which uses analog systems, and has led to the concept of digital terrestrial television transmission. As a result of these advances, digital terrestrial television transmission has been a significant research topic worldwide since the early 1990s [1].

The alternative to decommissioning analog broadcasts in Europe was the first-generation European standard for providing Digital Terrestrial Television; this standard is called Digital Video Broadcasting Terrestrial (DVB-T). DVB-T introduces a new range of frequencies located in the band of Ultra-High Frequency (UHF) and opportunities for unique services like broadcasting of HDTV, on-demand video, and handheld Television. DVB-T was the most widely DTT that supplies terrestrial air services for different countries worldwide [2].

The increasing demand for broadcasting services is continual, and these services required a more efficient broadcasting system. DVB-T was limited by frequency capacity, so a new standard was needed to accomplish market demands by boosting the spectral efficiency to carry additional services. DVB project introduces the development of DVB-T known as Digital Video Broadcasting Terrestrial Second-Generation [3].

DVB-T2 technology has the features of being the world's most developed DTT system, where it presents a terrestrial transmission system with high performance and good broadcasting robustness. DVB-T2 can increase channel capacity over different terrestrial environments, which considers another good point for the DVB-T2 standard [2]. DVB-T is used as base technology in building the DVB-T2 system, where it's passed through specific developing steps. DVB-T2 uses all available concepts for the DVB-T standard to minimize overhead to produce a new transmission technology with an output approach to theoretical channel capacity [4].

The most prominent advantage of DVB-T2 is the ability to boost DTT capacity. Compared with DVB-T, DVB-T2 can obtain a more net data rate with 30% to 67% higher and achieve preferable suitability with handheld usage. Many different applications need high data throughput and require a system to be rugged with variable mobile circumstances [5]. DVB-T2 standard benefits when dealing with impulsive and multipath interference than the old DVB-T mode. The fixed reception mode is the basic layout of the DVB-T2 standard. It can also deal with mobile and portable applications if a compatible specification is utilized [6].

There are several essential differences between DVB-T2 and the base standard DVB-T. These differences make the standard flexible regarding transmission robustness in many terrestrial circumstances and allow the new standard to operate with a high capacity [3]. The several improvements introduce by DVB-T2 are recent Forward Error Correction (FEC) coding, modulation techniques, guard intervals, Fast Fourier Transform (FFT) sizes, new pilot patterns, multiple antenna technologies, constellations rotation, and cyclic delay schemes [4], [7].

Terrestrial DVB systems use Coded Orthogonal Frequency Division Multiplexing (COFDM) technology to minimize multipath interference [4]. COFDM supplies a low complex and efficient scheme to decrease inter-symbol interference during broadcasting over the fading channels. In addition to the COFDM scheme, DVB-T2 is characterized by several advanced specifications that made it suitable to improve the system performance in the fading environment [8].

One of these specifications is the constellation rotation and cyclic Q delay, which are considered the most developed specifications. System robustness can be enhanced with these features because when a particular effect happens to the data within one channel component, the second component can quickly regain the damaged data [9].

The Single Frequency Networks (SFNs) are considered another important feature of the DVB-T2 system, and its performance enhancement was an essential purpose for the standardization efforts [10]. DVB-T2 utilizes SFN because compared to Multi-Frequency Networks (MFNs) supplies more homogeneously arrangement in terms of field strength because of spatial diversity, which offers the same signal quality at a low transmission power. However, there is deep degradation in the signal's performance in the case of SFN generated by self-interferences [11]. One of the most efficient solutions for this issue is the Multi-antenna scheme such as Multiple-Input Single-Output antennas technology [5].

The DVB Project has included a contemporary profile called as T2-Lite in the most recent versions of the DVB-T2 standard. This profile is intended for mobile and portable reception, with the goal of simplifying receiver complexity and decreasing the cost and power consumption of mobile services. Based on the T2-Lite profile specification, DVB Project has proposed a Digital Video

Broadcasting Next Generation Handheld (DVB-NGH) for future broadcasting applications [9], [12].

DVB-NGH is the mobile extension of the high-performance DVB-T2 standard, with the most superior transmission technologies. One of the main modifications introduced by DVB-NGH is the advanced module of Bit-interleaved coded and modulation (BICM) [14]. This BICM depends on a subset of DVB-T2 BICM elements with particular improvements to minimize the receiver decoding complexity, boost system robustness, and optimize spectral efficiency [11], [15].

1.2 Literature Reviews

After studying many related works, the following is a summary of the literature reviews:

N. Cornillet et al., 2011, studied the capabilities of the second-generation terrestrial standard under SFNs. Besides, this study compares the transmission performance of the Alamouti algorithm with pair of transmit antennas to that of a traditional single input single output scheme. This paper used a 10^{-4} Quasi Error Free (QEF) criteria to test the system where the obtained MISO gain is 0.5dB compared to the SISO configuration [16].

O. KARAKUŞ, 2011, provided a simulation for the first and second-generation European terrestrial broadcasting systems. A comparative examination for both terrestrial systems has been presented when their signals are subjected to a multipath fading environment. The comparison has been made based on the needed C/N values for each standard, determined by the simulation. The work demonstrated that to achieve a target BER of $2*10^{-4}$ the DVB-T required an SNR of 10.5 dB while DVB-T2 required 4.8dB with a configuration of 1/2 coding rate and 16-QAM modulation [1].

L. Polak, and T. Kratochvil, 2012, studied the performance of the rotated constellation adopted in the second-generation terrestrial system. This investigation is carried out to display the differences between the performance of rotated and non-rotated constellations in fading environment by means of simulation The current paper used an error-free reception condition of 10^{-5} and offered a required SNR of 13.2dB, 9.8dB before and after rotation, respectively with QPSK and 1/2 coding rate [17].

L. Dai et al., 2012, began with a brief overview of first-generation terrestrial broadcasting systems, as well as the present state of emergent second-generation terrestrial broadcasting standards. Then, it centers on the fundamental technologies that underpin these standards, including the state-of-the-art, technological problems and the latest successes in the domain [18].

C. Douillard, and C. A. Nour, 2012, outlined the fundamental characteristics of the bit interleaved coding and modulation module for the DVB-NGH. The authors presented a performance comparison between DVB-NGH bit interleaved coding and modulation module with unconstrained Shannon limits and handheld DVB-H. This work used a frame error rate of 10^{-4} after inner decoding and found that DVB-NGH outperforms the DVB-H by around 2.0 dB over the AWGN channel [19].

L. Polak and T. Kratochvil, 2012, analyzed the transmission achievement of the digital video broadcasting first and second-generation terrestrial systems in fixed television environments. Moreover, short general explanations for both systems are presented in this research. The authors obtain and distinguish a bit error rate results for both systems with a certain parameter setting. The considered QEF for both systems was 10^{-5} and the required C/N for the DVB-T system was 14.9dB while for DVB-T2 was 6.9dB over AWGN and 64-QAM modulation [20].

D. Tralic et al., 2012, outlined performance simulation and measurement of the transmitted digital signal based on the new second-generation broadcasting system over some scenarios are in this article. The simulation was carried out with the settings used for the Croatian second-generation terrestrial broadcasting provider. It stated that the DVB-T2 system required 18.08dB, 18.49, and 20.42bB for AWGN, Ricean, and Rayleigh channels, respectively, with BER that equals 10^{-7} after inner coding [21].

D. Goz´alvez et al., 2013, looked at the possible benefits that rotated constellations can provide in next-generation handheld broadcasting. Therefore, the study analyzes the possible advantages produced by this scheme from an information-theoretic perspective based on mutual information [22].

M. Dąbrowski, 2013, investigated the operation of television digitization, especially in Poland, and studied the analysis of the second-generation terrestrial standard with its elder first-generation terrestrial standard. Also, evaluating coming trends for replacing the first-generation standard with the second-generation standard, considering the estimation and correct adoption of new receiver configurations. It stated that the DVB-T required 5.6 dB, and 6.1dB over AWGN, and Ricean channels, respectively, with QPSK modulation and 1/2 coding rate [23].

I. Eizmendi et al., 2014, supplied a review about the second-generation terrestrial system. The various important aspects of the DVB-T2 system and its advantages with trade-offs are detailed. Also, the impacts of some of the configuration options have been detailed in this study [24].

D. G´omez-Barquero et al., 2014, reviewed the key technological characteristics employed by next-generation handheld digital video broadcasting. Some of these characteristics include forward error correction codes, modulation type, capacity, and rotated constellations schemes. The

theoretical gain displayed was 3dB as compared to DVB-H over Rayleigh channels condition [25].

E. Dumic et al., 2014, examined the potential capacity improvements in the change from digital video broadcasting first-generation terrestrial to second-generation standard. Also, checking the minimal C/N ratio required for the first and second-generation terrestrial systems reception with Croatian broadcasting settings. The minimum C/N over Gaussian channel was 17.2dB for DVB-T and it was 18.1dB for DVB-T2 while over Ricean the minimum C/N was 18.7 dB versus 18.6 dB [26].

D. A. Samo et al. 2015, investigated the abilities of digital video broadcasting second-generation terrestrial standard with its additional profile T2-Lite. The investigation presented in this work employs some specific coding rates adopted in the T2-Lite system. Moreover, it performs a brief overview of the second-generation terrestrial and T2-Lite standards. For target packet error rate of 10^{-4} the DVB-T2 required an SNR of 10dB with 16-QAM modulation and 1/2 coding rate, While the T2-Lite system required 9.5dB for 1/3 coding rate [27].

M. Kaur, 2017, descripted of the performance requirements and characteristics of the digital video broadcasting terrestrial second-generation system. The present research focused on data transmission analysis with DVB-T2 based on the application of OFDM scheme. The SNR required to achieve BER of 10^{-10} was 8.9dB for Ricean and 10.3dB for Rayleigh conditions when considering 16-QAM modulation [28].

L. Andoni, and A. Biberaj, 2019, presented an overview of the multi-input single-output transmission mode introduced by digital video broadcasting second-generation terrestrial system. Therefore, the goal of this article is to show how the Multi-input single-output mode works over a single frequency

network and demonstrate limitations in terms of the guard interval and pilot pattern selection form theoretical point of view [29].

H. J. Kim et al., 2020, analyzed the performance of signal-to-noise ratio gain to check the feasibility of the three-layered division multiplexing. The present research concentrated on layered division multiplexing and time-division multiplexing systems when transmitting three physical layer pipes with the same data rate over digital video broadcasting second-generation. The required SNR is 7.6 dB for 16-QAM modulation and coding rate of 3/5 with one physical layer pipe [30].

L. Polak et al., 2021, investigated the performance analysis of second-generation digital video broadcasting terrestrial system using multi-antennas schemes at special fixed transmission scenarios. The used scenarios are characterized by different channel conditions between the transmitters and receiver sides [31].

The researchers in the above reviews explore the DVB-T2 standard without using different parameters configuration with the available technologies in terms of coding rates, modulation mode, time interleaver types, number of FEC block, and iteration number of inner decoding. Also, using certain channel conditions that do not reflect the real system performance in different scenarios. Moreover, some works, especially those that deal with DVB-NGH, depend on the perspective of information theory based on mutual information in their results.

All the mentioned works only interact with evaluating the DVB-T2 system or a single approach adopted in the system. Therefore, the works present in this thesis are separated into four main objectives. The first and second objectives simulate the constellation rotation and MISO transmission techniques, respectively, to show their performance with the DVB-T2 standard.

The third objective simulates the T2-Lite profile with and without constellation rotation. The fourth objective simulates the BICM module belong to the futuristic DVB-NGH with the T2-Lite profile instead of its traditional one to obtain the new improvements of the proposed system.

The following important aspects distinguish the thesis from the works included in the reviews:

- Simulating the DVB-T2 system with and without constellation rotation technique based on several parameters configurations and different fading channels such as Gaussian, Ricean, Rayleigh, 0 dB Echo, DTGlong, DTGmedium, DTGshort, and TU06 channels.
- Simulating the DVB-T2 system when applying the MISO transmission technique based on a modified Alamouti coding scheme in the condition of SFNs areas with different parameters configurations and MISO fading channels. Also adopting rotation technique together with MISO mode in SFNs condition.
- Simulating and comparing the performance of the T2-Lite profile with and without constellation rotation, including different parameters configuration and multipath channel models.
- Simulating the T2-Lite profile with the proposed DVB-NGH BICM module beside different coding rates, constellation modes, and fading channel models.
- Applying two and four-dimensional constellations rotation techniques supported by DVB-NGH BICM module.

1.3 Thesis Objectives

The main objectives behind this thesis are included in the following four parts:

i. The first part aims to simulate and evaluate the overall chain of DVB-T2 standard and obtain the system performance gain with and without applying the constellation rotation technique. Several fading channels have been considered, such as AWGN, Ricean, Rayleigh, 0 dB Echo, DTGlong, DTGmedium, DTGshort, and TU06 channels. Furthermore, it evaluates the parameters configuration to produce optimal performance suitable for each channel's conditions.

ii. The purpose of the second part is to test the DVB-T2 effectiveness in SFNs context. The diversity gain and BER from employing the MISO technique based on a modified Alamouti coding scheme are obtained and compared with traditional SISO operations. In this part, the MISO mode operation is also evaluated before and after using the constellation rotation technique and Q delay schemes. Different fading channels are included for both SISO and MISO mode simulations.

iii. The third part deals with the evaluation of the T2-Lite profile with and without the constellation rotation technique. The rotation and cyclic Q delay schemes are applied according to the original BICM structure. The results of the present part are essential in the subsequent comparisons because the T2-Lite system is considered a base for the next-generation broadcasting implementation.

iv. Finally, in the fourth part, the T2-Lite BICM is changed with the new proposed DVB-NGH BICM module and displays diversity gain for two and four-dimensional constellations rotation techniques. Additionally, this gain is compared to the T2-Lite system with its conventional BICM module.

1.4 Thesis Organization

The thesis is organized as follows:

a. Chapter One, "***Introduction***", has presented a background of the thesis, literature review, thesis objectives, and thesis organization.

b. Chapter Two, "***Digital Video Broadcasting Terrestrial Second Generation***", submits an introduction, DVB-T2 system structure (input processing, BICM module, frame builder, OFDM generation) with their sub-block, T2-Lite system beside (restrictions, elements excluded, and elements added in T2-Lite), digital video broadcasting next-generation handheld (BICM Module for DVB-NGH with all sub-blocks), multipath fading channels (DVB-T2 channel models including types of channels models and MISO model).

c. Chapter Three, "***Proposed Systems Structures***", represents an explanation of the simulated systems and processes sequence in MATLAB, also sub-divided into four main parts DVB-T2 system, DVB-T2 with MISO transmission mode, T2-Lite profile, and T2-Lite system with DVB-NGH BICM module.

d. Chapter Four, "***Results and Discussion***", shows the achieved results for all simulated systems and their discussion.

e. Chapter Five, "***Conclusions and Suggestions For Future Works***", summarizes the conclusions and recommendations for future studies.

Chapter Two

Digital Video Broadcasting Terrestrial Second Generation

2.1 Introduction

Several digital terrestrial television broadcasting standards have been adopted in different parts of the world, where DVB standards consisting of DVB-T and DVB-T2 are viewed as the most deployed worldwide. DVB-T2 standard is globally considered the most advanced Digital Terrestrial Transmission (DTT) system, allowing efficiency and high robustness for the terrestrial environment . Fig. 2.1 shows the deployment map of digital terrestrial television broadcasting standards.

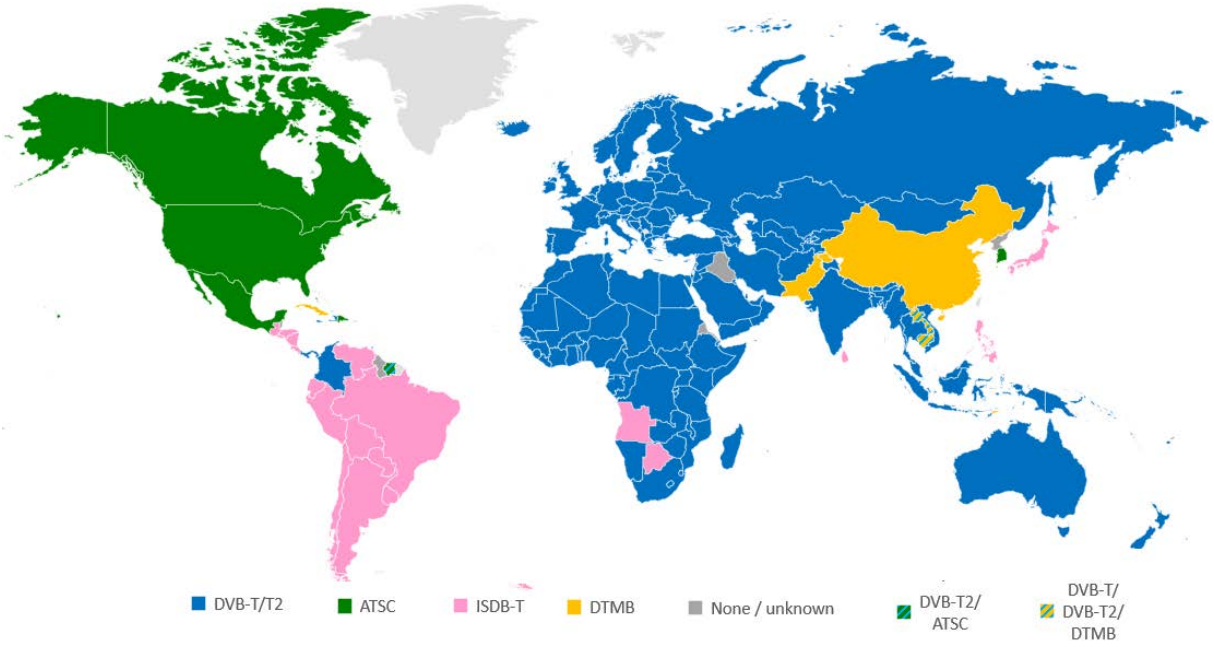

Fig. 2.1 Worldwide digital terrestrial broadcasting standards [31].

This chapter provides a theoretical view of the DVB-T2 specifications. It consists of several main sub-sections, such as input processing, bit interleaved coding and modulation, frame builder, and OFDM generation. Furthermore, it supports information about T2-Lite profile, DVB-NGH, and fading channel models.

2.2 DVB-T2 System Structure

The DVB-T2 system consists of several functional blocks. Each block performs a certain operation. The high-level transmitter architecture of the DVB-T2 system is shown in Fig. 2.2. It consists of several sub-parts and each one will be discussed in the following sections [32].

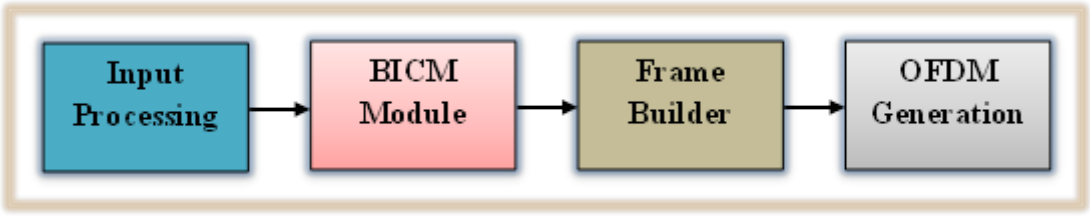

Fig. 2.2 High-level DVB-T2 system structure [32].

2.2.1 Input Processing

The first block of DVB-T2 is the input processing, which accomplishes two functions; mode adaptation and stream adaptation as shown in Fig. 2.3 [32].

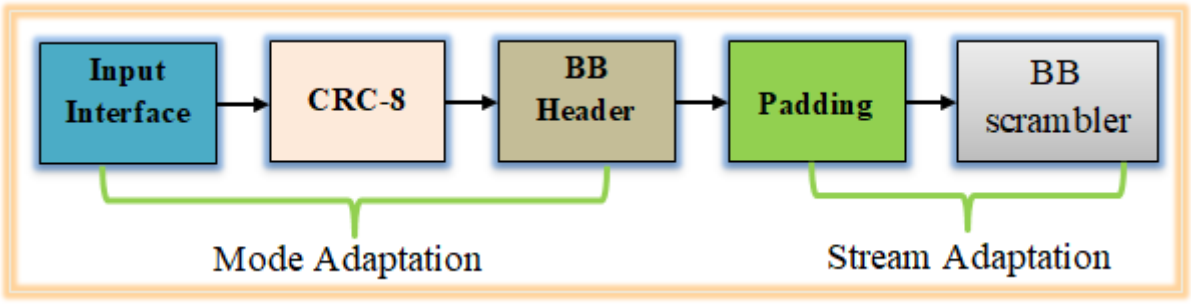

Fig. 2.3 DVB-T2 Input processing module [32].

i. Mode Adaptation

One or more data streams must be supplied to the DVB-T2 as input. One Physical Layer Pipe (PLP) transports a single data stream. The mode adaptation module works individually on the field of every physical layer pipe. This module divides the input data stream into data fields where these data fields will generate baseband frames after the input processing block [33].

The mode adaptation module includes the input interface, input stream synchronizer, null packet deletion, and the CRC-8 encoder. The last three sub-block of the mode adaptation module are optional. Each data field contains a baseband header (BBHEADER) at its beginning inserted by mode adaptation where the structure of BBHEADER is given in Fig. 2.4 [32].

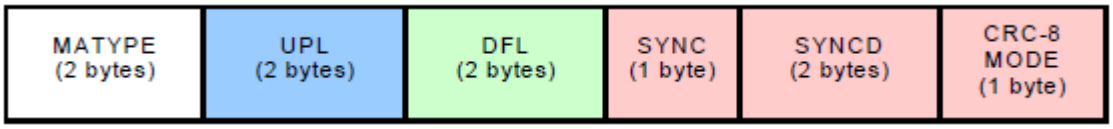

Fig. 2.4 BBHEADER structure [33].

The input formats of a given PLP may be Transport Stream (TS), Generic Encapsulated Stream (GSE), Generic Continuous Stream (GCS), and Generic Fixed-length Packetized Stream (GFPS). TS has constant User Packets (UP) length of 188*8 bits. The stream of GSE is featured by a variable or fixed packet length, while GCS has a continuous stream of bits [33]. It should be noticed that a variable or a fixed packet length with more than 64 kbit must be handled as GCS Stream. The last type of input format is GFPS, characterized by fixed user packets length with a 64 kbit maximum [5].

a. Input Interface

The input interface performs the input map into an internal logical form of bits. The first input bit applied to the input interface section referred to as Most Significant Bit (MSB). The Input Interface arranges the received bits into a data field with a Data Field Length (DFL) as presented in Eq. 2.1 [32].

$$0 \leq \mathrm{DFL} \leq (\mathrm{K_{bch}} - 80) \qquad 2.1$$

DFL's highest size is determined by the Low-Density Parity-Check code (LDPC) employed, which provides number of bits of Bose Chaudhuri Hocquengham (BCH) un-coded block (K_{bch})bits a protected payload. The 80 bits baseband header are placed at the beginning of this data field [1].

The Input Interface performs two types of operations based on the method of input bits allocation. The first one is known as fragmentation, where the number of input bits is placed to the possible capacity of the data field by dividing UPs into subset data fields. The second operation is no fragmentation, where the data field consists of an integer number of UPs [16].

When in-band signaling has not applied, the capacity of the data field is (K_{bch} - 80) and less when in-band is employed. If the data field length less than (K_{bch} - 80), the stream adapter must insert a padding field to keep the LDPC /BCH coding block capacity complete [33].

b. Input Stream Synchronizer

The user information may have a changeable transmission delay during data processing in the modulator of the DVB-T2 system. For each input form, the Input Stream Synchronizer (ISSY) must produce appropriate ways of ensuring Constant Bit Rate (CBR) and fixed delay. For PLPs conveying GSE, GCS, and GFPS input formats, applying ISSY is optional [16].

If PLP conveying TS formats, ISSY should always be employed unless the following five requirements are met. These requirements are using only one PLP, the data field is (K_{bch} - 80) in each BBFRAME, the number of FEC blocks of PLP is equal to the maximum FEC blocks in interleaving frame, Null Packet Deletion (NPD) is not employed, and Future Extension Frames (FEF) are not used [25], [34].

The ISSY field is two or three bytes conveying a counter state that can be utilized by the receiver to reproduce the regenerated output stream's correct timing. The conveyance of ISSY fields is determined by the input stream format and the mode type [35].

For a collection of data PLPs and the associated common PLP, the interleaving parameters such as Number of T2-frames to which each

Interleaving Frame is mapped (P_I) and Number of TI-blocks in an Interleaving Frame (N_{TI}) as well as the Frame Interval (I_{JUMP}), may be varied. The TS reintegrated mechanism is important at the receiver. To implement this mechanism without needing additional memory, the input TS is delayed in the modulator after adding the ISSY field [35].

The TS principles need a fixed overall delay for bit rates at the transmitter output and the de-multiplexer input of the receiver. A substantial portion of null packets is present to handle inconstant bit-rate applications at a fixed rate for some input TS [33].

TS null-packets must be discovered and eliminated in this situation to minimize extra transmission overhead. The method must satisfy accurate re-insertion of the deleted null-packets at the receiver in the precise position where they were initially located [32].

c. Deleted Null Packets

After sending a UP, a counter named Deleted Null Packets (DNP) of one byte must be reset and then increased by one at every removed null packet. The DNP owns a maximum allowable value of 255. If the DNP reaches its maximum and the following package is also a null one, it will be held and transmitted as a helpful packet. The process of null packet deletion is displayed in Fig. 2.5 [35].

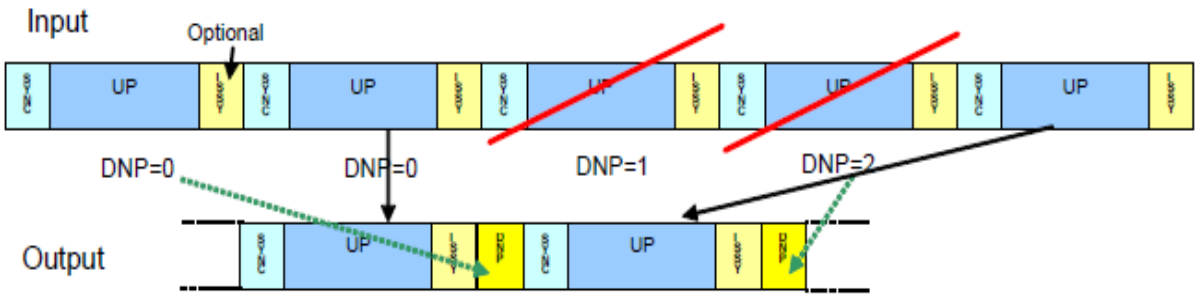

Fig. 2.5 Null packet deletion process [35].

d. Cyclic Redundancy Check

A Cyclic Redundancy Check (CRC-8) is implemented to detect errors at the user packet level for normal mode and packetized streams. The User Packet bits with a Length (UPL) of UPL-8 are processed by eight bits systematic CRC encoder. Following CRC application, the result is added after the user packet. The systematic CRC-8 encoder is specified in appendix A [1].

ii. Stream Adaptation

Stream adaptation module is a subsystem of input processing of DVB-T2, supports scheduling, padding, and scrambling operations. The scheduling is applied for multi-frame interleaving and padding to keep fixed BBFRAME bits length or handle in-band signaling. The scrambling is employed to dissipate energy [16].

The BBHEADER with DATA FIELD is the input of the stream adaptation module. The output of this process is the BBFRAME stream, as given in Fig. 2.6 [16].

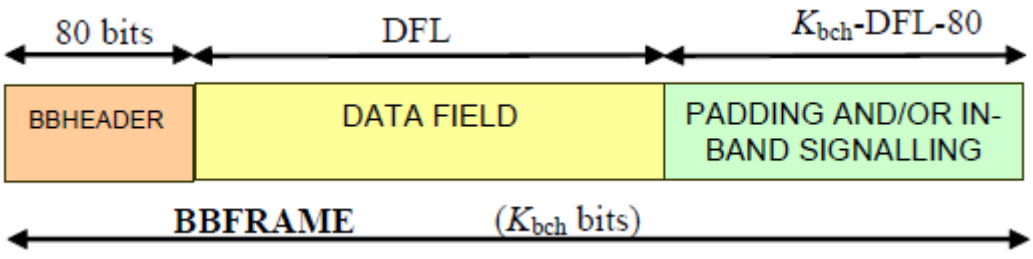

Fig. 2.6 Stream adaptation output format [16].

a. Scheduler

The scheduler must determine the DVB-T2 signal cells that transport data related to physical layer pipes essential to produce the information needed for dynamic signaling. The scheduler must establish the accurate configuration of the frame structure, despite the fact that this process has no influence on the data stream at this step [33].

The beginning of every FEC block is calculated individually for every physical layer pipes starting by first interleaving frame. Then for every PLP, the values of dynamic parameters are determined by the scheduler. The scheduler delivers determined values to the in-band signaling addition [32].

b. Padding

Padding can be used if the amount of accessible user data to be handled is insufficient to populate a baseband frame fully or if the amount of user packets in a BBFRAME is allocated an integer number. The numbers of padding zero bits are given by Eq. 2.2. These bits are added after the DATA FIELD to produce fixed bits length of K_{bch} [35].

$$\text{padding} = K_{bch} - DFL - 80 \qquad 2.2$$

The field of padding can be employed to support in-band signaling. There are two kinds of in-band signals, type A and type B. The field of PADDING can include one kind of these in-band signals or both of them. When both in-band signals are used, a type A block should appear first, followed by a type B block. Both signaling types A and B present only in the first BBFRAME of a given interleaving frame. Fig. 2.7 shows the padding field signaling format when in-band signals are provided [33].

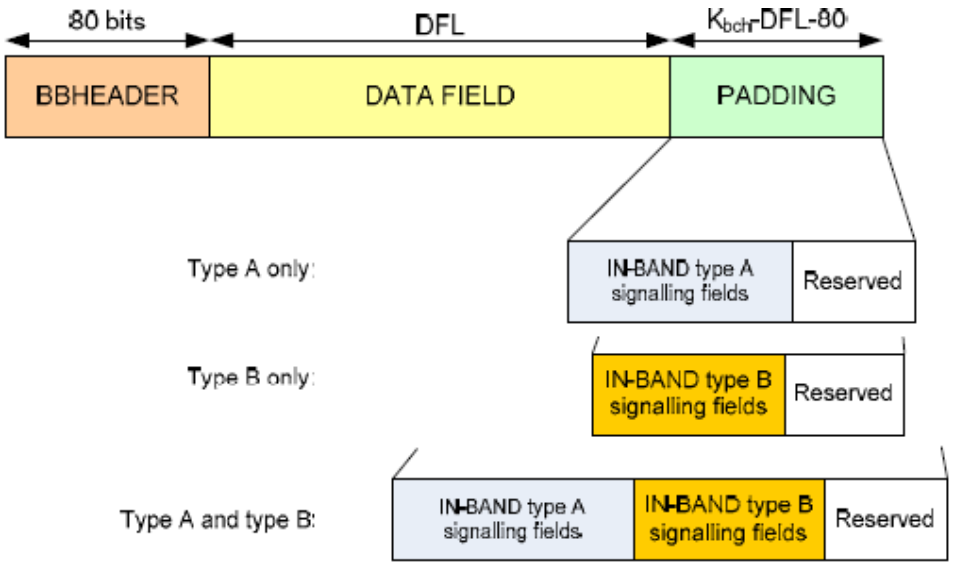

Fig. 2.7 Padding field format of stream adaptation [33].

In-band type A signaling is responsible for providing updated and co-scheduled information. For handling more than one PLP, in-band type A constantly applies. In-band type B signaling offers extra information associated with the input processing module of PLPs having TS or GFPS stream. It should include additional ISSY information specifically to allow faster initial acquisition. The application of In-band type B is optional [5].

c. BB Scrambling

Randomization of the entire baseband format is required. The randomization process is synchronized with the BBFRAME. The process begins at MSB and completes after K_{bch} BBFRAME bits. For this purpose, a feedback shift register is used to produce the scrambling sequence as shown in Fig. 2.8 [16].

The Pseudo-Random Binary Sequence (PRBS) polynomial is given in Eq. 2.3. At each beginning of BBFRAME, the PRBS register should be initialized with the (100101010000000) sequence [16].

$$1 + x^{14} + x^{15} \qquad 2.3$$

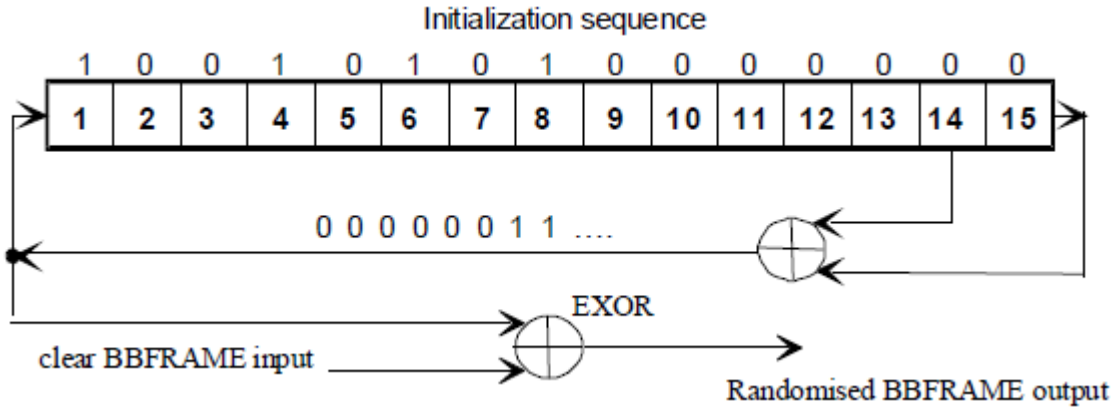

Fig. 2.8 PRBS implementation for BB scrambling [16].

2.2.2 Bit Interleaved Coding and Modulation

The second block of the DVB-T2 system is bit interleaved coding and modulation module. The BICM module has been utilized to handle Shannon

limit with low complexity in communications systems. This module includes mainly of seven sub-block, as illustrated in Fig. 2.9 [5].

The BICM module input possibly contains one or more data streams, where a single PLP conveys every data stream. Then service-specific robustness becomes achievable because every PLP has its individual configuration of the FEC, constellation, and depth of time interleaving. The output of the BICM module is fed to the frame builder block [36].

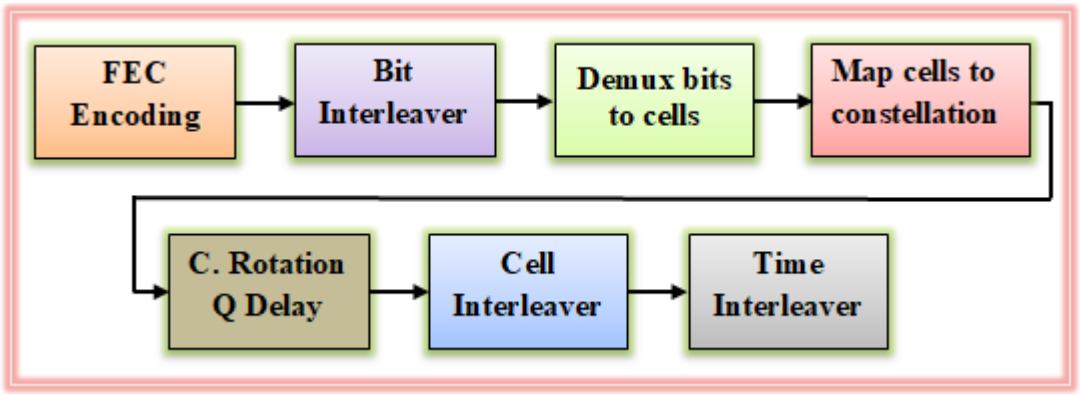

Fig. 2.9 DVB-T2 BICM module [5].

i. FEC Encoding

The FEC encoding is the BICM module sub-system which consists of BCH outer coding, and LDPC inner coding. The DVB-T2 adopts a similar FEC coding process from the DVB-S2 by LDPC/BCH concatenation codes [37].

The use of LDPC codes produces an achievement that is near to AWGN capacity, and the BCH code eliminates the existence of error floors. The connection of LDPC and BCH schemes can be better than convolutional, and Reed Solomon codes (RS) belong to the first-generation around 3 dB in AWGN [9].

The input of the FEC encoding subsystem is BBFRAMEs, while the output stream is FECFRAMEs. The BBFRAME with K_{bch} bits is applied to the FEC to produce the FECFRAME having N_{ldpc} bits. The systematic BCH parity

check bits are attached after BBFRAME, and the LDPC parity check bits are attached after the BCHFEC field, as illustrated in Fig. 2.10 [16].

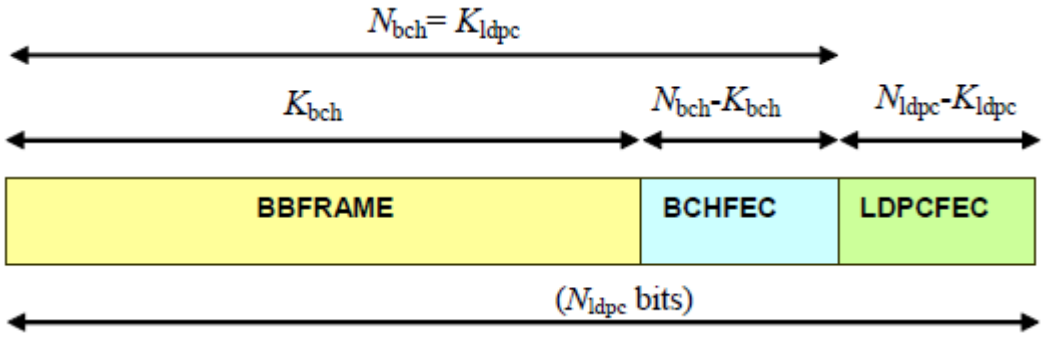

Fig. 2.10 FEC encoding format [16].

The FECFRAME length comes with two options normal and short frame length based on N_{ldpc} parameters of 64800 and 16200 bits, respectively. The FEC coding parameters for normal and short structures are given in Table 2.1[38].

1. Outer Encoding

The BCH code is a type of cyclic error-correcting code made up of polynomials over a Galois field. In 1959 Alexis Hocquenghem, a French mathematician, invents BCH codes and separately in 1960 by Bose and Chaudhuri. One of the most important characteristics of BCH codes is that the symbol error numbers that the code can correct may be precisely controlled during code generation at the transmitter [35].

Particularly, binary BCH codes can be constructed to fix multiple bit errors. Another benefit of BCH codes is their ease of decoding, which is accomplished via an algebraic method called syndrome decoding. In DVB-T2, every BBFRAME has BCH (N_{bch}, K_{bch}) with error-correcting ability (t) to obtain an error-protected packet. The parameters of the DVB-T2 BCH code are given in Table 2.1. The BCH encoder with t error-correcting ability is produced by using the generator polynomial presented in Table 2.2 [32].

Table 2.1(a) FEC parameters for normal frame length [32]

Code Rates	**K_{bch} (bits)**	**$N_{bch} = K_{ldpc}$ (bits)**	**BCH-t**
1/2	32208	32400	12
3/5	38688	38880	12
2/3	43040	43200	10
3/4	48408	48600	12
4/5	51648	51840	12
5/6	53840	54000	10

Table 2.1(b) FEC parameters for short frame length [32]

Code Rates	**K_{bch} (bits)**	**$N_{bch} = K_{ldpc}$ (bits)**	**BCH-t**
1/2	7032	7200	12
3/5	9552	9720	12
2/3	10632	10800	12
3/4	11712	11880	12
4/5	12432	12600	12
5/6	13152	13320	12

2. Inner Encoding

The LDPC code employed in DVB-T2 is a linear error-correcting code. This code is developed by the American electrical engineer R. Gallager in 1960. A sparse Tanner graph is applied to create the LDPC codes. The LDPC encoders are employed as inner encoders in DVB-T2 systems because of their great error-correcting achievement [35].

Table 2.2 (a) Outer coder Generator polynomial for normal frame length [35]

g(x)	Polynomial
$g_1(x)$	$1+x^2+x^3+x^5+x^{16}$
$g_2(x)$	$1+x+x^4+x^5+x^6+x^8+x^{16}$
$g_3(x)$	$1+x^2+x^3+x^4+x^5+x^7+x^8+x^9+x^{10}+x^{11}+x^{16}$
$g_4(x)$	$1+x^2+x^4+x^6+x^9+x^{11}+x^{12}+x^{14}+x^{16}$
$g_5(x)$	$1+x+x^2+x^3+x^5+x^8+x^9+x^{10}+x^{11}+x^{12}+x^{14}+x^{16}$
$g_6(x)$	$1+x^2+x^4+x^5+x^7+x^8+x^9+x^{10}+x^{12}+x^{13}+x^{14}+x^{15}+x^{16}$
$g_7(x)$	$1+x^2+x^5+x^6+x^8+x^9+x^{10}+x^{11}+x^{13}+x^{15}+x^{16}$
$g_8(x)$	$1+x+x^2+x^5+x^6+x^8+x^9+x^{12}+x^{13}+x^{14}+x^{16}$
$g_9(x)$	$1+x^5+x^7+x^9+x^{10}+x^{11}+x^{16}$
$g_{10}(x)$	$1+x+x^2+x^5+x^7+x^8+x^{10}+x^{12}+x^{13}+x^{14}+x^{16}$
$g_{11}(x)$	$1+x^2+x^3+x^5+x^9+x^{11}+x^{12}+x^{13}+x^{16}$
$g_{12}(x)$	$1+x+x^5+x^6+x^7+x^9+x^{11}+x^{12}+x^{16}$

Table 2.2 (b) Outer coder Generator polynomial for short frame length [35]

g(x)	Polynomial
$g_1(x)$	$1+x+x^3+x^5+x^{14}$
$g_2(x)$	$1+x^6+x^8+x^{11}+x^{14}$
$g_3(x)$	$1+x+x^2+x^6+x^9+x^{10}+x^{14}$
$g_4(x)$	$1+x^4+x^7+x^8+x^{10}+x^{12}+x^{14}$
$g_5(x)$	$1+x^2+x^4+x^6+x^8+x^9+x^{11}+x^{13}+x^{14}$
$g_6(x)$	$1+x^3+x^7+x^8+x^9+x^{13}+x^{14}$
$g_7(x)$	$1+x^2+x^5+x^6+x^7+x^{10}+x^{11}+x^{13}+x^{14}$
$g_8(x)$	$1+x^5+x^8+x^9+x^{10}+x^{11}+x^{14}$
$g_9(x)$	$1+x+x^2+x^3+x^9+x^{10}+x^{14}$
$g_{10}(x)$	$1+x^3+x^6+x^9+x^{11}+x^{12}+x^{14}$
$g_{11}(x)$	$1+x^4+x^{11}+x^{12}+x^{14}$
$g_{12}(x)$	$1+x+x^2+x^3+x^5+x^6+x^7+x^8+x^{10}+x^{13}+x^{14}$

The outer encoding output N_{BCH} is processed by LDPC encoder as a block of size K_{ldpc} information and systematically produces N_{ldpc} code-word size [2]. The parameters of inner coding are given in Table 2.1 for both frame types. The complete steps for data encoding with outer and inner codes are given in Appendix B [32].

ii. Bit Interleaver

Deep fading or erasure occurrences can be very damaging to LDPC codes. If a number of bits linked to the same inner coding check node are deeply faded or erased, the updated information cannot be supported correctly by this check node to the related variable nodes [36].

Moreover, the affected check node no longer contributes to the iterative process adequately, resulting in a waste of performance. When high constellations size are applied, erasures and fading occur at the cell field, affecting all the cell's bits identically. Consequently, the bit interleaver's purpose is to keep bits from being sent in the same constellation cell attached to one check node [35].

The type of bit interleaver employed in the DVB-T2 system is a block interleaver. It combines parity interleaving and column-twist interleaving and is applied at the field of LDPC codeword. It is employed with all modulation modes except when the QPSK modulation is used [7], [39].

The fundamental block interleaver process is applied immediately to the field LDPC; thus, several constellation symbols include many coded bits attached to the same check node. Hence, the parity interleaver is built so that the parity and information sections of the parity check matrix have a similar structure [5].

The operation of the parity interleaver part is described by Eq. 2.4 for the information bits section and Eq. 2.5 for the parity section. Where $0 \leq s < 360$, $0 \leq$

t < Q_{ldpc}, a is the LDPC output, u the output of parity interleaver in bits, and Q_{ldpc} is the LDPC constant for each coding rate given in Table 2.3 [35].

$$u_i = a_i \text{ for } 0 \leq i < K_{ldpc} \quad 2.4$$

$$u_{K_{ldpc}+360t+s} = a_{K_{ldpc}+Q_{ldpc}.s+t} \quad 2.5$$

Table 2.3 Q_{ldpc} values for normal and short frame length

Code Rates	**Normal Q_{ldpc}**	**Short Q_{ldpc}**
1/2	90	25
3/5	72	18
2/3	60	15
3/4	45	12
4/5	36	10
5/6	30	8

The operation of the column twist interleaver section is done by serially writing the output of parity interleaver, information and interleaved parity bits, column-wise and sequential readout row-wise. The writing start point is twisted with integer value t_c for every column. The column twist interleaver arrangement and value of t_c parameters are given in Table 2.4. The reading process is started from the MSB of BBHEADER, as illustrated in Fig. 2.11 [1].

The write and read scheme of the column-twist interleaver can be more clarified by mathematical expression, where the input bit is addressed to column C_i, row R_i as given in Eq. 2.6. and the output bit is obtained according to Eq. 2.7, where $0 \leq i, j < N_{ldpc}$ [38].

$$C_i = i \; div \; N_r, \; R_i = \left(i + t_{c_i}\right) mod \; N_r \quad 2.6$$

$$R_j = j \; div \; N_c, \; C_j = j \; mod \; N_c \quad 2.7$$

Table 2.4 The column twist configuration and t_c parameters

Mod.	**N_c**	**N_{ldpc}**	**t_c**															
			0	1	2	3	4	5	6	7	8	9	10	11	12	13	14	15
16-QAM	8	64800	0	0	2	4	4	5	7	7								
		16200	0	0	0	1	7	20	20	21								
64-QAM	12	64800	0	0	2	2	3	4	4	5	5	7	8	9				
		16200	0	0	0	2	2	2	3	3	3	6	7	7				
256-QAM	16	64800	0	2	2	2	2	3	7	15	16	20	22	22	27	27	28	32
	8	16200	0	0	0	1	7	20	20	21								

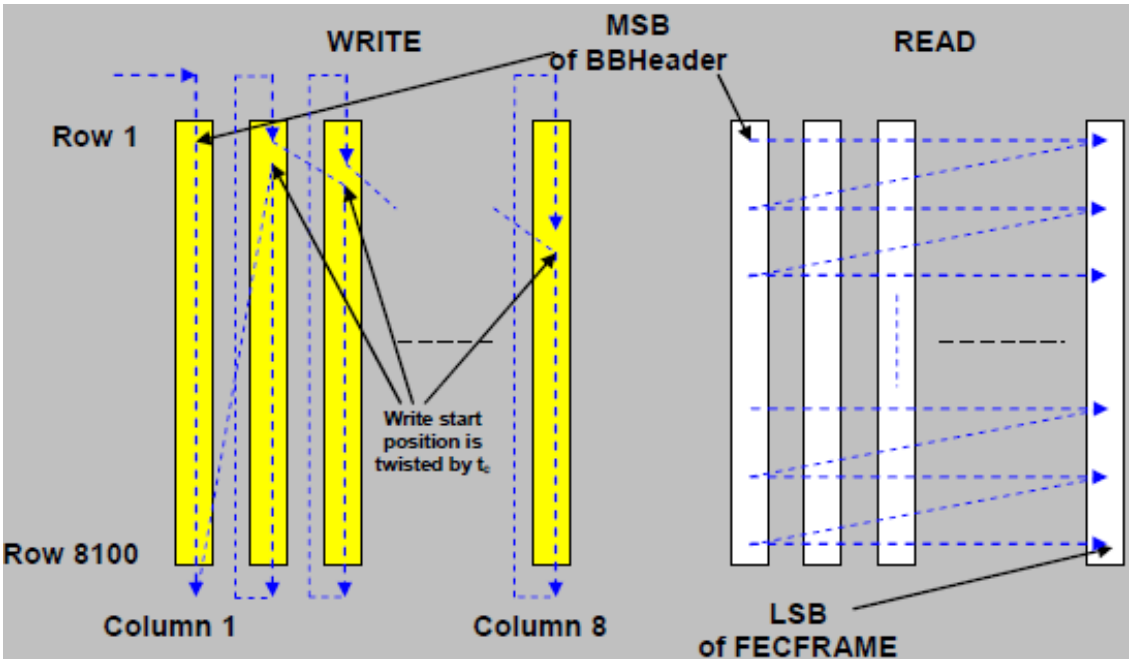

Fig. 2.11 Bit interleaver process for 16-QAM constellation and normal frame length [38].

iii. Bit to Cell Word de-multiplexer

A coded and modulated FEC block is obtained from mapping every FECFRAME field. The process is done by initially splitting the input stream into groups of cells and converting it into constellation values. Table 2.5 displays the number of data cells and effective bits per cell [32].

An extra bit to cell de-multiplexer is used to provide a more precise optimization of the association between the modulation and the LDPC code. It is located between the stage of the bit interleaver and the constellation mapper. The de-multiplexer separates the bit stream (v_i) at the bit interleaver's output into several sub-streams (b), as shown in Fig. 2.12. The bits per one constellation cell is a multiple of this sub-stream, as seen in Table 2.6 [1].

The parameters for de-multiplexing are a function of the code rate, constellation size, and FECFRAM length, as given in Appendix C.

Table 2.5 Configuration of mapping bits onto constellations

N_{ldpc}	Modulation	n_{MOD}	Cells
64800	QPSK	2	32400
	16-QAM	4	16200
	64-QAM	6	10800
	256-QAM	8	8100
16200	QPSK	2	8100
	16-QAM	4	4050
	64-QAM	6	2700
	256-QAM	8	2052

Table 2.6 Sub-streams numbers of the de-multiplexer

Modulation	**N_{ldpc}**	**$N_{substreams}$**
QPSK	64800 or 16200	2
16-QAM		8
64-QAM		12
256-QAM	64800	16
	16200	8

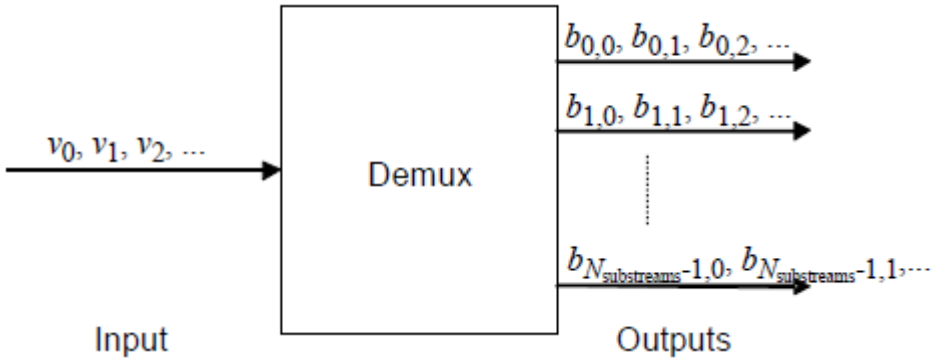

Fig. 2.12 Bit to cell de-multiplexer scheme [1].

iv. Map Cells to Constellation

The powerful performance of error-correction codes permits the DVB-T2 system to employ constellation modulation with high order. The DVB-T2 uses constellation schemes of QPSK, 16-QAM, and 64-QAM as in the DVB-T system. It also supports a 256-QAM constellation with 8 bits in every OFDM cell, allowing an improvement by 33% in the spectral efficiency compared to DVB-T [5].

The constellation point (z_q) is produced by modulating every cell of the de-multiplexer output with any selected constellation type. After applying the constellation modulation, the resulting points are normalized by a certain factor

to obtain the correct value of the complex cell. Fig. 2.13 shows an example for current mapper with QPSK and 16-QAM modulation [1].

The normalization factors for each constellation type are addressed in Table 2.7. For each constellation, the correct component of the real and imaginary values and corresponding bit pattern are specified in Appendix D [32].

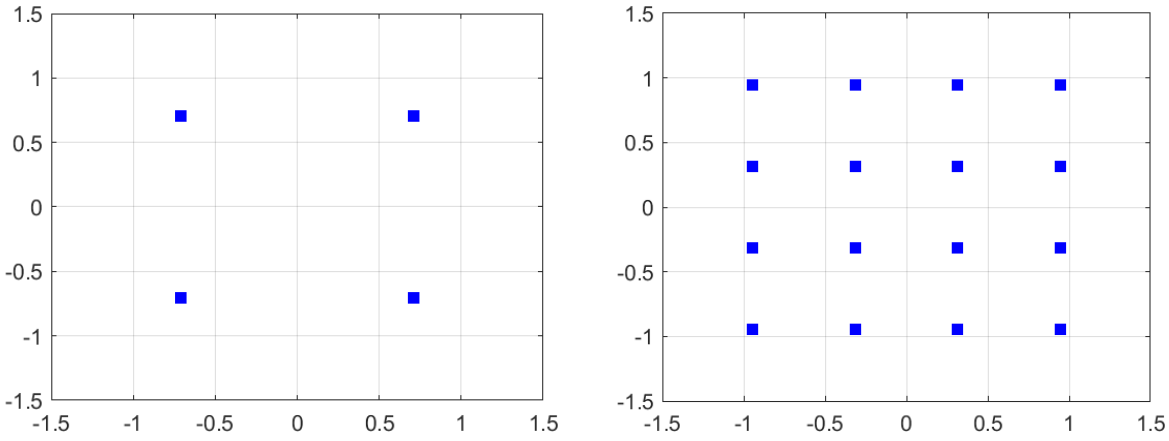

(a) (b)

Fig. 2.13 DVD-T2 constellation diagram after normalization (a) QPSK, (b) 16-QAM [32].

Table 2.7 Data cells normalization factors

Modulation	Normalization
QPSK	$\frac{z_q}{\sqrt{2}}$
16-QAM	$\frac{z_q}{\sqrt{10}}$
64-QAM	$\frac{z_q}{\sqrt{42}}$
256-QAM	$\frac{z_q}{\sqrt{170}}$

v. Rotated Constellation and Q Delay

The DVB-T2 system applies two constellation modes, the standard non-rotation and the new constellation rotation modes. If employing traditional constellations mode, then every real I or imaginary Q component contains half of the binary information conveyed within the signal [40].

As a result, when a particular event fades the signal, both parts of I and Q fade out in the same way. The information conveyed on both the in-phase and quadrature components experiences a high loss in complex fading [41].

The new constellation rotation technique is an optional feature supported by the DVB-T2 system. However, the application of this technique makes both I and Q components carry the entire signal binary content. Each I and Q component has its individual axes projections [2].

The rotation is accomplished by rotating the normalized cell values from the output of the constellation mapper in the complex plane. Then, the rotation is applied on every FEC block using the rotation phasor (R_{RQD}) given in Eq. 2.8. The rotation phasor angle θ relies on the constellation type, as supplied in Table 2.8 [40].

$$R_{RQD} = e^{j\frac{2\pi\theta}{360}} \qquad 2.8$$

Table 2.8 Values of rotation angle according to each constellation size

Modulation	QPSK	16-QAM	64-QAM	256-QAM
θ in degrees	29	16.8	8.6	3.6

Next, an extra invention called Q cyclic delay is applied. The delay denotes that the Q component's status is shifted to the upcoming cell within the FEC block. This shift is done cyclically and achieved individually in the FEC

levels. The operation of constellation rotation with cyclic Q delay is explained in Eq. 2.9 and 2.10 where F_0 is the constellation mapper output [18], [32].

$$G_0 = Re\left(R_{RQD}\, F_0\right) + j\, Im\left(R_{RQD}\, F_{Ncells-1}\right) \quad 2.9$$

$$G_q = Re\left(R_{RQD}\, F_q\right) + j\, Im\left(R_{RQD}\, F_{q-1}\right), q = 1,2, \ldots . N_{cells} - 1 \quad 2.10$$

vi. Cell Interleaver

The primary function of the Cell Interleaver (CI) and Time Interleaver (TI) is to defend against impulsive noise and time-selective fading. The CI uses a pseudo-random permutation to distribute the cells in the FEC codeword evenly. Its intentions to guarantee an uncorrelated pattern of channel distortions and interference over the FEC code-words in the receiver and improve cell detachment [9].

The Cell Interleaver processes the input sequence from the constellation rotation and cyclic Q delay to give the output vector of Eq. 2.11. Where $L_r(q)$ is a permutation function utilized to each FEC block index (r) within the time interleaver block. The permutation function depends on a maximum length sequence having an order of (N_d-1) with N_d given by Eq. 2.12. This function toggles MSB at every new location production [32].

$$d_{r,L_r(q)} = g_{r,q}\; q = 1,2, \ldots , N_{cells} - 1 \quad 2.11$$

$$N_d = \lceil log_2(N_{cells}) \rceil \quad 2.12$$

When a location is formed with a length more than or equal to N_{cells}, it is rejected, and a new one is formed. A constant shift (modulo N_{cells}) is attached to the permutation to create various permutations for various FEC blocks, with values higher than or equal to N_{cells} rejected. The $L_r(q)$ permutation function is presented by Eq. 2.13 [1].

$$L_r(q) = [L_0(q) + P(r)] mod N_{cells} \quad 2.13$$

The $L_0(q)$ is the basic permutation function illustrate in the algorithm given in Appendix E and P(r) is the shift value for index r. The cell interleaver scheme is displayed in Fig. 2.14 [16].

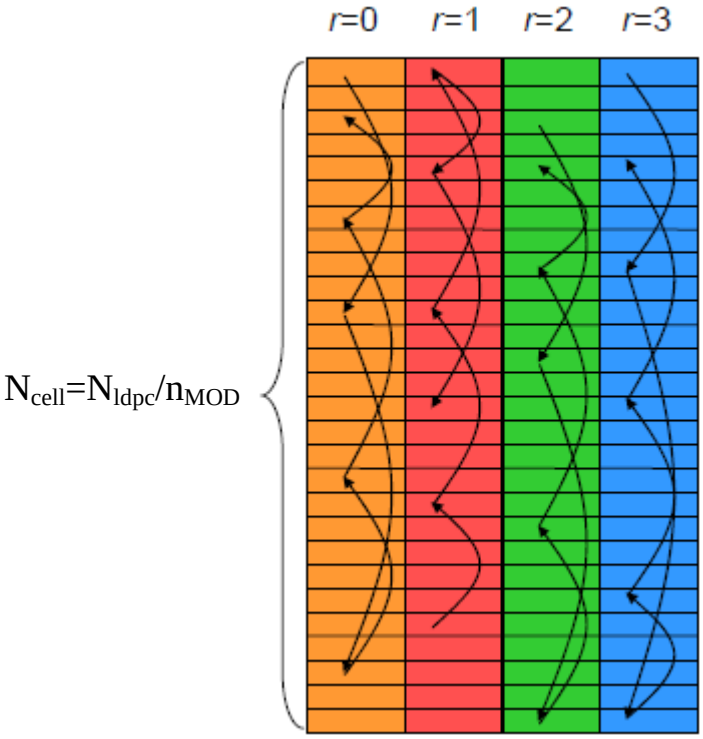

Fig. 2.14 Cell interleaver process [16].

vii. Time Interleaver

A further key development of DVB-T2 over DVB-T is the addition of time interleaving which considerably enhances the system's robustness upon fading conditions. The time interleaver performs at the PLP field. In the DVB-T2 system, the time interleaving parameters may change for various PLPs [42].

The smallest part of the frame construction is named the Interleaving Frame (IF). The IF is formed by arranging the cell interleaver FEC blocks for a given PLP assigned to a single or multiple T2-frames. Because each PLP's data rate varies, each IF can have a dynamically different amount of FEC blocks [43].

Every IF is either assigned immediately to a single T2-frame or split across multiple T2-frames. This IF is also additionally broken into single or multiple time-interleaved blocks (N_{TI}), each of which representing one-time interleaver memory consumption. A varied number of forward error correction blocks can be found in every block of the TI inside an IF [42].

The IF must be assigned to only a single T2-frame if it is split into several TI-blocks. As a result, each PLP has three possibilities for time interleaving they are [7]:

- Single TI-block in each IF and is assigned immediately to a single T2-frame.
- Single TI-block in each IF and is assigned to a multiple T2-frame.
- Each IF is partitioned into many TI-blocks and is assigned immediately to a single T2-frame.

The third choice for time interleaving are explained in Fig. 2.15. For multiple TI-block per IF, i.e. $N_{TI}>1$, then the number of available FEC blocks in TI-block for a given IF is expressed by Eq. 2.14. This guarantees that the $N_{FEC-TI}(n,s)$ values for the TI-blocks inside an IF vary by no more than a single FEC block, and the TI-blocks appear first to be the smallest [32].

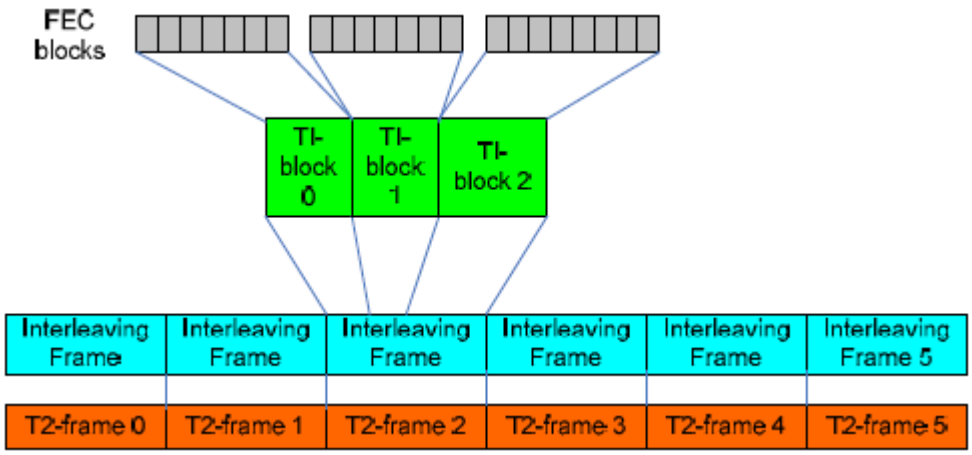

Fig. 2.15 Time interleaver for $N_{TI}>1$[32].

$$N_{FEC-TI}(n,s) = \begin{cases} \left\lfloor \frac{N_{BLOCKS\_IF}(n)}{N_{TI}} \right\rfloor, & s < N_{TI} - \left[N_{BLOCKS\_IF}(n) \; mod \; N_{TI}\right] \\ \left\lfloor \frac{N_{BLOCKS\_IF}(n)}{N_{TI}} \right\rfloor + 1, & s \geq N_{TI} - \left[N_{BLOCKS\_IF}(n) \; mod \; N_{TI}\right] \end{cases} \quad 2.14$$

Where $0 \leq s < N_{TI}$ is TI-block index, n is IF index, N_{BLOCK_IF} is the total number of FEC blocks per IF. The $N_{FEC-TI}(n,s)$ may change over time from a value of 0 to a maximum value given in Eq. 2.15 [32].

$$N_{FEC\_TI\_MAX} = \left\lceil \frac{N_{BLOCKS\_IF\_MAX}}{N_{TI}} \right\rceil \quad 2.15$$

The $N_{BLOCK-IF-MAX}$ is defined as the maximum FEC blocks per one IF. The maximum value of TI memory per PLP is $M_{TI}=2^{19}+2^{15}$ and if there is a common PLP, this memory must be divided between this common one and data PLP. As a result, for PLPs without a common one, the values of TI-blocks and maximum FEC blocks per IF must be selected according to the formula given in Eq. 2.16 [9].

$$N_{FEC\_TI\_MAX} * N_{cells} \leq M_{TI} \quad 2.16$$

The time interleaver is a row-column block interleaver with the row number equal to the FEC block cells divided by five according to the DVB-T2 standard. The column number of TI is given by multiplication the total number of FEC blocks from each TI-blocks by five. Therefore, The TI column number loaded will change for each TI-block based on FEC blocks within it [1].

The parameters of the TI are listed in Table 2.9. The row-column block interleaver can be described graphically as in Fig. 2.16. The initial FEC block fills the initial five columns of TI in the column-wise path, and the next FEC block fills the following five columns, and so on. Thus, the reading process is done in a row-wise way [32].

Table 2.9 TI parameters

N_{ldpc}	Modulation	Cells	N_r
64800	QPSK	32400	6480
	16-QAM	16200	3240
	64-QAM	10800	2160
	256-QAM	8100	1620
16200	QPSK	8100	1620
	16-QAM	4050	810
	64-QAM	2700	540
	256-QAM	2052	405

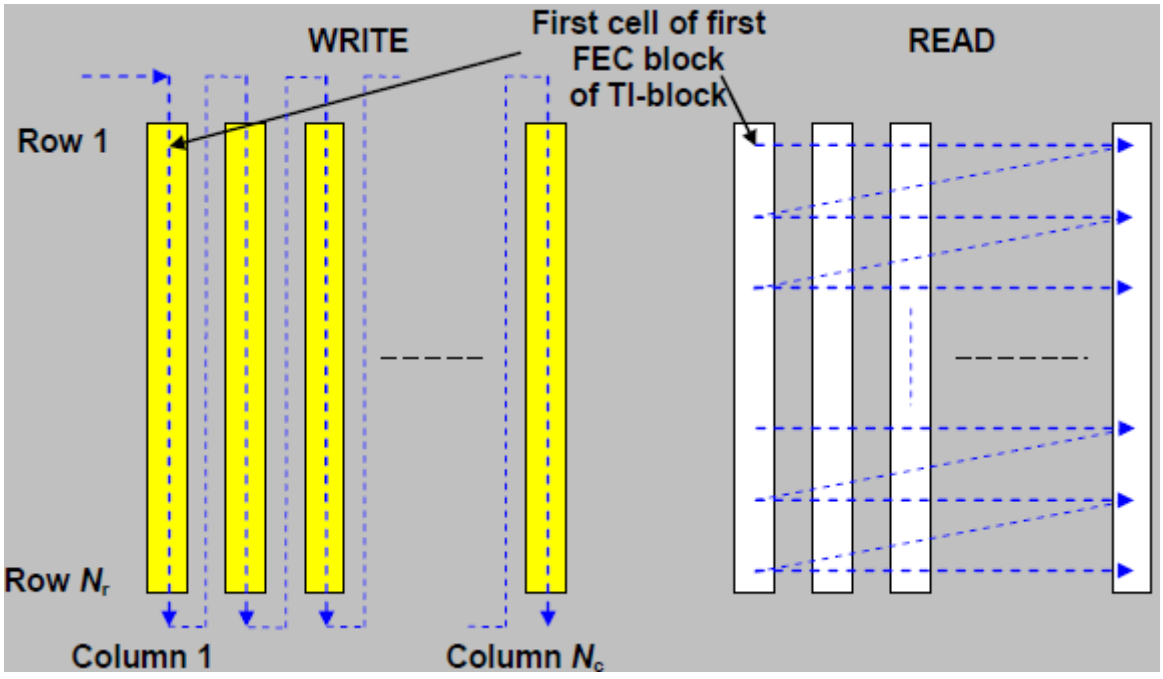

Fig. 2.16 Write and read scheme of time interleaver [32].

2.2.3 Frame Builder

The time interleaver output cells are mapped by the frame builder to arrays of OFDM cells. These cells belonged to the OFDM symbols that build up the whole frame arrangement. The mapping scheme is applied for every PLPs. The frame builder is controlled by the scheduler's dynamic information and the frame structure's setting [5].

Super-frames are divided into T2-frames in the DVB-T2 frame construction, where each DVB-T2 frame is formed from OFDM symbols. The Future Extension Frames sections could be present in the super-frame. The structure of DVB-T2 frame is displayed in Fig. 2.17 [35].

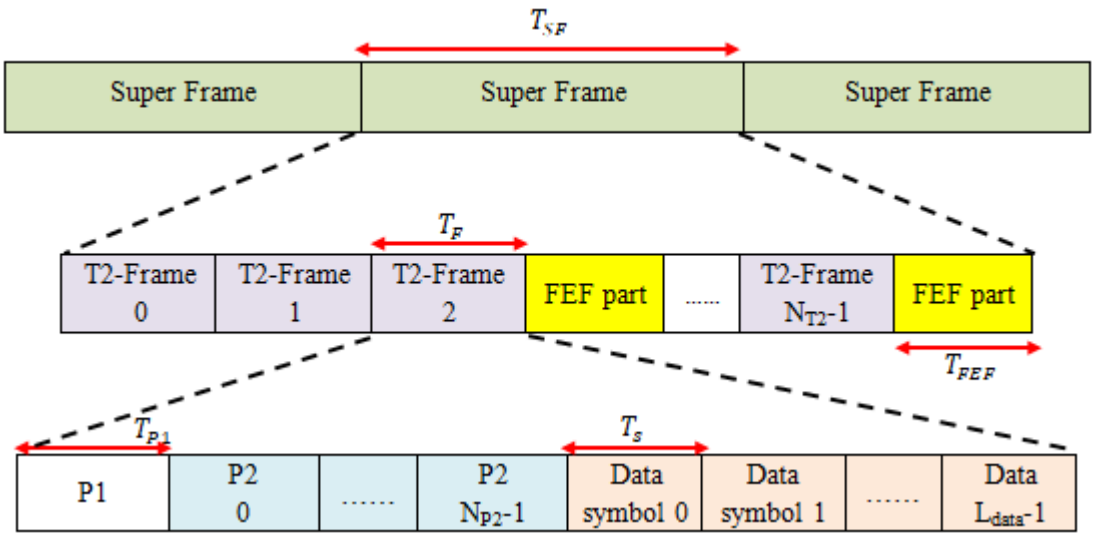

Fig. 2.17 The DVB-T2 frame structure [35].

The super-frame has configurable T2-frames numbers N_{T2}. They are counted from 0 to N_{T2}-1. Among T2-frames, an FEF portion can be included. In the super-frame, there may be many FEF portions, but no FEF segment should be near to another FEF segment. The super-frame structure is used to signal the FEF pieces' placement in time. The duration T_{SF} of a super-frame is defined by Eq. 2.17 [16].

$$T_{SF} = N_{T2} * T_F + N_{FEF} * T_{FEF} \qquad 2.17$$

The parameter N_{FEF} is the number of FEF and T_{FEF} is the time duration of single FEF sections. If Future Extension Frames are not employed, the maximum value for the super-frame duration T_{SF} is 63.75 s, and if used, the ultimate value is 127.5 s. It's also worth noting that T2-frames and N_{T2} indexing are unaffected by FEF. The N_{T2} is selected to achieve an integer number of IF in super-frame for every physical layer pipes [16].

a. DVB-T2 Frame Structure

The T2-frame involves a single P1 symbol, P2 symbols, and a configurable length of data symbols. In addition, for specific DVB-T2 parameters, a frame closing symbol must be inserted at the end of the data symbol. The preamble P2 symbols are primarily utilized to transport data, and preamble symbol indicates the frame starting [32].

The FFT modes decide the number of P2 symbols N_{P2}, whereas the amount of data symbols L_{data} in the T2-frame is a configurable element. The maximum number of N_{P2} symbols is given in Table 2.10. The total amount of symbols in a T2 frame is presented in Eq. 2.18, and hence the frame duration is given in Eq. 2.19 [32].

$$L_F = N_{P2} + L_{data} \quad 2.18$$

$$T_F = L_F * T_s + T_{P1} \quad 2.19$$

The parameter T_s denotes the entire duration of OFDM symbols, and T_{P1} denotes the P_1 symbol duration. The frame time T_F must not exceed 250 milliseconds, and the highest number OFDM symbols must be as specified in Table 2.11according to each Guard Interval fraction (GI) [5].

Table 2.10 P2 symbol numbers of T2 frame

FFT	1K	2K	4K	8K	16K	32K
N_{p2}	16	8	4	2	1	1

Table 2.11 Max. L_F number of OFDM symbol

FFT	GI						
	1/128	1/32	1/16	19/256	1/8	19/128	1/4
32K	68	66	64	64	60	60	
16K	138	135	131	129	123	121	111
8K	276	270	262	259	247	242	223
4K		540	524		495		446
2K		1081	1049		991		892
1K			2098		1982		1784

The permeable P2 and data symbols carry physical layer pipes, and auxiliary streams. Data symbols carry only common PLPs or data PLPs. The mapping of PLPs into the symbols is done at the OFDM cell level, and thus, P2 or data symbols can be shared between multiple PLPs. If there is free capacity left in the T2-frame, it is filled with auxiliary streams (if any) and dummy cells. [5].

Table 2.12 lists the number of accessible cells in each P2 symbol (C_{P2}). Table 2.13 shows the number of accessible cells in standard data symbols (C_{data}) as a function of the pilot pattern (PP_i). Finally, when a FC is applied, the active cells number (C_{FC}) listed in Table 2.14 is used [32].

Table 2.12 Data cells of P_2 symbol

FFT		32K	16K	8K	4K	2K	1K
C_{P2}	SISO	22432	8944	4472	2236	1118	558
	MISO	17612	8814	4398	2198	1098	546

Table 2.13 Data cells of one data symbol

FFT	**C_{data}**								**T_R**
	PP1	PP2	PP3	PP4	PP5	PP6	PP7	PP8	
32K		24886		26022		26592	26836	26812	288
16K	12418	12436	12988	13002	13272	13288	13416	13406	144
8K	6208	6214	6494	6498	6634		6698	6698	72
4K	3084	3092	3228	3234	3298		3328		36
2K	1522	1532	1596	1602	1632		1646		18
1K	764	768	798	804	818				10

Table 2.14 Active cells in F_C symbol

FFT	**C_{FC}**								**T_R**
	PP1	PP2	PP3	PP4	PP5	PP6	PP7	PP8	
32K		20952		22649		23603			288
16K	6437	10476	7845	11324	8709	11801	11170		144
8K	3218	5238	3922	5662	4354		5585		72
4K	1609	2619	1961	2831	2177		2792		36
2K	804	1309	980	1415	1088		1396		18
1K	402	654	490	707	544				10

The frame ending symbol is a unique FC symbol in some FFT modes, Pilot pattern, and guard interval choices. This features a larger weight of pilots to provide for frequency-only interpolation for the symbol and temporal interpolation for the symbols directly leading. Because more pilots mean fewer data cells, the increased pilot density would inevitably result in reducing symbol

capacity than others. The number of data cells in the FC symbol is given in Table 2.15, which also shows the lower capacity N_{FC} [35].

Table 2.15 Data cells in F_C symbol

FFT	**N_{FC}**								**T_R**
	PP1	PP2	PP3	PP4	PP5	PP6	PP7	PP8	
32K		22720		24992		26128			288
16K	9088	11360	11360	12496	12496	13064	13064		144
8K	4544	5680	5680	6248	6248		6532		72
4K	2272	2840	2840	3124	3124		3266		36
2K	1136	1420	1420	1562	1562		1632		18
1K	568	710	710	780	780				10

However, some of the cells do not have any modulation., i.e., their modulation amount is zero, resulting in a further drop in capacity. This is made to guarantee that FC has roughly the equivalent power as the usual symbols, in spite of, higher pilots in the frame-closing symbol and the same amount boost the pilots as in the normal symbol [5].

Thus, the capacity C_{FC} reported in Table 2.14 is the number of modulated data cells; as can be observed, these are lower than the comparable numbers in Table 2.15. At the frame-builder end, the un-modulated cells are nearby, and the frequency interleaver disseminates them around the spectrum. The un-modulated cells and the higher pilots density from the frame-closing symbol are illustrated in Fig. 2.18 [5].

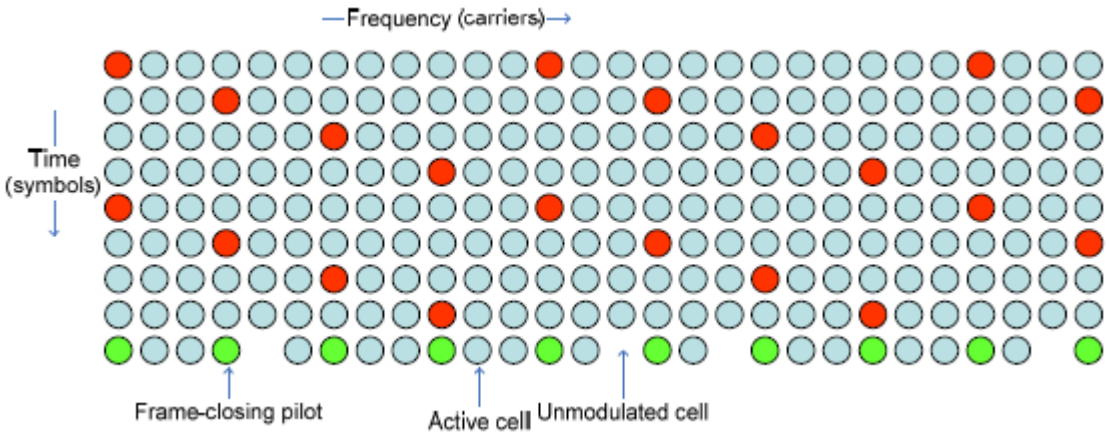

Fig. 2.18 Cells structure of frame-closing symbol

b. Dummy cells and Auxiliary streams

The overall cells number possible for physical layer pipes in a frame is not always a multiple of FEC block cells and relies on several elements of the DVB-T2 system. Since T2-Frame must have a complete number of FEC blocks, there may be cells in the frame that do not contain cells from any FEC block known as dummy cells. These cells will appear towards the end of the T2 frame [32].

The dummy cells don't hold any important information, so they're a waste of space. Applications that make utilization of these wasted cells may be established in the future, and the idea of an Auxiliary Stream is introduced for this reason. Auxiliary Streams could be used for transmitter signatures, audio streams, or information passed between network operators [5].

c. Future Extension Frames

FEF is optional parts that allow loading a frame specified in the future development of the DVB-T2 system. The DVB-T2 receivers in the current version have no ability to decode FEF but only can detect it. Any FEF must begin with a P1 symbol that all DVB-T2 receivers can identify [9].

For the T2-base system, the maximum duration of one FEF is 250 milliseconds. The FEF sections may comprise frames of different profiles. In addition, because every FEF section may include numerous frames, every section may contain numerous preamble P1 spaced at different intervals [26].

A super frame can include one or more FEF sections, allowing it to carry two various kinds of structures: T2-frames and FEF parts. When FEFs are employed, the ends of a super frame is an FEF section. The number of FEF sections in a super frame is given by Eq. 2.20 [5].

$$N_{FEF} = {}^{N_{T2}}/_{FEF\_interval} \qquad 2.20$$

d. Frequency Interleaver

The important step of frame building operation is the frequency interleaver scheme. The frequency interleaver plans the cells from the frame builder onto the potential carriers in each symbol N_{data}. It works with a single OFDM symbol's cells. The interleaved vector is given in Eq. 2.21 for symbol l of T2-frame m. While even and odd symbols of the frame are defined by Eq. 2.22 and Eq. 2.23, respectively [35].

$$A_{m,l} = (a_{m,l,0}, a_{m,l,1}, a_{m,l,2}, \ldots a_{m,l,N_{data}-1}) \qquad 2.21$$

$$a_{m,l,p} = x_{m,l,H_0(p)} \text{ , p=0,…, } N_{data}\text{-1} \qquad 2.22$$

$$a_{m,l,p} = x_{m,l,H_1(p)} \text{ , p=0,…, } N_{data}\text{-1} \qquad 2.23$$

The frequency interleaver is based on a set of permutation functions given by H(p), $H_0(p)$, and $H_1(p)$. These permutation functions are built by using R'_i sequences explained in Appendix F. The bit position of a permutation vector depends on the FFT modes, as shown in Table 2.16 for the 8K mode [16].

Table 2.16 Permutations of bits for 8K FFT

R'_i	11	10	9	8	7	6	5	4	3	2	1	0
H_0	5	11	3	0	10	8	6	9	2	4	1	7
H_1	8	10	7	6	0	5	2	1	3	9	4	11

2.2.4 OFDM Generation

In the DVB-T2 transmitter structure, the OFDM generation is the final step. The OFDM block diagram is made up of several sub-blocks, as seen in Fig. 2.19. The MISO Processing and PAPR reduction sub-blocks are optional which aren't employed in every situation [1].

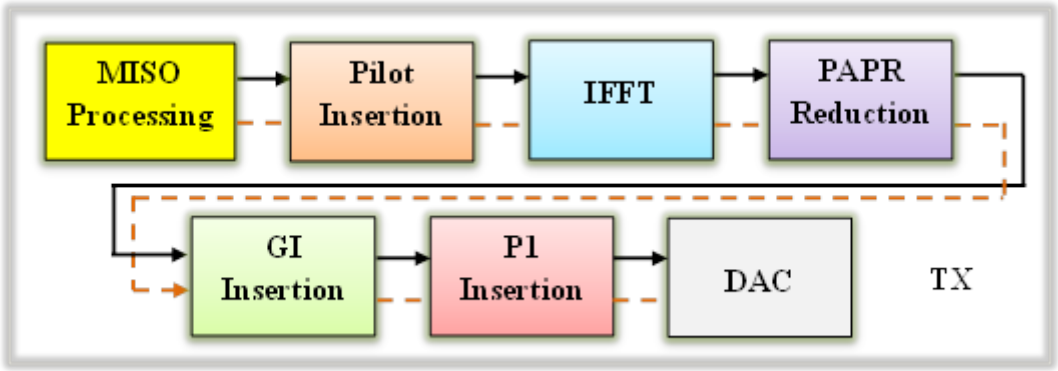

Fig. 2.19 DVB-T2 OFDM module [1]

The OFDM generating module aims to gather the output cells generated by the frame builder and insert the necessary reference data, named as pilots. These pilots enable the receiver to adjust for transmission channel distortions and generate the basis time domain signal for broadcast. The DVB-T2 signal is then finished by inserting guard intervals and, if necessary, employing a PAPR reduction scheme [44].

i. MISO Process

A modified Alamouti coding can be used to address the primary frequency-domain coefficients in an elective first step known as multiple input single output MISO scheme. It provides the T2 signal to be divided between two transmitters groups operating on the same frequency without interfering [45].

The channel frequency response has deep notches when signals are received from different transmitters. These notches have the potential to eliminate a large number of subcarriers and significantly reduce service quality. MISO aims to aggregate signals from several transmitters in the most efficient way possible and eliminates notches from the channel [46].

The MISO approach of the DVB-T2 system is built on a modified Alamouti code, a relatively simple space-frequency block code (SFBC) intended to improve system diversity with pair antennas DVB-T2 uses a code employed over two transmitters to increase reception in single frequency networks without requiring any changes to the existing network architecture [47]-[48].

The encoding operation is carried out on two OFDM payload cells (s_p, s_{p+1}) derived from the frequency interleaver output. The matrix for the modified Alamouti code provided in DVB-T2 is given in Eq. 2.24. Where p=0,2,4,…,N_{data}-2, * indicates the complex conjugation process, Tx1 is transmitter 1 belong to MISO group 1, and Tx2 is transmitter 2 belong to MISO group 2 [32], [49].

$$\begin{bmatrix} Tx1 \\ Tx2 \end{bmatrix} = \begin{bmatrix} s_p & s_{p+1} \\ -s^*_{p+1} & s^*_p \end{bmatrix} \qquad 2.24$$

The channel must stay essentially fixed over the transmission of symbols from the same pair to maintain the Alamouti code orthogonally. The channel is expected to experience significant differences between two consecutive OFDM

symbols, primarily in mobile settings, due to the extended duration of the OFDM symbols [50].

As a result, in DVB-T2, the Alamouti code is employed to successive subcarriers in the frequency domain rather than consecutive OFDM symbols in the time domain. The P1 symbols must be the same between the two transmitter groups, i.e., MISO not applied to P1 symbols. The input cells must be passed straight to the output if MISO scheme is not employed as presented in Eq. 2.25 [25], [32].

$$Tx = s_p,\ \text{p=0,1,2,…,}N_{data}\text{-1} \qquad 2.25$$

ii. Pilot Insertion

The pilots serve as a source of reference knowledge in the communication system. They enable the receiver to recognize and recompense for distortions caused by the transmission channel and generate the time domain signal for transmission from this. Frame, frequency, and time synchronization, besides estimation of the channel, are all carried out with the help of pilots [25], [51].

Pilots cells that include reference data are sent at a boosted power level compared to other OFDM cells. There are several kinds of pilots in DVB-T2 systems scattered, continual, edge, P2, and frame-closing pilots cells [52]-[53].

The modulation of pilots is based on the reference sequence ($r_{l,k}$). The $r_{l,k}$ sequence is created from PRBS symbol-level (w_k) and a frame-level pseudorandom sequence (P_{Nl}) as given in Eq. 2.26. Therefore, all pilots of every T2-frame symbol must be modulated with this reference sequence. The structure of reference sequence is illustrated in Fig. 2.20 [35].

$$r_{l,k} = w_k \oplus P_{Nl} \qquad 2.26$$

The PRBS symbol level sequence w_k is produced using the polynomial generator given in Eq. 2.27 where it initialized with all 1. At the same time, the

OFDM symbol from each T2-frame is processed by the frame-level P_{Nl} sequence. The length for P_{Nl} sequence is equal to the length of the T2-frame. In 8 MHz channel, the maximum length of the PN-sequence with various FFT modes is illustrated in Table 2.17 [32].

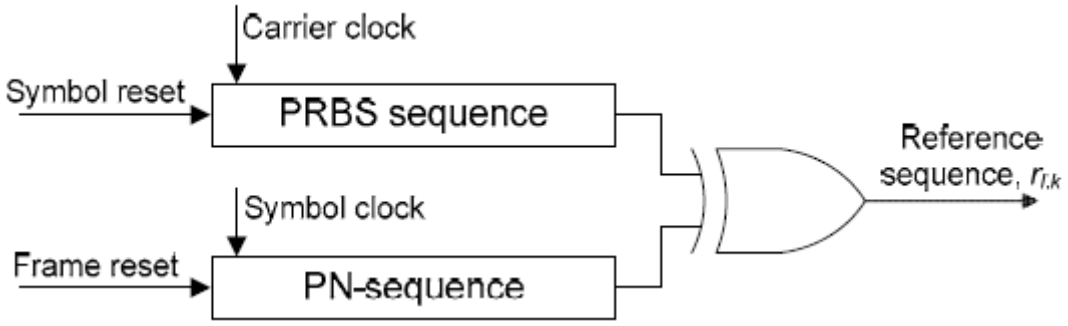

Fig. 2.20 Reference sequence scheme for pilots modulation [32].

$$X^{11} + X^2 + 1 \qquad 2.27$$

Table 2.17 The Max. frame-level PN length

FFT	1K	2K	4K	8K	16K	32K
$\mathbf{N_{pn}}$	2098	1081	540	276	138	68

Each T2-frame symbol carries reference data obtained from the reference sequence in the scattered pilots. Different pilot patterns, numbered PP1 through PP8, are possible to offer efficient solutions for various channel conditions. Positions of the Scattered Pilots (SP)are determined according to Eq. 2.28 and Table 2.18. The selection of suitable scattered pilot patterns is based on FFT modes, guard interval, and transmission mode, as given in Tables 2.19 and 2.20 [16].

$$\mathrm{k} \bmod(\mathrm{D_X D_Y}) = \mathrm{D_X}(\mathrm{l} \bmod \mathrm{D_Y}) \qquad 2.28$$

The parameter k is the carrier of OFDM, and l is the given symbol, D_X is pilot separation of bearing carriers, D_Y Number of symbols forming one scattered pilot sequence.

Table 2.18 Parameters determining SP patterns

Pilot pattern	PP1	PP2	PP3	PP4	PP5	PP6	PP7	PP8
D_X	3	6	6	12	12	24	24	6
D_Y	4	2	4	2	4	2	4	16

Table 2.19 Allowable scattered pilot pattern for SISO mode

FFT	**GI**						
	1/128	1/32	1/16	19/256	1/8	19/128	1/4
32K	PP7	PP4 PP6	PP2 PP8 PP4	PP2 PP8 PP4	PP2 PP8	PP2 PP8	
16K	PP7	PP 7 PP4 PP6	PP2 PP8 PP4 PP5	PP2 PP8 PP4 PP5	PP2 PP3 PP8	PP2 PP3 PP8	PP1 PP8
8K	PP7	PP7 PP4	PP8 PP4 PP5	PP8 PP4 PP5	PP2 PP3 PP8	PP2 PP3 PP8	PP1 PP8
4K, 2K		PP7 PP4	PP4 PP5		PP2 PP3		PP1
1K			PP4 PP5		PP2 PP3		PP1

Table 2.20 Allowable scattered pilot pattern for MISO mode

FFT	**GI**						
	1/128	1/32	1/16	19/256	1/8	19/128	1/4
32K	PP8 PP4 PP6	PP8 PP4	PP2 PP8	PP2 PP8			
16K	PP8 PP4 PP5	PP8 PP4 PP5	PP3 PP8	PP3 PP8	PP3 PP8	PP1 PP8	
8K	PP8 PP4 PP5	PP8 PP4 PP5	PP3 PP8	PP3 PP8	PP3 PP8	PP1 PP8	
4K, 2K		PP4 PP5	PP3				
1K			PP3				

The scattered pilots are modulated using Eq. 2.29. The patterns of scattered pilots and information about the other pilot types are explained in Appendix G [32]. Where A_{sp} is the scattered pilots amplitude according to Table 2.21.

$$Re\{c_{l,k}\} = 2\,A_{SP}(1/2 - r_{l,k}), Im\{c_{l,k}\} = 0 \qquad 2.29$$

Table 2.21 Values of pilots pattern amplitude

Pilot pattern	PP1, PP2	PP3, PP4	PP5, PP6, PP7, PP8
A_{sp}	4/3	7/4	7/3
Boost [dB]	2.5	4.9	7.4

iii. Inverse FFT

This section describes the OFDM transmission scheme. There are six distinct transmission modes in DVB-T2 systems: 1K, 2K, 4K, 8K, 16K, and 32K. Frames are used to structure a T2 broadcasted signal. every frame has a T_F time and is made up of OFDM symbols. A single super frame is formed of N_{T2} frames [35].

Every symbol has a time of T_S and is composed of a group of K_{total} carriers. A carrier is made up of two sections: a useful component with a T_U time and a guard interval with a Δ duration. Table 2.22 lists several significant OFDM parameters [32].

Table 2.22 OFDM parameters for DVB-T2 system

Parameters	**32K**	**16K**	**8K**	**4K**	**2K**	**1K**
K_{total}	27265	13633	6817	3409	1705	853
K_{min}	0	0	0	0	0	0
K_{max}	27264	13632	6816	3408	1704	852
T_U (μs)	3584	1792	896	448	224	112
Carriers Spacing	279 Hz	558 Hz	1116 Hz	2232 Hz	4464 Hz	8929 Hz
Spacing [K_{min} and K_{max}]	7.61MHz	7.61MHz	7.61MHz	7.61MHz	7.61MHz	7.61MHz

In an OFDM frame, the symbols are counted from 0 to L_F–1. Data and reference information are included in every symbol. The OFDM signal consists of many individually modulated carriers; every symbol can be split into cells,

each of which corresponds to the modulation provided on a single carrier during a single symbol duration [16].

The k parameters is used to indicate carriers arrangement, which is part of the K_{min} and K_{max} sets. $1/T_U$ defines the interval among neighboring carriers, while $(K_{total}-1)/T_U$ establishes the interval among K_{min} and K_{max} carriers. When PAPR scheme is not employed, the generated signal contains the addition of guard intervals. The guard intervals are included after PAPR scheme if it is applied [5].

iv. PAPR Reduction

The Peak-to-average power ratio (PAPR) can be reduced by making a pair of changes to the transmitted OFDM signal [54]. It's possible to employ both techniques at the same time. These techniques are Tone Reservation Technique (TR) and Active Constellation Extension Technique (ACE) [55]-[56].

TR technique utilizes some reserved OFDM cells known as dummy tone reservation in its process. IF both techniques are utilized, They're employed on each OFDM symbol's active region. Using rotating constellations or MISO, the ACE approach should not be employed on pilot or reserved tones. When both procedures are employed, the signal should be used the ACE technique first [32], [57].

In TR, the peaks of time domain signal are successively eliminated by employing kernel signal. The kernel's feature is akin to an impulse and defined as in Eq. 2.30. Where n is the sample index between zero and N_{FFT}, K_C is the index of the center carrier as given in Eq. 2.31, S_l is the group of the reserved carriers, and N_{TR} is the number of reserved carriers. To aid in providing a decent kernel, the reserved-carrier indices are chosen from Appendix H for given N_{TR} [5].

$$P_n = \frac{1}{N_{TR}} \sum_{k \in S_l} e^{j\frac{2\pi n(k-K_C)}{N_{FFT}}} \quad 2.30$$

$$K_C = (K_{max} + K_{\min})/2 \quad 2.31$$

v. Guard Interval

To meet the needs of a variety of broadcasters, DVB-T2 provides seven different options of guard intervals. The full guard interval fractions are represented in multiples of the fundamental interval T for each group of FFT size and guard interval fractions in Table 2.23. The elementary period T is selected based on the DVB-T2 bandwidth and is equal to 7/64 μs for 8 MHz [1].

Table 2.23 OFDM Guard interval duration

FFT	**GI Fraction**						
	1/128	1/32	1/16	19/256	1/8	19/128	1/4
32K	256T	1024T	2048T	2432T	4096T	4864T	
16K	128T	512T	1024T	1216T	2048T	2432T	4096T
8K	64T	256T	512T	608T	1024T	1216T	2048T
4K		128T	256T		512T		1024T
2K		64T	128T		256T		512T
1K			64T		128T		256T

vi. Preamble Symbol Insertion

Preamble P1 serves four functions as a preamble sign. It's first employed during the primary signal scan to quickly recognize the T2 signal, for which just recognizing the P1 is sufficient. Even if the receiver is set to the center frequency, each frequency offsets can be discovered immediately due to the symbol's structure. The receiver does not have to examine all of the available offsets individually, which reduces the scanning process [58].

The preamble's second function is to classify it as a T2 preamble. Thus, the P1 symbol has the ability to differentiate itself from others employed in FEF portions that are presented in one super-frame. The third purpose is to send essential TX elements that will be used to decode the remainder of the preamble, which will aid in the startup operation. Finally, the fourth function is to permit detection and adjust the frequency and temporal synchronization [32].

The P1 preamble is an OFDM symbol with 1K FFT mode and divided into two sections. The symbol duration is 224 µs in 8 MHz bandwidth. This duration consists of 112 µs for the useable component A and two adjusted interval parts C and B. These parts have 59 µs and 53 µs, respectively, as shown in Fig. 2.21[59].

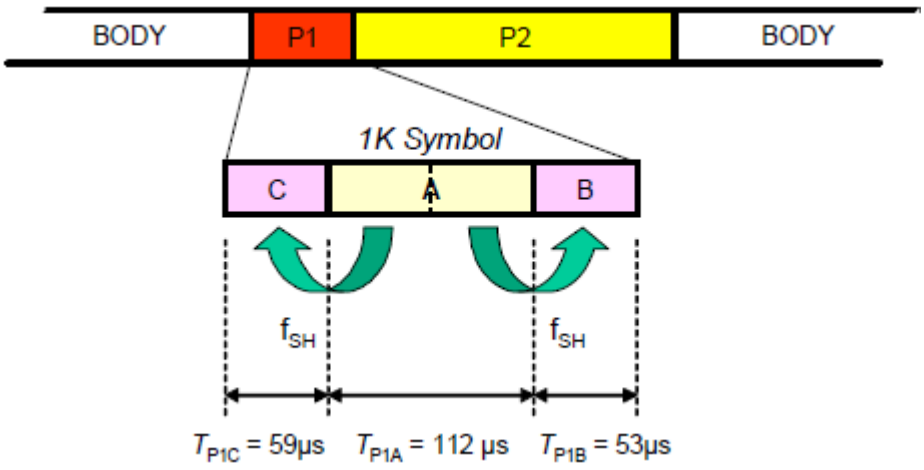

Fig. 2.21 Arrangement of P1 symbol [32].

P1 symbol has 853 available carriers, and just 384 carriers are handled, with the rest established to zero. From the center of the original 7,61 MHz bandwidth, the utilized carriers take around 6,83 MHz. Thus, the number 44 relates to the initial operating carrier, while the number 809 relates to the end, as illustrated in Fig. 2.22 [32], [59].

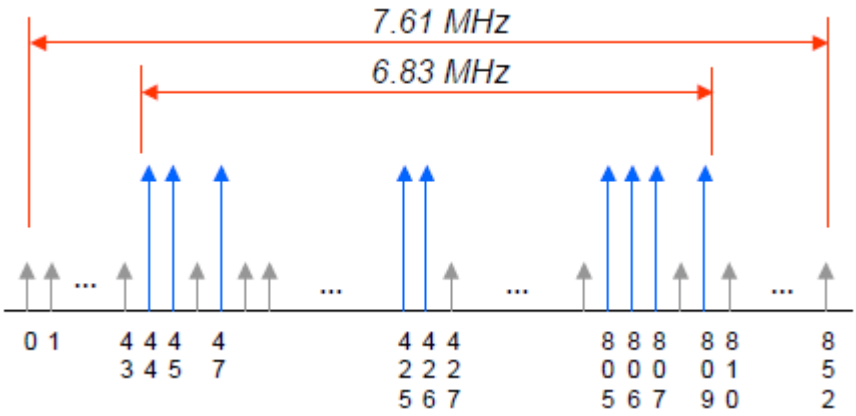

Fig. 2.22 P1 symbol available carriers

2.3 T2-Lite System

T2-Lite is a modern profile introduced in the latest versions of the DVB-T2 standard. The profile is designed for mobile and handheld reception. Therefore, it only includes modes that are possible to work in mobile environments. In addition, the profile was created to simplify the complexity of T2-Lite receivers, lowering the cost and power consumption of mobile services [60].

The cost of mobile services can be reduced by sets of limits in terms of data rate, forward error correction code rates, and TI memory. It further eliminates modes that aren't appropriate for providing portable applications in UHF band from the standard [9].

T2-Lite features a limited amount of new components to maintain greatest compatibility. In addition, the revised profile includes more resilient coding rates to allow receiver operation at low Signal-to-Noise Ratio (SNR) values and greater flexibility for multiplexing several T2 signals in one channel [5].

i. Restrictions of T2-Lite

The time interleaver memory of T2-Lite profiles is lowered from $2^{19} + 2^{15}$ to 2^{18} cells. This reduction has a significant influence on receiver cost due to the components needed. However, the time interleaver memory limitation reduces the highest interleaving period offered for any provided data rate. It is adequate in the application of T2-Lite because portable services are often sent at significantly lower data rates than fixed applications [9].

The maximum data rate of any data PLP in T2-Lite is limited to 4 Mbps. This rate enables a maximum of 10 services at 375 kbps in a single PLP, and it is recommended to use multiple PLPs in T2-Lite for different reasons. One of these reasons is to allow higher energy savings because receivers are only turned on for the time that matches a single service. However, since just the cells from

a single application need to be held in the TI memory, the highest interleaving time is greater [32].

ii. Elements excluded in T2-Lite

T2-Lite system does not use the 32K FFT mode because the obtained separation among subcarriers at ultra-high frequencies is insufficiently resistant versus Inter Carrier Interference (ICI) in portable circumstances. T2-Lite reception is not predicted at L-band or S-band frequencies; hence the 1K FFT mode is not applicable [28].

Three groups of FFT modes, pilot pattern, and GI are deleted from the remainder of the available arrangements to minimize the number of possible variations and make receiver implementation easier [28].

The T2-Lite system excludes PP8 pilot pattern from its mode combinations. The Coded Decision Directed Demodulation (CD3-OFDM) approach, in which the estimates are measured in data subcarriers following forward error correction decode the information, is meant to be utilized with PP8. However, with temporal interleaving or several PLPs, which are likely to play a key part in T2-Lite, this type of channel estimation may perform poorly [61].

The full set of allowable collections of FFT modes, pilot pattern, and GI elements for T2-Lite is displayed in Tables 2.24 and 2.25 [32].

The DVB-T2 system protects the broadcasted signal by using two concatenated forward error correction codes. There are two types of FEC frames regular 64K and short 16K frame lengths. The use of 64K frame length results in a performance improvement with a few decibels at the cost of some increased latency. The regular forward error correction length has been eliminated from the T2-Lite system to provide simple receiver implementation. In this method,

T2-Lite receivers require to execute the less complicated decoding of 16K frame length [28].

Table 2.24 T2-Lite Allowable scattered pilot pattern for SISO mode

FFT	**GI**						
	1/128	1/32	1/16	19/256	1/8	19/128	1/4
16K	PP7	PP7 PP6	PP4 PP5	PP2 PP4 PP5	PP2 PP3	PP2 PP3	PP1
8K	PP7	PP7 PP4	PP4 PP5	PP4 PP5	PP2 PP3	PP2 PP3	PP1
4K, 2K		PP7 PP4	PP4 PP5		PP2 PP3		PP1

Table 2.25 T2-Lite Allowable scattered pilot pattern for MISO mode

FFT	**GI**						
	1/128	1/32	1/16	19/256	1/8	19/128	1/4
16K	PP4 PP5	PP4	PP3	PP3	PP1	PP1	
8K	PP4 PP5	PP4 PP5	PP3	PP3	PP1	PP1	
4K, 2K		PP4 PP5	PP3		PP1		

In T2-Lite profile, the number of coding rates available has also been lowered compared to DVB-T2 base profile. Since higher-order modulation modes and more resilient coding rates are often favored in mobile environments, code rates 4/5 and 5/6 have been eliminated. Moreover, the configuration of

256-QAM constellation and 2/3 and 3/4 code rates doesn't offer reliable reception in handheld devices; it isn't allowable due to robustness deficiency. Table 2.26 lists the short inner codes that should be utilized for T2-Lite [32].

Table 2.26 Coding elements for T2-Lite system

Code Rates	K_{bch} (bits)	$N_{bch} = K_{ldpc}$ (bits)	BCH-t
1/3	5232	5400	12
2/5	6312	6480	12
4/9	7032	7200	12
3/5	9552	9720	12
2/3	10632	10800	12
11/15	11712	11880	12

The use of rotated constellations in conjunction with the 256-QAM constellation is also not involved since the outcome of the rotation scheme cant recompense for the additional complexity necessary for de-mapping in this scenario. By utilizing signal space diversity, rotated constellations increase system robustness in fading environments. As a condition for the agreement, the implementation in the receiver required a more complicated process than familiar constellations, particularly for 256-QAM constellations [9].

iii. Elements added in T2-Lite

The forward error correction code and the structure of future extension frame sections are among the new parameters attached for T2-Lite. Two code rates, 1/3 and 2/5, are appended to the concatenation forward error correction code along with their corresponding bit to cell de-multiplexer, as given in Appendix I [32].

The developed code rates were derived from digital video broadcasting satellite second-generation system to allow reception at weak signal-to-noise ratio thresholds. It is likely to increase the coverage of the T2-Lite system while sacrificing capacity in this case [25].

T2-Lite supports the parity interleaver introduced in the second-generation base profile for all high constellation types and extra code rates, as well as QPSK constellation. The parity interleaver is intended to develop inner decoding achievement in fading scenarios by guaranteeing that bits related to the one check node are sent in separate cells. All of the possible bit interleaver configurations for T2-Lite is shown in Table 2.27 [9].

The duration of the future extension frame for DVB-T2 is limited to 250 ms while extended to 1s for the T2-Lite signal. This increment provides extra freedom when multiplexing both signals in single frequency channels because the DVB-T2 signal is assumed to fill the main section of the transmission duration [5].

Table 2.27 T2-Lite bit interleaver usage

Code Rates	**Modulation**	
	QPSK	16, 64, 256-QAM
1/3	Parity	Parity & column twist
2/5	Parity	Parity & column twist
4/9	None	Parity & column twist
3/5	None	Parity & column twist
2/3	None	Parity & column twist
11/15	None	Parity & column twist

2.4 Digital Video Broadcasting Next-Generation Handheld

With the development of smartphones and tablets, interest in mobile multimedia broadcasting has resurfaced. Several mobile broadcast technologies, including Digital Video Broadcasting–Handheld (DVB-H) and Satellite to Handheld (DVB-SH), were created over the last decades to the widespread consumption of multimedia services like portable television [26].

Due to the absence of a viable business strategy and the related substantial costs with the introduction of modern mobile television networks, the penetration of mobile TV services has fallen short of expectations. Due to both consumers' and operators' ever-increasing demands and desires, the development of a new mobile generation broadcasting technology became necessary [12].

This generation should employ the most recent advancements in wireless communications to offer substantial capacity and coverage efficiency enhancements over first-generation portable broadcasting standards [9].

DVB-NGH was proposed to be the reference industry standard for mobile multimedia broadcasting. It significantly outperforms the current mobile broadcasting standards from where coverage, capacity, and more spectrum efficiency. Also, DVB-NGH is optimizing the DVB-T2 system in several features [12].

DVB-NGH is considered the first broadcasting scheme that utilizes the full benefits of a Multiple-Input Multiple-Output (MIMO) system, in terms of performance [62]-[64]. MIMO is the key technology to get through the Shannon limit of SISO wireless systems by employing spatial multiplexing without any further transmit power or bandwidth, this provides DVB-NGH be the future of the third-generation broadcasting system [65].

There are four broadcasting profiles defined by DVB-NGH specification known as the sheer-terrestrial, MIMO-terrestrial, hybrid terrestrial–satellite, and

hybrid-MIMO profiles [66]. DVB-NGH specification state that the sheer-terrestrial profile is compulsory, while the others are optional. The sheer-terrestrial profile, which is also called base profile, depended on the features of DVB-T2 and DVBT2-lite standards [13].

DVB-NGH system employs several developed physical-layer techniques to enhance robustness and reliability over different fading conditions. These techniques are BICM, complete provision of an Internet Protocol (IP) transport, new LDPC codes rate, time-frequency slicing (TFS), signal space diversity (SSD), scalable video coding (SVC), and enhanced spatial multiplexing multiple-input multiple-output (ESM-MIMO) [13], [67].

a. BICM Module for DVB-NGH

The BICM module of DVB-NGH depends on the DVB-T2 standard with specific improvements to minimize the receiver decoding complexity, extend the coverage area, and optimize spectral efficiency. This BICM module is considered the most advanced in coding modulation technology. The DVB-NGH combines the most efficient BICM module with OFDM that evaluated the favored choice of mobile broadcasting systems [12], [68].

The BICM can separate the continuous bits error caused by symbol burst errors to boost system diversity in a fading environment. BICM supports DVB-NGH with diversity gains in frequency and time by efficiently combining FEC codes and various interleaving schemes. DVB-NGH BICM module consists of several functional sub-block, as given in the block diagram of Fig. 2.23 [13].

i. FEC Encoding

To limit receiver complication, just the short frame length coding lengths are employed with similar encoding process, like in the T2-Lite profile. The values of coding rate are determined to consistently include the field from 5/15

to 11/15. Table 2.28 compiles the various coding rates and block sizes for DVB-NGH [9].

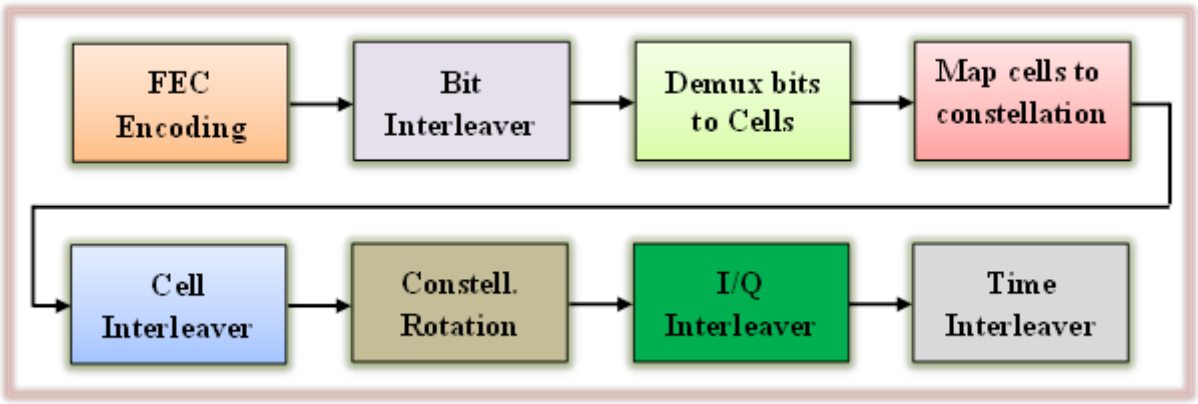

Fig. 2.23 DVB-NGH BICM module structure [9].

Table 2.28 FEC parameters of DVB-NGH

Code Rates	K_{bch} (bits)	$N_{bch} = K_{ldpc}$ (bits)	BCH-t
3/15	3072	3240	12
4/15	4152	4320	12
5/15	5232	5400	12
6/15	6312	6480	12
7/15	7392	7560	12
8/15	8472	8640	12
9/15	9552	9720	12
10/15	10632	10800	12
11/15	11712	11880	12

DVB-NGH extract several codes rate from the second generation T2 and T2-Lite configuration like 5/15, 6/15, 9/15, and 11/15. Code rates 4/15, 7/15, and 8/15, on the other hand, necessitate the creation of new DVB-NGH-certain codes. For the short frame block size, the outer BCH scheme is replica to the

one utilized in the terrestrial second generation and using an identical error-correcting generator polynomial (t) [13].

Several improvements were developed in this BICM to achieve transmission robustness, such as introducing a more powerful 3/15 inner LDPC coding rate, while the most robust coding rate in DVB-T2 and T2-Lite are 1/2 and 1/3, respectively. As in the hybrid scenarios, the employment of 3/15 and 4/15 coding rates is limited to QPSK and 16-QAM constellations size. They're designed to allow a hybrid single-frequency network to link terrestrial and satellite signals [25].

ii. Bit Interleaver

The bit interleaver construction of DVB-NGH was obtained from second-generation terrestrial T2, which is performed by parity interleaver succeeded by column-twist interleaver. It has been demonstrated that parity interleaving increases performance in fading conditions. It is implemented to every modulation size, including QPSK modulation and all coding rates, regardless of the coding rate [20].

All modulation types, except for QPSK modulation, apply column-twist interleaving. In every separate column, the initial write location is twisted by the constant t_c parameter, whose value varies based on the column sequence. For each constellation size, the bit interleaver and column-twist parameters arrangement is provided in Table 2.29 [13].

iii. Bit-to-Cell De-multiplexer

Like in second-generation terrestrial T2, a supplementary bit-to-cell de-multiplexer is included in the middle sequence of the bit interleaver and the constellation mapper. The purpose of a bit-to-cell de-multiplexer is to separate the bit interleaver output stream into several sub-streams. These sub-streams must be multiple of the bits number per modulated cell. Appendix J contains

more information on de-mux bits to sub-streams for the new coding rates [13], [20].

Table 2.29 DVB-NGH Bit interleaver and column-twist parameters

Modulation	**N_r**	**N_c**	**t_c**											
			0	1	2	3	4	5	6	7	8	9	10	11
16-QAM	2025	8	0	1	0	8	2	0	1	5				
64-QAM	1350	12	0	12	7	1	3	1	8	7	1	0	3	9
256-QAM	2025	8	0	1	0	8	2	0	1	5				

iv. Map Cells to Constellations

The cell's word obtained from bit-to-cell de-multiplexer is modulated to the appropriate constellation type for giving a constellation point. The same four constellation types used in second-generation terrestrial T2 are used in next-generation handheld: QPSK, 16-QAM, 64-QAM, and 256-QAM [9].

New non-uniform modulations have been added to the conventional 64-QAM and 256-QAM modulations. Furthermore, regular and non-uniform modulations may be done using rotated or non-rotated methods. As in T2-Lite, the 256-QAM modulation can't use the rotated constellation scheme to minimize the receiver de-mapping complexity [13].

v. Cell interleaver

The cell interleaver of next-generation has the same structures as in DVB-T2 standard. It evenly distributes the cells belong forward error correction codes to guarantee an uncorrelated allocation of channel effects and interference in the receiving device. The CI's maximum length permutation function changes between any two contiguous forward error correction blocks [32].

In contrast to DVB-T2, this unit is positioned before the constellation rotation sub-block in to prevent interference with the I/Q interleaver stage. Finally, it should be stated that when four dimension rotated constellations are employed, the cell interleaver is pair-wise implemented. In this case, the length of permutation function is $N_{cells}/2$, and the output cell interleaver is given in Eq. 2.32 with q=0,1, 2, ..., ($N_{cells}/2$-1) [26].

$$d_{r,2L_r(q)} = g_{r,2q} d_{r,2L_r(q)+1} = g_{r,2q+1} \qquad 2.32$$

vi. Rotated Constellations

Rotated constellation technique is provided to improve reception resilience over severe fading circumstances. DVB-NGH supports two dimensions (2D) rotation for all modulation types except 256-QAM constellation, as it does in the T2-Lite scenarios, to keep the de-mapper complexity low [12].

The idea of rotated constellations is further developed to a greater diversity scheme, known as four dimensions (4D) rotated constellations, for QPSK modulation and high coding rates. The number of rotation dimensions available for every constellation and coding rate is abstracted in Table 2.30 [23].

Table 2.30 Numbers of dimensional rotation for DVB-NGH

Modulation	**Code Rate**						
	5/15	6/15	7/15	8/15	9/15	10/15	11/15
QPSK	2D			4D			
16-QAM	2D						
64-QAM	2D						
256-QAM	No						

In contrast to the DVB-T2 or T2-Lite systems, next-generation handheld implements rotated constellation to the complex cells presented at the output of the cell interleaver. According to the number of rotation dimensions expressed by N_D, the rotation is accomplished by multiplying two or four real-component of CI output by a perpendicular matrix. The rotation matrix has a size of 2x2 and 4x4 for 2D and 4D rotations, respectively, as provided in Eq. 2.33 and Eq. 2.34 [13].

$$\begin{bmatrix} y_0 \\ y_1 \end{bmatrix} = \begin{bmatrix} +a & -b \\ +b & +a \end{bmatrix} \begin{bmatrix} x_0 \\ x_1 \end{bmatrix} \quad 2.33$$

$$\begin{bmatrix} y_0 \\ y_1 \\ y_2 \\ y_3 \end{bmatrix} = \begin{bmatrix} +a & -b & -b & -b \\ +b & +a & -b & +a \\ +b & +b & +a & -b \\ +b & -b & +b & +a \end{bmatrix} \begin{bmatrix} x_0 \\ x_1 \\ x_2 \\ x_3 \end{bmatrix} \quad 2.34$$

Vector x consist the number of rotation dimensions components of $N_D/2$ adjacent cells, as given in Eq. 2.35 and Eq. 2.36 for 2D and 4D rotation, respectively. The value of parameter b according to each constellation sizes and code rates is proposed in Table 2.31. While, parameter a is derived from N_D components and parameter b as given in Eq. 2.37 [13].

$$[x_0, x_1] = [Re(d_i), Im(d_i)] \quad 2.35$$

$$[x_0, x_1, x_2, x_3] = [Re(d_{2i+0}), Im(d_{2i+0}), Re(d_{2i+1}), Im(d_{2i+1})] \quad 2.36$$

$$a = \sqrt{1 - (N_D - 1)b^2} \quad 2.37$$

vii. I/Q Component Interleaver

Inside the forward error correction block of second-generation terrestrial T2, every rotating constellation quadrature's part is single-cell delayed cyclically. In next-generation handheld broadcasting, the cyclic Q delay scheme is changed by a more advanced In-phase-Quadrature component interleaver,

enabling improved temporal disconnection and channel diversity for both 2D and 4D rotations methods [12].

Table 2.31 Value of b parameters of DVB-NGH

Modulation	Code Rate	Rotation	b
QPSK	3/15 to 7/15	2D	0.4848
	8/15 to 11/15	4D	0.3162
16-QAM	All	2D	0.2890
64-QAM	All	2D	0.1495

Following the rotation scheme, I/Q component interleaving is implemented in three stages over every forward error correction block individually. In the first stage, the In-phase and Quadrature parts of cells in a forward error correction block are individually addressed column-wise into pairs of matrices with N_R rows equal to N_D. The couples of matrices have column numbers N_C as provided in Eq. 2.38 [13].

$$N_C = \lceil N_{cells}/N_R \rceil \qquad 2.38$$

An N_D /2 cyclic shift is performed for the Quadrature parts to every column of the matrix in a second stage. In the final stage, synchronously reading a couple of matrices in the row-wise method, output cells are produced by coupling every In-phase and quadrature components together. Fig. 2.24 depicts the three stages and the equivalent forward error correction blocks before and after applying the I/Q component interleaving stages [13].

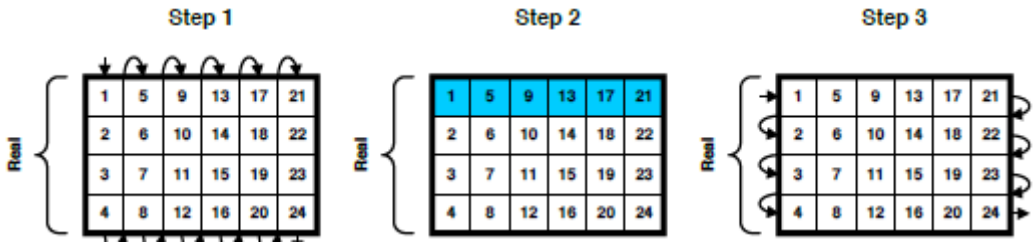

(a)

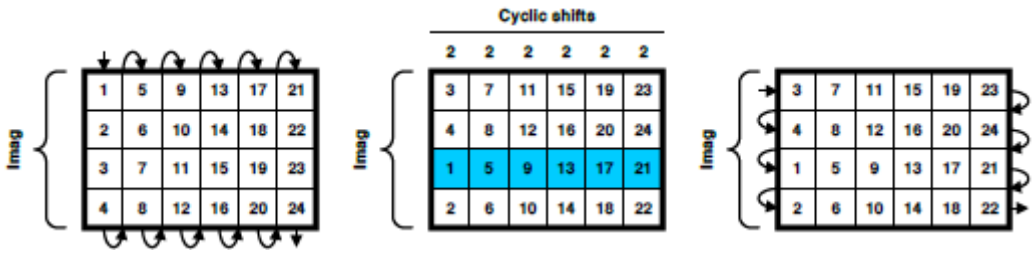

(b)

Fig. 2.24 I/Q component interleaver steps (a) Real, (b) Imaginary

viii. Time Interleaver

According to the utilization of the rotated constellations technique, the time interlever sub-block is connected to the I/Q component interleaver output or the CI output. It has a construction based on second-generation terrestrial T2; however, it also has the option of connecting a convolutional interleaver on top of the regular block interleaver. It works at the physical layers pipe fields, with different time interleaver settings from one physical layers pipe to the next [26].

Each physical layers pipes has two possibilities for time interleaving. Each interleaving frame comprises a single time interleaver block and is assigned to single or multiple frames this called Type one. The number of time interleaver blocks in interleaving frame N_{TI} is valued to one, so a convolutional interleaver and a block interleaver are used to create the overall time interleaver for this type [12].

In Type zero, Every IF is directly assigned to a single logical frame, and the IF is split into single or multiple time interleaver blocks. Fig. 2.25 shows the time interleaver structure of DVB-NGH [9].

For Type one time interleaver, the interleaved cells are addressed row by row into the time interleaver memory, and the addressing sequence is FEC block after FEC block. The interleaving frame is divided into N_{IU} interleaver units of roughly similar size, with N_{IU} equaling the value of logical frames addressed by every time interleaver block [9].

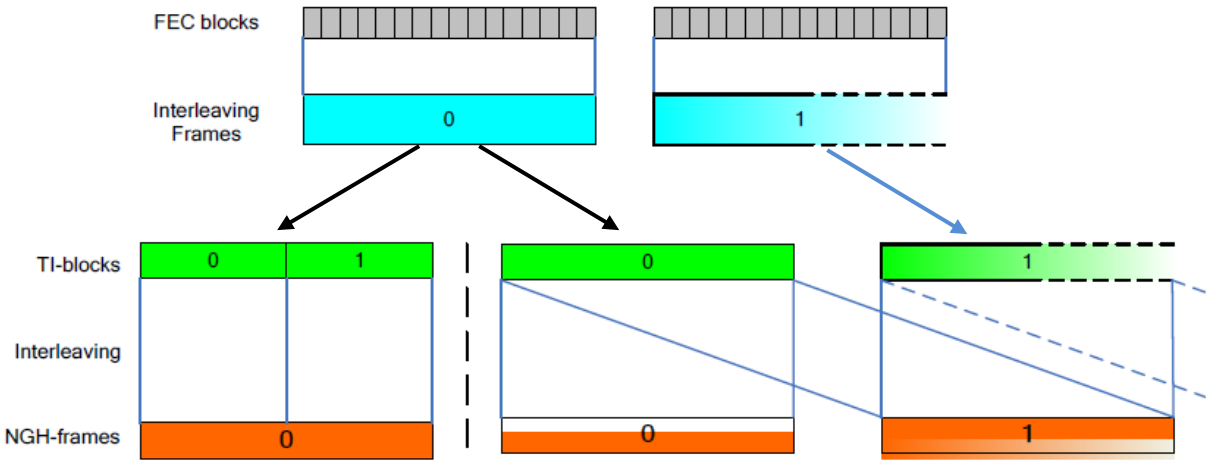

Fig. 2.25 DVB-NGH time interleaver types [13].

Every interleaver unit is sent via one of the convolutional interleaver's delay lines, and the cells are then read column by column. As a result, every input interleaving frame is split across N_{IU} logical frames [13].

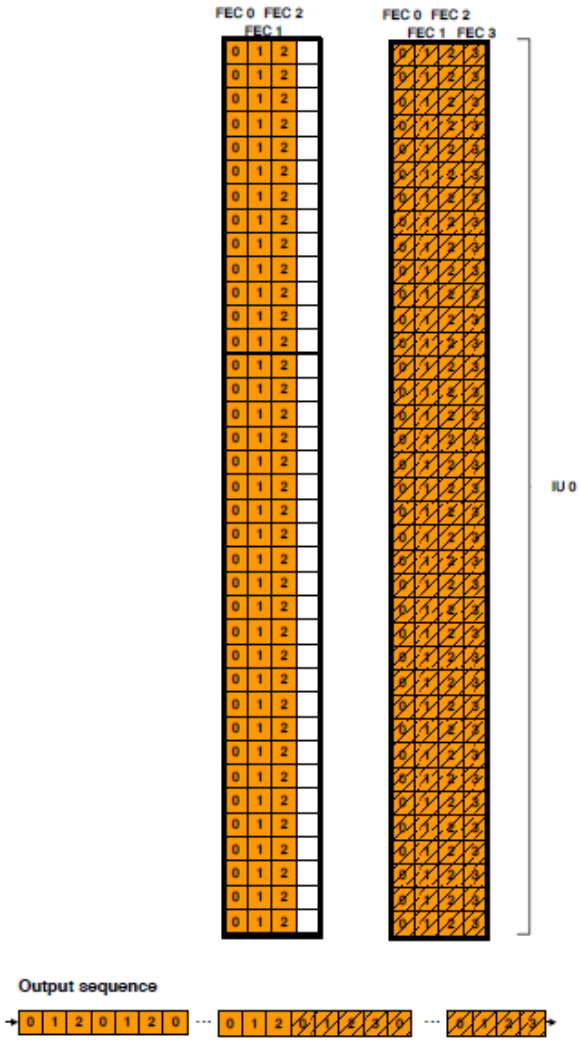

Fig. 2.26 Example of Type zero time interleaver process [13]

For Type zero, just a single N_{IU} of block interleaver for time interleaver block per IF is addressed column by column. This block interleaver is done row by row to create the output for the immediate time interleaver block. Following the same process, this subsequent TI-output block is added to the preceding TI-output; an example of this can be seen in Fig. 2.26 above. It's worth noting that the value of utilized columns varies amongst block interleavers due to the interleaving frame's dynamic element PLP block number [13].

2.5 Multipath Fading Channels

The channel constitutes a physical medium between the transmitter and the receiver sides of a communication system. The channel model shows the link between input and output mathematically or computationally. Wireless channels are not expected; contrast wired channels, which have fixed and expected properties. Notable amounts of interference, distortion, and noise are presented by these channels. One of the common complex aspects of wireless system design has been modeling wireless channels [38].

Several channel profiles have been established by the digital video broadcasting organization to get satisfactory results in software and real system simulations. Different digital video broadcasting systems, like DVB-T, DVB-T2, DVB-H, and others, provide information about these models [22].

i. DVB-T2 Channel models

The first-generation terrestrial system predicts three distinct situations for DVB-T signal reception: Additive Gaussian, Ricean, and Rayleigh receptions. In supplement to the first-generation terrestrial models, specific new channels have been introduced, some of which are unique to the second-generation terrestrial system [69].

These channels were adopted to test performance in a variety of reception environments, such as fixed, portable, mobile, as well as signal frequency networks, and a multi-input single output transmission mode [32].

a. AWGN Channel

Only Gaussian noise is introduced to the transmitted signal in this sort of channel model. It is expected that there would be simply one path without delay and phase shift. The best signal quality can be received with this model, but the terrestrial system is not only affected by this model [22].

b. Ricean Channel

This channel, also known as the F1 channel described in the first generation terrestrial specification, represents a fixed outdoor model's receiving conditions. This model does not contain Doppler frequency impact. The model has one component in the direct path, and 20 other paths have a different delay, attenuation, and phase shift, meaning that the total taps are 21 for this model. The F1 model is represented by Eq. 2.39 [36].

$$y(t) = \frac{\rho_0 x(t) + \sum_{i=1}^{N} \rho_i \, e^{-j\theta_i} \, x(t-\tau_i)}{\sqrt{\sum_{i=0}^{N} \rho_i{}^2}} \qquad 2.39$$

The signal x(t) represent the input term, and y(t) defines output signals of the channel. While τ is the path delay, ρ is the attenuation and θ is a phase shift, as given in Table 2.32. The value of ρ_0 is directly related to the Ricean factor K. This factor specifies the strength ratio of the LOS beam to the reflecting paths. In the DVB-T2 specifications, it is recommended to use a Ricean factor of K = 10 dB for the simulation cases. Accordingly, the value of ρ will be as provided in Eq. 2.40 [5].

$$\rho_0 = \sqrt{10 \, \sum_{i=1}^{N} \rho_i{}^2} \qquad 2.40$$

c. Rayleigh Channel

The Rayleigh channel is characterized by no direct path of the transmitted signal and heavy multipath. This model presents the portable outdoor or indoor channel conditions known as the P1 fading channel model. P1 channel was also established in first-generation terrestrial broadcasting and does not carry Doppler frequency impact. It has 20 taps of multipath components, and each scattered path comes with distinct time-delay and phase-shift. Eq. 2.41 expresses mathematical model of the Rayleigh channel [2], [5].

Table. 2.32 Ricean and Rayleigh channels parameters

Path Number	ρ	τ (μs)	θ degree
1	0.057 662	1.003019	4.855121
2	0.176 809	5.422091	3.419109
3	0.407 163	0.518650	5.864470
4	0.303 585	2.751772	2.215894
5	0.258 782	0.602895	3.758058
6	0.061 831	1.016585	5.430202
7	0.150 340	0.143556	3.952093
8	0.051 534	0.153832	1.093586
9	0.185 074	3.324866	5.775198
10	0.400 967	1.935570	0.154459
11	0.295 723	0.429948	5.928383
12	0.350 825	3.228872	3.053023
13	0.262 909	0.848831	0.628578
14	0.225 894	0.073883	2.128544
15	0.170 996	0.203952	1.099463
16	0.149 723	0.194207	3.462951
17	0.240 140	0.924450	3.664773
18	0.116 587	1.381320	2.833799
19	0.221 155	0.640512	3.334290
20	0.259 730	1.368671	0.393889

$$y(t) = k \sum_{i=1}^{N} \rho_i \, e^{-j\theta_i} \, x(t - \tau_i) \qquad 2.41$$

Where x(t), y(t), τ, ρ, and θ have the definition of the same parameters from previous equation, whereas the factor k value is given in Eq. 2.42.

$$k = \frac{1}{\sqrt{\sum_{i=1}^{N} \rho_i{}^2}} \qquad 2.42$$

d. 0 dB Echo Channel

The 0 dB echo channel model composes of two paths with identical amplitude. The directions are separated by a time equal to 0.9 from Guard Interval (GI), i.e., 90% GI. The second path comes with a 1 Hz frequency shift. The parameters for this model are displayed in Table 2.33, where Δ, and Δf are GI, and frequency shifting of the individual path, sequentially [70].

Table. 2.33 0 dB echo channel parameters

Path Number	Power [dB]	Delay [μs]	Δf [Hz]
1	0	0	0
2	0	0.9Δ	1

e. DTG Channels

The Digital Television Group (DTG) defined three type of channels, DTGlong, DTGmedium and DTGshort. The First two have Ricean, and the last one Rayleigh distribution. Each of them consists of 6 signal paths. Table 2.34 shows signal attenuation and Table 2.35 shows signal delay for these channels [22].

Table. 2.34 Attenuation values for DTG channels

Path Number	DTGlong [dB]	DTGmedium [dB]	DTGshort [dB]
1	0	0	-2.8
2	-9	-8.6	0
3	-22	-12.6	-3.8
4	-25	-18	-0.1
5	-27	-20.7	-2.6
6	-28	-22.2	-1.3

DTGlong represents conditions where one signal path is a direct one and others are highly attenuated, with delay reaching 75 μs. Frequency response

varies often from minimum to maximum, but the lowest value is not lower than -8 dB. DTGmedium channel is similar to DTGlong, with signal delay up to 21 μs. DTGshort channel has much lower path delays, reaching only 2.8 μs, but components signals are attenuated, which complicates reception [22].

Table. 2.35 Delay values for DTG channels

Path Number	DTGlong [μs]	DTGmedium [μs]	DTGshort [μs]
1	0	0	0
2	5	1	0.05
3	14	5	0.4
4	35	8	1.45
5	54	12	2.3
6	75	21	2.8

f. Typical Urban Channel

This profile reproduces the terrestrial propagation in an urban area. This channels was originally defined by European Cooperation in the fields of Scientific and Technical research (COST207) as a Typical Urban (TU6) profile. It is made of 6 paths having wide dispersion in delay and relatively strong power as shown in Table 2.36. It reproduces the terrestrial propagation in an urban area. This channel profile has also been used for Global System for Mobile Communications (GSM) and Digital Audio Broadcasting (DAB) tests [71].

Table. 2.36 Attenuation and Delay values for TU06 channel

Path Number	Power [dB]	Delay [μs]
1	-3	0
2	0	0.2
3	-2	0.5
4	-6	1.6
5	-8	2.3
6	-10	5

g. MISO Channels

The MISO mode employs two transmitting antennas, each one for a particular transmitter. Therefore, the MISO channel models require two separate fading paths. The First transmitter utilizes the characteristics of the same paths given in Table 2.32, while the parameters specified in Table 2.37 are adopted for the second transmitter. DVB-T2 specifications define two types of MISO channels, Ricean and Rayleigh MISO profiles [5].

i. Ricean MISO Model

The first path of Ricean MISO channel model is similar to the F1 profile with the exception of the second path insertion. For the second path, the Ricean F2 channel applies according to Table 2.37 with 21-taps for each path [5].

ii. Rayleigh MISO Model

The Rayleigh MISO profile, like the Ricean channel, is made up of two independent routes, one for transmitter group 1 and the other for transmitter group 2, which is identical to the P1 Rayleigh profile. The P2 is defined by the parameters listed in Table 2.37. The P2 path is made up of 20 scattered, time-delayed, and phase-shifted components [5].

Table. 2.37 Ricean and Rayleigh MISO channels parameters

Path Number	ρ	τ (μs)	θ (degree)
1	0.057 662	2.003 019	1.855 121
2	0.176 809	2.422 091	2.419 109
3	0.407 163	1.518 650	3.864 470
4	0.303 585	0.751 772	1.215 894
5	0.258 782	3.602 895	0.758 058
6	0.061 831	0.016 585	2.430 202
7	0.150 340	5.143 556	4.952 093
8	0.051 534	1.153 832	0.093 586

9	0.185 074	2.324 866	4.775 198
10	0.400 967	4.935 570	6.154 459
11	0.295 723	3.429 948	1.928 383
12	0.350 825	1.228 872	2.053 023
13	0.262 909	1.848 831	1.628 578
14	0.225 894	3.073 883	2.128 544
15	0.170 996	1.203 952	4.099 463
16	0.149 723	4.194 207	3.462 951
17	0.240 140	1.924 450	3.664 773
18	0.116 587	2.381 320	3.833 799
19	0.221 155	0.640 512	3.334 290
20	0.259 730	3.368 671	0.393 889

Chapter Three

Proposed Systems Structures

3.1 Introduction

The second-generation terrestrial system has particular transmitter implementations based on its published standard. The main functional blocks of the DVB-T2 transmitter have been discussed in detail in the previous chapter. The primary issue with this standard emerges when attempting to implement a receiver side since there is no special arrangement for the receiver implementation.

To this end, the DVB project produced a document titled “Implementation Guideline for DVB-T2 systems” in order to demonstrate the way to DVB-T2 system designers. There is no specified receiver configuration in this document; instead, there are concepts and some alternative system architectures. In this thesis, the overall DVB-T2 system chain is simulated according to the standard and implementation guideline principles. The DVB-T2 system is simulated using Script M-file of the computational program MATLAB version R2020b.

As a result, the works presented in this thesis are divided into four primary parts, the first two of which simulate the constellation rotation and MISO techniques to demonstrate their performance with the DVB-T2 standard. The third part simulates the T2-Lite system profile with and without using constellation rotation technique.

Finally, the fourth part proposes insertion of BICM module from the futuristic DVB-NGH with the T2-Lite system profile rather than its usual one to gain the additional benefits implemented with this module. In the sections that follow, the aforementioned parts will be explored in greater depth.

3.2 DVB-T2 System

This part is significant because it represents the overall DVB-T2 system chain that will be the base system for all following parts. DVB-T2 transmitter chain divides into several signal processing sub-blocks, and every sub-block has its own function. The high-level of the simulated DVB-T2 transmitter structure is displayed in Fig. 3.1.

i. Technical Description

The structure of the DVB-T2 transmitter side is made up of several sub-blocks that will be discussed in the following sections. Each sub-block performs a certain operation from the transmitter's central function. Simulation was done using publicly available DVB-T2 Common Simulation Platform (CSP) simulator, implemented in MATLAB. The main configuration parameters employed in this simulation for the first two parts are presented in Table 3.1, while for the last two parts some of these parameters are modified. Furthermore, The technical description for each sub-block is given in the following sections.

Table 3.1 DVB-T2 System parameters configuration

Parameters	Configuration
OFDM FFT Mode	8K
Guard Interval	1/8
Constellation Type	QPSK, 16-QAM, 64-QAM
Scattered Pattern	PP8
PLP Numbers	one
Coding Rate	1/2, 3/5, 2/3, 3/4, 4/5, 5/6
FEC Length	64800 Bits
FEC Blocks	48 Block
Data Symbols	83 Symbol
Max. LDPC decoding Iterations	50 Iteration
Bandwidth	8 MHz

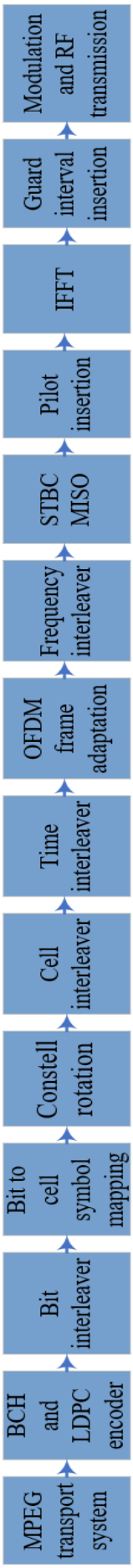

Fig. 3.1Transmitter structure of simulated DVB-T2 system

a. MPEG Transport System

The MPEG sub-block performs the generation of MPEG transport stream data for the DVB-T2 chain. The data generator produces a random data sequence based on the built-in random number generator in MATLAB. This sub-block determines the data field length and generates a random transport stream with a fixed user packet length of 188*8 bits corresponding one MPEG Packet. The number of MPEG Packets generated is based on the selected parameters configuration.

b. BCH and LDPC Encoding

The assigning and scheduling operation is one of the elements of the DVB-T2 standard, and it may be accomplished in any form as long as the signaling inside the BBFrames properly explain it. During the allocation procedure, every physical layer pipe in every Interleaving Frame is assigned a certain number of BBFrames, leading to a specific number of forward error correction blocks for every physical layer pipe in every Interleaving Frame.

The bits assigning in BBFrames and scheduling data over the chain structure should be performed before the encoding stage. The element N_{BLOCKS} specifies the number of BBFRAMES per IF and input bits are assigned in such a way that the available capacity is entirely filled. This enables the N_{BLOCKS} to be a vector with each member representing the number of BBFRAMES in a certain IF. The BB Scrambling applies the scrambling sequence on the pre-prepared BBframes. It generates the pseudo-random binary sequence used to scramble the BB Frame within the stream adaption module, according to PRBS polynomial given in Eq. 2.3.

The Bit-interleaved coding and modulation module consists of several functional sub-blocks. Each sub-block executes a specific process of the main BICM chain. BCH encoding provides outer encoding function for DVB-T2

chain. The outer encoding process follows the specified parameters configuration of the DVBT2 structure. The parity bits are computed employing input data and the generator polynomial of BCH code. They are attached following the data to form a complete BCH encoder. The parameters and generator polynomial of BCH code given in Table 2.1.

The inner encoding function for the simulated DVB-T2 is handled by the LDPC encoding. As in the case of outer coding, The DVB-T2 structure's settings are utilized for the inner encoding procedure. This encoder uses a built-in function called dvbs2ldpc from digital video broadcasting satellite second-generation to offers the parity matrix for LDPC process. The parity check matrix is obtained from the considered function based on the required coding rate and normal or short FECFRAME as explained in Table 2.1.

c. Bit Interleaver

The Bit Interleaver sub-block provides bit interleaving in which the parity and column twist interleaving are carried out in sequence. This process is only used for 16-QAM, 64-QAM, and 256-QAM constellations, and it is skipped in the case of the QPSK constellation.

The parity section is located and interleaved using Eq. 2.4 where dependent constant of inner coding rate is presented in Table 2.3. The numbers of row and column for the twist column interleaver is taken according to the parameters configuration while t_c twists the write start location of each column as already defined in Table 2.4.

d. Bit to Cell Symbol Mapping

The Bit to Cell mapping sub-block performs certain of processing steps. The first process is carried out by splitting the input into several sub-streams according to modulation mode and regular or short FECFRAME. All needed parameters values of this step are defined in Tables 2.5 and 2.6. The second step

is to map the bits of each sub-stream into new bits arrangements to agree with the DVB-T2 specification, as given in Appendix C. The new bits structures are limited by coding rate, modulation format, and type of frame length.

Cell word mapping into I/Q constellations is made by cell mapper step. It maps every cell word into QPSK, 16-QAM, and 64-QAM modulation producing constellation points. According to their modulation mode, every value of imaginary and real parts is mapped into their corresponding constellation symbol as specified in the DVB-T2 standard and illustrated with detail in Appendix D. Finally, the normalizing factor of Table 2.7 is practiced to the resultant constellation points to get the right complex cell value to utilize.

e. Constellation Rotation

The central function of constellation Rotation sub-block is to increase the diversity order of the BICM module giving an overall performance-boosting for the DVB-T2 system. The output of Cell Mapper is applied to this sub-block when the constellation rotation technique is used and is skipped if this technique is not used. The process in this part is admitted one of the main important optional DVB-T2 features simulated in the thesis.

The selection of rotation angle relies on the modulation mode given by the DVB-T2 chain parameter configurations as defined in Table 2.8. There are two basic steps to fulfill the constellation rotation function. The first one is by applying the rotation phasor given in Eq. 2.8 for both in-phase and quadrature components that belong to the normalized cell values for every FEC block. The second step delays the quadrature component by a single cell inside the current FEC block in a cyclic manner, as defined in Eq. 2.10.

The constellation rotation allows each symbol to be transmitted across the in-phase and quadrature components separately, so each component has its individual right information to estimate the transmitted symbol. The cyclic delay

causes the transmitted components to be fading separately. Fig. 3.2 illustrates this important technique more precisely.

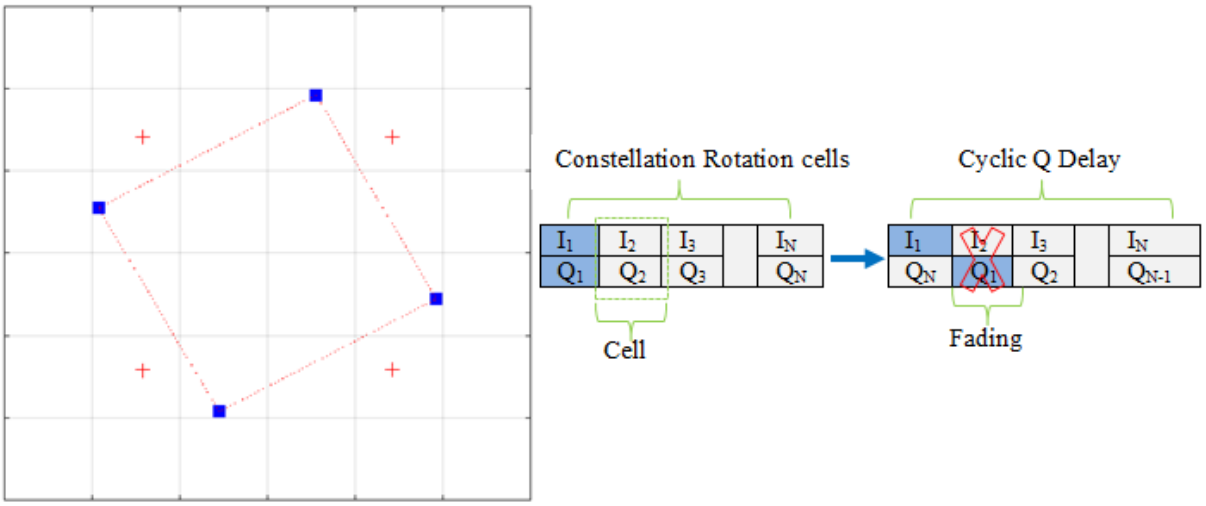

(a) (b) (c)

Fig. 3.2 Process of constellation rotation (a) Constellation points (b) Rotated cells (c) Cyclic Q delay cells

f. Cell Interleaver

The essential function of the Cell Interleaver sub-block is to interleave the cells defined as the data input following the parameters configuration of DVB-T2 structure. To evenly distribute the cells in the forward error correction block, the current interleaver uses a pseudo-random permutation given in Eq. 2.13.

To guarantee an uncorrelated distribution of channel distortions and interference during the reception, the input cells mapped to a second position created by the pseudo-random means. The sub-block generates the basic permutation function and the shift value addressed in Appendix E and needed to build the final permutation function.

g. Time Interleaver

After the first interleaving process, the cells are then delivered to a second interleaving step, which is the time interleaving sub-block. The operation of this

sub-block is carried at the physical layer pipe field to improve the system's resistance for burst errors.

The simulated system deals with the third time interleaver option where each IF is divided into many TI-blocks (N_{TI}>1) and allocated to a single T2-frame right away. The input to the time interleaver is loaded column by column where the number of columns is equal to five times FEC Blocks Per one TI block of the Interleaving Frame. The output to the time interleaver is read row by row, where the row numbers are specified for each modulation mode and FECFRAME type as provided in Table 2.9.

By determining the value of TI Block, number of rows, and the number of columns for a given parameters configuration beside applying Eq. 2.14 and 2.15, the time interleaver process can be carried out based on MATLAB build-in functions. The configuration of N_{TI} applied in the simulation is 3.

h. OFDM Frame Adaptation

The frame adaptation gathers the time interleaver output cells for a given physical layer pipe. The gathered cells are arranged into active OFDM cells for every appropriate OFDM symbol to form the whole frame arrangement. This sub-block performs several internal operations that involve assembling the cells of the physical layer pipe to P2 and data symbols. Also, producing and preparing the cells of bias balancing, dummy, and un-modulated FC fields. The simulated parameters configuration controllers all mapping operations for each mentioned cells type.

Because of the varied pilot models, several symbols of a frame carry varying numbers of data cells. The output data of the frame builder is described as a rectangular array having C_{DATA} cells per symbol, offering total cells for every data symbol. The length of data symbols L_{data} is chosen to be 83 symbol while the length of P2 symbol is given in Table 2.10. However, there are fewer

data cells in the P2 and frame closing symbols, which hold unused cells at the symbol's edge.

j. Frequency Interleaver

The frequency interleaver sub-block is the final step in the interleaving process for the simulated DVB-T2 chain. The data cells from the frame builder, which correspond to a single OFDM symbol, are transferred to ready data carriers in the assigned symbol. The possible carries numbers are directly reflected by the chain parameters configuration.

The first step in implementing a frequency interleaver is to produce the appropriate permutation functions H(p), H_0(p), and H_1(p) and bit positions given in Table 2.16 for 8K FFT mode. According to the DVB-T2 standard's restriction, the permutation rules are separated into even and odd portions for each OFDM symbol defined by Eq. 2.22 and Eq. 2.23, respectively. Finally, the symbol interleaver is performed using produced even and odd symbol permutation matrices.

k. Pilot Insertion

The OFDM generation carries more than one function of the simulated DVB-T2 chain. This part consists of pilots and dummy reserved carriers insertion, inverse FFT, PAPR reduction, guard interval insertion, and P1 insertion. The pilots insertion performs modulation for specific input cells with reference information. These cells carry information about SP, Continual Pilot CP, edge, P2, and frame-closing pilot cells. A reference sequence is used to modulate the pilots, where this sequence is obtained from symbol field PRBS and a frame-field PN-sequence as provided in Eq. 2.26.

This sub-block produces OFDM symbols with pilot carriers and boosting process based on the parameters configuration and the chosen FFT mode. The setting of tone reservation locations is also done here, and dummy data TR

locations are inserted so they don't get loaded with data. After all pilots types are modulated and placed into their appropriate carriers according to the stated parameters, the data carriers are outlined, defining the unoccupied location in the OFDM symbol.

l. IFFT

Zero paddings are utilized in the IFFT sub-block to achieve the right symbol length based on the specified FFT mode. Then, to transform the signal into the time-domain representation, IFFT is done using the built-in MATLAB function on the input data as defined by carrier locations. This sub-block required certain OFDM parameters that can be selected from Table 2.22.

The PAPR reduction fulfills the tone-reservation technique, incorporating improvements in the latest version of the DVB-T2 standard. The improvements involve restricting the amplitude of reserved carriers and running the process exclusively on P2 symbols. The number of iterations is set to one and clipping level is 3 are selected as recommended in the DVB-T2 specifications.

m. Guard Interval insertion

This sub-block Inserts the guard interval to the OFDM signal following the configuration parameters of the DVBT2 structure, such as guard interval fraction and FFT number of points given in Table 2.23. The insertion of the GI is at the start of the OFDM symbol according to the determined number of cyclic prefix samples. Finally, the P1 preamble is added to the data being sent. the central purpose of this stage is to carry out P1 preamble generation and insertion. The generation of the P1 symbol is done based on the algorithm and specification given in Appendix K according to DVB-T2 standard. Next, the P1 preamble is added to the data being sent.

ii. Channel Models

The channel models are used to generate channel response via a given channel scenario. These channels use to evaluate performance in several different receiving situations. There are eight channel models for this part of the simulation as given below. The path numbers, power, delay, and phase shift are presented in section 2.5 of chapter two.

- **Gaussian**
- **Ricean F1**
- **Rayleigh P1**
- **0 dB Echo**
- **DTGlong**
- **DTGmedium**
- **DTGshort**
- **TU06 (0.27 Hz at 730 MHz)**

The output of the transmitter chain is fed directly to the channel model's input. There are particular significant processing steps employed by the channel models. Each channel type has its propagation scenario, and the first step is to get the channel response. The channel response generates the attenuation, delay, and phase for the echoes of a considered channel as specified by the DVB-T2 standard.

The second step is to perform the convolution between the input data and the time domain of the channel response, which is skipped for the AWGN channel. The time-domain of the channel response is calculated by taking the IFFT function for the frequency domain response. The last stage is to produce and incorporate Gaussian noise into the signal.

iii. DVB-T2 Receiver Side

The arrangement comprises many sub-blocks in the DVB-T2 receiver side, which will be explored briefly in the coming sections. Each sub-block is responsible for the opposite of the associated transmitter module that is most commonly applied. The first processing step of the receiver side is to complete the de-modulation of OFDM given on the transmitter side. It consists of P1 extraction, guard interval removal, FFT, and pilot and dummy reserved carriers removal sub-blocks. It also offers channel estimation and equalization function.

a. Channel Estimation and Equalization

This sub-block estimates the channel and equalizes input data following the configuration parameters of the DVB-T2 chain. Estimation of channels involves calculating an estimate for individual carriers in every symbol, which originates at the transmitter and reaches the receiver through the specified frequency domain coefficient. For clarity, the received (complex) carrier amplitudes can be defined by Eq. 3.1.

$$Y_{k,l} = H_{k,l}\, X_{k,l} + N_{k,l} \tag{3.1}$$

The $Y_{k,l}$ represents received carrier-amplitude. $X_{k,l}$ represents the complex modulation applied on carrier k, symbol l. $H_{k,l}$ is channel frequency response and $N_{k,l}$ represents the additive receiver noise.

The frequency response of the considered channel is computed immediately, given the channel characteristics for multipath profiles. The class of channel estimation implemented here is perfect because it supplies the most reliable response estimation at any frequency and on individual symbols. The channel response is determined using the parameters obtained from the chosen channel model, thus providing an accurate depiction function of the channel's impact.

i. Zero Forcing Equalizer

The first kind of channel equalizer executed in the simulated DVB-T2 chain is the Zero Forcing (ZF) equalizer. In this kind, the equalization procedure is carried out by dividing the cell value of the received signal by the channel response affecting the same cell as given in Eq. 3.2. Finally, the estimated channel response is moved up the receiver structure to the Log-likelihood Ratio (LLR) de-mapper. It is utilized to compute the proper LLR for every bit. Where $X^{\wedge}_{k,l}$ is equalized cell value and $H^{\wedge}_{k,l}$ is the estimated channel response.

$$X^{\wedge}_{k,l} = \frac{Y_{k,l}}{H^{\wedge}_{k,l}} \qquad 3.2$$

ii. Minimum Mean Square Error Equalizer

There is an option to use Minimum Mean Square Error (MMSE) as a second type of equalization process. MMSE equalizer minimize the mean square error between the transmitted vector and its estimate. This approach takes into account the effect of AWGN and offsets the inverse matrix with the noise variance as given in Eq. 3.3 where H^{*} represents the conjugate transpose of H and σ^2 represents the channel noise variance.

$$X^{\wedge} = (H^{*}H + \sigma^{2})^{-1} H^{*} Y \qquad 3.3$$

Following the process of channel estimation and equalization, all pilots types and tone reservation carriers should be removed. Then OFDM symbols are recovered from input data following the configuration parameters of the DVB-T2 chain according to the location of data carriers per symbol. Furthermore, frequency de-interleaver and frame extraction perform the opposite of the transmitter side process.

b. Constellation Rotation De-mapping

The de-modulation of the BICM module is made up of several sub-blocks started from time de-interleaver and ended with BCH decoder. Each sub-block performs an inverse function of the main BICM transmitter module. The time de-interleaver performs the inverse operation of the time interleaver sub-block. The number of FEC blocks per TI Block is calculated using FEC blocks in each interleaved frame and the number of TI blocks per Interleaving Frame. This number is an essential de-interleaver element to count the number of needed columns and length of received data per TI Block.

In this part, the procedure is inverted as compared to transmitter side where the number or row becomes equal to five times FEC Blocks per one TI block of the Interleaving Frame. The column numbers are given by parameters configuration for each constellation size and FEC type. The cell and bit de-interleaver is performed by using transmitter functions but with opposite processes.

If the constellation rotation technique is applied at the transmitter side, then the first step executed by this sub-block is to remove the cyclic Q delay from the complex part of the received cells. The second step is to determine Log Likelihood-Ratios (LLRs) for every bit in the constellation. The LLR implemented in this simulation adopted the option of Genie-aided de-mapping.

- **Genie-aided de-mapping**

Genie-aided de-mapping is the considered bounding case of the advantages of the iterative scheme, where the inner decoding does have knowledge about those other bits. In this computation, just the other bits transported in the same constellation are utilized, not the bit presently holding decoded. It follows that only two constellation points could possibly have been transmitted, which two points of course depending on the values of the bits

except bi. One of these two points corresponds to bi = 1, and the other to bi = 0 as shown in Fig. 3.3.

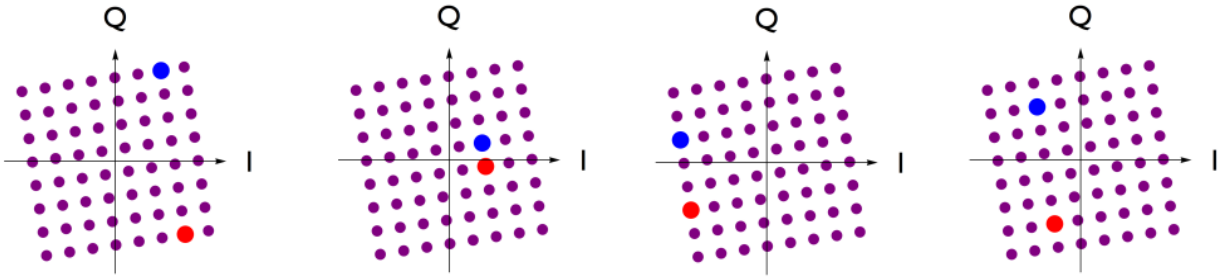

Fig. 3.3 Genie-aided de-mapping for 64-QAM (blue represent 0, red represent 1)

According to this assumption, the numerator in the LLR expression will contain only one state x (corresponding to the point for which bi = 1) for which the probability product is non-zero and identical to unity. This is because the product is of terms since the decoding is known to be error-free) take a value of either 0 or 1, and thus the product is non-zero, and equal to 1, only in the case of the state x that corresponds to the bi = 1, together with the known values of the other bits. Let the transmitted coordinates of this state be I_1, Q_1.

Similar reasoning also applies to the denominator, with a different single state corresponding to the point for which bi = 0. Let the transmitted coordinates of this state be I_0, Q_0. In effect, the constellation has been reduced to a special case of BPSK. It follows that the LLR becomes a simple function of I, Q as given in Eq. 3.4. So this sub-block will produce stream of cells, each cell result from LLR and represent the correct cell value ready to be feed to the next stage.

$$\mathrm{LLR(bi)} = \ln\left\{\frac{e^{-\frac{(I-\rho_I I_1)^2+(Q-\rho_Q Q_1)^2}{2\sigma^2}}}{e^{-\frac{(I-\rho_I I_0)^2+(Q-\rho_Q Q_0)^2}{2\sigma^2}}}\right\} \qquad 3.4$$

iv. Simulation Description

Simulation results were obtained using the DVB-T2 test 'dvbt2bl_ber_snr_VV_dico' which performed dichotomic search for Signal to Noise Ratio, e.g. added Gaussian noise at target bit error rate of 10^{-7} (after LDPC decoder). It starts from widely spaced SNR values guaranteed to bracket

the desired BER and performing interval bisection. Only one frame is simulated at each SNR value and so the procedure rapidly homes in on the approximate SNR achieving the target BER. It is possible to calculate more precise SNR value using similar test and testing SNR by small increments, however, it takes much longer to calculate desired SNR which will be around 0.1dB different than SNR obtained by using dichotomic search.

3.3 DVB-T2 with STBC MISO Mode

MISO mode is without a doubt one of the most innovative approaches to the DVB-T2 system. The second part of this thesis is dealing with the MISO transmission mode in SFNs condition. There are two types of simulation; the first one simulates the traditional DVB-T2 SISO SFNs. While the second simulates the DVB-T2 with MISO SFNs configuration.

This part basically uses the same system configuration presented in the first part. Furthermore, there are several modifications and certain block addition for the transmitter and receiver sides. Also, the channel models should be modified to handle this type of transmission. The transmitter side has the same basic sub-blocks displayed previously but with the consideration of STBC MISO sub-block. Moreover, all the process following the MISO should take care of the applied modification.

i. STBC MISO Process

The principle of MISO technology utilized in second-generation system relies on a modified Alamouti coding scheme as depicted in Fig. 3.4. This SFBC principle presents excellent benefits because the signals from the transmitter of groups 1 and 2 are no longer correlated. This makes it potential to eliminate the notches that are typical in SFNs.

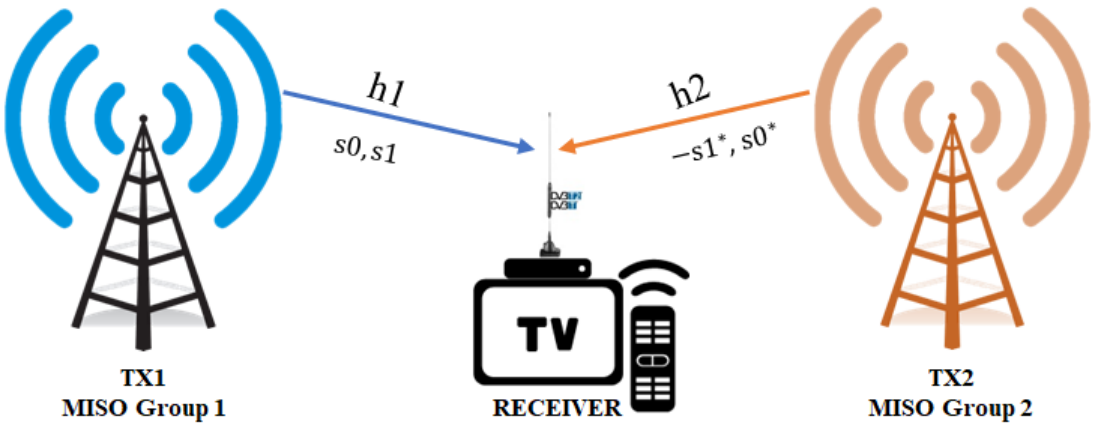

Fig. 3.4 Modified Alamouti scheme

The MISO sub-block makes the conjugation and swapping of the Alamouti processing. It makes two copies of the input data. The first copy is passed without any modification and represents the data from TX1 that belongs to MISO group 1. The second copy is modified by applying the Eq. 2.24 given in chapter two and represents the data from TX2 that belongs to MISO group 2 . The output data of this sub-block becomes two sections, one for each TX group.

For the simulation of DVB-T2 SISO SFNs mode, the current processing sub-block also performs two copy inputs. Still, the second copy remains the same as the first copy, i.e., without modification. All sub-block lying under the OFDM generation process should handle the modification and addition of MISO processing. Where all sub-block deals with two inputs, each one belongs to the MSIO group. Any OFDM sub-block modification must follow the configuration parameters of the simulated DVB-T2 chain.

ii. MISO Channel Model

Considering that the two transmitter groups are adequately far from each other, It can conclude that the two signals associated with each station transmit over two separate channel paths. Each channel's path characterizes by Channel Impulse Response (CIR). Channel impulse response h1 describes the channel path between MISO group 1 and the receiver, while h2 defines the channel path as MISO group 2.

In DVB-T2 MISO SFNs simulation, three models of fading channels utilize Gaussian, Ricean MISO, and Rayleigh MISO. The first step prepared by the channel model is to get the channel response. The channel response produces two fading paths, one for each MISO group. The Ricean F1 or Rayleigh P1 are generated for TX1 belonging to MISO group 1 when using Ricean or Rayleigh MISO channel scenarios.

The second path is formed for TX2 belonging to MISO group 2 using Ricean F2 or Rayleigh P2 according to selected MISO channel situations. The path numbers, power, delay, and phase shift of the MISO group 2 are provided in Table 2.32. The following step is done by taking the convolution between each MISO group's input data and the time domain of the corresponding channel response.

iii. DVB-T2 MISO Receiver Side

To correctly decode the received signal, the receiver side should be modified to take care of the change presented at the transmitter. The receiver side consists of several sub-block. Some of these sub-blocks are assigned to deals with MISO transmission mode while the others achieve the same functions as part one. The following sections discuss only the presented modification.

a. MISO Estimation

This process performs MISO channel estimation within OFDM de-modulation module, i.e., two channels estimation. It Computes the channel response for both MISO groups. The channel response is calculated using the parameters acquired from the channel model of choice (delay, attenuation, phase). This results in an ideal representation of the channel's influence for each MISO group. Then these channel responses are arranged following the data carrier locations.

b. MISO Equalization

For the system simulated in part one, the channel equalization is applied immediately after the channel estimation process. In this part, the channel equalization has a separated process. This process is delayed after the pilot and dummy reserved carriers removal section. It is essential since MISO equalization is carried out on pairs of cells, which may be broken up by pilots or

dummy reserved carriers. As a result, the resulting data cells can rejoin in their MISO pairs only after the pilots are removed.

The receiving pair of cells in MISO mode holds together a couple of transmitted constellations. For each pair of cells from each transmitter group, four related frequency responses are obtained from the channel gain. This can be clearly understood by the MISO processing block diagram displayed in Fig. 3.5. Where the received complex values r1 and r2 for a pair of MISO cells are indicated by Eq. 3.5 and Eq. 3.6.

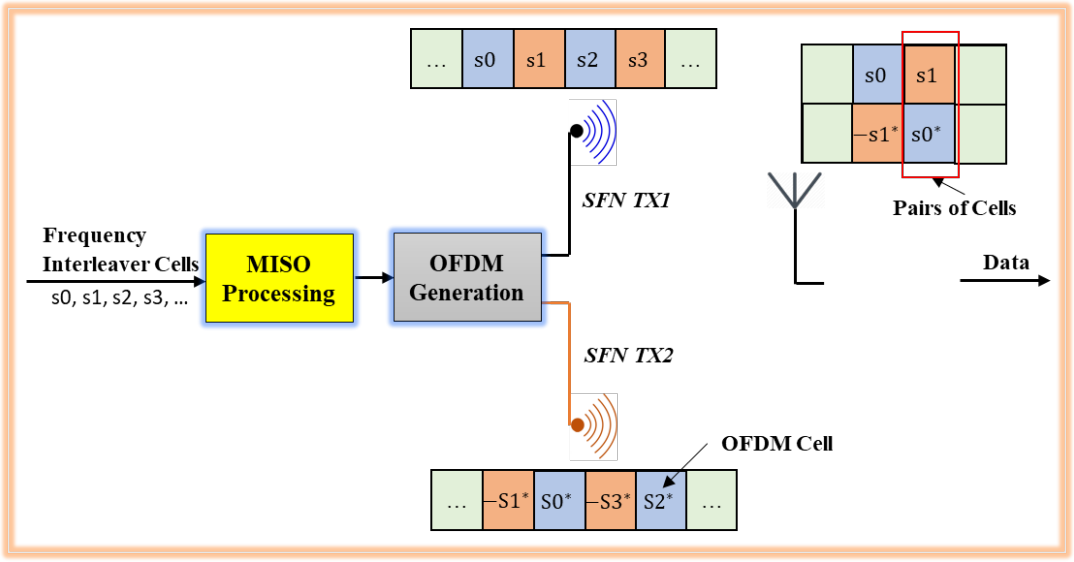

Fig. 3.5 DVB-T2 MISO processing

$$r_1 = h_1 s_0 - h_2 s_1^* + n_1 \qquad 3.5$$

$$r_2 = h_1 s_1 + h_2 s_0^* + n_2 \qquad 3.6$$

The * sign indicates complex conjugate operation, n characterizing the noise terms. In matrix notation, these equations can be expressed by Eq. 3.7.

$$\begin{bmatrix} r_1 \\ r_2^* \end{bmatrix} = \begin{bmatrix} h_1 & -h_2 \\ h_2^* & h_1^* \end{bmatrix} + \begin{bmatrix} s_0 \\ s_1^* \end{bmatrix} + \begin{bmatrix} n_1 \\ n_2^* \end{bmatrix} \qquad 3.7$$

The MISO equalizer sub-block applies the matrix inverse process, describing the ZF equalizer, as provided in Eq. 3.8 and Eq.3.9.

$$r = \begin{bmatrix} r_1 \\ r_2{}^* \end{bmatrix} = h\, s + n \qquad 3.8$$

$$\hat{s} = h^{-1}\, r \qquad 3.9$$

3.4 T2-Lite Profile

The system considered in this part is a special case of part One. It deals with the simulation of a modern T2-Lite profile designed for mobile and handheld reception. The system simulated in this part is based on the original DVB-T2 chain with some modifications. The T2-lite transmitter side has the same sub-blocks as the system given in Fig. 3.1. All given sub-blocks are internally modified to handle the short FEC frame length, i.e., 16k. This affects MPEG transport stream data, BBframe lengths, number of output data cells, the interleaved cells, and number of rows for time interleaver.

The bit-interleaved coding and modulation module for T2-Lite consists of the same number of sub-blocks as the main DVB-T2 system. Also, each sub-block performs the same functions. The main changes are given in terms of BCH encoding where the generator polynomials used with short FECFRAME length. LDPC encoding applies the short FECFRAME length with new coding rates given for the T2-Lite profile presented in Table 2.26, with their consideration in terms of N_{bch} and K_{bch}. The coding rates simulated in this part are 1/3, 2/5, 3/5, 2/3,11/15.

The parity interleaver is also applied for code rates 1/3 or 2/5 when selecting the QPSK constellation. For this condition, the column twist interleaving is not used. In the remaining constellation types and coding rates, the number of rows, columns, and twisting parameter t_c of the bit interleaver structure is changed according to the provided configuration as offered in Tables 2.2 and 2.27 .

The first step of bit to cell symbol mapping process is performed input splitting into several sub-streams according to modulation mode and short FEC frame length only. Furthermore, it provides the de-multiplexing parameters for the new coding rates (1/2 and 2/5). The previous and the new coding rate de-multiplexing parameters for short frame length is provided in Appendix I. The

cell and time interleavers applying the same process while the number of cells should be considered according to the limitation of T2-Lite profile.

3.5 T2-Lite System with DVB-NGH BICM Module

This part of the simulation deals with the utilization of DVB-NGH BICM module, which is at the cutting edge of coded modulation technologies proposed for DVB-NGH. DVB-NGH is not implemented yet, and it's suggested for future broadcasting applications. This module is derived from a sub-set of T2-Lite BICM components with extra features. So the system simulated in part three is essential for current part because the T2-Lite system is considered a base toward next-generation broadcasting implementation.

This part fundamentally uses the same system configuration presented in T2-Lite system by considering the sheer-terrestrial DVB-NGH broadcasting profiles. Furthermore, the modification is represented by proposing the implementing of DVB-NGH BICM module instead the original T2-Lite BICM module. The subsequent sections show the implementation of DVB-NGH BICM module.

i. DVB-NGH BICM Module

All of the main sub-blocks given in the transmitter structure having identical functions to the T2-Lite except for the BICM module and its sub-blocks. The BICM of DVB-NGH depends on the T2-Lite profile with particular improvements to minimize the receiver decoding complexity, power consumption and improve system robustness over fading channels. This BICM module is considered the most advanced in coding modulation technology.

It consists of certain sub-blocks, some of them similar to the original T2-Lite module while others having a different functions. It also includes a new sub-block known as the I/Q component interleaver. The different sub-blocks are explained in the next section. The structure of DVB-NGH BICM module is illustrated in Fig. 3.6.

Fig. 3.6 DVB-NGH BICM module structure

a. BCH and LDPC encoder

The BCH and LDPC encoding sub-blocks apply the same processes introduced in the simulated T2-Lite system. The DVB-NGH BICM has other different coding rates from the T2-Lite as presented in Table 2.28, but they aren't adopted in the current simulation. The reason behind that is to make the comparison fair between them by examining similar coding rates. The coding rates simulated in this part are 5/15, 6/15, 9/15, 10/15, and 11/15.

b. Bit interleaver

The bit interleaver has the same processing steps as the T2-Lite system with certain modifications. The first modification is to apply only the parity interleaver operation for all coding rates when the system is configured with the QPSK modulation type. The second is to change the twisting parameter t_c of column twist interleaver for all remaining modulation modes as addressed in Table 2.29.

c. Bit to cell symbol mapper & Cell interleaver

Since the chosen code rates and modulation modes are the same as the simulated T2-Lite system, the bit to cell symbol mapper sub-block has the same structure. The cell interleaver sub-block performs its function identically as the T2-lite system by following similar rules with some modifications. The first necessary modification is the position changing in the BICM chain to precede constellation rotation sub-block.

The second modification includes holding pairs of neighboring cells together while using four-dimensional constellation rotation. This case is applied when managing QPSK for specific code rates according to the configuration parameters i.e., with 9/15, 10/15, and 11/15 coding rates. For the same condition, the permutation function length is halved, i.e., half the cells number according to Eq. 2.32.

d. Constellation rotation

The constellation rotation sub-block uses the dimension rotation procedure to employ the rotation scheme. The two-dimension rotation technique is employed but with different structures for all modulation modes and code rates, excluding QPSK modulation with 9/15, 10/15, and 11/15 code rates. The 2D constellation rotation approach is extended to four-dimensional to provide a greater diversity scheme. The four-dimensional is applied when simulation parameters configuration are QPSK modulation with 9/15, 10/15, and 11/15 code rates.

The two and four-dimensional are accomplished by multiplying output vectors of cell interleaver by a rotation matrix having an orthogonal feature of size (2x2) Eq. 2.33 or (4x4) Eq. 2.34, respectively. The process of the input vector x to produce $N_D/2$ adjacent cells is proffered in Eq. 2.35 and Eq. 2.36. Furthermore, the a and b parameters required in the DVB-NGH rotation process are individually given in Eq. 2.37 and Table 2.31.

e. I/Q Component Interleaver

Following implementing the rotating constellation scheme, the quadrature Q component of the T2-Lite system is delayed using a cyclic Q delay. The current sub-block replaces the cyclic Q delay with an extra sophisticated interleaver. moreover, utilized when finishing from constellation process sub-block.

The I/Q component interleaver sub-block is carried out individually on each FEC block and completed in four steps, as explained in chapter two section 2.4. The row number is set equal to the number of rotated dimensions, while the number of columns is obtained from simulated parameter configurations according to Eq. 2.38.

f. Time Interleaver

The output of the I/Q component interleaver is fed to the time interleaver sub-block. The DVB-NGH time interleaver has two interleaving options, type zero and type one. For the current simulation, type zero is performed because interleaved frame is divided into multiple interleaved blocks, so every IF is immediately allocated to a single logical frame.

Considering the above condition, only a one-time interleaver unit of block interleaver per TI-block per interleaver frame is addressed column per column. The number of used columns for the block interleaver is directly related to the block numbers of the interleaving frame for a given physical layer pipe. The reading process is similar to the T2-Lite, but the number of rows is different for the same modulation mode. This difference is because the number of rows for the time interleaver of T2-Lite is constant and related to the modulation mode.

In comparison, it's equal to the number of cells per FEC Block of a given modulation mode following the simulated structure configuration parameters displayed in Table 2.9. Additionally, the variable $N_{FEC\text{-}TI}(n,s)$ has a value marked according to Eq. 2.15 given in chapter two.

Chapter Four

Results and Discussion

4.1 Introduction

This chapter is very important because it displays the performance of simulated systems over several channel conditions. Tables and figures will be used to display the outcomes of the performance of the simulated systems. MATLAB R2020b software has been used to acquire the results of all simulation parts in this thesis. The results that have been obtained and recorded in this chapter are divided into four parts according to the number of simulated systems.

The first part displays the results of the DVB-T2 system with rotated and non-rotated constellation techniques. The second one covers the results obtained from the simulation of the DVB-T2 system with MISO transmission mode in SFNs environments. This part also displays the results of employing DVB-T2 SISO mode in SFNs areas. The third part includes the results of simulating the T2-Lite profile. The rotated and non-rotated constellation techniques are also applied to T2-Lite profile simulation.

The final part simulates the T2-Lite profile by employing DVB-NGH BICM module instead of its original one. This part is characterized by employing the new features of DVB-NGH BICM module with both two and four dimensional constellation rotation schemes. In addition, the achieved results for all parts will be discussed at the end of this chapter.

4.2 DVB-T2 Results

This part is further divided into two sections as presented below, one for the DVB-T2 simulation results before using the constellation rotation. The second section is for the results of the constellation rotation cyclic Q delay

simulation. The DVB-T2 standard defines several configurations. The right choice of a specific configuration makes the system suitable for various uses, from portable services with a low data rate to broadcast programs with HD resolution. In this part, a specific parameters configuration is used to simulate both rotated and no rotated constellation cases. The main configuration parameters employed in this simulation are presented previously in Table 3.1.

i. DVB-T2 Results Before Constellation Rotation

This section deals with the simulation of the DVB-T2 system without employing constellation rotation and cyclic Q delay. Many outputs can be displayed for each sub-blocks for both transmitter and receiver sides. Still, all sections considered in the thesis display only the results that are reflected essential information. Therefore, the constellation diagrams of the data cells after applying the cell mapper sub-block are given in Fig. 4.1.

The output of the cell mapper sub-block is fed directly to the cell interleaver since the constellation rotation technique is not used. The process of the DVB-T2 BICM module is completed after applying the time interleaver sub-block.

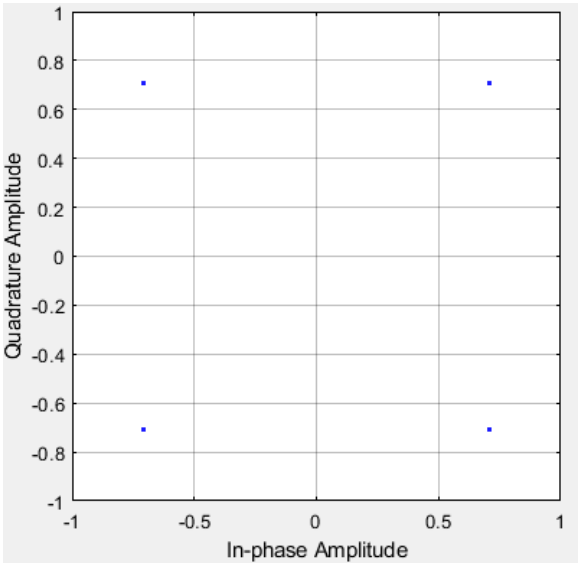

(a)

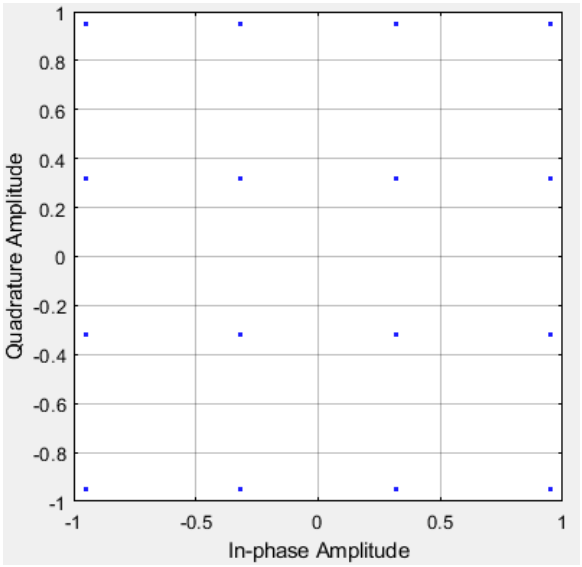

(b)

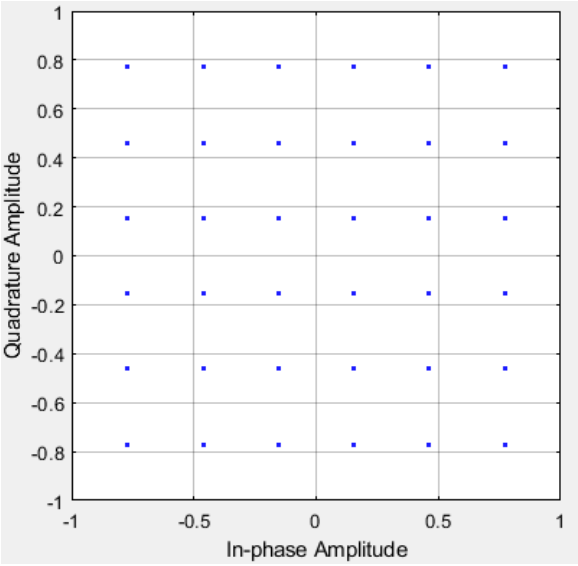

(c)

Fig. 4.1 Cell mapper output for (a) QPSK, (b)16-QAM, (c) 64-QAM

The output of the cell mapper sub-block is fed directly to the cell interleaver since the constellation rotation technique is not used. The process of the DVB-T2 BICM module is completed after applying the time interleaver sub-block.

The succeeding stages involve passing BICM output cells to the frame builder, frequency interleaver, and OFDM generation. The first sub-block of the OFDM module is the pilot insertion. The output of this sub-block is essential when comparing the input and output of the channel estimation. The reason behind this is that the inserted pilots have not yet been removed. The production of this sub-block is manifested in Fig. 4.2.

The result of the pilot insertion is applied to the subsequent OFDM generation sub-blocks. The generated DVB-T2 signals after employing the last sub-block of OFDM generation are provided in Fig. 4.3 for QPSK modulation mode as an illustration.

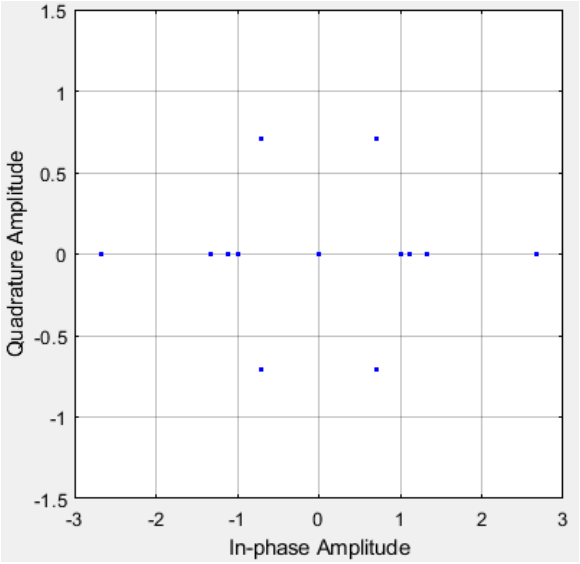

Fig. 4.2 Pilot insertion output for QPSK modulation

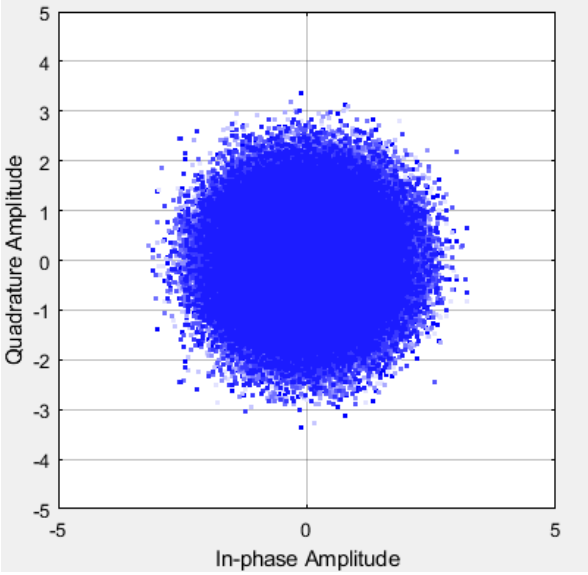

Fig. 4.3 Transmitted DVB-T2 signals with QPSK modulation

The output of the DVB-T2 transmitter chain is applied to the channel models block. The channel models are necessary for demonstrating the DVB-T2 system performance. The models consist of eight scenarios: AWGN, Ricean F1, Rayleigh P1, 0 dB Echo, DTGlong, DTGmedium, DTGshort, and TU06 channels. The responses in time and frequency for the first four channel are displayed in Fig. 4.4. Accordingly, the received DVB-T2 signal with QPSK modulation over the AWGN channel can be seen in Fig. 4.5.

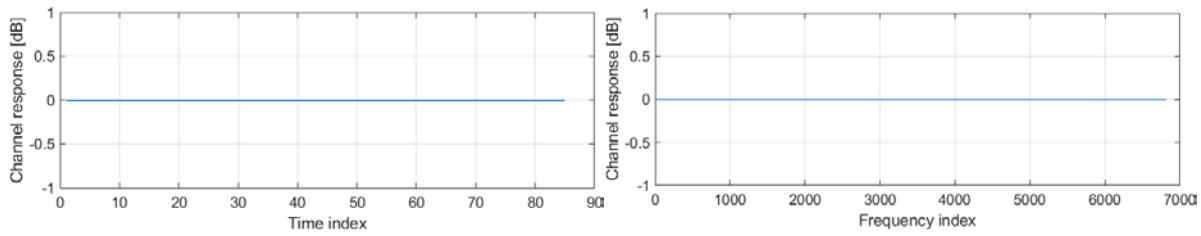

(a)

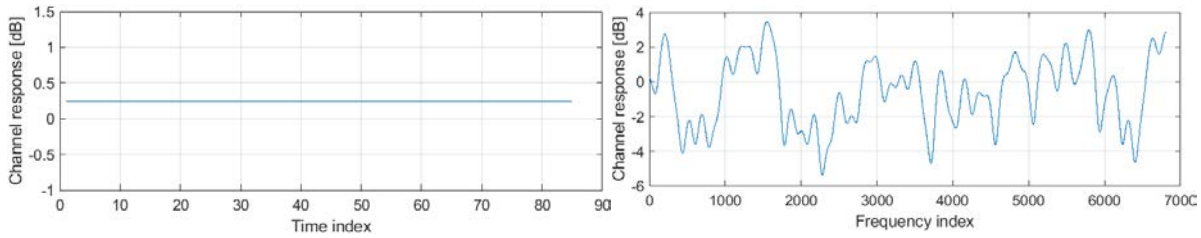

(b)

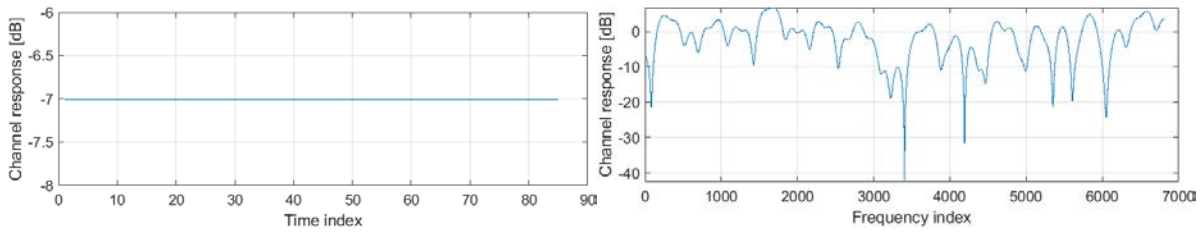

(c)

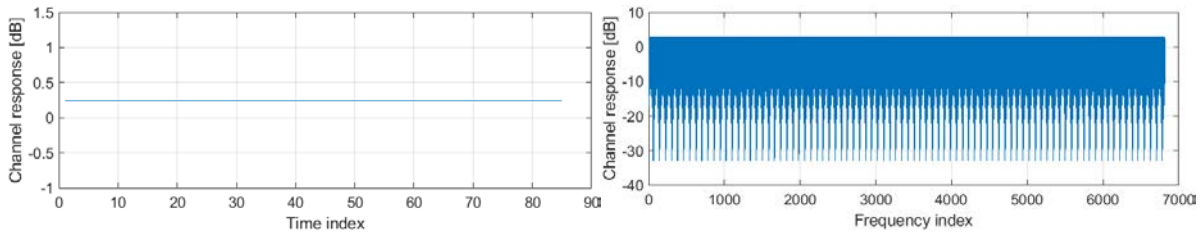

(d)

Fig. 4.4 Channel response in dB (a) AWGN, (b) Ricean, (c) Rayleigh, (d) 0db echo

The output of the FFT sub-block from the OFDM de-modulation module is forded to the channel estimation and equalization sub-block. Channel estimation computes channel response according to the simulated channel profile. Add to the above; the DVB-T2 simulated system equalized the channel impact by employing the Zero Forcing equalizer. Consequently, Fig. 4.6 and Fig. 4.7 illustrate the received signal before and after channel equalization function.

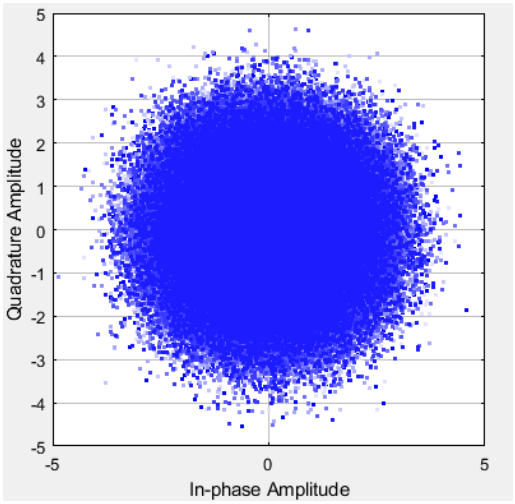

Fig. 4.5 Received DVB-T2 signal over AWGN channel QPSK modulation

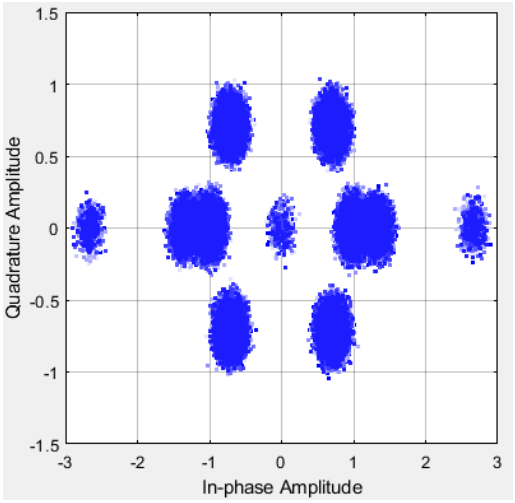

(a)

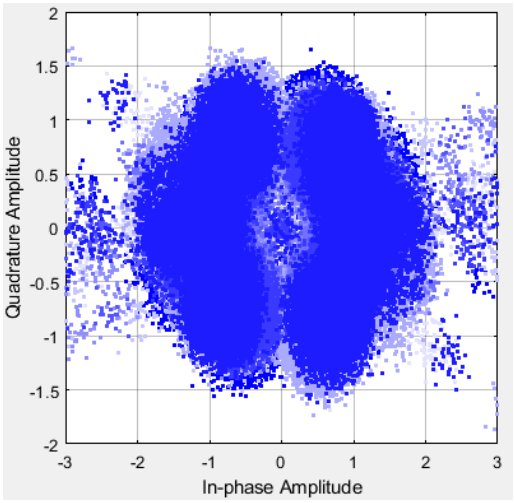

(b)

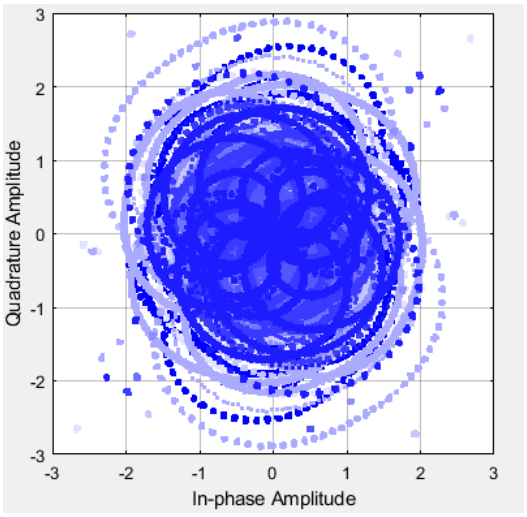

(c)

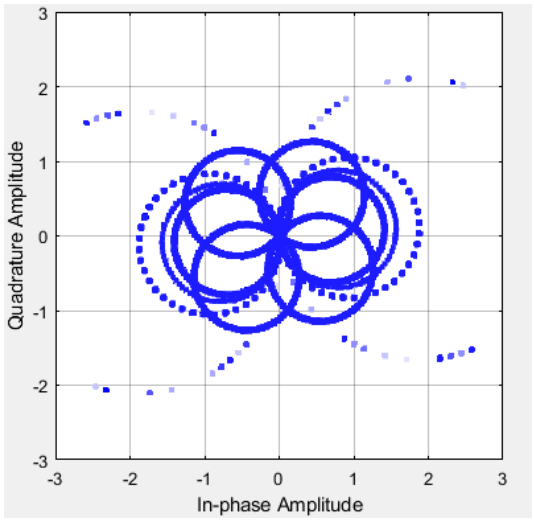

(d)

Fig. 4.6 Received signal before equalization with QPSK modulation for (a)AWGN, (b) Ricean, (c) Rayleigh, (d) 0db echo

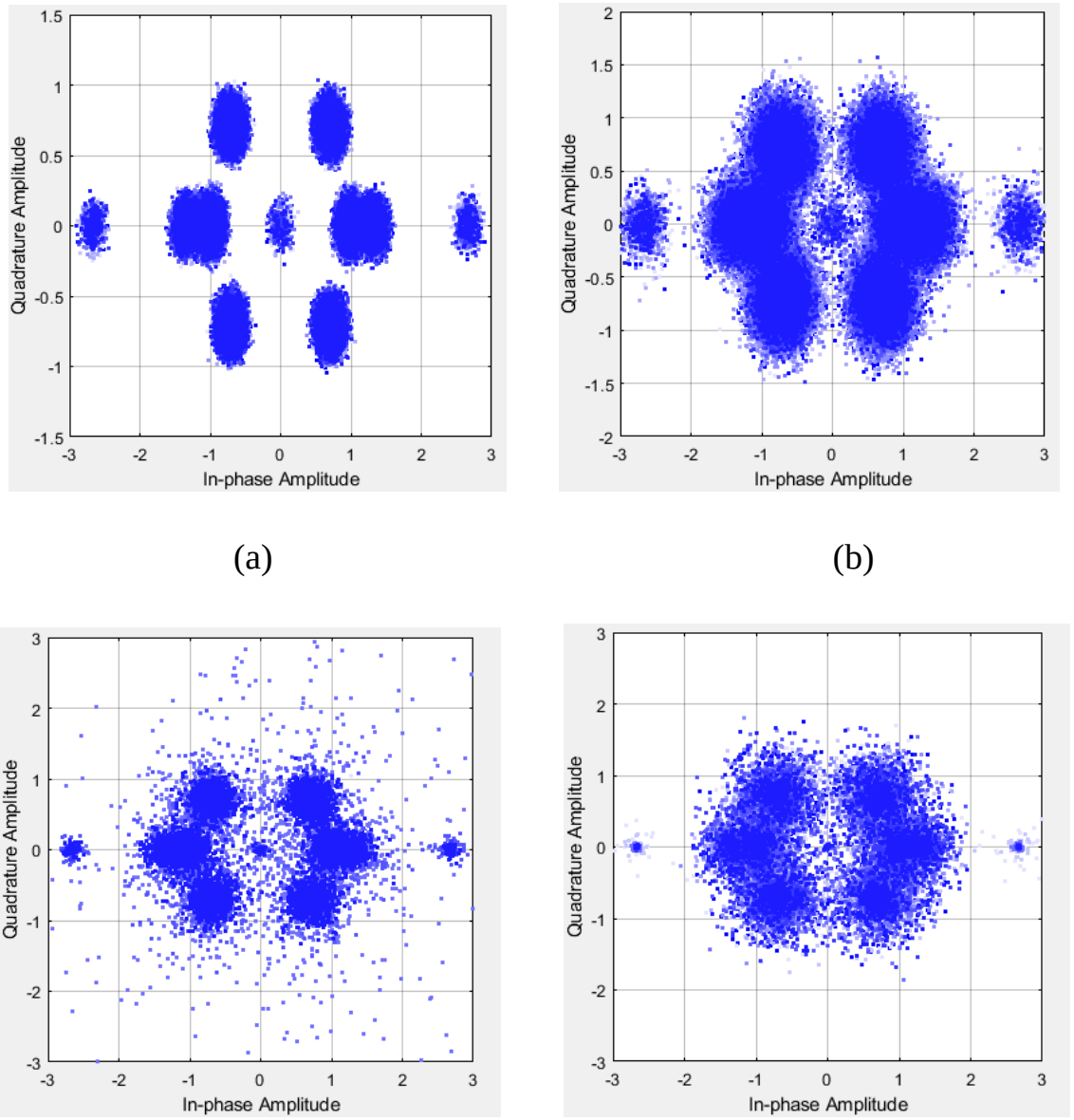

Fig. 4.7 Received signal after equalization with QPSK modulation for (a)AWGN, (b) Ricean, (c) Rayleigh, (d) 0db echo

This phase intends to determine the signal-to-noise ratio (SNR) value using QEF criteria. As stipulated in the DVB-T2 implementation standards, the QEF is a minimum limit defined as BER of less than or equal to $1*10^{-7}$ after inner decoder LDPC. This phase employs all six coding rates provided in the DVB-T2 standard with three constellation types. Tables 4.1(a & b) show the results for all eight channels before applying constellation rotation scheme.

ii. DVB-T2 Results After Constellation Rotation

This section considers the simulation of the DVB-T2 system by applying constellation rotation and the cyclic Q delay technique. The data cells resulting from the cell mapper sub-block are passed to the constellation rotation module. The input cells are rotated by applying specified rotation angles matching each modulation mode in this module. The output after applying the rotation scheme is presented in Fig. 4.8.

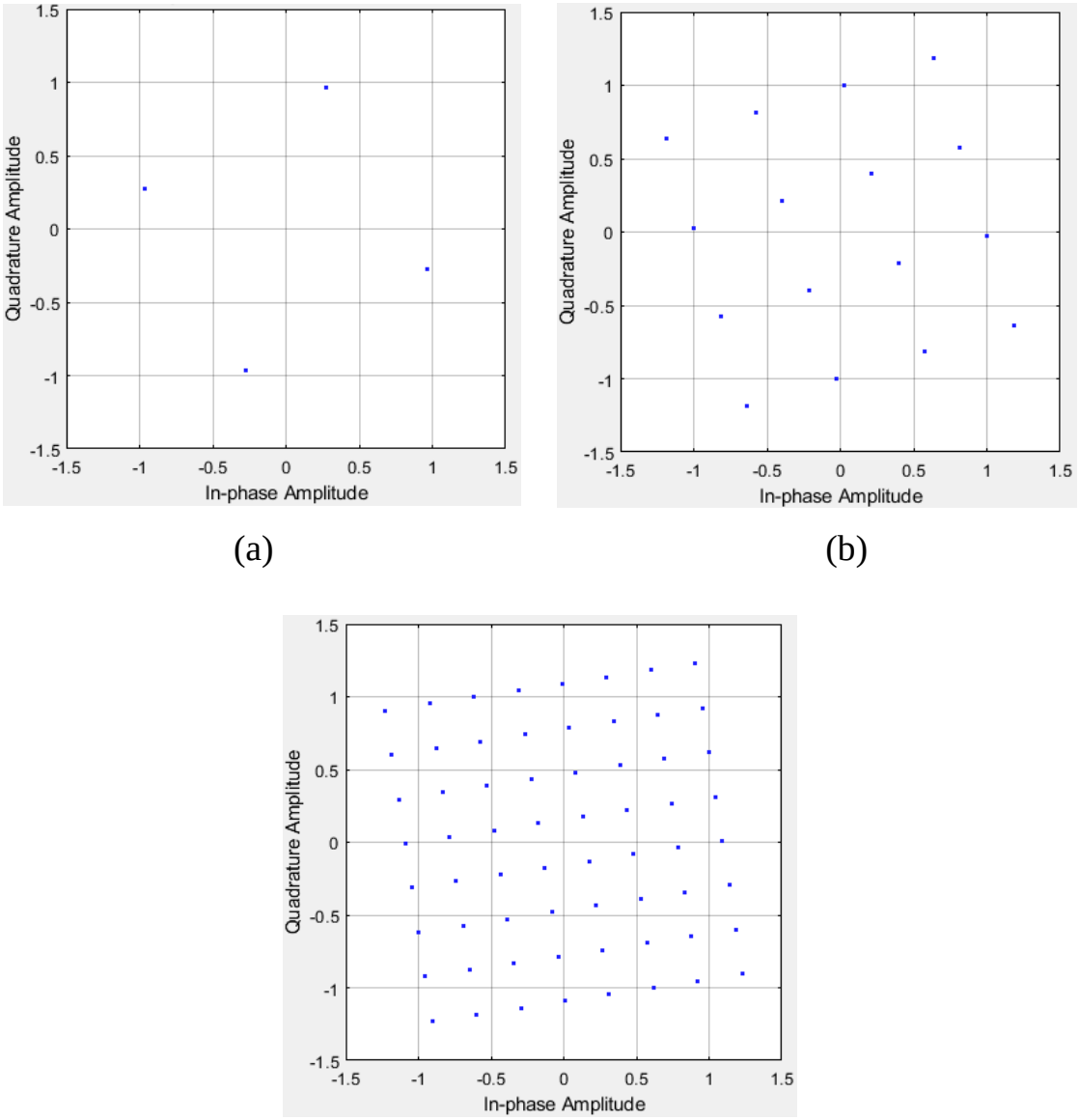

(a) (b)

(c)

Fig. 4.8 Data cells after applying constellation rotation (a) QPSK, (b) 16-QAM, (c) 64-QAM

The second process after constellation rotation is the cyclic Q delay by delaying the Q components. This interleaver leads to twice sending the same information in different cells over the channel. The obtained constellation is called the virtual constellation, which seems to be broadcasting a high-order constellation. For example, QPSK modulation's virtual constellation appears to be an irregular 16-QAM constellation. The output cells of the rotation constellation sub-block after applying Q delay are given in Fig. 4.9.

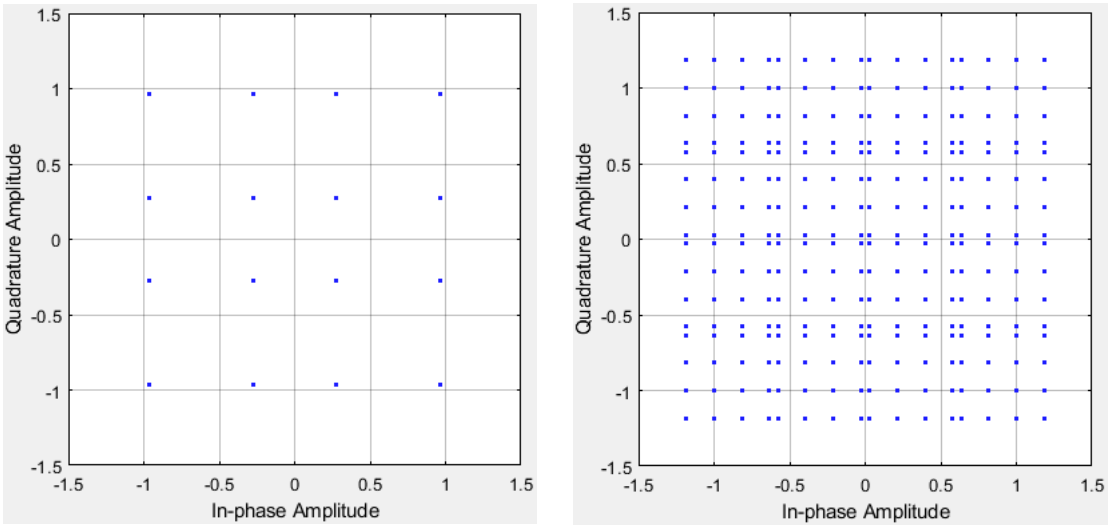

(a) (b)

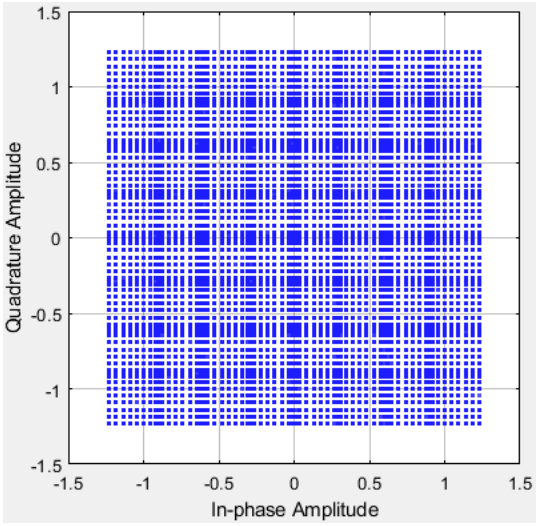

(c)

Fig. 4.9 Constellation rotation output (a) QPSK, (b) 16-QAM, (c) 64-QAM

As stated previously, the output of the pilot insertion sub-block is valuable for comparing the input and output of the channel estimation module. In the event of using the constellation rotation technique, the output of the pilot insertion is addressed in Fig. 4.10.

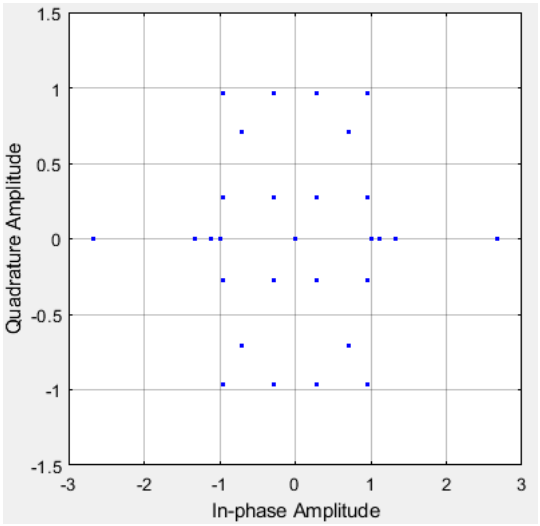

Fig. 4.10 Pilot insertion output for QPSK modulation with constellation rotation

To make a clear sequence of results presentation as in section (i), the received signal before and after the channel equalization sub-block is given in Fig. 4.11 and Fig. 4.12 as samples of two fading channel models.

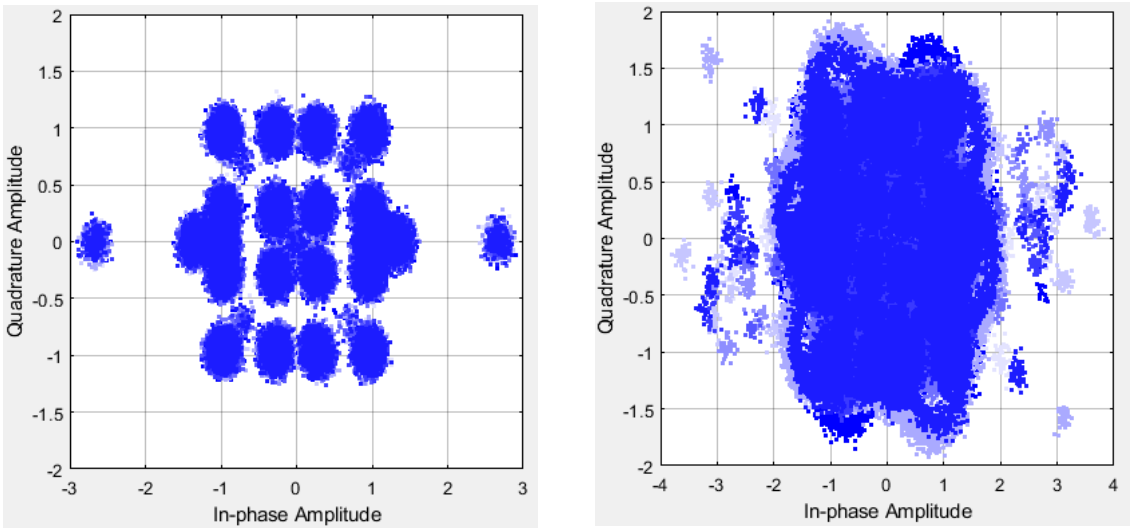

(a) (b)

Fig. 4.11 Received signal before equalization with QPSK modulation for (a) AWGN, (b) Ricean

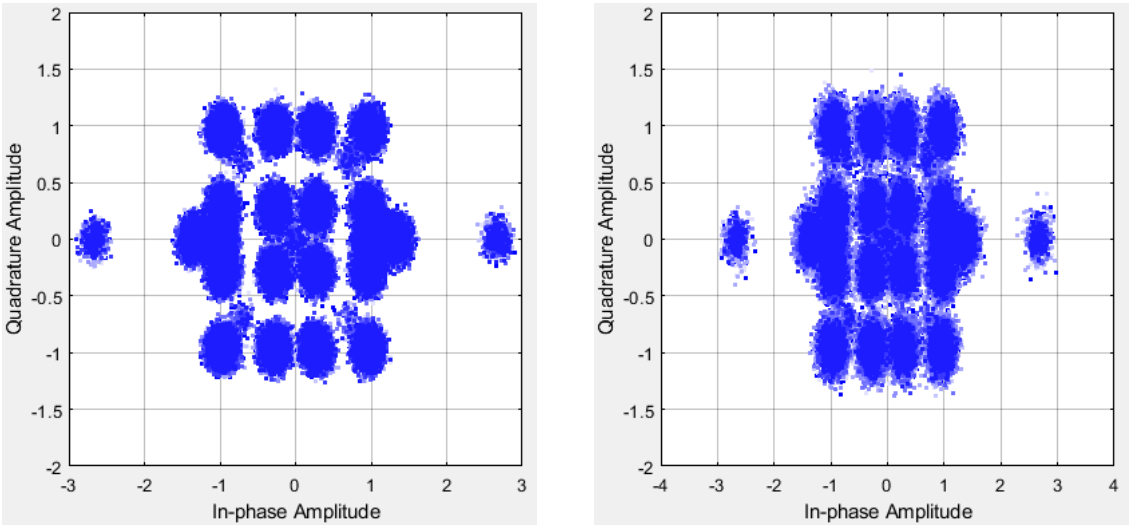

(c) (d)

Fig. 4.12 Received signal after equalization with QPSK modulation for (a) AWGN, (b) Ricean

Table 4.1(a & b) also shows the required SNRs for all four channels to achieve BER of less than or equal to $1*10^{-7}$ following inner decoder LDPC when using the constellation rotation and cyclic Q delay approaches. The SNRs resulting from employing the constellation rotation technique are compared with system performance before using it. The essential factor in this comparison is to obtain the achieved gain. Accordingly, the performance gains achieved with rotated constellations for different modulation modes, code rates, and channels models are presented in the same table.

The diversity gain occurring from constellation rotation adoption is related to modulation modes, coding rates, and fading type. This association can be easily distinguished graphically, as seen in Fig. 4.13. According to Fig. 4.13 (a) for QPSK modulation mode and code rate of 4/5, there is no gain from adopting rotation in the case of the AWGN channel. At the same time, the rotation gains are 0.3, 2.3, and 3 dB for Ricean, Rayleigh, and 0 dB Echo channel models, respectively.

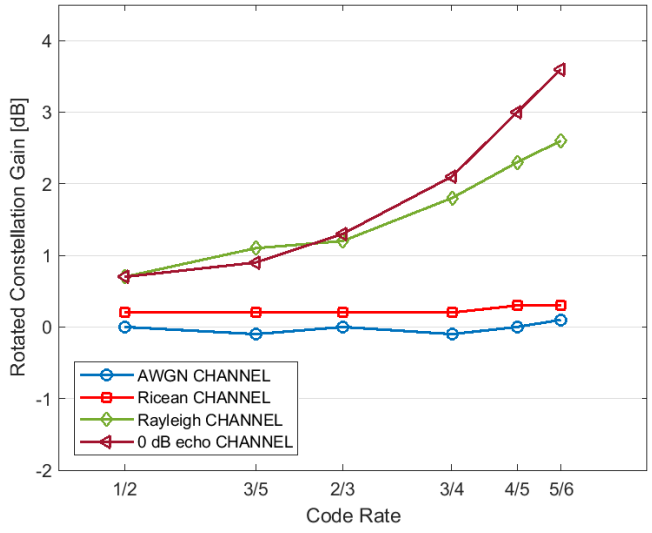

(a)

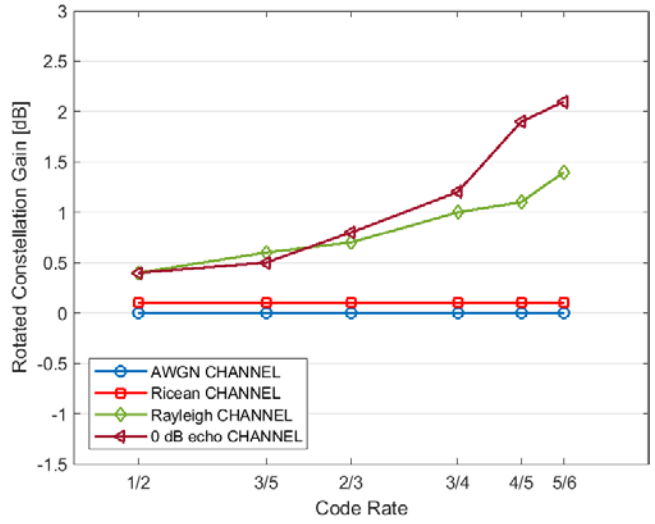

(b)

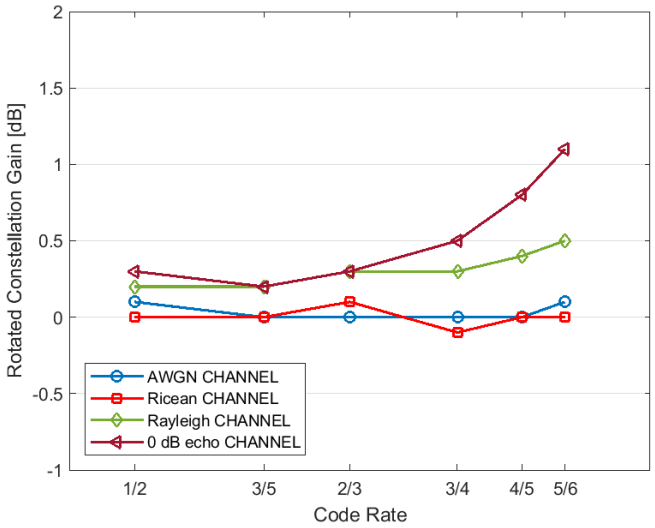

(c)

Fig. 4.13 Constellation rotation diversity gain for (a) QPSK, (b)16-QAM, (c) 64-QAM

The BER curves for QPSK modulation with three code rates of 1/2, 3/4, and 5/6 are simulated. The first four channel profiles are used to test this configuration. The simulation displays BER curves for the DVB-T2 system with and without constellation rotation are shown in Fig. 4.14. The DVB-T2 system without constellation rotation requires an SNR of 2.5 dB to obtain a BER of $1*10^{-5}$ with the Rayleigh channel in the case of QPSK modulation and 1/2 coding rate, as shown in Fig. 4.14(a) below. Furthermore, the system requires an SNR of 1.8 dB under the same circumstance but with constellation rotation.

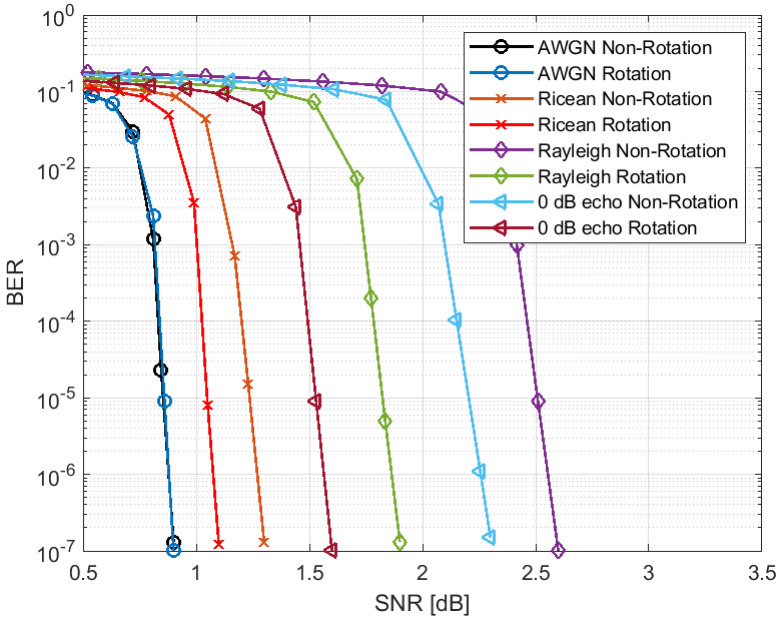

(a)

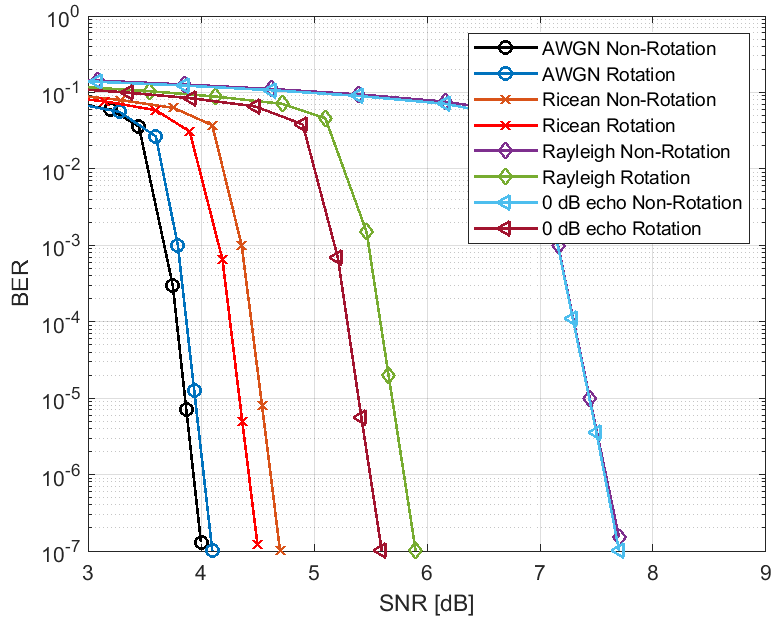

(b)

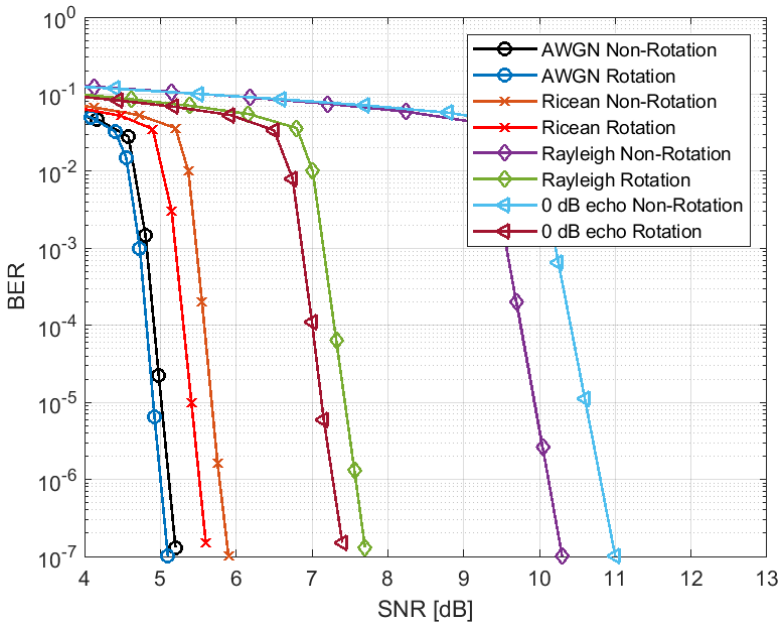

(c)

Fig. 4.14 DVB-T2 BER with QPSK modulation and code rate (a) 1/2 (b) 3/4 (c) 5/6

- **MMSE Equalizer Results**

The above results are obtained using the zero forcing equalizer process. When using the MMSE equalizer, there will be a difference between the required SNR for the two equalization processes. The MMSE outperforms the zero-forcing in term of BER because its take into account the offsets effect of channel noise variance as shown in Fig. 4.15.

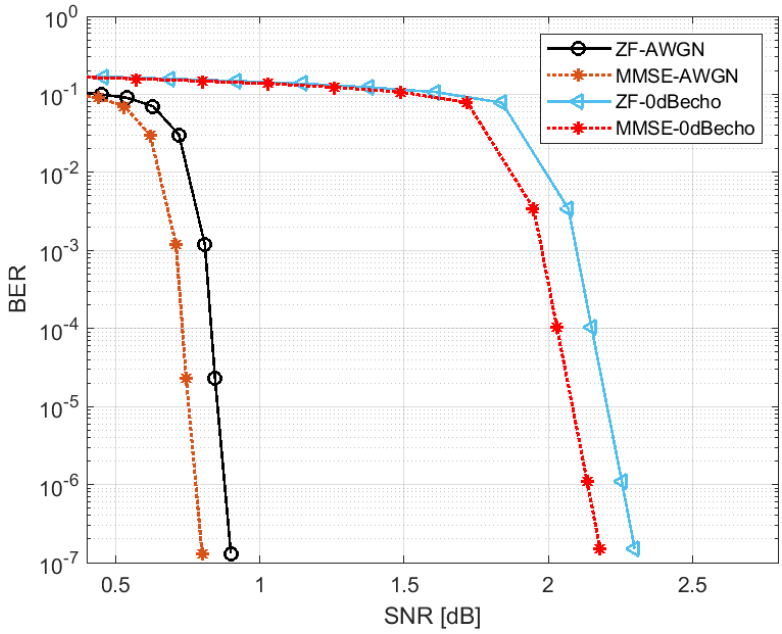

(a)

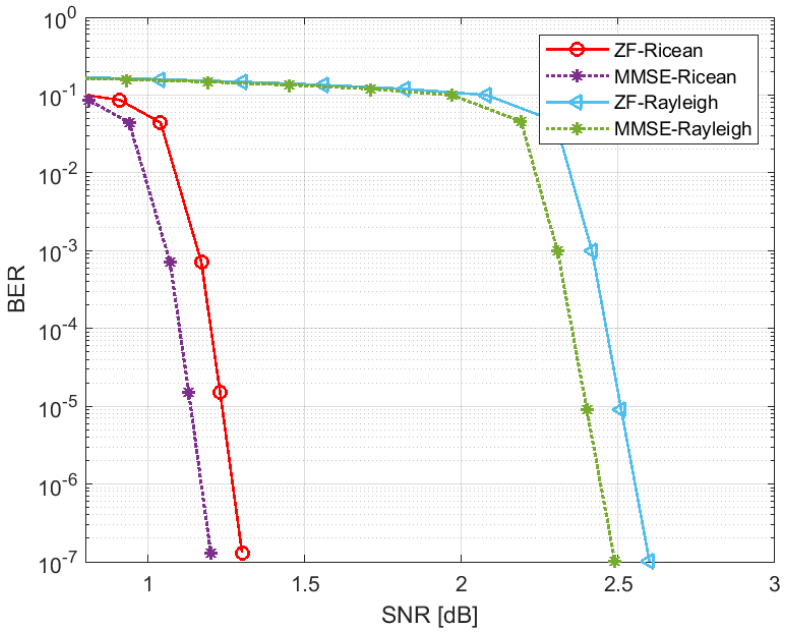

(b)

Fig. 4.15 DVB-T2 BER with ZF and MMSE for QPSK and 1/2 code rate (a) AWGN and 0 dB echo (b) Ricean and Rayleigh

4.3 DVB-T2 MISO Transmission Mode Results

The MISO transmission mode in SFN situations is the subject of this part. There are two sorts of simulation results: the first is for the traditional DVB-T2 SISO SFNs. The second is for the DVB-T2 with MISO SFNs configuration. This part adopts the same parameters configuration presented in Table 3.1 which are used to test the first phase.

Two transmitters and one receiver are introduced in this section, with the first transmitter, Tx1, belonging to MISO group 1 and the second transmitter, Tx2, belonging to MISO group 2. Besides, three types of channel models are used: AWGN, Ricean, and Rayleigh for both SISO and MISO SFNs simulation cases.

This part is based on the same BER criteria as part one, where the displayed SNR achieves BER less than or equal to $1*10^{-7}$ after the inner decoder. Two modulation modes have been considered with all available six code rates given in the DVB-T2 specification.

In traditional SISO mode SFNs, all cooperating transmitters broadcast signals synchronously in content, time, and frequency. This can result in interference of more-or-less similar signals at the receiver. The SNR results from simulating DVB-T2 SISO in SFN are given in Table 4.2 for the mentioned configuration parameters.

For SFNs with MISO mode, the unmodified signal transmitted from transmitter one belongs to MISO group 1. In contrast, transmitter two from MISO group 2 sends a spectrally uncorrelated signal in which the cells (symbols) of the neighboring carriers are swapped. At the same time, Table 4.2 displays the required SNR values for applying MISO scheme.

Table 4.2 also display the SNR results from adopting the constellation rotation with MISO mode over the same channels module. By comparing the MISO and SISO modes, the influence of MISO diversity (gain1)on reception quality in SFNs can be determined in the same table. Furthermore, the gain of applying both constellation rotation and MISO (gain2) is likewise presented.

The relationship between MISO diversity gain (gain1), constellation type, code rates, and fading conditions can be clearly understood graphically, as viewed in Fig. 4.16 . The values of diversity gain from utilizing MISO transmission mode in DVB-T2 system for AWGN, Ricean, and Rayleigh channels, respectively, are 0.1, 0.3, and 3 dB for 16-QAM modulation and coding rate of 5/6 as shown in Fig. 4.16(b).

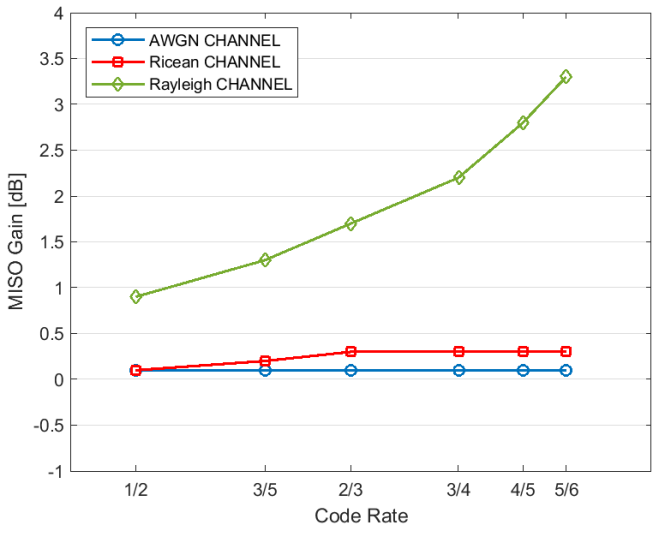

(a)

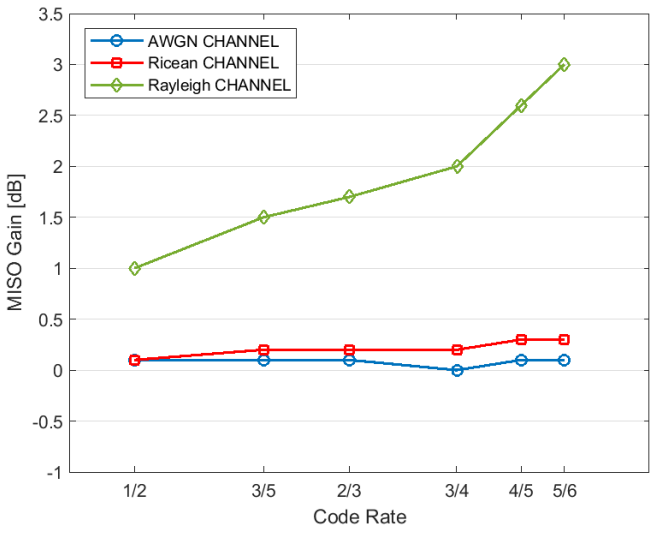

(b)

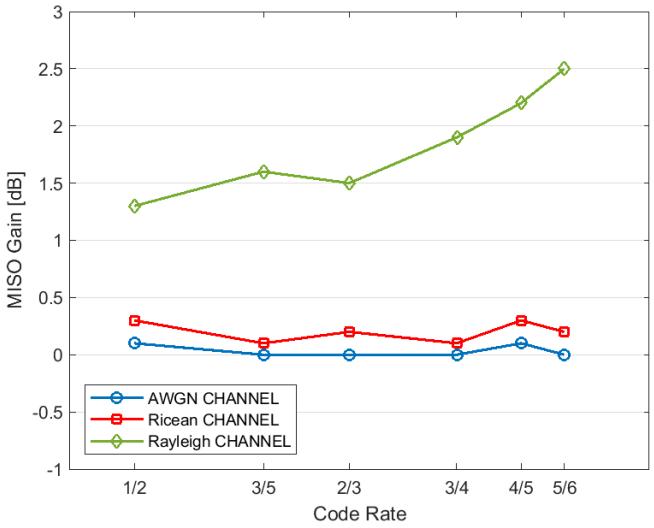

(c)

Fig. 4.16 MISO diversity gain for (a) QPSK and (b)16-QAM (c) 64-QAM

The Bit Error curves for the QPSK constellation are simulated using the same three coding rates: 1/2, 3/4, and 5/6. The three-channel profiles outlined above are used to evaluate this configuration. Fig. 4.17 compares the BER performance of the DVB-T2 system with SISO and MISO modes in the AWGN, Ricean, and Rayleigh channels, respectively.

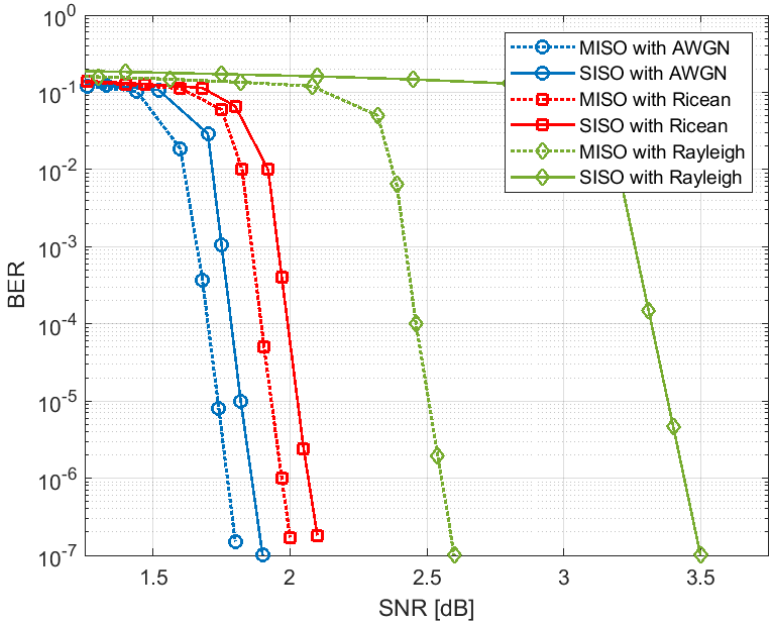

(a)

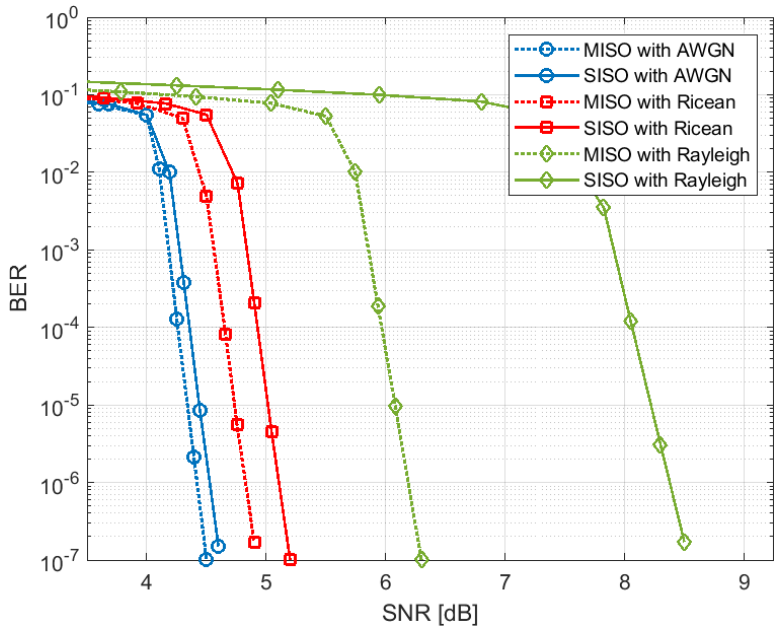

(b)

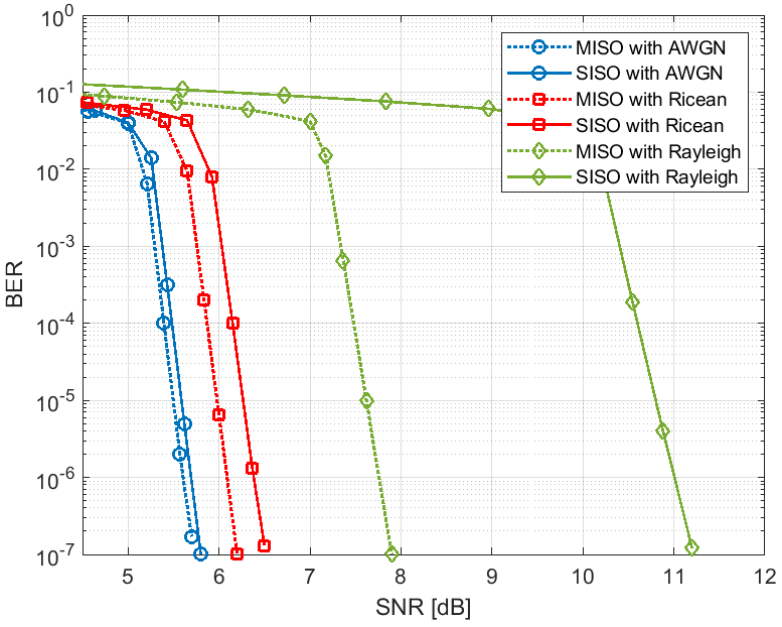

(c)

Fig. 4.17 DVB-T2 MSIO and SISO BER for code rates (a) 1/2 (b) 3/4 (c) 5/6

To achieve a BER of $1*10^{-5}$ with the Rayleigh channel in the case of QPSK modulation and 3/4 coding rate, the DVB-T2 system with SISO in single-frequency networks requires an SNR of 8.3 dB, as illustrated in Fig. 4.17 (b). Under identical conditions, but with MISO transmission mode, the system requires an SNR of 6.1 dB.

4.4 T2-Lite Profile Results

This part aims to simulate the T2-Lite profile before and after applying constellation rotation and Q delay techniques specified by its original BICM module. The same parameter configurations of Table 3.1 are used in this section, excluding the FEC frame length, scattered pattern, and code rates. It adopts an FEC frame length of 16200 and a PP2 scattered pattern. Besides, the selected code rates are 1/3, 2/5, 3/5, 2/3, and 11/15.

The Ricean, Rayleigh, and 0 dB Echo channel models with and without constellation rotation simulation are employed. Also, the same BER criteria as in the previous sections are used. So Table 4.3 shows the results before and after applying a constellation rotation scheme for QPSK, 16-QAM, and 64-QAM modes. Moreover, the same table presents diversity gains produced by adopting the constellation rotation in the T2-Lite system. Simultaneously, the graphical representation for diversity gains and BER curves are kept pending the next part.

4.5 T2-Lite Profile with DVB-NGH BICM Module Results

This part covers the modification of the T2-lite profile by replacing its original BICM module. This module is replaced by DVB-NGH BICM module. It is made up of a subset of T2-Lite BICM components with more added functionality. For the current part, the same parameter configurations from the previous part are adopted with code rates of 5/15, 6/15, 9/15, 10/15, and 11/15.

The simulation includes three types of fading channel profiles: Ricean, Rayleigh, and 0 dB Echo channels. Furthermore, the current part involves three modulation modes: QPSK, 16-QAM, and 64-QAM.

DVB-NGH BICM module is simulated using both constellation rotation techniques, two and four-dimensional constellation rotation, for the same BER consideration as in previous parts. It's worth mentioning that the four-dimensional rotation is applied to the configuration of QPSK and 9/15, 10/15, and 11/15 coding rates, while all other configurations adopt two-dimensional rotation.

The generated data are passed through the several sub-blocks of the transmitter chain as previously explained till they reach to constellation rotation sub-block of DVB-NGH BICM module. The NGH constellation rotation performs two types of rotation schemes two and four-dimensional rotation. The two-dimensional technique uses a distinct rotation process based on a 2x2 rotation matrix to complete the same output arrangement as previous systems.

The four-dimensional technique uses a 4x4 orthogonal rotation matrix to achieve the rotation scheme. This matrix is formed by using a and b parameters according to QPSK mode and coding rates. The input vector of the rotation matrix in 4D rotation must be the real and imaginary parts of two adjacent cells from the cell interleaver sub-block. Fig. 4.18 displays the output of constellation rotation sub-block with the 4D technique.

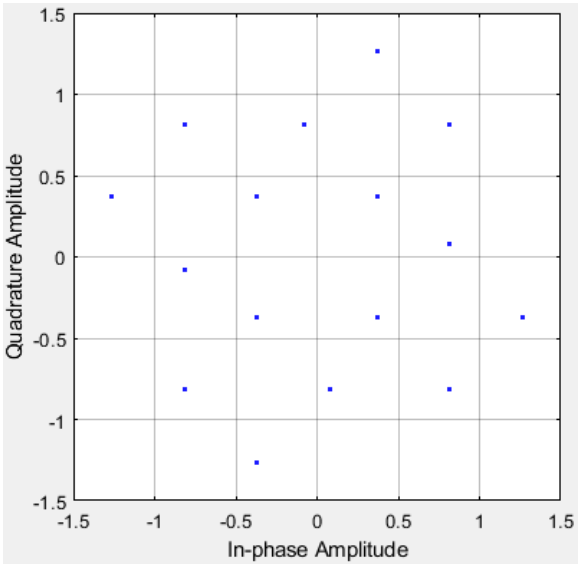

Fig. 4.18 Four-dimensional rotation for QPSK modulation with DVB-NGH BICM module

The following process is the advanced I/Q component interleaver. For the current configuration, the number of dimension rotation N_D is four and $N_r=N_D$ while the cyclic shift of the quadrature component is equal to $N_D/2$ for every column. The output cells of the I/Q component interleaver are produced by combining the In-phase and quadrature parts of the two matrices in the row-wise reading arrangement.

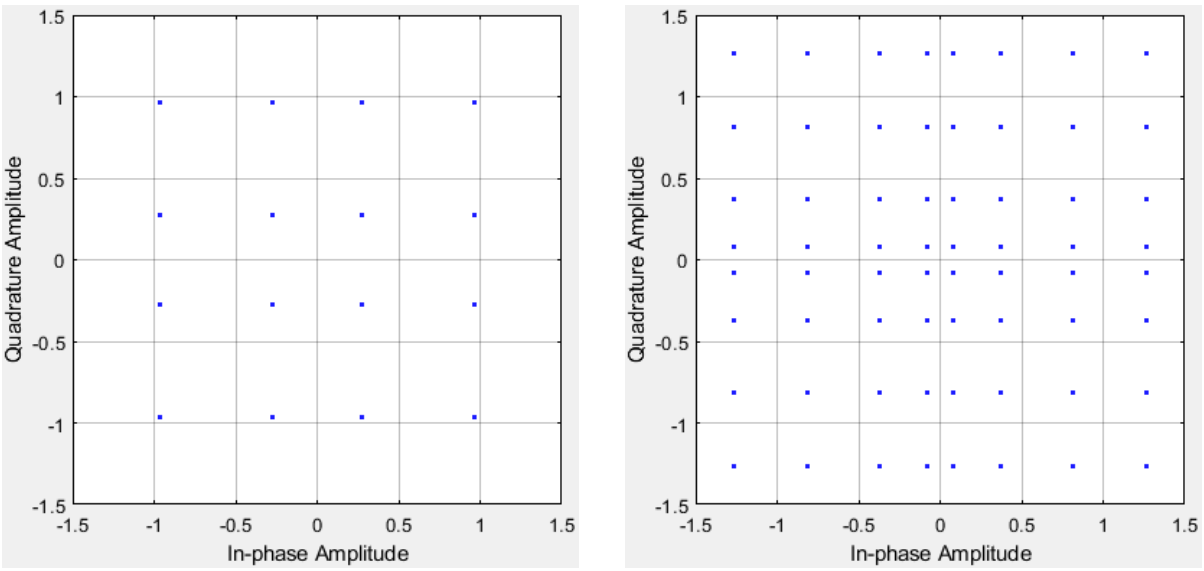

(a) (b)

Fig. 4.19 Virtual constellation after I/Q component interleaver with (a) 2D, and (b) 4D rotation

The obtained virtual constellation after applying I/Q component interleaver is similar to transmit high-order constellation sizes. For the QPSK modulation with 2D or 4D rotation configuration, the virtual constellation seems to be an irregular 16-QAM or 64-QAM constellation, respectively. The output of the I/Q component interleaver for both dimensions rotation is given in Fig. 4.19 above.

The output of the pilot insertion sub-block from the OFDM generation module is displayed in Fig. 4.20. This output is according to the case of four-dimensional constellation rotation with QPSK modulation. The pilot insertion output is essential for the channel estimate comparison as presented below.

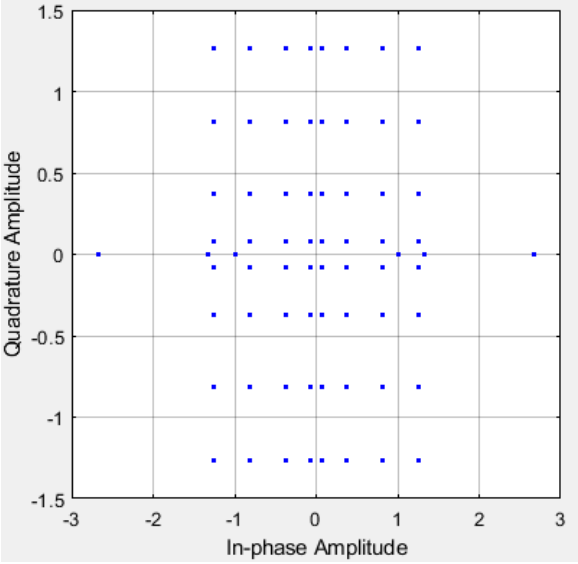

Fig. 4.20 Pilot insertion output for QPSK and four-dimensional rotation

The received T2-Lite signal with DVB-NGH BICM before and after the channel equalization sub-block is given in Fig. 4.21 and Fig. 4.22 as illustrations with Ricean and Rayleigh channel models. These figures are considered according to QPSK modulation mode with a four-dimensional rotation approach.

The results of the T2-Lite with DVB-NGH BICM module for the supplied modulation modes and channel models are shown in Table 4.4. Simultaneously,

it displays the diversity gains obtained by replacing the T2-Lite BICM with the DVB-NGH BICM module.

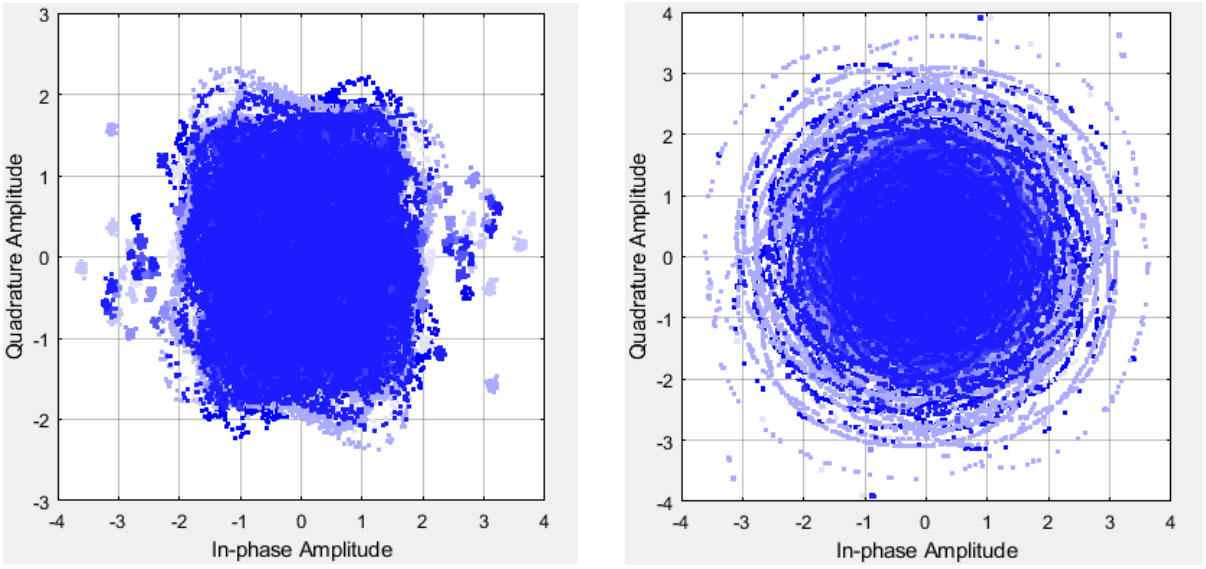

(a) (b)

Fig. 4.21 Received T2-Lite signal with DVB-NGH BICM before equalization with 4D rotation and QPSK modulation (a) Ricean, (b) Rayleigh

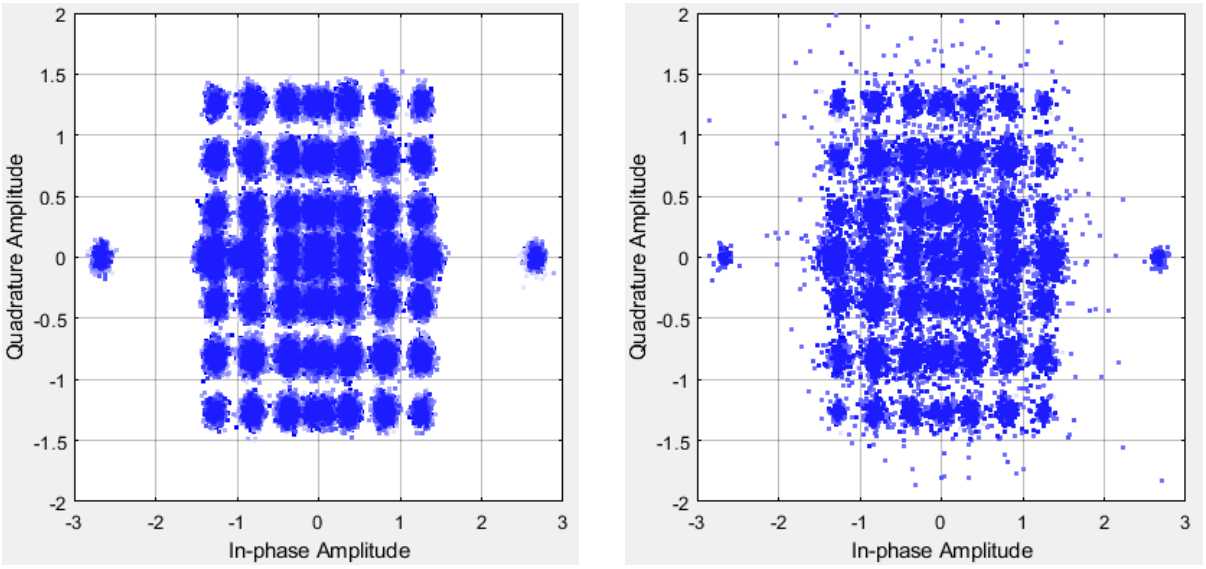

(a) (b)

Fig. 4.22 Received T2-Lite with DVB-NGH BICM signal after equalization with 4D rotation and QPSK modulation (a) Ricean, (b) Rayleigh

Fig. 4.23 shows the diversity gain obtained with the T2-Lite system and constellation rotation. The same figure depicts the diversity gain after replacing the existing T2-Lite BICM with DVB-NGH BICM Module. The DVB-NGH BICM module's resulting gain is linked to the use of 2D and 4D rotation schemes based on coding rate and constellation size.

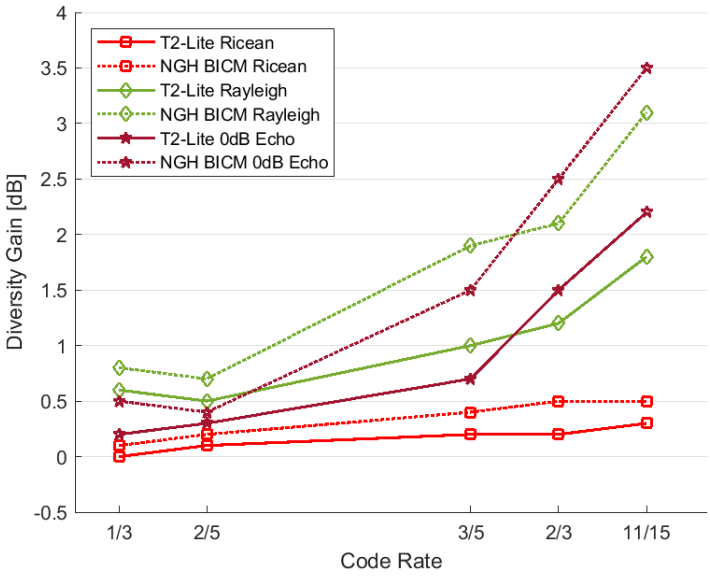

(a)

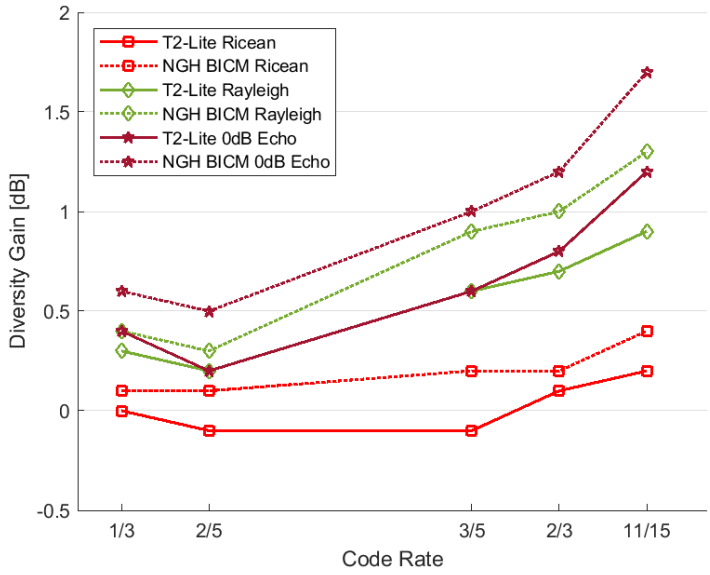

(b)

Fig. 4.23 T2-Lite diversity gain with and without DVB-NGH BICM (a) QPSK and (b)16-QAM

As demonstrated in Fig. 4.23 (a), the diversity gains from using constellation rotation in the T2-Lite profile for Ricean, Rayleigh, and 0 dB Echo channels are 0.3, 1.8, and 2.2 dB with QPSK modulation and coding rate of 11/15, respectively. In addition, When adopting the DVB-NGH BICM module with the four-dimensional constellation rotation scheme instead of the original T2-Lite BICM module, the gain values are 0.5, 3.1, and 3.5 dB for the same system configuration and channel condition.

Three coding rates are used to compute the Bit Error curves for the T2-Lite profile with QPSK modulation type: 3/5, 2/3, and 11/15. The T2-Lite BER curves are computed for the case of applying constellation rotation and cyclic Q delay scheme.

For T2-Lite with DVB-NGH BICM module, the BER curves are obtained for the same modulation type and code rates of 9/15, 10/15, and 11/15. These configuration parameters represent the state of four-dimensional constellation rotation. In Fig. 4.24, the simulation shows the BER curves for the T2-Lite profile with and without DVB-NGH BICM module.

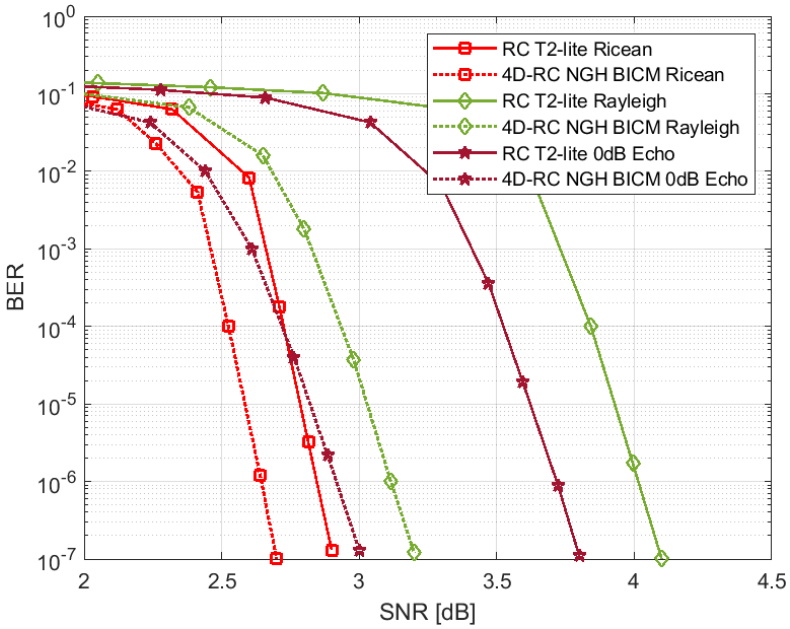

(a)

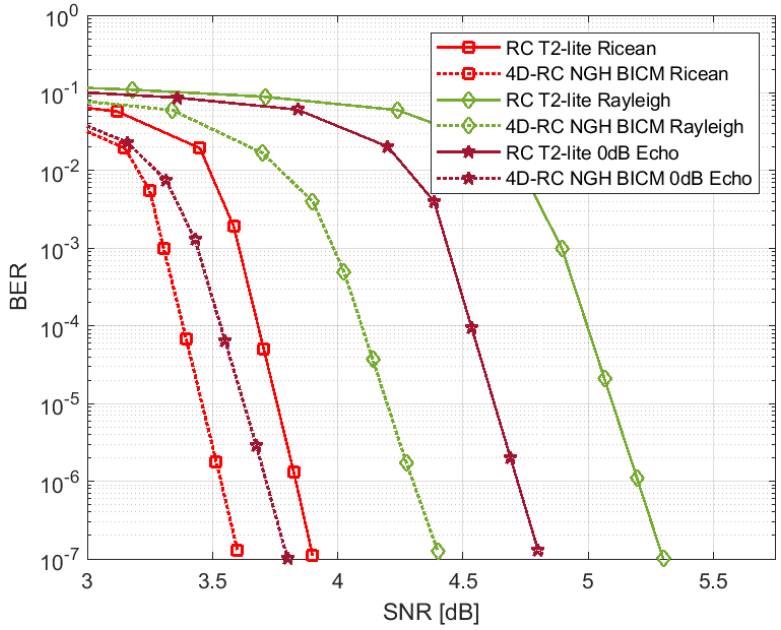

(b)

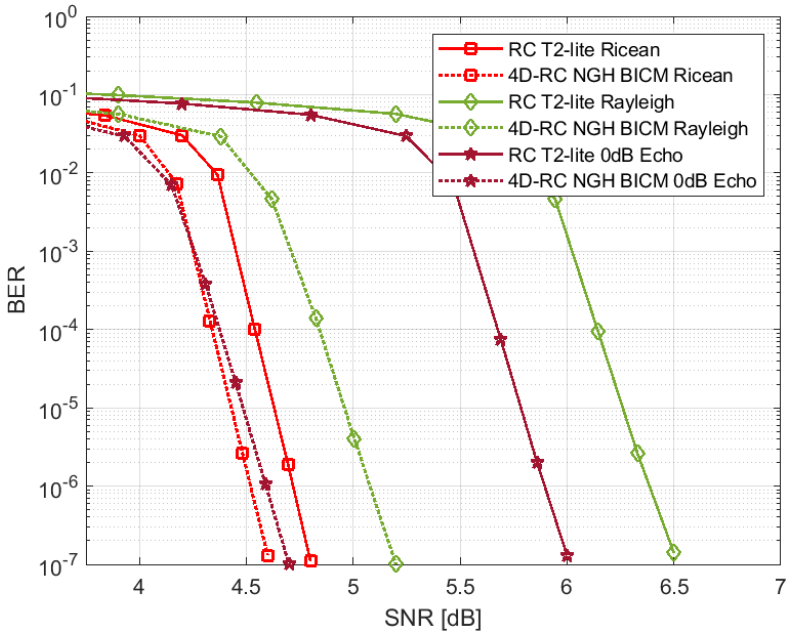

(c)

Fig. 4.24 T2-Lite BER with and without DVB-NGH BICM for QPSK modulation and code rate of (a) 3/5, (b) 2/3, and (c) 11/15

The T2-Lite profile needs an SNR of 6.26 dB to achieve a BER of $1*10^{-5}$ after LDPC coding when it applies constellation rotation with QPSK modulation and code rate of 11/15 over the Rayleigh channel model. This value of SNR

becomes 4.96 dB when adopting the DVB-NGH BICM module instead of the T2-Lite BICM module to achieve the corresponding BER for the same system configuration and fading module. The gain, in this case, results in additional diversity to enhance the T2-Lite system robustness obtained from using the DVB-NGH BICM module.

- **Non-uniform 64-QAM Results**

Non-uniform constellations provided by DVB-NGH BICM module attempt to make the constellation distribution broadcast appear more Gaussian. The equivalent improvement is referred to as non-uniform gain, and it adds up to the coding gain of coded modulation schemes. Each code rate has a specific constellation point value to form constellation diagram according to a given coding rate as illustrated in Fig. 4.25 for NU-64-QAM and 5/15 coding rate. Moreover, Table 4.5 show the results of NU-64-QAM before and after applying constellation rotation scheme with the achieved gain for T2-Lite when adopting DVB-NGH BICM module.

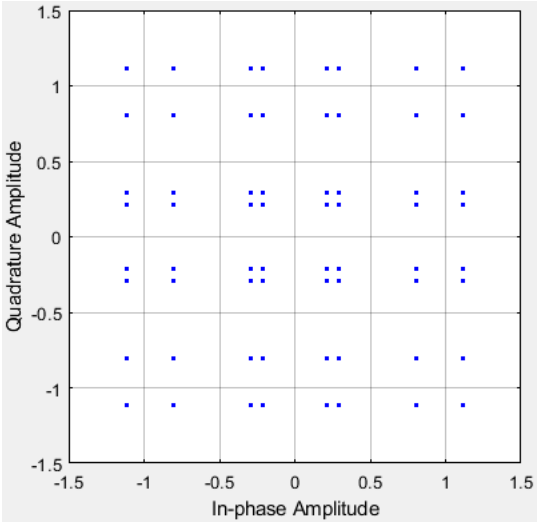

Fig. 4.25 Cell mapper output for NU-64-QAM and 5/15 coding rate

The work presented in [18] studied the performance of the rotated constellation adopted in the second-generation terrestrial system. In order to compare the thesis with this work there are certain points should be cleared. The author was used only 0db echo channel with a bit error rate criteria of $1*10^{-5}$. Moreover, the performance is tested only with one coding rate (1/2) and two modulation mode and no mention for the used type of time interleaver and the number of FEC blocks.

The work supplied by [30] presented an overview of the multi-input single-output transmission mode and demonstrate limitations in terms of the guard interval and pilot pattern selection form theoretical point of view. There are many different between this research and the thesis such as applying the MISO mode by using physical layer simulation with different type of fading scenarios given for MISO channel transmission mode. Furthermore, the MISO mode is tested with SISO mode in SFNs environments with different modulation modes and all coding rate supported by DVB-T2 system. The other important points is employing the constellation rotation and cyclic Q delay together with MISO mode and display the diversity gain resulting from adopting both schemes in the SFNs environments.

4.6 Discussion

The achieved results are discussed in the following points:

- **In the first part,** the performance of the DVB-T2 system with and without the constellation rotation technique has been simulated. This performance is directly related to the diversity gain. It is a central parameter viewed in the comparison to show the performance associated with the constellation rotation, and BER curves are also considered.

  It has been demonstrated that constellation rotation features can provide a high diversity gain in the presence of severe fading. For low constellation

sizes, such as QPSK, this advantage is significant. It has also been found that employing a high coding rate 5/6 can yield excellent gains by 3.6 dB from Table 4.1 rather than a low rate because the system relies on the diversity provided by this feature.

- **In the second part,** the MISO diversity gain for the DVB-T2 in SFNs environment has been investigated. The obtained gain shows the benefit of using MISO mode as compared to the traditional SISO mode in SFNs. BER curves are also considered in the comparison to deliver the performance connected with the MISO mode.

  It has been shown that the modified Alamouti MISO mode essentially improves the signal reception quality in SFN areas. The simulation results show that maximum MISO gain is 3.3 dB can be achieved from low modulation type QPSK and high code rate 5/6 in the Rayleigh MISO channel profile as given in Table 4.2. At the same condition and system configuration parameters this gain can be extended to 4.3 dB when adopting both MISO transmission mode and constellation rotation with cyclic Q delay schemes.

- **In the third part,** the T2-Lite profile has been simulated with and without the constellation rotation technique. Also, the diversity gain for the T2-Lite BICM module with constellation rotation has been obtained.

  It has been shown that the T2-Lite BICM with constellation rotation trait can supply a good diversity gain of 2.2 and 1.8 dB for the 0 dB echo and Rayleigh channel models, respectively, when employing QPSK modulation and the 11/15 coding rate as marked in Table 4.3.

- **In the fourth part,** the T2-Lite profile with DVB-NGH BICM module has been proposed and simulated. The diversity gain from performing this modification has been obtained for two and four-dimensional constellation

rotation techniques. This module can provide an excellent diversity gain of 3.5 and 3.1 dB for the same T2-lite BICM configurations regarding the constellation, coding rates, and fading models as addressed in Table 4.4.

Chapter Five

Conclusions and Suggestions for Future Works

5.1 Conclusions

In this thesis, some concluding remarks are provided on which points are the following:

i. The first objective involves obtaining diversity gain for DVB-T2 system when adopting constellation rotation technique.

ii. The simulation was curried out on eight fading channels, AWGN, Ricean, Rayleigh, 0 dB Echo, DTGlong, DTGmedium, DTGshort, and TU06 with different parameters configurations.

iii. The diversity gain is 3.6 dB, when adopting small constellation sizes and a high coding rate (QPSK with 5/6 code rate over 0 dB Echo fading), as given in Table 4.1.

iv. The additional diversity enhances the operation of the BICM module in various fading channel environments, resulting in an overall improvement of DVB-T2 performance.

v. The second objective aims to obtain the diversity gain associated with the MISO transmission mode for the DVB-T2 system in single-frequency networks operation.

vi. MISO transmission mode improves DVB-T2 system performance due to the elimination of destructive interference at the receiver, resulting from overlaying the two SISO signals in SFNs.

vii. The maximum MISO diversity gain 3.3dB is realized with QPSK mode and the high coding rate (5/6) in the Rayleigh MISO channel model, as given in Table 4.2.

viii. The MISO diversity gain can be extended to 4.3dB when adopting both MISO transmission mode and constellation rotation with cyclic Q delay schemes in SFNs, as specified in Table 4.2.

ix. The MISO gain submit extra robustness to enhance the data rate while keeping the same field strength by increasing the modulation order or the coding rate.

x. The third objective focuses on gaining diversity from utilizing the constellation rotation technique and cyclic Q delay with the T2-Lite profile.

xi. A good T2-Lite diversity gain 2.2dB can be obtained from constellation rotation with QPSK modulation and the 11/15 coding rate over the 0 dB Echo model, as illustrated in Table 4.3.

xii. The fourth objective covers the diversity gain from combining the DVB-NGH BICM module with the T2-Lite profile with two and four-dimensional constellation rotation techniques.

xiii. Combining the high code rate 11/15 and BICM module of DVB-NGH with four-dimensional constellation rotation (QPSK) supplies additional robustness presented by diversity gain of 3.5dB as shown in Table 4.4.

xiv. This robustness improves the proposed system performance, making DVB-NGH a promising technology for future terrestrial multimedia broadcasting systems over existing mobile broadcasting standards.

xv. The four-dimensional rotation is used only with QPSK modulation due to complexity consideration at the de-mapper process.

5.2 Suggestions for Future Works

The following ideas can be utilized as future development to the existing work:

i. The possibility of using MIMO terrestrial profile of DVB-NGH such as MIMO rate-1, MIMO rate-2 techniques and enhanced single-frequency networks (eSFN).

ii. Applying Time-Frequency Slicing (TFS) together with inter frame interleaving proposed in the next-generation handheld.

iii. Implement the overall DVB-T2 system by using field-programmable gate array (FPGA) boards.

REFERENCES

[1] L. Julianawati, Q. A'yun, M. E. Anggraeni and R. Faradisa, "Performance Evaluation of DVB-T2 TV Broadcast For Fixed Reception," *2019 International Electronics Symposium (IES)*, pp. 510-515, 2019.

[2] A. C. Honfoga, M. Dossou and V. Moeyaert, "Performance comparison of new waveforms applied to DVB-T2 transmissions," *2020 IEEE International Symposium on Broadband Multimedia Systems and Broadcasting (BMSB)*, pp. 1-6, 2020.

[3] M. Mendicute, I.Sobrón, L. Martínez, and P. Ochandiano, "DVB-T2: new signal processing algorithms for a challenging digital video broadcasting standard", *Digital Video*, Floriano De Rango, IntechOpen, Croatia, pp. 185-206, 2010.

[4] L. Vangelista et al., "Key technologies for next-generation terrestrial digital television standard DVB-T2," *in IEEE Communications Magazine*, vol. 47, no. 10, pp. 146-153, October 2009.

[5] ETSI TS 102 831, Technical Specification, "*Digital Video Broadcasting (DVB), Implementation guidelines for a second generation digital terrestrial television broadcasting system (DVB-T2)*," v 1.2.1, 2012.

[6] L. Polak, O. Kaller, L. Klozar, J. Sebesta, and T. Kratochvil, "Exploring and measuring possible co-existences between DVB-T2-Lite and LTE systems in ideal and portable fading channels," *Journal of Applied Research and Technology*, vol. 13, no. 1, pp. 32-44, 2015.

[7] W. Fischer, "*Digital video and audio broadcasting technology a practical engineering guide*", Fourth Edition, Springer Nature Switzerland, pp. 759-804, 2020.

[8] R. Beutler, "*The digital dividend of terrestrial broadcasting*," Germany, Springer Science+Business Media, LLC, 2012.

[9] D. Gomez-Barquero, "*Next generation mobile broadcasting*," CRC Press, Taylor & Francis Group, LLC, 2013.

[10] K. Staniec, "Analysis of the single frequency network gain in digital audio broadcasting networks," *Sensors*, vol. 21, no. 2, 569, 2021.

[11] M. V. Guerra et al., "Channel characteristics for fixed and portable DTV reception in a single frequency network," *Journal of Microwaves, Optoelectronics and Electromagnetic Applications*, vol. 18, no. 3, pp. 439-451, 2019.

[12] W. Wen, J. Tian, M. Li and G. Li, "Reduction of physical layer signaling overhead in DVB-NGH systems," *2015 10th International Conference on Communications and Networking in China (ChinaCom)*, , pp. 719-723, 2015.

[13] ETSI EN 303 105, DVB Document A160, "*Digital Video Broadcasting (DVB), "Next Generation Broadcasting System to Handheld, Physical Layer Specification (DVB-NGH)*,", v 1.1.1, 2013.

[14] C. Abdel Nour and C. Douillard, "Rotated QAM constellations to improve BICM performance for DVB-T2," *2008 IEEE 10th International Symposium on Spread Spectrum Techniques and Applications*, pp. 354-359, 2008.

[15] D. Pérez-Calderón et al., "Rotated constellation for DVB-T2," *XXIV Conference on Design of Circuits and Integrated Systems*, University of Zaragoza, 2009.

[16] N. Cornillet et al., "Performance of the DVB-T2 system in a Single Frequency Network: Analysis of the distributed alamouti scheme," *2011 IEEE International Symposium on Broadband Multimedia Systems and Broadcasting (BMSB)*, pp. 1-4, 2011.

[17] O. Karakuş, “European terrestrial digital television receiver performance comparison study under strong multipath interference”, Master Thesis, *The Graduate School of Engineering and Sciences of İzmir Institute of Technology*, İZMİR, 2011.

[18] L. Polak, and T. Kratochvil, “Performance of the rotated constellation in DVB-T2,” *ICDT 2012: The Seventh International Conference on Digital Telecommunications*, Chamonix / Mont Blanc, France, 2012.

[19] L. Dai et al., “Next-generation digital television terrestrial broadcasting systems: Key technologies and research trends,” *in IEEE Communications Magazine*, vol. 50, no. 6, pp. 150-158, 2012.

[20] C. Douillard and C. Abdel Nour, “The bit interleaved coded modulation module for DVB-NGH: enhanced features for mobile reception,” *2012 19th International Conference on Telecommunications (ICT)*, pp. 1-6, 2012.

[21] L. Polak and T. Kratochvil, “DVB-T and DVB-T2 performance in fixed terrestrial TV channels,” *2012 35th International Conference on Telecommunications and Signal Processing (TSP)*, pp. 725-729, 2012.

[22] D. Tralic et al., “Simulation and measurement of DVB-T2 channel characteristics,” *Proceedings ELMAR-2012*, Zadar, Croatia, pp. 83-88, 2012.

[23] D. Gozálvez et al., “Rotated Constellations for Improved Time and Frequency Diversity in DVB-NGH,” *in IEEE Transactions on Broadcasting*, vol. 59, no. 2, pp. 298-305, 2013.

[24] M. Dąbrowski, “Investigation of digital terrestrial television receiver architectures for DVB-T2 standard,” Ph. D. Thesis, *Warsaw University of Technology*, Warsaw, 2013.

[25] I. Eizmendi et al., “DVB-T2: The second generation of terrestrial digital video broadcasting system,” *in IEEE Transactions on Broadcasting*, vol. 60, no. 2, pp. 258-271, 2014.

[26] D. Gómez-Barquero, et al., “DVB-NGH: The Next Generation of Digital Broadcast Services to Handheld Devices,” *in IEEE Transactions on Broadcasting*, vol. 60, no. 2, pp. 246-257, 2014.

[27] E. Dumic et al., “Simulating DVB-T to DVB-T2 migration opportunities in Croatian TV broadcasting,” *2014 22nd International Conference on Software, Telecommunications and Computer Networks (SoftCOM)*, pp. 206-210, 2014.

[28] D. A. Samoa et al. , “A performance study of DVB-T2 and DVB-T2-Lite for mobile reception”, *Digital Signal Processing*, Elsevier Inc., vol. 37, pp. 35-42, 2015.

[29] M. Kaur, “Performance improvement of data transmission through DVB-T2 based Wireless system.” Master Thesis, *Lovely Professional University Punjab*, India, 2017.

[30] L. Andoni and A. Biberaj, “Multi-Antenna systems in DVB-T2/SFN networks, *International Refereed Journal of Engineering and Science (IRJES),*” vol. 8, no. 1, pp. 66-70, 2019.

[31] H. J. Kim et al., “Performance Analysis of LDM and TDM systems for Three PLPs in DVB-T2,” *2020 International Conference on Electronics, Information, and Communication (ICEIC)*, pp. 1-3, 2020.

[32] L. Polak et al., “On the Performance of DVB-T2 MISO System: Special Fixed Transmission Scenarios,” *2021 31st International Conference Radioelektronika (RADIOELEKTRONIKA)*, pp. 1-4, 2021.

[33] DTT system implemented or adopted, (Source: DVB/EBU/BNE DTT Deployment Database, April 2021), Available at: https://dvb.org/solutions/dtt-deployment-data/, Access Time: 1/9/2021.

[34] ETSI EN 302 755, European Standard, “*Digital Video Broadcasting (DVB), Frame structure channel coding and modulation for a second*

generation digital terrestrial television broadcasting system (DVB-T2)," v 1.4.1, 2015.

[35] S. Correia et al., "DVB-T2 modulator design supporting multiple PLP and auxiliary streams," *2010 IEEE International Symposium on Broadband Multimedia Systems and Broadcasting (BMSB)*, pp. 1-6, 2010.

[36] R. N. C. Khalanyane, F. Takawira and O. O. Oyerinde, "PLP scheduling schemes for MPLP transmission of SVC services in DVB-T2," *2017 Global Wireless Summit (GWS)*, pp. 175-180, 2017.

[37] H. A. Fahmy Amin, "Efficient design and implementation of DVB-T2 modules on FPGA," Master Thesis, *Arab Academy for Science, Technology and Maritime Transport*, Cairo, 2015.

[38] A. -C. Honfoga, M. Dossou, P. Dassi and V. Moeyaert, "Joint use of 5G waveform UFMC and Non Uniform Constellations in DVB-T2," *2020 6th IEEE Congress on Information Science and Technology (CiSt)*, pp. 430-435, 2020.

[39] L. Polak and T. Kratochvil, "Behavior of the BICM module of the DVB-T2 standard in the MRE channel with erasures," *2013 23rd International Conference Radioelektronika (RADIOELEKTRONIKA)*, pp. 316-319, 2013.

[40] M. LI, "Design, implementation and prototyping of an iterative receiver for bit-interleaved coded modulation system dedicated to DVB-T2," Ph.D. Thesis, *Signal and Image processing, Télécom Bretagne, Université de Bretagne-Sud*, 2012.

[41] I. Kang, K. Ok, Y. Kim, J. H. Seo, H. M. Kim and H. Kim, "Design of a bit interleaver for the high-order constellation DVB-T2 system," *2014 IEEE International Symposium on Broadband Multimedia Systems and Broadcasting*, pp. 1-4, 2014.

[42] ITU-RBT.2254-4, "Frequency and network planning aspects of DVBT-2," BT Series Broadcasting service (television), 2020.

[43] D. Alfonso Pérez, “Diversity techniques for DVB cutting-edge systems,” Ph.D. Thesis, *Higher Technical School of Engineering, Sevilla University*, Sevilla, 2017.

[44] D. Gozalvez, D. Gomez-Barquero, D. Vargas and N. Cardona, “Time diversity in mobile DVB-T2 systems,” *in IEEE Transactions on Broadcasting*, vol. 57, no. 3, pp. 617-628, 2011.

[45] D. Gozalvez, D. Vargas, D. Gómez-Barquero and N. Cardona, "Performance evaluation of DVB-T2 time interleaving in mobile environments," *2010 IEEE 72nd Vehicular Technology Conference-Fall*, pp. 1-5, 2010.

[46] A. Eldieb, M. Saleh, and S. Elramly, “A comparative study of channel estimation techniques for OFDM in DVB-T2,” *International Journal of Computer Applications*, vol. 91, no. 14, pp. 21-25, 2014.

[47] N. Surantha et al., “ Channel estimation for a MISO DVB-T2 system in high-speed environments,” *Journal of Signal Processing*, vol. 17, no. 5, pp. 179-188, 2013.

[48] M. Tormos, C. Tanougast, A.Dandache, D. Masse and P. Kasser, “Modeling and performance evaluations of Alamouti technique in a single frequency network for DVB-T2,” *EURASIP Journal on Wireless Communications and Networking 2013*, 78, 2013.

[49] S.D Santumon and B.R. Sujatha, “Space-Time Block Coding (STBC) for wireless networks,” *International Journal of Distributed and Parallel Systems (IJDPS)*, vol. 3, no. 4, 2012.

[50] A. Omri, R. Hamila, A. Hazmi, R. Bouallegue and A. Al-Dweik, “Enhanced Alamouti decoding scheme for DVB-T2 systems in SFN channels,” *2011 IEEE 22nd International Symposium on Personal, Indoor and Mobile Radio Communications*, pp. 1626-1630, 2011.

[51] S. M. Alamouti, “A simple transmit diversity technique for wireless communications,” *in IEEE Journal on Selected Areas in Communications*, vol. 16, no. 8, pp. 1451-1458, 1998.

[52] B. Akbarian, and S. G. Maghrebi, “Better performance of new generation of digital video broadcasting-terrestrial (DVB-T2) using Alamouti scheme with cyclic delay diversity,” *Journal of Information Systems and Telecommunication*, vol. 3, no. 2, 2015.

[53] L. Fu, S. Sun, X. Jing and H. Huang, “Analysis of pilot patterns and channel estimation for DVB-T2,” *2010 2nd IEEE International Conference on Network Infrastructure and Digital Content*, pp. 609-613, 2010.

[54] H. Khoshnevis, “Pilot signature based detection of DVB-T2 broadcasting signal for cognitive radio,” *2012 Third International Conference on The Network of the Future (NOF)*, pp. 1-5, 2012.

[55] T. Kratochvil and L. Polak, “Measurement of the DVB-T2 with 256QAM rotated constellation and 32K extended mode in relation to variable pilot patterns,” *2013 IEEE International Symposium on Broadband Multimedia Systems and Broadcasting (BMSB)*, pp. 1-4, 2013.

[56] T. Mata, P. Boonsrimuang and P. Boontra, “A PAPR reduction scheme based on improved PTS with ABC algorithm for OFDM signal,” 2018 15th International Conference on Electrical Engineering/Electronics, Computer, Telecommunications and Information Technology (ECTI-CON), pp. 469-472, 2018.

[57] M. Mroué, A. Nafkha and J. Palicot, “An innovative low complexity PAPR reduction TR-based technique for DVB-T2 system,” *International Congress on Ultra Modern Telecommunications and Control Systems*, pp. 148-153, 2010.

[58] Z. Zheng and G. Li, “An efficient FPGA design and performance testing of the ACE algorithm for PAPR reduction in DVB-T2 systems,” in IEEE Transactions on Broadcasting, vol. 63, no. 1, pp. 134-143, 2017.

[59] M. Mroue, A. Nafkha, J. Palicot, B. Gavalda, and N. Dagorne, “Performance and implementation evaluation of TR PAPR reduction methods for DVB-T2,” *International Journal of Digital Multimedia Broadcasting*, vol. 2010, ID 797393, 2010.

[60] S. Cazalens, G. Lesthievent, B. Ros and C. Boustie, “Theoretical study of P1 detection (synchronisation for DVB-T2 standard),” *2013 36th International Conference on Telecommunications and Signal Processing (TSP)*, pp. 249-253, 2013.

[61] C. Dai, Q. Gu, F. Liu and H. Sun, “Robust preamble design for OFDM broadcast system over dispersive fading channels,” *2014 9th IEEE Conference on Industrial Electronics and Applications*, pp. 888-890, 2014.

[62] L. Polak, D. Plaisner, O. Kaller, J. Milos and T. Kratochvil., “Coexistence between DVB-T2-Lite and LTE downlink networks in advanced mobile fading channels-partial overlapping RF spectrum,” *2016 39th International Conference on Telecommunications and Signal Processing (TSP)*, pp. 458-461, 2016.

[63] L. Martínez, J. Robert, H. Meuel, I. Sobrón and M. Mendicute, “Improved robustness for channel estimation without pilots for DVB-T2,” *2010 IEEE International Symposium on Broadband Multimedia Systems and Broadcasting (BMSB)*, pp. 1-5, 2010.

[64] D. Vargas, D. Gozalvez, D. Gómez-Barquero and N. Cardona. “Multi antenna techniques for Digital Video Broadcasting (DVB) systems,” *Waves*, (4), pp. 79-88, 2012.

[65] I. G. P. Astawa and T. B. Santoso, “Analysis of performance DVB-T2 using MIMO system over MMSE channel estimation,” *2016 IEEE Region 10 Symposium (TENSYMP)*, pp. 299-304, 2016.

[66] E. Miloud Reyouchi, K. Ghoumid, K. Amezian, and O. Mrabet, “MIMO-OFDM coded for digital terrestrial television broadcasting systems,” *International Journal of Electronics and Communication Engineering*, vol. 7, no. 4, 2013.

[67] D. Vargas, D. Gozalvez, D. Gomez-Barquero and N. Cardona, “MIMO for DVB-NGH, the next generation mobile TV broadcasting,” *in IEEE Communications Magazine*, vol. 51, no. 7, pp. 130-137, 2013.

[68] S. Cho, S. Ji, I. Hwang, C. You, “Obtaining diversity and coding gains for digital terrestrial television by using a coded cooperative MIMO transmission scheme,” *Wireless Personal Communications*, vol. 78, pp. 561–577, 2014.

[69] Z. Wu, X. Gao and C. Jiang, “Nonbinary LDPC-coded spatial multiplexing for rate-2 MIMO of DVB-NGH system,” *in IEEE Transactions on Broadcasting*, vol. 64, no. 2, pp. 201-210, 2018.

[70] T. H. Chowdhury, S. E. Razzaque, and A. Sultana, “Performance analysis of DVB- T2 using MIMO-OFDM technique,” *International Journal of Computer Applications*, vol. 69, no. 20, 2013.

[71] Digital Video Broadcasting (DVB), “Framing structure, channel coding and modulation for digital terrestrial television,” *ETSI EN 300 744*, V1.6.2, 2015.

[72] I. Eizmendi, G. Prieto, G. Berjon-Eriz, M. M. Vélez, A. Arrinda and P. Angueira, “DVB-T2 performance in presence of multipath laboratory tests,” *2011 IEEE International Symposium on Broadband Multimedia Systems and Broadcasting (BMSB)*, pp. 1-6, 2011.

[73] ETSI TR 101 290, Technical Report, “*Digital Video Broadcasting (DVB); Measurement guidelines for DVB systems*,” v1.4.1, 2020.

Appendix A
Calculation of the CRC word

The implementation of Cyclic Redundancy Check codes (CRC-codes) allows the detection of transmission errors at the receiver side. For this purpose CRC words shall be included in the transmitted data. These CRC words shall be defined by the result of the procedure described in this Appendix.

A CRC code is defined by a polynomial of degree *n*:

$$G_n(x) = x^n + g_{n-1}x^{n-1} + \ldots + g_2x^2 + g_1x + 1$$

with $n \geq 1$:

and: $$g_i \in \{0,1\}, \quad i = 1.....n-1$$

The CRC calculation may be performed by means of a shift register containing *n* register stages, equivalent to the degree of the polynomial (see figure A(1). The stages are denoted by b_0... b_{n-1}, where b_0 corresponds to 1, b_1 to *x*, b_2 to x^2,..., b_{n-1} to x^{n-1}. The shift register is tapped by inserting XORs at the input of those stages, where the corresponding coefficients g_i of the polynomial are '1'.

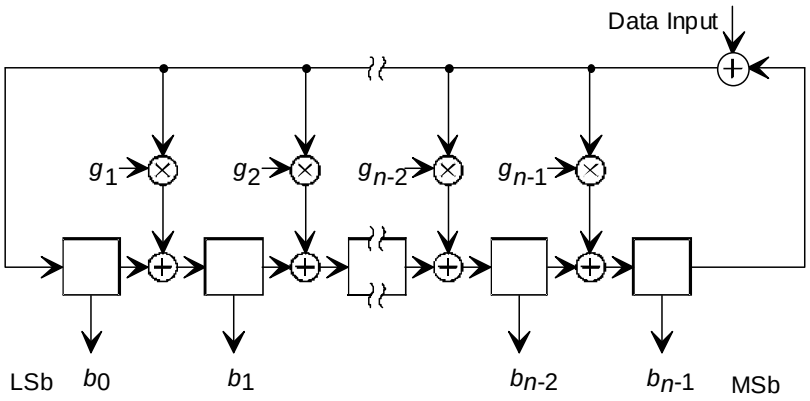

Figure A(1): General CRC block diagram

At the beginning of the CRC-8 calculation (used for GFPS and TS, NM only and BBHEADER), all register stage contents are initialized to zeros.

After applying the first bit of the data block (MSB first) to the input, the shift clock causes the register to shift its content by one stage towards the MSB stage (b_{n-1}), while loading the tapped stages with the result of the appropriate XOR operations. The procedure is then repeated for each data bit. Following the shift after applying the last bit (LSB) of the data block to the input, the shift register contains the CRC word which is then read out. Data and CRC word are transmitted with MSB first.

The CRC codes used in the DVB-T2 system are based on the following polynomial:

- $G_8(x) = x^8 + x^7 + x^6 + x^4 + x^2 + 1$

Appendix B

1. Outer encoding (BCH)

The bits of the baseband frame form the message bits $M = (m_{K_{bch}-1}, m_{K_{bch}-2}, ..., m_1, m_0)$ for BCH encoding, where $m_{K_{bch}-1}$ is the first bit of the BBHEADER and m_0 is the last bit of the BBFRAME (or padding field if present). BCH encoding of information bits $M = (m_{K_{bch}-1}, m_{K_{bch}-2}, ..., m_1, m_0)$ onto a codeword is achieved as follows:

- Multiply the message polynomial $m(x) = m_{K_{bch}-1}x^{k_{bch}-1} + m_{K_{bch}-2}x^{k_{bch}-2} + ... + m_1 x + m_0$ by $x^{N_{bch}-K_{bch}}$.
- Divide $x^{N_{bch}-K_{bch}}\, m(x)$ by $g(x)$, the generator polynomial. Let $d(x) = d_{N_{bch}-K_{bch}-1}x^{N_{bch}-K_{bch}-1} + ... + d_1 x + d_0$ be the remainder.
- Construct the output codeword I, which forms the information word I for the LDPC coding, as follows:

$$I = (i_0, i_1, ..., i_{N_{bch}-1}) = (m_{K_{bch}-1}, m_{K_{bch}-2}, ..., m_1, m_0, d_{N_{bch}-K_{bch}-1}, d_{N_{bch}-K_{bch}-2}, ..., d_1, d_0)$$

NOTE: The equivalent codeword polynomial is $c(x) = x^{N_{bch}-K_{bch}}\, m(x) + d(x)$.

2. Inner encoding (LDPC)

The LDPC encoder treats the output of the outer encoding, $I = (i_0, i_1, ..., i_{K_{ldpc}-1})$, as an information block of size $K_{ldpc} = N_{BCH}$, and systematically encodes it onto a codeword Λ of size N_{ldpc}, where:

$$\Lambda = (\lambda_0, \lambda_1, \lambda_2, ..., \lambda_{N_{LDPC}-1}) = (i_0, i_1, ..., i_{K_{ldpc}-1}, p_0, p_1, ... p_{N_{ldpc}-K_{ldpc}-1}).$$

The LDPC code parameters (N_{ldpc}, K_{ldpc}) are given in table 2.1.

2.1 Inner coding for normal FECFRAME

The task of the encoder is to determine $N_{ldpc} - K_{ldpc}$ parity bits $(p_0, p_1, ..., p_{n_{ldpc}-k_{ldpc}-1})$ for every block of k_{ldpc} information bits, $(i_0, i_1, ..., i_{K_{ldpc}-1})$. The procedure is as follows:

- Initialize $p_0 = p_1 = p_2 = ... = p_{N_{ldpc}-K_{ldpc}-1} = 0$
- Accumulate the first information bit, i_0, at parity bit addresses specified in the first row of tables A.1 through A.6. For example, for rate 2/3 (see table A.3), (all additions are in GF(2)):

$$p_{317} = p_{317} \oplus i_0 \qquad p_{6700} = p_{6700} \oplus i_0$$

$$p_{2255} = p_{2255} \oplus i_0 \qquad p_{9101} = p_{9101} \oplus i_0$$

$$p_{2324} = p_{2324} \oplus i_0 \qquad p_{10057} = p_{10057} \oplus i_0$$

$$p_{2723} = p_{2723} \oplus i_0 \qquad p_{12739} = p_{12739} \oplus i_0$$

$$p_{3538} = p_{3538} \oplus i_0 \qquad p_{17407} = p_{17407} \oplus i_0$$

$$p_{3576} = p_{3576} \oplus i_0 \qquad p_{21039} = p_{21039} \oplus i_0$$

$$p_{6194} = p_{6194} \oplus i_0$$

- For the next 359 information bits, i_m, $m = 1, 2, ..., 359$ accumulate i_m at parity bit addresses $\{x + m \bmod 360 \times Q_{ldpc}\} \bmod (N_{ldpc} - K_{ldpc})$ where x denotes the address of the parity bit accumulator corresponding to the first bit i_0, and Q_{ldpc} is a code rate dependent constant specified in table 2.3. Continuing with the example, $Q_{ldpc} = 60$ for rate 2/3. So for example for information bit i_1, the following operations are performed:

$$p_{377} = p_{377} \oplus i_1 \qquad p_{6760} = p_{6760} \oplus i_1$$

$$p_{2315} = p_{2315} \oplus i_1 \qquad p_{9161} = p_{9161} \oplus i_1$$

$$p_{2384} = p_{2384} \oplus i_1 \qquad p_{10117} = p_{10117} \oplus i_1$$

$$p_{2783} = p_{2783} \oplus i_1 \qquad p_{12799} = p_{12799} \oplus i_1$$

$$p_{3598} = p_{3598} \oplus i_1 \qquad p_{17467} = p_{17467} \oplus i_1$$

$$p_{3636} = p_{3636} \oplus i_1 \qquad p_{21099} = p_{21099} \oplus i_1$$

$$p_{6254} = p_{6254} \oplus i_1$$

- For the 361st information bit i_{360}, the addresses of the parity bit accumulators are given in the second row of the tables A.1 through A.6. In a similar manner the addresses of the parity bit accumulators for the following 359 information bits $i_m, m = 361, 362, ..., 719$ are obtained using the formula $\{x + (m \bmod 360) \times Q_{ldpc}\} \bmod (N_{ldpc} - K_{ldpc})$ where x denotes the address of the parity bit accumulator corresponding to the information bit i_{360}, i.e. the entries in the second row of the tables B.1 through B.6.

- In a similar manner, for every group of 360 new information bits, a new row from tables B.1 through B.6 are used to find the addresses of the parity bit accumulators.

After all of the information bits are exhausted, the final parity bits are obtained as follows:

- Sequentially perform the following operations starting with $i = 1$.

$$p_i = p_i \oplus p_{i-1}, \quad i = 1, 2, ..., N_{ldpc} - K_{ldpc} - 1$$

- Final content of p_i, $i = 0, 1, .., N_{ldpc} - K_{ldpc} - 1$ is equal to the parity bit p_i.

2.2 Inner coding for short FECFRAME

K_{ldpc} BCH encoded bits shall be systematically encoded to generate N_{ldpc} bits as described in clause 2.1, replacing table 2.3 with table 2.4, the tables of B with the tables of BB.

Table 2.4 Q_{ldpc} values for short frames

Code Rate	Q_{ldpc}
1/4	36
1/3	30
2/5	27
1/2	25
3/5	18
2/3	15
3/4	12
4/5	10
5/6	8

Table B For Appendix B
Addresses of parity bit accumulators for N_{ldpc} = 64 800

Example of interpretation of the table B.1.

$p_{54} = p_{54} \oplus i_0$ $p_{9318} = p_{9318} \oplus i_0$ $p_{14392} = p_{14392} \oplus i_0$ $p_{27561} = p_{27561} \oplus i_0$ $p_{26909} = p_{26909} \oplus i_0$ $p_{10219} = p_{10219} \oplus i_0$
$p_{2534} = p_{2534} \oplus i_0$ $p_{8597} = p_{8597} \oplus i_0$

$p_{144} = p_{144} \oplus i_1$ $p_{9408} = p_{9408} \oplus i_1$ $p_{14482} = p_{14482} \oplus i_1$ $p_{27651} = p_{27651} \oplus i_1$ $p_{26999} = p_{26999} \oplus i_1$ $p_{10309} = p_{10309} \oplus i_1$
$p_{2624} = p_{2624} \oplus i_1$ $p_{8687} = p_{8687} \oplus i_1$

: : : : : : : : :

: : : : : : : : :

$p_{32364} = p_{32364} \oplus i_{359}$ $p_{9228} = p_{9228} \oplus i_{359}$ $p_{14302} = p_{14302} \oplus i_{359}$ $p_{27471} = p_{27471} \oplus i_{359}$ $p_{26819} = p_{26819} \oplus i_{359}$
$p_{10129} = p_{10129} \oplus i_{359}$ $p_{2444} = p_{2444} \oplus i_{359}$ $p_{8507} = p_{8507} \oplus i_{359}$

$p_{55} = p_{55} \oplus i_{360}$ $p_{7263} = p_{7263} \oplus i_{360}$ $p_{4635} = p_{4635} \oplus i_{360}$ $p_{2530} = p_{2530} \oplus i_{360}$ $p_{28130} = p_{28130} \oplus i_{360}$
$p_{3033} = p_{3033} \oplus i_{360}$ $p_{23830} = p_{23830} \oplus i_{360}$ $p_{3651} = p_{3651} \oplus i_{360}$

: : : : : : : : :

: : : : : : : : :

Table B1: Rate 1/2 (N_{ldpc} = 64 800)

54 9318 14392 27561 26909 10219 2534 8597	20 19978 27197
55 7263 4635 2530 28130 3033 23830 3651	21 27060 15071
56 24731 23583 26036 17299 5750 792 9169	22 6071 26649
57 5811 26154 18653 11551 15447 13685 16264	23 10393 11176
58 12610 11347 28768 2792 3174 29371 12997	24 9597 13370
59 16789 16018 21449 6165 21202 15850 3186	25 7081 17677
60 31016 21449 17618 6213 12166 8334 18212	26 1433 19513
61 22836 14213 11327 5896 718 11727 9308	27 26925 9014
62 2091 24941 29966 23634 9013 15587 5444	28 19202 8900
63 22207 3983 16904 28534 21415 27524 25912	29 18152 30647
64 25687 4501 22193 14665 14798 16158 5491	30 20803 1737
65 4520 17094 23397 4264 22370 16941 21526	31 11804 25221
66 10490 6182 32370 9597 30841 25954 2762	32 31683 17783
67 22120 22865 29870 15147 13668 14955 19235	33 29694 9345
68 6689 18408 18346 9918 25746 5443 20645	34 12280 26611
69 29982 12529 13858 4746 30370 10023 24828	35 6526 26122
70 1262 28032 29888 13063 24033 21951 7863	36 26165 11241
71 6594 29642 31451 14831 9509 9335 31552	37 7666 26962
72 1358 6454 16633 20354 24598 624 5265	38 16290 8480
73 19529 295 18011 3080 13364 8032 15323	39 11774 10120
74 11981 1510 7960 21462 9129 11370 25741	40 30051 30426
75 9276 29656 4543 30699 20646 21921 28050	41 1335 15424
76 15975 25634 5520 31119 13715 21949 19605	42 6865 17742
77 18688 4608 31755 30165 13103 10706 29224	43 31779 12489
78 21514 23117 12245 26035 31656 25631 30699	44 32120 21001
79 9674 24966 31285 29908 17042 24588 31857	45 14508 6996
80 21856 27777 29919 27000 14897 11409 7122	46 979 25024
81 29773 23310 263 4877 28622 20545 22092	47 4554 21896
82 15605 5651 21864 3967 14419 22757 15896	48 7989 21777
83 30145 1759 10139 29223 26086 10556 5098	49 4972 20661
84 18815 16575 2936 24457 26738 6030 505	50 6612 2730
85 30326 22298 27562 20131 26390 6247 24791	51 12742 4418
86 928 29246 21246 12400 15311 32309 18608	52 29194 595
87 20314 6025 26689 16302 2296 3244 19613	53 19267 20113
88 6237 11943 22851 15642 23857 15112 20947	
89 26403 25168 19038 18384 8882 12719 7093	
0 14567 24965	
1 3908 100	
2 10279 240	
3 24102 764	
4 12383 4173	
5 13861 15918	
6 21327 1046	
7 5288 14579	
8 28158 8069	
9 16583 11098	
10 16681 28363	
11 13980 24725	
12 32169 17989	
13 10907 2767	
14 21557 3818	
15 26676 12422	
16 7676 8754	
17 14905 20232	
18 15719 24646	
19 31942 8589	

Table B.2: Rate 3/5 (N_{ldpc} = 64 800)

22422 10282 11626 19997 11161 2922 3122 99 5625 17064 8270 179 25087 16218 17015 828 20041 25656 4186 11629 22599 17305 22515 6463 11049 22853 25706 14388 5500 19245 8732 2177 13555 11346 17265 3069 16581 22225 12563 19717 23577 11555 25496 6853 25403 5218 15925 21766 16529 14487 7643 10715 17442 11119 5679 14155 24213 21000 1116 15620 5340 8636 16693 1434 5635 6516 9482 20189 1066 15013 25361 14243 18506 22236 20912 8952 5421 15691 6126 21595 500 6904 13059 6802 8433 4694 5524 14216 3685 19721 25420 9937 23813 9047 25651 16826 21500 24814 6344 17382 7064 13929 4004 16552 12818 8720 5286 2206 22517 2429 19065 2921 21611 1873 7507 5661 23006 23128 20543 19777 1770 4636 20900 14931 9247 12340 11008 12966 4471 2731 16445 791 6635 14556 18865 22421 22124 12697 9803 25485 7744 18254 11313 9004 19982 23963 18912 7206 12500 4382 20067 6177 21007 1195 23547 24837 756 11158 14646 20534 3647 17728 11676 11843 12937 4402 8261 22944 9306 24009 10012 11081 3746 24325 8060 19826 842 8836 2898 5019 7575 7455 25244 4736 14400 22981 5543 8006 24203 13053 1120 5128 3482 9270 13059 15825 7453 23747 3656 24585 16542 17507 22462 14670 15627 15290 4198 22748 5842 13395 23918 16985 14929 3726 25350 24157 24896 16365 16423 13461 16615 8107 24741 3604 25904 8716 9604 20365 3729 17245 18448 9862 20831 25326 20517 24618 13282 5099 14183 8804 16455 17646 15376 18194 25528 1777 6066 21855 14372 12517 4488 17490 1400 8135 23375 20879 8476 4084 12936 25536 22309 16582 6402 24360 25119 23586 128 4761 10443 22536 8607 9752 25446 15053 1856 4040 377 21160 13474 5451 17170 5938 10256 11972 24210 17833 22047 16108 13075 9648 24546 13150 23867 7309 19798 2988 16858 4825 23950 15125 20526 3553 11525 23366 2452 17626 19265 20172 18060 24593 13255 1552 18839 21132 20119 15214 14705 7096 10174 5663 18651 19700 12524 14033 4127 2971 17499 16287 22368 21463 7943 18880 5567 8047 23363 6797 10651 24471 14325 4081 7258 4949 7044 1078 797 22910 20474 4318 21374 13231 22985 5056 3821 23718 14178 9978 19030 23594 8895 25358 6199 22056 7749 13310 3999 23697 16445 22636 5225 22437 24153 9442 7978 12177 2893 20778 3175 8645 11863 24623 10311 25767 17057 3691 20473 11294 9914 22815 2574 8439 3699 5431 24840 21908 16088 18244 8208 5755 19059 8541 24924 6454 11234 10492 16406 10831 11436 9649 16264 11275 24953 2347 12667 19190 7257 7174 24819 2938 2522 11749 3627 5969 13862 1538 23176 6353 2855 17720 2472 7428 573 15036 0 18539 18661 1 10502 3002 2 9368 10761 3 12299 7828 4 15048 13362 5 18444 24640 6 20775 19175 7 18970 10971 8 5329 19982 9 11296 18655 10 15046 20659 11 7300 22140 12 22029 14477 13 11129 742 14 13254 13813 15 19234 13273	16 6079 21122 17 22782 5828 18 19775 4247 19 1660 19413 20 4403 3649 21 13371 25851 22 22770 21784 23 10757 14131 24 16071 21617 25 6393 3725 26 597 19968 27 5743 8084 28 6770 9548 29 4285 17542 30 13568 22599 31 1786 4617 32 23238 11648 33 19627 2030 34 13601 13458 35 13740 17328 36 25012 13944 37 22513 6687 38 4934 12587 39 21197 5133 40 22705 6938 41 7534 24633 42 24400 12797 43 21911 25712 44 12039 1140 45 24306 1021 46 14012 20747 47 11265 15219 48 4670 15531 49 9417 14359 50 2415 6504 51 24964 24690 52 14443 8816 53 6926 1291 54 6209 20806 55 13915 4079 56 24410 13196 57 13505 6117 58 9869 8220 59 1570 6044 60 25780 17387 61 20671 24913 62 24558 20591 63 12402 3702 64 8314 1357 65 20071 14616 66 17014 3688 67 19837 946 68 15195 12136 69 7758 22808 70 3564 2925 71 3434 7769

Table B.3: Rate 2/3 (N_{ldpc} = 64 800)

317 2255 2324 2723 3538 3576 6194 6700 9101 10057 12739 17407 21039	10574 11268 17932
1958 2007 3294 4394 12762 14505 14593 14692 16522 17737 19245 21272 21379	15442 17266 20482
127 860 5001 5633 8644 9282 12690 14644 17553 19511 19681 20954 21002	390 3371 8781
2514 2822 5781 6297 8063 9469 9551 11407 11837 12985 15710 20236 20393	10512 12216 17180
1565 3106 4659 4926 6495 6872 7343 8720 15785 16434 16727 19884 21325	4309 14068 15783
706 3220 8568 10896 12486 13663 16398 16599 19475 19781 20625 20961 21335	3971 11673 20009
4257 10449 12406 14561 16049 16522 17214 18029 18033 18802 19062 19526 20748	9259 14270 17199
412 433 558 2614 2978 4157 6584 9320 11683 11819 13024 14486 16860	2947 5852 20101
777 5906 7403 8550 8717 8770 11436 12846 13629 14755 15688 16392 16419	3965 9722 15363
4093 5045 6037 7248 8633 9771 10260 10809 11326 12072 17516 19344 19938	1429 5689 16771
2120 2648 3155 3852 6888 12258 14821 15359 16378 16437 17791 20614 21025	6101 6849 12781
1085 2434 5816 7151 8050 9422 10884 12728 15353 17733 18140 18729 20920	3676 9347 18761
856 1690 12787	350 11659 18342
6532 7357 9151	5961 14803 16123
4210 16615 18152	2113 9163 13443
11494 14036 17470	2155 9808 12885
2474 10291 10323	2861 7988 11031
1778 6973 10739	7309 9220 20745
4347 9570 18748	6834 8742 11977
2189 11942 20666	2133 12908 14704
3868 7526 17706	10170 13809 18153
8780 14796 18268	13464 14787 14975
160 16232 17399	799 1107 3789
1285 2003 18922	3571 8176 10165
4658 17331 20361	5433 13446 15481
2765 4862 5875	3351 6767 12840
4565 5521 8759	8950 8974 11650
3484 7305 15829	1430 4250 21332
5024 17730 17879	6283 10628 15050
7031 12346 15024	8632 14404 16916
179 6365 11352	6509 10702 16278
2490 3143 5098	15900 16395 17995
2643 3101 21259	8031 18420 19733
4315 4724 13130	3747 4634 17087
594 17365 18322	4453 6297 16262
5983 8597 9627	2792 3513 17031
10837 15102 20876	14846 20893 21563
10448 20418 21478	17220 20436 21337
3848 12029 15228	275 4107 10497
708 5652 13146	3536 7520 10027
5998 7534 16117	14089 14943 19455
2098 13201 18317	1965 3931 21104
9186 14548 17776	2439 11565 17932
5246 10398 18597	154 15279 21414
3083 4944 21021	10017 11269 16546
13726 18495 19921	7169 10161 16928
6736 10811 17545	10284 16791 20655
10084 12411 14432	36 3175 8475
1064 13555 17033	2605 16269 19290
679 9878 13547	8947 9178 15420
3422 9910 20194	5687 9156 12408
3640 3701 10046	8096 9738 14711
5862 10134 11498	4935 8093 19266
5923 9580 15060	2667 10062 15972
1073 3012 16427	6389 11318 14417
5527 20113 20883	8800 18137 18434
7058 12924 15151	5824 5927 15314
9764 12230 17375	6056 13168 15179
772 7711 12723	3284 13138 18919
555 13816 15376	13115 17259 17332

Table B.4: Rate 3/4 (N_{ldpc} = 64 800)

0 6385 7901 14611 13389 11200 3252 5243 2504 2722 821 7374	23 5865 1768
1 11359 2698 357 13824 12772 7244 6752 15310 852 2001 11417	24 2655 14957
2 7862 7977 6321 13612 12197 14449 15137 13860 1708 6399 13444	25 5565 6332
3 1560 11804 6975 13292 3646 3812 8772 7306 5795 14327 7866	26 4303 12631
4 7626 11407 14599 9689 1628 2113 10809 9283 1230 15241 4870	27 11653 12236
5 1610 5699 15876 9446 12515 1400 6303 5411 14181 13925 7358	28 16025 7632
6 4059 8836 3405 7853 7992 15336 5970 10368 10278 9675 4651	29 4655 14128
7 4441 3963 9153 2109 12683 7459 12030 12221 629 15212 406	30 9584 13123
8 6007 8411 5771 3497 543 14202 875 9186 6235 13908 3563	31 13987 9597
9 3232 6625 4795 546 9781 2071 7312 3399 7250 4932 12652	32 15409 12110
10 8820 10088 11090 7069 6585 13134 10158 7183 488 7455 9238	33 8754 15490
11 1903 10818 119 215 7558 11046 10615 11545 14784 7961 15619	34 7416 15325
12 3655 8736 4917 15874 5129 2134 15944 14768 7150 2692 1469	35 2909 15549
13 8316 3820 505 8923 6757 806 7957 4216 15589 13244 2622	36 2995 8257
14 14463 4852 15733 3041 11193 12860 13673 8152 6551 15108 8758	37 9406 4791
15 3149 11981	38 11111 4854
16 13416 6906	39 2812 8521
17 13098 13352	40 8476 14717
18 2009 14460	41 7820 15360
19 7207 4314	42 1179 7939
20 3312 3945	43 2357 8678
21 4418 6248	44 7703 6216
22 2669 13975	0 3477 7067
23 7571 9023	1 3931 13845
24 14172 2967	2 7675 12899
25 7271 7138	3 1754 8187
26 6135 13670	4 7785 1400
27 7490 14559	5 9213 5891
28 8657 2466	6 2494 7703
29 8599 12834	7 2576 7902
30 3470 3152	8 4821 15682
31 13917 4365	9 10426 11935
32 6024 13730	10 1810 904
33 10973 14182	11 11332 9264
34 2464 13167	12 11312 3570
35 5281 15049	13 14916 2650
36 1103 1849	14 7679 7842
37 2058 1069	15 6089 13084
38 9654 6095	16 3938 2751
39 14311 7667	17 8509 4648
40 15617 8146	18 12204 8917
41 4588 11218	19 5749 12443
42 13660 6243	20 12613 4431
43 8578 7874	21 1344 4014
44 11741 2686	22 8488 13850
0 1022 1264	23 1730 14896
1 12604 9965	24 14942 7126
2 8217 2707	25 14983 8863
3 3156 11793	26 6578 8564
4 354 1514	27 4947 396
5 6978 14058	28 297 12805
6 7922 16079	29 13878 6692
7 15087 12138	30 11857 11186
8 5053 6470	31 14395 11493
9 12687 14932	32 16145 12251
10 15458 1763	33 13462 7428
11 8121 1721	34 14526 13119
12 12431 549	35 2535 11243
13 4129 7091	36 6465 12690
14 1426 8415	37 6872 9334
15 9783 7604	38 15371 14023
16 6295 11329	39 8101 10187
17 1409 12061	40 11963 4848
18 8065 9087	41 15125 6119
19 2918 8438	42 8051 14465
20 1293 14115	43 11139 5167
21 3922 13851	44 2883 14521
22 3851 4000	

Table B.5: Rate 4/5 (N_{ldpc} = 64 800)

0 149 11212 5575 6360 12559 8108 8505 408 10026 12828	0 5647 4935
1 5237 490 10677 4998 3869 3734 3092 3509 7703 10305	1 4219 1870
2 8742 5553 2820 7085 12116 10485 564 7795 2972 2157	2 10968 8054
3 2699 4304 8350 712 2841 3250 4731 10105 517 7516	3 6970 5447
4 12067 1351 11992 12191 11267 5161 537 6166 4246 2363	4 3217 5638
5 6828 7107 2127 3724 5743 11040 10756 4073 1011 3422	5 8972 669
6 11259 1216 9526 1466 10816 940 3744 2815 11506 11573	6 5618 12472
7 4549 11507 1118 1274 11751 5207 7854 12803 4047 6484	7 1457 1280
8 8430 4115 9440 413 4455 2262 7915 12402 8579 7052	8 8868 3883
9 3885 9126 5665 4505 2343 253 4707 3742 4166 1556	9 8866 1224
10 1704 8936 6775 8639 8179 7954 8234 7850 8883 8713	10 8371 5972
11 11716 4344 9087 11264 2274 8832 9147 11930 6054 5455	11 266 4405
12 7323 3970 10329 2170 8262 3854 2087 12899 9497 11700	12 3706 3244
13 4418 1467 2490 5841 817 11453 533 11217 11962 5251	13 6039 5844
14 1541 4525 7976 3457 9536 7725 3788 2982 6307 5997	14 7200 3283
15 11484 2739 4023 12107 6516 551 2572 6628 8150 9852	15 1502 11282
16 6070 1761 4627 6534 7913 3730 11866 1813 12306 8249	16 12318 2202
17 12441 5489 8748 7837 7660 2102 11341 2936 6712 11977	17 4523 965
18 10155 4210	18 9587 7011
19 1010 10483	19 2552 2051
20 8900 10250	20 12045 10306
21 10243 12278	21 11070 5104
22 7070 4397	22 6627 6906
23 12271 3887	23 9889 2121
24 11980 6836	24 829 9701
25 9514 4356	25 2201 1819
26 7137 10281	26 6689 12925
27 11881 2526	27 2139 8757
28 1969 11477	28 12004 5948
29 3044 10921	29 8704 3191
30 2236 8724	30 8171 10933
31 9104 6340	31 6297 7116
32 7342 8582	32 616 7146
33 11675 10405	33 5142 9761
34 6467 12775	34 10377 8138
35 3186 12198	35 7616 5811
0 9621 11445	0 7285 9863
1 7486 5611	1 7764 10867
2 4319 4879	2 12343 9019
3 2196 344	3 4414 8331
4 7527 6650	4 3464 642
5 10693 2440	5 6960 2039
6 6755 2706	6 786 3021
7 5144 5998	7 710 2086
8 11043 8033	8 7423 5601
9 4846 4435	9 8120 4885
10 4157 9228	10 12385 11990
11 12270 6562	11 9739 10034
12 11954 7592	12 424 10162
13 7420 2592	13 1347 7597
14 8810 9636	14 1450 112
15 689 5430	15 7965 8478
16 920 1304	16 8945 7397
17 1253 11934	17 6590 8316
18 9559 6016	18 6838 9011
19 312 7589	19 6174 9410
20 4439 4197	20 255 113
21 4002 9555	21 6197 5835
22 12232 7779	22 12902 3844
23 1494 8782	23 4377 3505
24 10749 3969	24 5478 8672
25 4368 3479	25 4453 2132
26 6316 5342	26 9724 1380
27 2455 3493	27 12131 11526
28 12157 7405	28 12323 9511
29 6598 11495	29 8231 1752
30 11805 4455	30 497 9022
31 9625 2090	31 9288 3080
32 4731 2321	32 2481 7515
33 3578 2608	33 2696 268
34 8504 1849	34 4023 12341
35 4027 1151	35 7108 5553

Table B.6: Rate 5/6 (N_{ldpc} = 64 800)

0 4362 416 8909 4156 3216 3112 2560 2912 6405 8593 4969 6723	20 4766 2697	10 7868 5731
1 2479 1786 8978 3011 4339 9313 6397 2957 7288 5484 6031 10217	21 4069 6675	11 6121 10732
2 10175 9009 9889 3091 4985 7267 4092 8874 5671 2777 2189 8716	22 1117 1016	12 4843 9132
3 9052 4795 3924 3370 10058 1128 9996 10165 9360 4297 434 5138	23 5619 3085	13 580 9591
4 2379 7834 4835 2327 9843 804 329 8353 7167 3070 1528 7311	24 8483 8400	14 6267 9290
5 3435 7871 348 3693 1876 6585 10340 7144 5870 2084 4052 2780	25 8255 394	15 3009 2268
6 3917 3111 3476 1304 10331 5939 5199 1611 1991 699 8316 9960	26 6338 5042	16 195 2419
7 6883 3237 1717 10752 7891 9764 4745 3888 10009 4176 4614 1567	27 6174 5119	17 8016 1557
8 10587 2195 1689 2968 5420 2580 2883 6496 111 6023 1024 4449	28 7203 1989	18 1516 9195
9 3786 8593 2074 3321 5057 1450 3840 5444 6572 3094 9892 1512	29 1781 5174	19 8062 9064
10 8548 1848 10372 4585 7313 6536 6379 1766 9462 2456 5606 9975	0 1464 3559	20 2095 8968
11 8204 10593 7935 3636 3882 394 5968 8561 2395 7289 9267 9978	1 3376 4214	21 753 7326
12 7795 74 1633 9542 6867 7352 6417 7568 10623 725 2531 9115	2 7238 67	22 6291 3833
13 7151 2482 4260 5003 10105 7419 9203 6691 8798 2092 8263 3755	3 10595 8831	23 2614 7844
14 3600 570 4527 200 9718 6771 1995 8902 5446 768 1103 6520	4 1221 6513	24 2303 646
15 6304 7621	5 5300 4652	25 2075 611
16 6498 9209	6 1429 9749	26 4687 362
17 7293 6786	7 7878 5131	27 8684 9940
18 5950 1708	8 4435 10284	28 4830 2065
19 8521 1793	9 6331 5507	29 7038 1363
20 6174 7854	10 6662 4941	0 1769 7837
21 9773 1190	11 9614 10238	1 3801 1689
22 9517 10268	12 8400 8025	2 10070 2359
23 2181 9349	13 9156 5630	3 3667 9918
24 1949 5560	14 7067 8878	4 1914 6920
25 1556 555	15 9027 3415	5 4244 5669
26 8600 3827	16 1690 3866	6 10245 7821
27 5072 1057	17 2854 8469	7 7648 3944
28 7928 3542	18 6206 630	8 3310 5488
29 3226 3762	19 363 5453	9 6346 9666
0 7045 2420	20 4125 7008	10 7088 6122
1 9645 2641	21 1612 6702	11 1291 7827
2 2774 2452	22 9069 9226	12 10592 8945
3 5331 2031	23 5767 4060	13 3609 7120
4 9400 7503	24 3743 9237	14 9168 9112
5 1850 2338	25 7018 5572	15 6203 8052
6 10456 9774	26 8892 4536	16 3330 2895
7 1692 9276	27 853 6064	17 4264 10563
8 10037 4038	28 8069 5893	18 10556 6496
9 3964 338	29 2051 2885	19 8807 7645
10 2640 5087	0 10691 3153	20 1999 4530
11 858 3473	1 3602 4055	21 9202 6818
12 5582 5683	2 328 1717	22 3403 1734
13 9523 916	3 2219 9299	23 2106 9023
14 4107 1559	4 1939 7898	24 6881 3883
15 4506 3491	5 617 206	25 3895 2171
16 8191 4182	6 8544 1374	26 4062 6424
17 10192 6157	7 10676 3240	27 3755 9536
18 5668 3305	8 6672 9489	28 4683 2131
19 3449 1540	9 3170 7457	29 7347 8027

Table BB For Appendix B
Addresses of parity bit accumulators for N_{ldpc} = 16 200

Table BB.1: Rate 1/4 (N_{ldpc} = 16 200)

6295 9626 304 7695 4839 4936 1660 144 11203 5567 6347 12557
10691 4988 3859 3734 3071 3494 7687 10313 5964 8069 8296 11090
10774 3613 5208 11177 7676 3549 8746 6583 7239 12265 2674 4292
11869 3708 5981 8718 4908 10650 6805 3334 2627 10461 9285 11120
7844 3079 10773
3385 10854 5747
1360 12010 12202
6189 4241 2343
9840 12726 4977

Table BB.2: Rate 1/2 (N_{ldpc} = 16 200)

20 712 2386 6354 4061 1062 5045 5158	5 5924 290
21 2543 5748 4822 2348 3089 6328 5876	6 1467 4049
22 926 5701 269 3693 2438 3190 3507	7 7820 2242
23 2802 4520 3577 5324 1091 4667 4449	8 4606 3080
24 5140 2003 1263 4742 6497 1185 6202	9 4633 7877
0 4046 6934	10 3884 6868
1 2855 66	11 8935 4996
2 6694 212	12 3028 764
3 3439 1158	13 5988 1057
4 3850 4422	14 7411 3450

Table BB.3: Rate 3/5 (N_{ldpc} = 16 200)

71 1478 1901 2240 2649 2725 3592 3708 3965 4080 5733 6198	2820 4109 5307
393 1384 1435 1878 2773 3182 3586 5465 6091 6110 6114 6327	2088 5834 5988
160 1149 1281 1526 1566 2129 2929 3095 3223 4250 4276 4612	3725 3945 4010
289 1446 1602 2421 3559 3796 5590 5750 5763 6168 6271 6340	1081 2780 3389
947 1227 2008 2020 2266 3365 3588 3867 4172 4250 4865 6290	659 2221 4822
3324 3704 4447	3033 6060 6160
1206 2565 3089	756 1489 2350
529 4027 5891	3350 3624 5470
141 1187 3206	357 1825 5242
1990 2972 5120	585 3372 6062
752 796 5976	561 1417 2348
1129 2377 4030	971 3719 5567
6077 6108 6231	1005 1675 2062
61 1053 1781	

Table BB.4: Rate 2/3 (N_{ldpc} = 16 200)

0 2084 1613 1548 1286 1460 3196 4297 2481 3369 3451 4620 2622	1 2583 1180
1 122 1516 3448 2880 1407 1847 3799 3529 373 971 4358 3108	2 1542 509
2 259 3399 929 2650 864 3996 3833 107 5287 164 3125 2350	3 4418 1005
3 342 3529	4 5212 5117
4 4198 2147	5 2155 2922
5 1880 4836	6 347 2696
6 3864 4910	7 226 4296
7 243 1542	8 1560 487
8 3011 1436	9 3926 1640
9 2167 2512	10 149 2928
10 4606 1003	11 2364 563
11 2835 705	12 635 688
12 3426 2365	13 231 1684
13 3848 2474	14 1129 3894
14 1360 1743	
0 163 2536	

Table BB.5: Rate 3/4 (N_{ldpc} = 16 200)

3 3198 478 4207 1481 1009 2616 1924 3437 554 683 1801 4 2681 2135 5 3107 4027 6 2637 3373 7 3830 3449 8 4129 2060 9 4184 2742 10 3946 1070 11 2239 984 0 1458 3031 1 3003 1328 2 1137 1716 3 132 3725 4 1817 638 5 1774 3447 6 3632 1257 7 542 3694	8 1015 1945 9 1948 412 10 995 2238 11 4141 1907 0 2480 3079 1 3021 1088 2 713 1379 3 997 3903 4 2323 3361 5 1110 986 6 2532 142 7 1690 2405 8 1298 1881 9 615 174 10 1648 3112 11 1415 2808

Table BB.6: Rate 4/5 (N_{ldpc} = 16 200)

5 896 1565 6 2493 184 7 212 3210 8 727 1339 9 3428 612 0 2663 1947 1 230 2695 2 2025 2794 3 3039 283 4 862 2889 5 376 2110 6 2034 2286 7 951 2068 8 3108 3542 9 307 1421 0 2272 1197 1 1800 3280 2 331 2308	3 465 2552 4 1038 2479 5 1383 343 6 94 236 7 2619 121 8 1497 2774 9 2116 1855 0 722 1584 1 2767 1881 2 2701 1610 3 3283 1732 4 168 1099 5 3074 243 6 3460 945 7 2049 1746 8 566 1427 9 3545 1168

Table BB.7: Rate 5/6 (N_{ldpc} = 16 200)

3 2409 499 1481 908 559 716 1270 333 2508 2264 1702 2805 4 2447 1926 5 414 1224 6 2114 842 7 212 573 0 2383 2112 1 2286 2348 2 545 819 3 1264 143 4 1701 2258 5 964 166 6 114 2413 7 2243 81 0 1245 1581 1 775 169 2 1696 1104 3 1914 2831 4 532 1450 5 91 974	6 497 2228 7 2326 1579 0 2482 256 1 1117 1261 2 1257 1658 3 1478 1225 4 2511 980 5 2320 2675 6 435 1278 7 228 503 0 1885 2369 1 57 483 2 838 1050 3 1231 1990 4 1738 68 5 2392 951 6 163 645 7 2644 1704

Table BB.8: Rate 1/3 (N_{ldpc} = 16 200) - T2-Lite only

416 8909 4156 3216 3112 2560 2912 6405 8593 4969 6723 6912
8978 3011 4339 9312 6396 2957 7288 5485 6031 10218 2226 3575
3383 10059 1114 10008 10147 9384 4290 434 5139 3536 1965 2291
2797 3693 7615 7077 743 1941 8716 6215 3840 5140 4582 5420
6110 8551 1515 7404 4879 4946 5383 1831 3441 9569 10472 4306
1505 5682 7778
7172 6830 6623
7281 3941 3505
10270 8669 914
3622 7563 9388
9930 5058 4554
4844 9609 2707
6883 3237 1714
4768 3878 10017
10127 3334 8267

Table BB.9: Rate 2/5 (N_{ldpc} = 16 200) - T2-Lite only

5650 4143 8750 583 6720 8071 635 1767 1344 6922 738 6658
5696 1685 3207 415 7019 5023 5608 2605 857 6915 1770 8016
3992 771 2190 7258 8970 7792 1802 1866 6137 8841 886 1931
4108 3781 7577 6810 9322 8226 5396 5867 4428 8827 7766 2254
4247 888 4367 8821 9660 324 5864 4774 227 7889 6405 8963
9693 500 2520 2227 1811 9330 1928 5140 4030 4824 806 3134
1652 8171 1435
3366 6543 3745
9286 8509 4645
7397 5790 8972
6597 4422 1799
9276 4041 3847
8683 7378 4946
5348 1993 9186
6724 9015 5646
4502 4439 8474
5107 7342 9442
1387 8910 2660

Appendix C

Parameters of bits De-multiplexing into sub-streams according to coding rates and modulation modes

Table C(1): Parameters for de-multiplexing of bits to sub-streams for code rates 1/2, 3/4, 4/5 and 5/6

Modulation format	**QPSK**	
Input bit-number, *di* mod $N_{substreams}$	0	1
Output bit-number, *e*	0	1

Modulation format	**16-QAM**							
Input bit-number, *di* mod $N_{substreams}$	0	1	2	3	4	5	6	7
Output bit-number, *e*	7	1	4	2	5	3	6	0

Modulation format	**64-QAM**											
Input bit-number, *di* mod $N_{substreams}$	0	1	2	3	4	5	6	7	8	9	10	11
Output bit-number, *e*	11	7	3	10	6	2	9	5	1	8	4	0

Modulation format	**256-QAM (N_{ldpc} = 64 800)**															
Input bit-number, *di* mod $N_{substreams}$	0	1	2	3	4	5	6	7	8	9	10	11	12	13	14	15
Output bit-number, *e*	15	1	13	3	8	11	9	5	10	6	4	7	12	2	14	0

Modulation format	**256-QAM (N_{ldpc} = 16 200)**							
Input bit-number, *di* mod $N_{substreams}$	0	1	2	3	4	5	6	7
Output bit-number, *e*	7	3	1	5	2	6	4	0

Table C(2): Parameters for de-multiplexing of bits to sub-streams for code rate 3/5 only

Modulation format	**QPSK**	
Input bit-number, *di* mod $N_{substreams}$	0	1
Output bit-number, *e*	0	1

Modulation format	**16-QAM (N_{ldpc} = 64 800)**							
Input bit-number, *di* mod $N_{substreams}$	0	1	2	3	4	5	6	7
Output bit-number, *e*	0	5	1	2	4	7	3	6

Modulation format	**16-QAM (N_{ldpc} = 16 200)**							
Input bit-number, *di* mod $N_{substreams}$	0	1	2	3	4	5	6	7
Output bit-number, *e*	7	1	4	2	5	3	6	0

Modulation format	**64-QAM(N_{ldpc} = 64 800)**											
Input bit-number, *di* mod $N_{substreams}$	0	1	2	3	4	5	6	7	8	9	10	11
Output bit-number, *e*	2	7	6	9	0	3	1	8	4	11	5	10

Modulation format	**64-QAM (N_{ldpc} = 16 200)**											
Input bit-number, *di* mod $N_{substreams}$	0	1	2	3	4	5	6	7	8	9	10	11
Output bit-number, *e*	11	7	3	10	6	2	9	5	1	8	4	0

Modulation format	**256-QAM (N_{ldpc} = 64 800)**															
Input bit-number, *di* mod $N_{substreams}$	0	1	2	3	4	5	6	7	8	9	10	11	12	13	14	15
Output bit-number, *e*	2	11	3	4	0	9	1	8	10	13	7	14	6	15	5	12

Modulation format	**256-QAM (N_{ldpc} = 16 200)**							
Input bit-number, *di* mod $N_{substreams}$	0	1	2	3	4	5	6	7
Output bit-number, *e*	7	3	1	5	2	6	4	0

Table C(3): Parameters for de-multiplexing of bits to sub-streams for code rate 2/3 only

Modulation format	**QPSK**	
Input bit-number, *di* mod $N_{substreams}$	0	1
Output bit-number, *e*	0	1

Modulation format	**16-QAM**							
Input bit-number, *di* mod $N_{substreams}$	0	1	2	3	4	5	6	7
Output bit-number, *e*	7	1	4	2	5	3	6	0

Modulation format	**64-QAM**											
Input bit-number, *di* mod $N_{substreams}$	0	1	2	3	4	5	6	7	8	9	10	11
Output bit-number, *e*	11	7	3	10	6	2	9	5	1	8	4	0

Modulation format	**256-QAM (N_{ldpc} = 64 800)**															
Input bit-number, *di* mod $N_{substreams}$	0	1	2	3	4	5	6	7	8	9	10	11	12	13	14	15
Output bit-number, *e*	7	2	9	0	4	6	13	3	14	10	15	5	8	12	11	1

Modulation format	**256-QAM (N_{ldpc} = 16 200)**							
Input bit-number, *di* mod $N_{substreams}$	0	1	2	3	4	5	6	7
Output bit-number, *e*	7	3	1	5	2	6	4	0

Appendix D

The exact values of the real and imaginary components Re(z_q) and Im(z_q) for each combination of the relevant input bits $y_{e,q}$ are given in tables C(1) to C(8) for the various constellations and the corresponding bit patterns are defined in Figure D

Table D(1): Constellation mapping for real part of QPSK

$y_{0,q}$	1	0
Re(z_q)	-1	1

Table D(2): Constellation mapping for imaginary part of QPSK

$y_{1,q}$	1	0
Im(z_q)	-1	1

Table D(3): Constellation mapping for real part of 16-QAM

$y_{0,q}$ $y_{2,q}$	1 0	1 1	0 1	0 0
Re(z_q)	-3	-1	1	3

Table D(4): Constellation mapping for imaginary part of 16-QAM

$y_{1,q}$ $y_{3,q}$	1 0	1 1	0 1	0 0
Im(z_q)	-3	-1	1	3

Table D(5): Constellation mapping for real part of 64-QAM

$y_{0,q}$ $y_{2,q}$ $y_{4,q}$	1 0 0	1 0 1	1 1 1	1 1 0	0 1 0	0 1 1	0 0 1	0 0 0
Re(z_q)	-7	-5	-3	-1	1	3	5	7

Table D(6): Constellation mapping for imaginary part of 64-QAM

$y_{1,q}$ $y_{3,q}$ $y_{5,q}$	1 0 0	1 0 1	1 1 1	1 1 0	0 1 0	0 1 1	0 0 1	0 0 0
Im(z_q)	-7	-5	-3	-1	1	3	5	7

Table D(7): Constellation mapping for real part of 256-QAM

$y_{0,q}$ $y_{2,q}$ $y_{4,q}$ $y_{6,q}$	1 0 0 0	1 0 0 1	1 0 1 1	1 0 1 0	1 1 1 0	1 1 1 1	1 1 0 1	1 1 0 0	0 1 0 0	0 1 0 1	0 1 1 1	0 1 1 0	0 0 1 0	0 0 1 1	0 0 0 1	0 0 0 0
Re(z_q)	-15	-13	-11	-9	-7	-5	-3	-1	1	3	5	7	9	11	13	15

Table D(8): Constellation mapping for imaginary part of 256-QAM

$y_{1,q}$ $y_{3,q}$ $y_{5,q}$ $y_{7,q}$	1 0 0 0	1 0 0 1	1 0 1 1	1 0 1 0	1 1 1 0	1 1 1 1	1 1 0 1	1 1 0 0	0 1 0 0	0 1 0 1	0 1 1 1	0 1 1 0	0 0 1 0	0 0 1 1	0 0 0 1	0 0 0 0
Im(z_q)	-15	-13	-11	-9	-7	-5	-3	-1	1	3	5	7	9	11	13	15

The constellations, and the details of the Gray mapping applied to them, are illustrated in figures 15 and 16.

Table D(9): Constellation mapping for real part of QPSK

$y_{0,q}$	1	0
$\mathrm{Re}(z_q)$	-1	1

Table D(10): Constellation mapping for imaginary part of QPSK

$y_{1,q}$	1	0
$\mathrm{Im}(z_q)$	-1	1

Table D(11): Constellation mapping for real part of 16-QAM

$y_{0,q}$ $y_{2,q}$	1 0	1 1	0 1	0 0
$\mathrm{Re}(z_q)$	-3	-1	1	3

Table D(12): Constellation mapping for imaginary part of 16-QAM

$y_{1,q}$ $y_{3,q}$	1 0	1 1	0 1	0 0
$\mathrm{Im}(z_q)$	-3	-1	1	3

Table D(13): Constellation mapping for real part of 64-QAM

$y_{0,q}$ $y_{2,q}$ $y_{4,q}$	1 0 0	1 0 1	1 1 1	1 1 0	0 1 0	0 1 1	0 0 1	0 0 0
$\mathrm{Re}(z_q)$	-7	-5	-3	-1	1	3	5	7

Table D(14): Constellation mapping for imaginary part of 64-QAM

$y_{1,q}$ $y_{3,q}$ $y_{5,q}$	1 0 0	1 0 1	1 1 1	1 1 0	0 1 0	0 1 1	0 0 1	0 0 0
$\mathrm{Im}(z_q)$	-7	-5	-3	-1	1	3	5	7

Table D(15): Constellation mapping for real part of 256-QAM

$y_{0,q}$ $y_{2,q}$ $y_{4,q}$ $y_{6,q}$	1 0 0 0	1 0 0 1	1 0 1 1	1 0 1 0	1 1 1 0	1 1 1 1	1 1 0 1	1 1 0 0	0 1 0 0	0 1 0 1	0 1 1 1	0 1 1 0	0 0 1 0	0 0 1 1	0 0 0 1	0 0 0 0
$\mathrm{Re}(z_q)$	-15	-13	-11	-9	-7	-5	-3	-1	1	3	5	7	9	11	13	15

Table D(16): Constellation mapping for imaginary part of 256-QAM

$y_{1,q}$ $y_{3,q}$ $y_{5,q}$ $y_{7,q}$	1 0 0 0	1 0 0 1	1 0 1 1	1 0 1 0	1 1 1 0	1 1 1 1	1 1 0 1	1 1 0 0	0 1 0 0	0 1 0 1	0 1 1 1	0 1 1 0	0 0 1 0	0 0 1 1	0 0 0 1	0 0 0 0
$\mathrm{Im}(z_q)$	-15	-13	-11	-9	-7	-5	-3	-1	1	3	5	7	9	11	13	15

The constellations, and the details of the Gray mapping applied to them, are illustrated in figures 15 and 16.

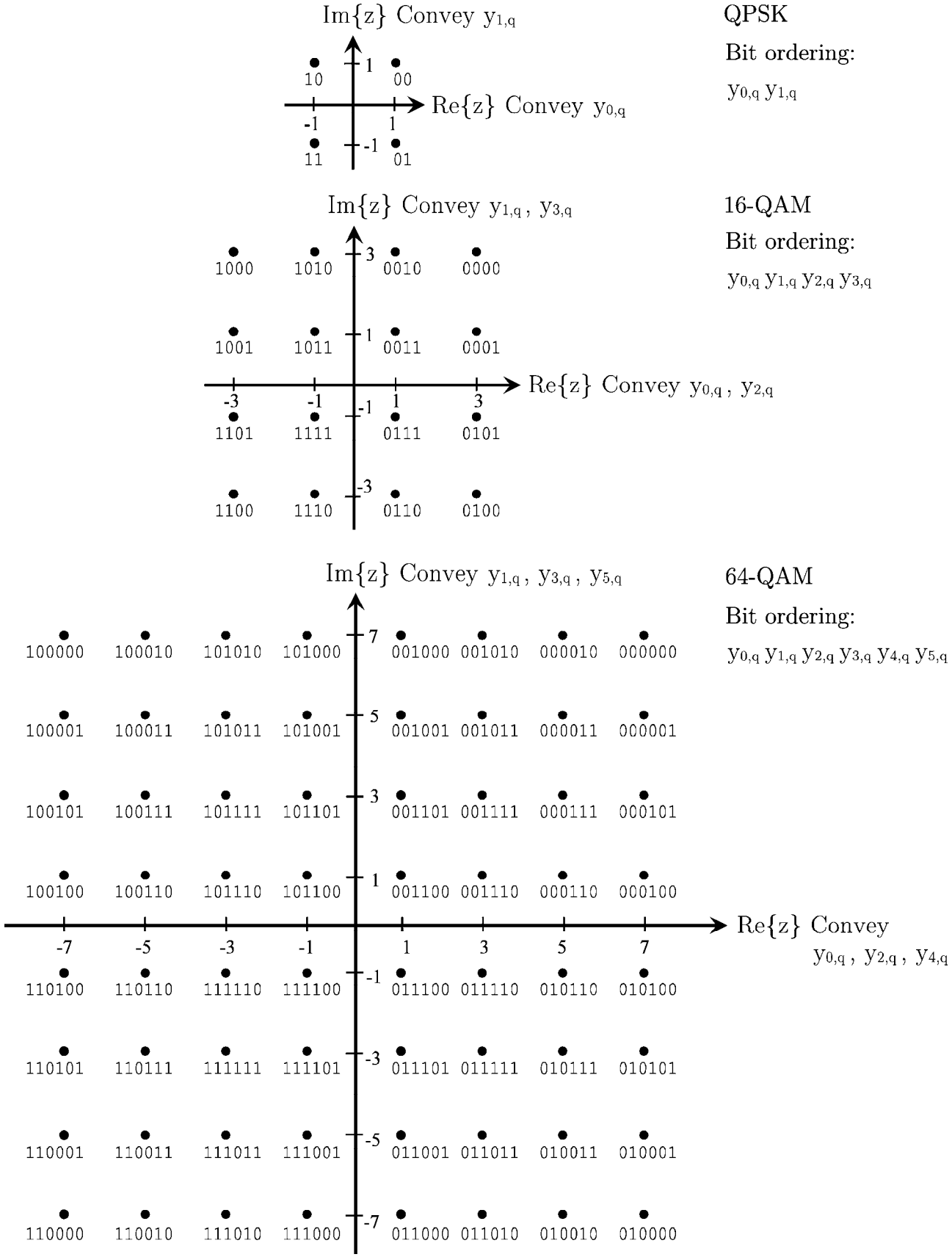

Figure D.1: The QPSK, 16-QAM and 64-QAM mappings and the corresponding bit patterns

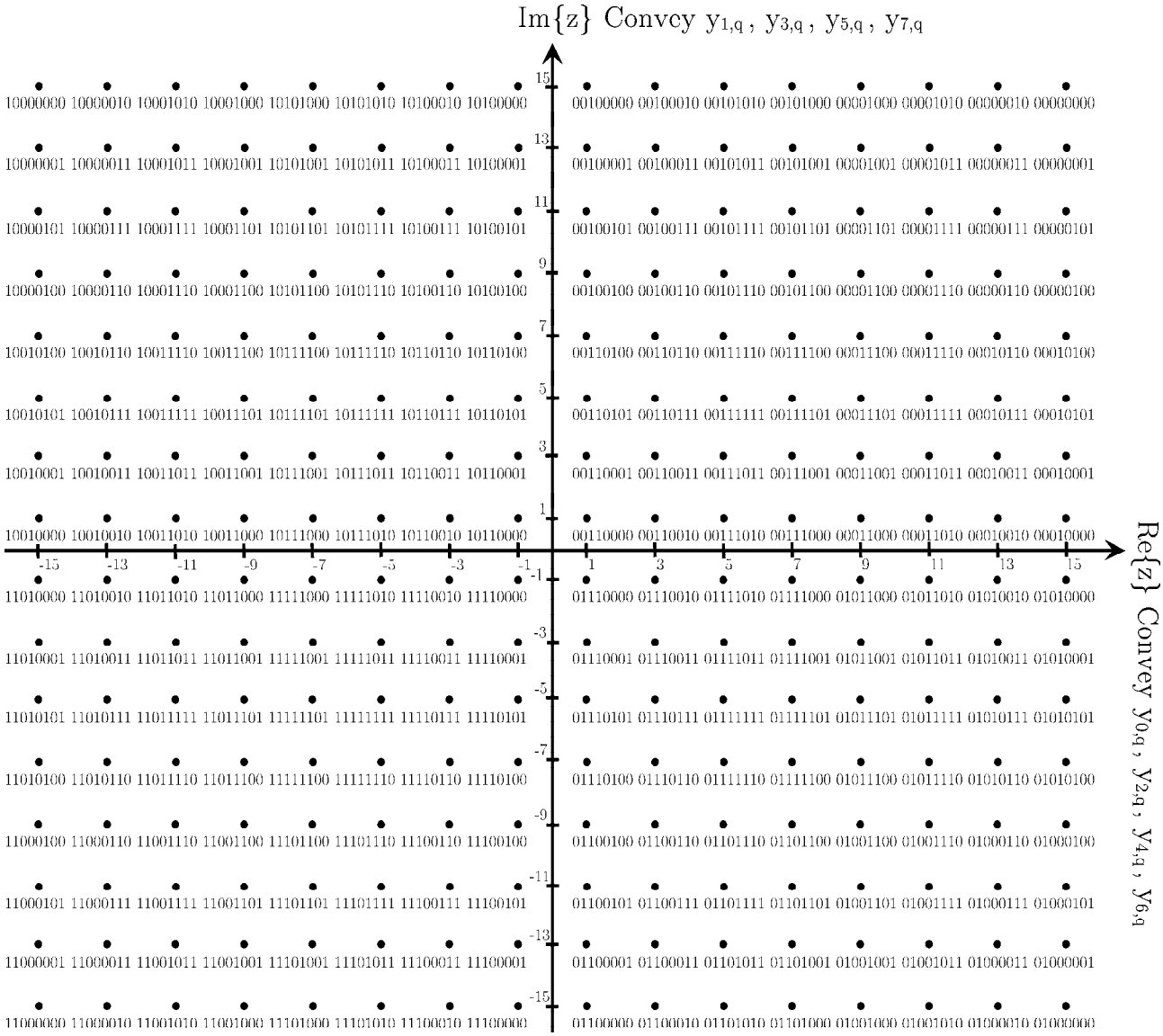

Figure D.2: The 256-QAM mapping and the corresponding bit pattern

Appendix E

The basic permutation function $L_0(q)$ is defined by the following algorithm.

An N_d bit binary word S_i is defined as follows:

For all i,

$S_i[N_d\text{-}1] = (i \bmod 2)$ // (toggling of top bit)

$i = 0,1$:

$S_i[N_d\text{-}2, N_d\text{-}3,...,1,0] = 0,0,...,0,0$

$i = 2$:

$S_2[N_d\text{-}2, N_d\text{-}3,...,1,0] = 0,0,...,0,1$

$2 < i < 2^{N_d}$:

$S_i[N_d\text{-}3, N_d\text{-}4,...,1,0] = S_{i-1}[N_d\text{-}2, N_d\text{-}3,...,2,1]$;

for $N_d = 11$: $S_i[9] = S_{i-1}[0] \oplus S_{i-1}[3]$

for $N_d = 12$: $S_i[10] = S_{i-1}[0] \oplus S_{i-1}[2]$

for $N_d = 13$: $S_i[11] = S_{i-1}[0] \oplus S_{i-1}[1] \oplus S_{i-1}[4] \oplus S_{i-1}[6]$

for $N_d = 14$: $S_i[12] = S_{i-1}[0] \oplus S_{i-1}[1] \oplus S_{i-1}[4] \oplus S_{i-1}[5] \oplus S_{i-1}[9] \oplus S_{i-1}[11]$

for $N_d = 15$: $S_i[13] = S_{i-1}[0] \oplus S_{i-1}[1] \oplus S_{i-1}[2] \oplus S_{i-1}[12]$.

The sequence $L_0(q)$ is then generated by discarding values of S_i greater than or equal to N_{cells} as defined in the following algorithm:

$q = 0$;

for ($i = 0$; $i < 2^{\text{Nd}}$; $i = i + 1$)

{

$$L_0(q) = \sum_{j=0}^{N_d - 1} S_i(j) \cdot 2^j \ ;$$

if ($L_0(q) < N_{\text{cells}}$)

$q = q+1$;

}

The shift $P(r)$ to be applied in FEC block index r is calculated by the following algorithm. The FEC block index r is the index of the FEC block within the TI-block and counts up to $N_{FEC\_TI}(n,s)$ - 1, where $N_{FEC\_TI}(n,s)$ is the number of FEC blocks in TI-block index 's' of Interleaving Frame 'n' (see clause 6.5.2). $P(r)$ is the conversion to decimal of the bit-reversed value of a counter k in binary notation over N_d bits. The counter is incremented if the bit-reversed value is too great.

k=0;

for (r=0; r<$N_{FEC\_TI}(n,s)$; r++)

{

$P(r)$=N_{cells};

while ($P(r)$>=N_{cells})

{

$$P(r) = \sum_{j=0}^{N_d-1} \left\lfloor \frac{k - \left\lfloor \frac{k}{2^{j+1}} \right\rfloor 2^{j+1}}{2^j} \right\rfloor \cdot 2^{N_d-1-j} \; ;$$

k= k+1;

}

}

So for N_{cells}= 10 800, N_d= 14, and the shift $P(r)$ to be added to the permutation for r =0, 1, 2, 3, etc. would be 0, 8 192, 4 096, 2 048, 10 240, 6 144, 1 024, 9 216, etc.

Appendix F

$H(p)$, $H_0(p)$ and $H_1(p)$ are permutation functions based on sequences R'_i defined by the following.

An $(N_r - 1)$ bit binary word R'_i is defined, with $N_r = \log_2 M_{max}$, where R'_i takes the following values:

$i = 0,1$: $R'_i [N_r\text{-}2, N_r\text{-}3,...,1,0] = 0,0,...,0,0$

$i = 2$: $R'_i [N_r\text{-}2, N_r\text{-}3,...,1,0] = 0,0,...,0,1$

$2 < i < M_{max}$: { $R'_i [N_r\text{-}3, N_r\text{-}4,...,1,0] = R'_{i-1} [N_r\text{-}2, N_r\text{-}3,...,2,1]$;

in the 1k mode: $R'_i [8] = R'_{i-1} [0] \oplus R'_{i-1} [4]$

in the 2k mode: $R'_i [9] = R'_{i-1} [0] \oplus R'_{i-1} [3]$

in the 4k mode: $R'_i [10] = R'_{i-1} [0] \oplus R'_{i-1} [2]$

in the 8k mode: $R'_i [11] = R'_{i-1} [0] \oplus R'_{i-1} [1] \oplus R'_{i-1} [4] \oplus R'_{i-1} [6]$

in the 16k mode: $R'_i [12] = R'_{i-1} [0] \oplus R'_{i-1} [1] \oplus R'_{i-1} [4] \oplus R'_{i-1} [5] \oplus R'_{i-1} [9] \oplus R'_{i-1} [11]$

in the 32k mode: $R'_i [13] = R'_{i-1} [0] \oplus R'_{i-1} [1] \oplus R'_{i-1} [2] \oplus R'_{i-1} [12]$ }

A vector R_i is derived from the vector R'_i by the bit permutations given in tables F(1) to F(7).

Table F(1): Bit permutations for the 1k mode

R'_i bit positions	8	7	6	5	4	3	2	1	0
R_i bit positions (H_0)	4	3	2	1	0	5	6	7	8
R_i bit positions (H_1)	3	2	5	0	1	4	7	8	6

Table F(2): Bit permutations for the 2k mode

R'_i bit positions	9	8	7	6	5	4	3	2	1	0
R_i bit positions (H_0)	0	7	5	1	8	2	6	9	3	4
R_i bit positions (H_1)	3	2	7	0	1	5	8	4	9	6

Table F(3): Bit permutations for the 4k mode

R'_i bit positions	10	9	8	7	6	5	4	3	2	1	0
R_i bit positions (H_0)	7	10	5	8	1	2	4	9	0	3	6
R_i bit positions (H_1)	6	2	7	10	8	0	3	4	1	9	5

Table F(4): Bit permutations for the 8k mode

R'_i bit positions	11	10	9	8	7	6	5	4	3	2	1	0
R_i bit positions (H_0)	5	11	3	0	10	8	6	9	2	4	1	7
R_i bit positions (H_1)	8	10	7	6	0	5	2	1	3	9	4	11

Table F(5): Bit permutations for the 16k mode

R'_i bit positions	12	11	10	9	8	7	6	5	4	3	2	1	0
R_i bit positions (H_0)	8	4	3	2	0	11	1	5	12	10	6	7	9
R_i bit positions (H_1)	7	9	5	3	11	1	4	0	2	12	10	8	6

Table F(6): Bit permutations for the 32k mode

R'_i bit positions	13	12	11	10	9	8	7	6	5	4	3	2	1	0
R_i bit positions	6	5	0	10	8	1	11	12	2	9	4	3	13	7

The permutation function $H(p)$ is defined by the following algorithm:

$p = 0$;

for ($i = 0$; $i < M_{max}$; $i = i + 1$)

$$\{ H(p) = (i \bmod 2).2^{N_r - 1} + \sum_{j=0}^{N_r - 2} R_i(j).2^j;$$

if ($H(p) < N_{data}$) $p = p + 1$; }

Appendix G

1. Continual pilot insertion

In addition to the scattered pilots described, a number of continual pilots are inserted in every symbol of the frame except for P1 and P2 and the frame closing symbol (if any). The number and location of continual pilots depends on both the FFT size and scattered pilot pattern PP1-PP8.

The continual pilot locations are taken from one or more "CP groups" depending on the FFT mode. Table G(1) indicates which CP groups are used in each FFT mode. The pilot locations belonging to each CP group depend on the scattered

pilot pattern in use; table G.1 gives the carrier indices $k_{i,32K}$ for each pilot pattern in the 32K mode. In other FFT modes, the carrier index for each CP is given by $k = k_{i,32K} \bmod K_{mod}$, where K_{mod} for each FFT size is given

in table G(1).

Table G(1): Continual Pilot groups used with each FFT size

FFT size	CP Groups used	K_{mod}
1K	CP_1	1 632
2K	CP_1, CP_2	1 632
4K	CP_1, CP_2, CP_3	3 264
8K	CP_1, CP_2, CP_3, CP_4	6 528
16K	CP_1, CP_2, CP_3, CP_4, CP_5	13 056
32K	CP_1, CP_2, CP_3, CP_4, CP_5, CP_6	NA

The continual pilots are transmitted at boosted power levels, where the boosting depends on the FFT size. Table G(2) gives the modulation amplitude A_{CP} for each FFT size.

Table G(2): Boosting for the continual pilots

FFT size	1K		4K		16K	32K
A_{CP}	4/3	4/3	$(4\sqrt{2})/3$	8/3	8/3	8/3

When a carrier's location is such that it would be both a continual and scattered pilot, the boosting value for the scattered pilot pattern shall be used (A_{SP}).

The phases of the continual pilots are derived from the reference sequence given above. The

modulation value for the continual pilots is given by:

$$\mathrm{Re}\{c_{m,l,k}\} = 2\, A_{CP}\, (1/2 - r_{l,k})$$

$$\mathrm{Im}\{\, c_{m,l,k}\,\} = 0.$$

2. Edge pilot insertion

The edge carriers, carriers $k=K_{min}$ and $k=K_{max}$, are edge pilots in every symbol except for the P1 and P2 symbol(s). They are inserted in order to allow frequency interpolation up to the edge of the spectrum. The modulation of these cells is exactly the same as for the scattered pilots.

$$\mathrm{Re}\{c_{m,l,k}\} = 2\,A_{SP}\,(1/2 - r_{l,k})$$

$$\mathrm{Im}\{\,c_{m,l,k}\,\} = 0.$$

3. P2 pilot insertion

In 32K SISO mode, cells in the P2 symbol(s) for which k mod 6 = 0 are P2 pilots.

In all other modes (including 32K MISO), cells in the P2 symbol(s) for which k mod 3 = 0 are P2 pilots.

In extended carrier mode, all cells for which $K_{min} \leq k < K_{min} + K_{ext}$ and for which $K_{max} - K_{ext} < k \leq K_{max}$ are also P2 pilots.

The pilot cells in the P2 symbol(s) are transmitted at boosted power levels. Table G(3) gives the modulation amplitude A_{P2} for the P2 pilots.

Table G(3): Amplitude of P2 pilots

Mode	A_{P2}
32K SISO	$\frac{\sqrt{37}}{5}$
All other modes (including 32K MISO)	$\frac{\sqrt{31}}{5}$

The corresponding modulation is given by:

$$\mathrm{Re}\{c_{m,l,k}\} = 2\,A_{P2}\,(1/2 - r_{l,k})$$

$$\mathrm{Im}\{c_{m,l,k}\} = 0$$

where m is the T2-frame index, k is the frequency index of the carriers and l is the symbol index.

4. frame closing pilots

When any of the combinations of FFT size, guard interval and scattered pilot pattern listed in table G(4) (for SISO mode) is used, the last symbol of the frame is a special frame closing symbol. Frame closing symbols are always used in MISO mode, except with pilot pattern PP8, when frame closing symbols are never used.

Table G(4): Combinations of FFT size, guard interval and pilot pattern for which frame closing symbols are used in SISO mode

FFT size	Guard interval						
	1/128	1/32	1/16	19/256	1/8	19/128	1/4
32K		PP6	PP4	PP4	PP2	PP2	NA
16K		PP7 PP6	PP4 PP5	PP4 PP5	PP2 PP3	PP2 PP3	PP1
8K		PP7	PP4 PP5	PP4 PP5	PP2 PP3	PP2 PP3	PP1
4K, 2K	NA	PP7	PP4 PP5	NA	PP2 PP3	NA	PP1
1K	NA	NA	PP4 PP5	NA	PP2 PP3	NA	PP1
NOTE: The entry 'NA' indicates that the corresponding combination of FFT size and guard interval is not allowed. An empty entry indicates that the combination of FFT size and guard interval is allowed, but frame closing symbols are never used.							

The cells in the frame closing symbol for which $k \bmod D_X = 0$, except when $k = K_{min}$ and $k = K_{max}$, are frame closing pilots, where D_X is the value from table 2.18 for the scattered pilot pattern in use. With an FFT size of 1K with pilot patterns PP4 and PP5, and with an FFT size of 2K with pilot pattern PP7, carrier K_{max}-1 shall be an additional frame closing pilot.

NOTE: Cells in the frame closing symbol for which $k = K_{min}$ or $k = K_{max}$ are edge pilots.

The frame closing pilots are boosted by the same factor as the scattered pilots, A_{SP}. The corresponding modulation is given by:

$$\mathrm{Re}\{c_{m,l,k}\} = 2\,A_{SP}\,(1/2 - r_{l,k})$$

$$\mathrm{Im}\{c_{m,l,k}\} = 0$$

Where m is the T2-frame index, k is the frequency index of the carriers and l is the time index of the symbols.

5. Locations of the continual pilots

Table G(5) gives the carrier indices for the continual pilots for each of the pilot patterns in 32K.

Table G(5): Continual pilot groups for each pilot pattern

Group	PP1	PP2	PP3	PP4	PP5	PP6	PP7	PP8
CP_1 [*All modes*]	116 255 285 430 518 546 601 646 744 1662 1893 1995 2322 3309 3351 3567 3813 4032 5568 5706	116 318 390 430 474 518 601 646 708 726 1752 1758 1944 2100 2208 2466 3792 5322 5454 5640	116 318 342 426 430 518 582 601 646 816 1758 1764 2400 3450 3504 3888 4020 4932 5154 5250 5292 5334	108 116 144 264 288 430 518 564 636 646 828 2184 3360 3396 3912 4032 4932 5220 5676 5688	108 116 228 430 518 601 646 804 1644 1680 1752 1800 1836 3288 3660 4080 4932 4968 5472		264 360 1848 2088 2112 2160 2256 2280 3936 3960 3984 5016 5136 5208 5664	
CP_2 [*2K-32K*]	1022 1224 1302 1371 1495 2261 2551 2583 2649 2833 2925 3192 4266 5395 5710 5881 8164 10568 11069 11560 12631 12946 13954 16745 21494	1022 1092 1369 1416 1446 1495 2598 2833 2928 3144 4410 4800 5710 5881 6018 6126 10568 11515 12946 13954 15559 16681	1022 1495 2261 2551 2802 2820 2833 2922 4422 4752 4884 5710 8164 10568 11069 11560 12631 12946 16745 21494	601 1022 1092 1164 1369 1392 1452 1495 2261 2580 2833 3072 4320 4452 5710 5881 6048 10568 11515 12946 13954 15559 16681	852 1022 1495 2508 2551 2604 2664 2736 2833 3120 4248 4512 4836 5710 5940 6108 8164 10568 11069 11560 12946 13954 21494		116 430 518 601 646 1022 1296 1368 1369 1495 2833 3024 4416 4608 4776 5710 5881 6168 7013 8164 10568 10709 11515 12946 15559 23239 24934 25879 26308 26674	
CP_3 [*4K-32K*]		2261 8164	13954	8164	648 4644 16745		456 480 2261 6072 17500	
CP_4 [*8K-32K*]		10709 19930		10709 19930	12631		1008 6120 13954	116 132 180 430 518 601 646 1022 1266 1369 1495 2261 2490 2551 2712 2833 3372 3438 4086 4098 4368 4572 4614 4746 4830 4968 5395 5710 5881 7649 8164 10568 11069 11560 12631 12946 13954

Group	PP1	PP2	PP3	PP4	PP5	PP6	PP7	PP8
								15760 16612 16745 17500 19078 19930 21494 22867 25879 26308
CP_5 [*16K-32K*]	1369 7013 7215 7284 7649 7818 8025 8382 8733 8880 9249 9432 9771 10107 10110 10398 10659 10709 10785 10872 11115 11373 11515 11649 11652 12594 12627 12822 12984 15760 16612 17500 18358 19078 19930 20261 20422 22124 22867 23239 24934 25879 26308 26674	6744 7013 7020 7122 7308 7649 7674 7752 7764 8154 8190 8856 8922 9504 9702 9882 9924 10032 10092 10266 10302 10494 10530 10716 11016 11076 11160 11286 11436 11586 12582 13002 17500 18358 19078 22124 23239 24073 24934 25879 26308	1369 5395 5881 6564 6684 7013 7649 8376 8544 8718 8856 9024 9132 9498 9774 9840 10302 10512 10566 10770 10914 11340 11418 11730 11742 12180 12276 12474 12486 15760 16612 17500 18358 19078 19930 20261 20422 22124 22867 23239 24934 25879 26308 26674	6612 6708 7013 7068 7164 7224 7308 7464 7649 7656 7716 7752 7812 7860 8568 8808 8880 9072 9228 9516 9696 9996 10560 10608 10728 11148 11232 11244 11496 11520 11664 11676 11724 11916 17500 18358 19078 21284 22124 23239 24073 24934 25879 26308	1369 2261 5395 5881 6552 6636 6744 6900 7032 7296 7344 7464 7644 7649 7668 7956 8124 8244 8904 8940 8976 9216 9672 9780 10224 10332 10709 10776 10944 11100 11292 11364 11496 11532 11904 12228 12372 12816 15760 16612 17500 19078 22867 25879	116 384 408 518 601 646 672 960 1022 1272 1344 1369 1495 1800 2040 2261 2833 3192 3240 3768 3864 3984 4104 4632 4728 4752 4944 5184 5232 5256 5376 5592 5616 5710 5808 5881 6360 6792 6960 7013 7272 7344 7392 7536 7649 7680 7800 8064 8160 8164 8184 8400 8808 8832 9144 9648 9696 9912 10008 10200 10488 10568 10656 10709 11088 11160 11515 11592 12048 12264 12288 12312 12552 12672 12946 13954 15559 16681 17500 19078 20422 21284 22124 23239 24934 25879	6984 7032 7056 7080 7152 7320 7392 7536 7649 7704 7728 7752 8088 8952 9240 9288 9312 9480 9504 9840 9960 10320 10368 10728 10752 11448 11640 11688 11808 12192 12240 12480 12816 16681 22124	6720 6954 7013 7026 7092 7512 7536 7596 7746 7758 7818 7986 8160 8628 9054 9096 9852 9924 10146 10254 10428 10704 11418 11436 11496 11550 11766 11862 12006 12132 12216 12486 12762 18358 20261 20422 22124 23239 24934

Group	PP1	PP2	PP3	PP4	PP5	PP6	PP7	PP8
						26308 26674		
CP_6 [*32K only*]		13164 13206 13476 13530 13536 13764 13848 13938 13968 14028 14190 14316 14526 14556 14562 14658 14910 14946 15048 15186 15252 15468 15540 15576 15630 15738 15840 16350 16572 16806 17028 17064 17250 17472 17784 17838 18180 18246 18480 18900 18960 19254 19482 19638 19680 20082 20310 20422 20454 20682 20874 21240 21284 21444 21450 21522 21594 21648 21696 21738 22416 22824 23016 23124 23196		13080 13152 13260 13380 13428 13572 13884 13956 14004 14016 14088 14232 14304 14532 14568 14760 14940 15168 15288 15612 15684 15888 16236 16320 16428 16680 16812 16908 17184 17472 17508 17580 17892 17988 18000 18336 18480 18516 19020 19176 19188 19320 19776 19848 20112 20124 20184 20388 20532 20556 20676 20772 21156 21240 21276 21336 21384 21816 21888 22068 22092 22512 22680 22740 22800		13080 13368 13464 13536 13656 13728 13824 14112 14232 14448 14472 14712 14808 14952 15000 15336 15360 15408 15600 15624 15648 16128 16296 16320 16416 16536 16632 16824 16848 17184 17208 17280 17352 17520 17664 17736 17784 18048 18768 18816 18840 19296 19392 19584 19728 19752 19776 20136 20184 20208 20256 21096 21216 21360 21408 21744 21768 22200 22224 22320 22344 22416 22848 22968 23016	13416 13440 13536 13608 13704 13752 14016 14040 14112 14208 14304 14376 14448 14616 14712 14760 14832 14976 15096 15312 15336 15552 15816 15984 16224 16464 16560 17088 17136 17256 17352 17400 17448 17544 17928 18048 18336 18456 18576 18864 19032 19078 19104 19320 19344 19416 19488 19920 19930 19992 20424 20664 20808 21168 21284 21360 21456 21816 22128 22200 22584 22608 22824 22848 22944	10709 11515 13254 13440 13614 13818 14166 14274 14304 14364 14586 14664 15030 15300 15468 15474 15559 15732 15774 16272 16302 16428 16500 16662 16681 16872 17112 17208 17862 18036 18282 18342 18396 18420 18426 18732 19050 19296 19434 19602 19668 19686 19728 19938 20034 21042 21120 21168 21258 21284 21528 21594 21678 21930 21936 21990 22290 22632 22788 23052 23358 23448 23454 23706 23772

Group	PP1	PP2	PP3	PP4	PP5	PP6	PP7	PP8
		23238		22836		23040	22992	24048
		23316		22884		23496	23016	24072
		23418		23304		23688	23064	24073
		23922		23496		23904	23424	24222
		23940		23568		24048	23448	24384
		24090		23640		24168	23472	24402
		24168		24120		24360	23592	24444
		24222		24168		24408	24192	24462
		24324		24420		24984	24312	24600
		24342		24444		25152	24360	24738
		24378		24456		25176	24504	24804
		24384		24492		25224	24552	24840
		24540		24708		25272	24624	24918
		24744		24864		25344	24648	24996
		24894		25332		25416	24672	25038
		24990		25536		25488	24768	25164
		25002		25764		25512	24792	25314
		25194		25992		25536	25080	25380
		25218		26004		25656	25176	25470
		25260		26674		25680	25224	25974
		25566		26944		25752	25320	26076
		26674				25992	25344	26674
		26944				26016	25584	26753
							25680	26944
							25824	
							26064	
							26944	

6. Pilot patterns

This part illustrates each of the scattered pilot patterns, showing the pattern of pilots at the low frequency edge of the ensemble and for the last few symbols of a frame. It shows first the patterns in SISO mode figures G(6) to G(13). Continual pilots and reserved carriers are not shown.

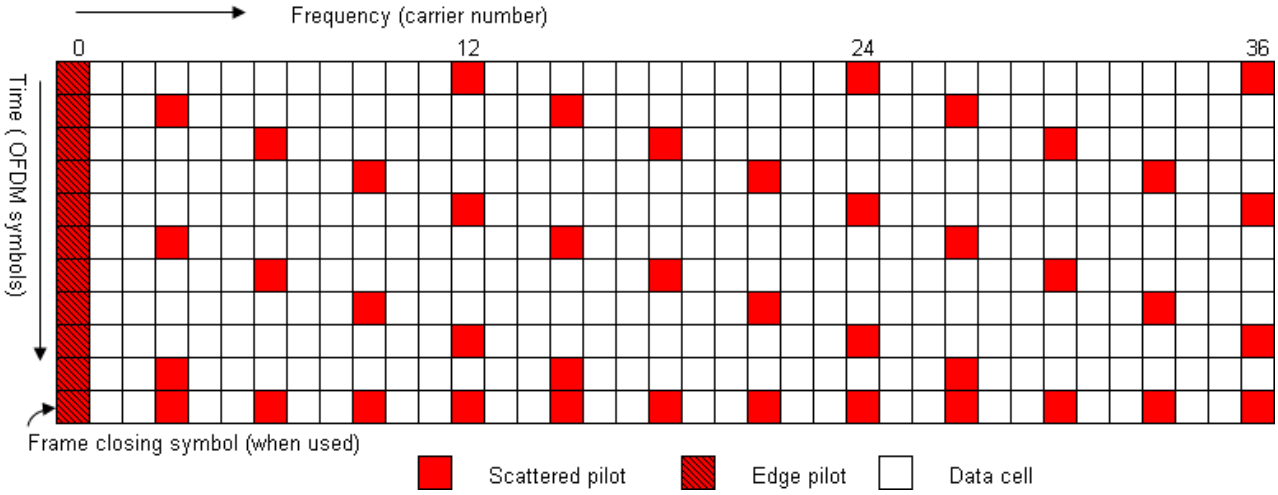

Figure G(6): Scattered pilot pattern PP1 (SISO)

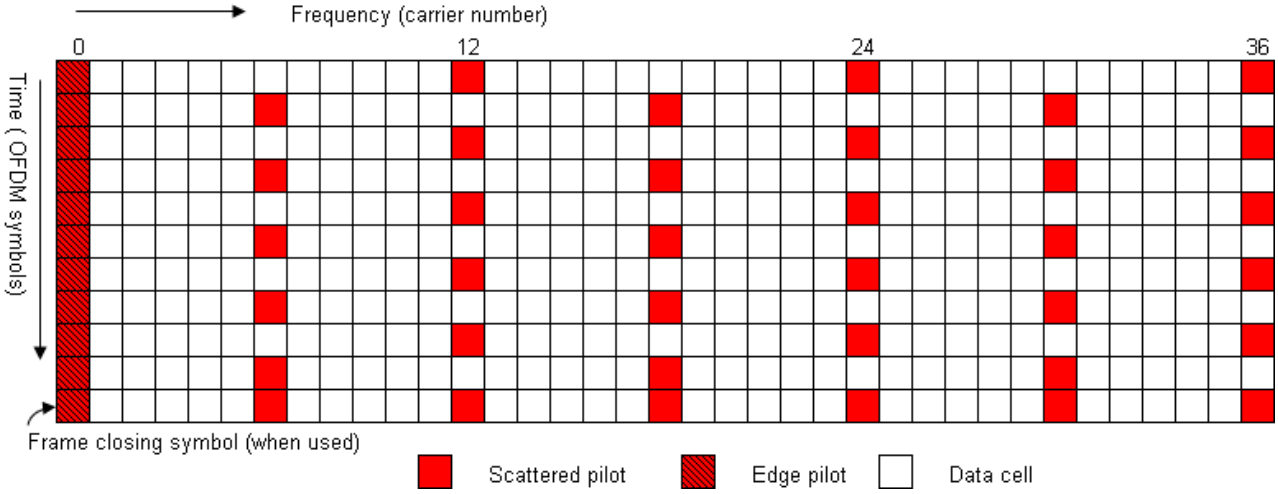

Figure G(6): Scattered pilot pattern PP2 (SISO)

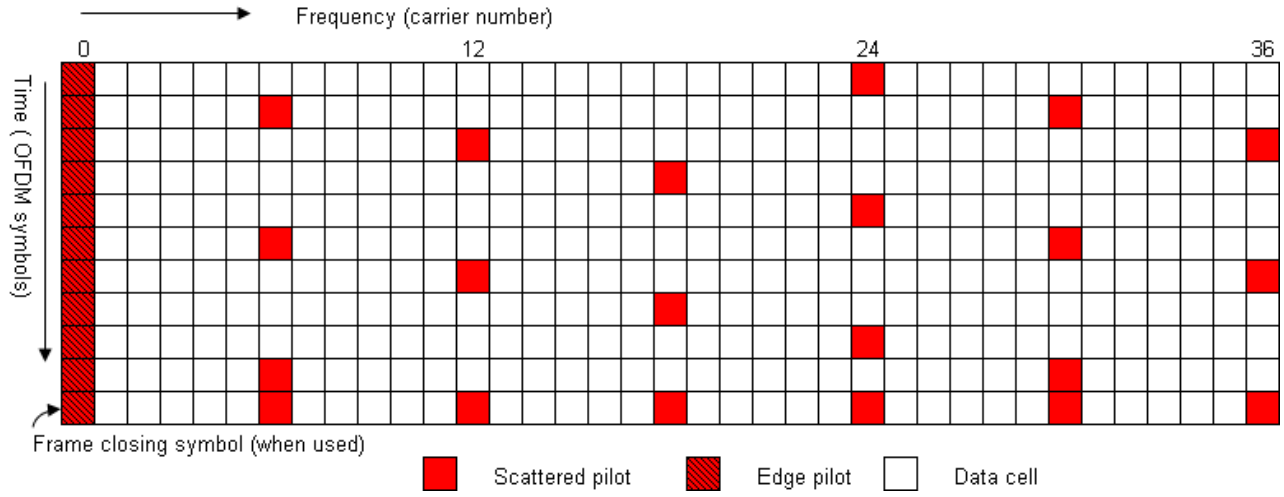

Figure G(8): Scattered pilot pattern PP3 (SISO)

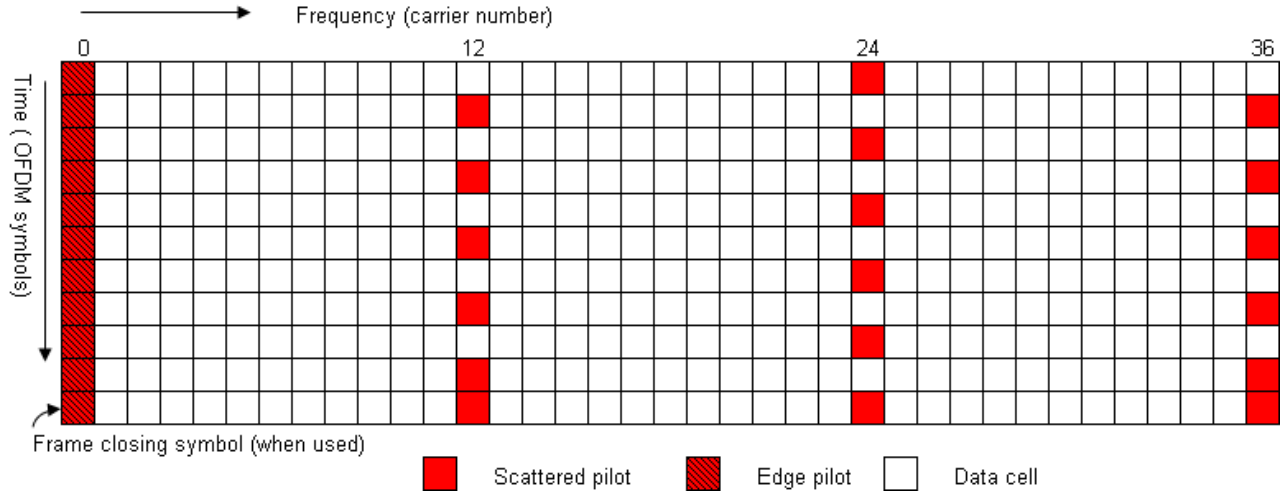

Figure G(9): Scattered pilot pattern PP4 (SISO)

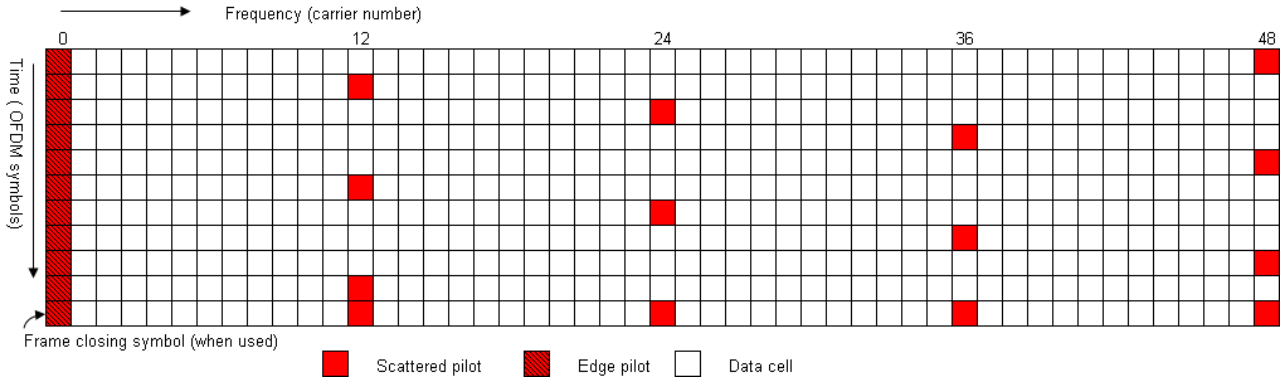

Figure G(10): Scattered pilot pattern PP5 (SISO)

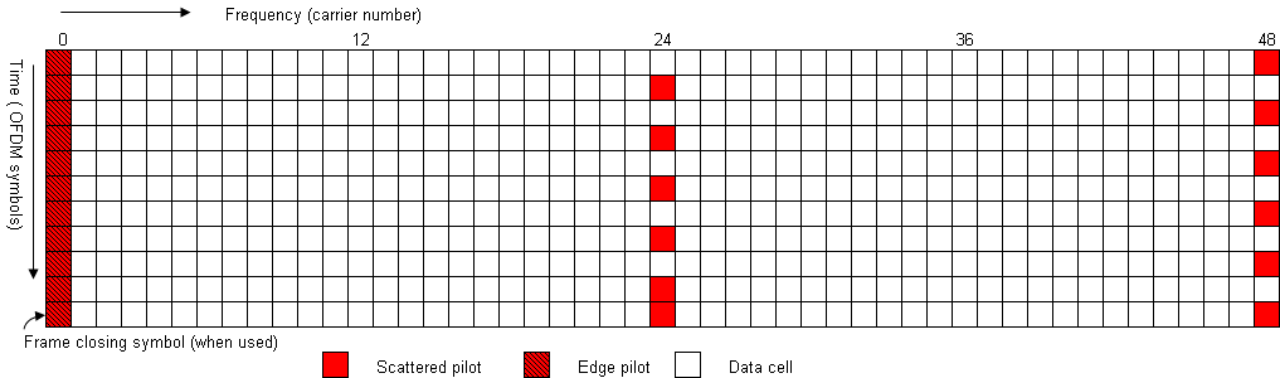

Figure G(11): Scattered pilot pattern PP6 (SISO)

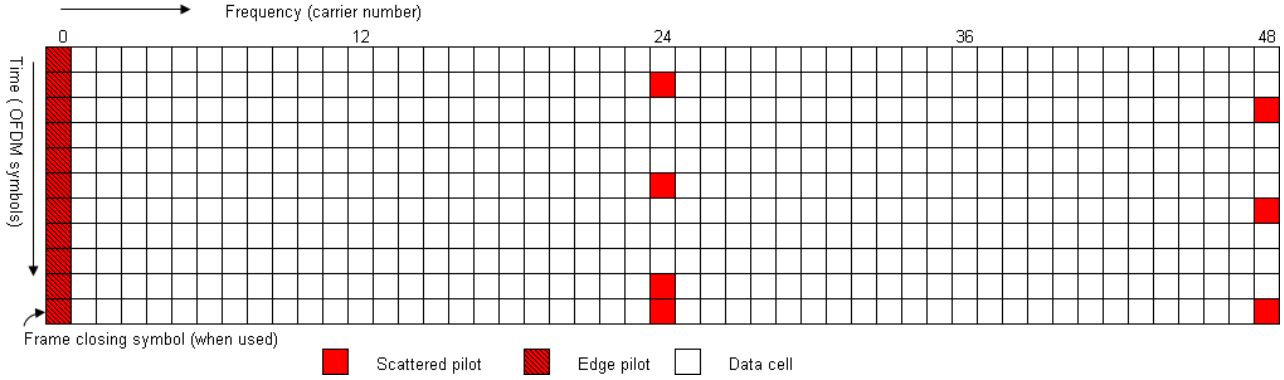

Figure G(12): Scattered pilot pattern PP7 (SISO)

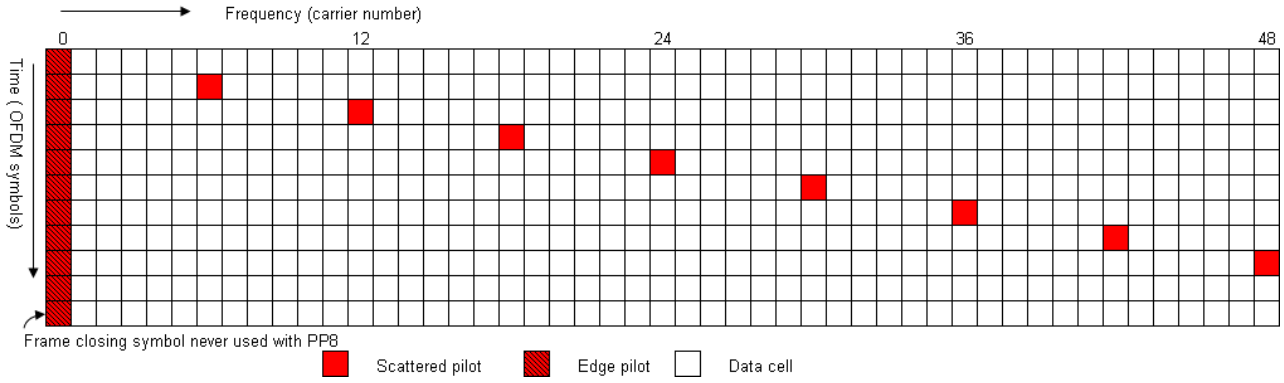

Figure G(13): Scattered pilot pattern PP8 (SISO)

Appendix H

Reserved carrier indices for PAPR reduction

Table H(1) gives the indices of the reserved carriers for the P2 symbol. Table H(2) gives the starting indices for the reserved carriers for pilot patterns PP1-8.

Table H(1): Reserved carrier indices for P2 symbol

FFT size (Number of reserved carriers)	Reserved Carrier Indices
1K (10)	116, 130, 134, 157, 182, 256, 346, 478, 479, 532
2K (18)	113, 124, 262, 467, 479, 727, 803, 862, 910, 946, 980, 1201, 1322, 1342, 1396, 1397, 1562, 1565
4K (36)	104, 116, 119, 163, 170, 173, 664, 886, 1064, 1151, 1196, 1264, 1531, 1736, 1951, 1960, 2069, 2098, 2311, 2366, 2473, 2552, 2584, 2585, 2645, 2774, 2846, 2882, 3004, 3034, 3107, 3127, 3148, 3191, 3283, 3289
8K (72)	106, 109, 110, 112, 115, 118, 133, 142, 163, 184, 206, 247, 445, 461, 503, 565, 602, 656, 766, 800, 922, 1094, 1108, 1199, 1258, 1726, 1793, 1939, 2128, 2714, 3185, 3365, 3541, 3655, 3770, 3863, 4066, 4190, 4282, 4565, 4628, 4727, 4882, 4885, 5143, 5192, 5210, 5257, 5261, 5459, 5651, 5809, 5830, 5986, 6020, 6076, 6253, 6269, 6410, 6436, 6467, 6475, 6509, 6556, 6611, 6674, 6685, 6689, 6691, 6695, 6698, 6701
16K (144)	104, 106, 107, 109, 110, 112, 113, 115, 116, 118, 119, 121, 122, 125, 128, 131, 134, 137, 140, 143, 161, 223, 230, 398, 482, 497, 733, 809, 850, 922, 962, 1196, 1256, 1262, 1559, 1691, 1801, 1819, 1937, 2005, 2095, 2308, 2383, 2408, 2425, 2428, 2479, 2579, 2893, 2902, 3086, 3554, 4085, 4127, 4139, 4151, 4163, 4373, 4400, 4576, 4609, 4952, 4961, 5444, 5756, 5800, 6094, 6208, 6658, 6673, 6799, 7208, 7682, 8101, 8135, 8230, 8692, 8788, 8933, 9323, 9449, 9478, 9868, 10192, 10261, 10430, 10630, 10685, 10828, 10915, 10930, 10942, 11053, 11185, 11324, 11369, 11468, 11507, 11542, 11561, 11794, 11912, 11974, 11978, 12085, 12179, 12193, 12269, 12311, 12758, 12767, 12866, 12938, 12962, 12971, 13099, 13102, 13105, 13120, 13150, 13280, 13282, 13309, 13312, 13321, 13381, 13402, 13448, 13456, 13462, 13463, 13466, 13478, 13492, 13495, 13498, 13501, 13502, 13504, 13507, 13510, 13513, 13514, 13516
32K (288)	104, 106, 107, 109, 110, 112, 113, 115, 118, 121, 124, 127, 130, 133, 136, 139, 142, 145, 148, 151, 154, 157, 160, 163, 166, 169, 172, 175, 178, 181, 184, 187, 190, 193, 196, 199, 202, 205, 208, 211, 404, 452, 455, 467, 509, 539, 568, 650, 749, 1001, 1087, 1286, 1637, 1823, 1835, 1841, 1889, 1898, 1901, 2111, 2225, 2252, 2279, 2309, 2315, 2428, 2452, 2497, 2519, 3109, 3154, 3160, 3170, 3193, 3214, 3298, 3331, 3346, 3388, 3397, 3404, 3416, 3466, 3491, 3500, 3572, 4181, 4411, 4594, 4970, 5042, 5069, 5081, 5086, 5095, 5104, 5320, 5465, 5491, 6193, 6541, 6778, 6853, 6928, 6934, 7030, 7198, 7351, 7712, 7826, 7922, 8194, 8347, 8350, 8435, 8518, 8671, 8861, 8887, 9199, 9980, 10031, 10240, 10519, 10537, 10573, 10589, 11078, 11278, 11324, 11489, 11642, 12034, 12107, 12184, 12295, 12635, 12643, 12941, 12995, 13001, 13133, 13172, 13246, 13514, 13522, 13939, 14362, 14720, 14926, 15338, 15524, 15565, 15662, 15775, 16358, 16613, 16688, 16760, 17003, 17267, 17596, 17705, 18157, 18272, 18715, 18994, 19249, 19348, 20221, 20855, 21400, 21412, 21418, 21430, 21478, 21559, 21983, 21986, 22331, 22367, 22370, 22402, 22447, 22535, 22567, 22571, 22660, 22780, 22802, 22844, 22888, 22907, 23021, 23057, 23086, 23213, 23240, 23263, 23333, 23369, 23453, 23594, 24143, 24176, 24319, 24325, 24565, 24587, 24641, 24965, 25067, 25094, 25142, 25331, 25379, 25465, 25553, 25589, 25594, 25655, 25664, 25807, 25823, 25873, 25925, 25948, 26002, 26008, 26102, 26138, 26141, 26377, 26468, 26498, 26510, 26512, 26578, 26579, 26588, 26594, 26597, 26608, 26627, 26642, 26767, 26776, 26800, 26876, 26882, 26900, 26917, 26927, 26951, 26957, 26960, 26974, 26986, 27010, 27013, 27038, 27044, 27053, 27059, 27061, 27074, 27076, 27083, 27086, 27092, 27094, 27098, 27103, 27110, 27115, 27118, 27119, 27125, 27128, 27130, 27133, 27134, 27140, 27143, 27145, 27146, 27148, 27149

Table H(2): Reserved carrier indices for PP 1, 2, 3, 4, 5, 6, 7 and 8

FFT size (Number of reserved carriers)	Reserved Carrier Indices
1K (10)	109, 117, 122, 129, 139, 321, 350, 403, 459, 465
2K (18)	250, 404, 638, 677, 700, 712, 755, 952, 1125, 1145, 1190, 1276, 1325, 1335, 1406, 1431, 1472, 1481
4K (36)	170, 219, 405, 501, 597, 654, 661, 745, 995, 1025, 1319, 1361, 1394, 1623, 1658, 1913, 1961, 1971, 2106, 2117, 2222, 2228, 2246, 2254, 2361, 2468, 2469, 2482, 2637, 2679, 2708, 2825, 2915, 2996, 3033, 3119
8K (72)	111, 115, 123, 215, 229, 392, 613, 658, 831, 842, 997, 1503, 1626, 1916, 1924, 1961, 2233, 2246, 2302, 2331, 2778, 2822, 2913, 2927, 2963, 2994, 3087, 3162, 3226, 3270, 3503, 3585, 3711, 3738, 3874, 3902, 4013, 4017, 4186, 4253, 4292, 4339, 4412, 4453, 4669, 4910, 5015, 5030, 5061, 5170, 5263, 5313, 5360, 5384, 5394, 5493, 5550, 5847, 5901, 5999, 6020, 6165, 6174, 6227, 6245, 6314, 6316, 6327, 6503, 6507, 6545, 6565
16K (144)	109, 122, 139, 171, 213, 214, 251, 585, 763, 1012, 1021, 1077, 1148, 1472, 1792, 1883, 1889, 1895, 1900, 2013, 2311, 2582, 2860, 2980, 3011, 3099, 3143, 3171, 3197, 3243, 3257, 3270, 3315, 3436, 3470, 3582, 3681, 3712, 3767, 3802, 3979, 4045, 4112, 4197, 4409, 4462, 4756, 5003, 5007, 5036, 5246, 5483, 5535, 5584, 5787, 5789, 6047, 6349, 6392, 6498, 6526, 6542, 6591, 6680, 6688, 6785, 6860, 7134, 7286, 7387, 7415, 7417, 7505, 7526, 7541, 7551, 7556, 7747, 7814, 7861, 7880, 8045, 8179, 8374, 8451, 8514, 8684, 8698, 8804, 8924, 9027, 9113, 9211, 9330, 9479, 9482, 9487, 9619, 9829, 10326, 10394, 10407, 10450, 10528, 10671, 10746, 10774, 10799, 10801, 10912, 11113, 11128, 11205, 11379, 11459, 11468, 11658, 11776, 11791, 11953, 11959, 12021, 12028, 12135, 12233, 12407, 12441, 12448, 12470, 12501, 12548, 12642, 12679, 12770, 12788, 12899, 12923, 12939, 13050, 13103, 13147, 13256, 13339, 13409
32K (288)	164, 320, 350, 521, 527, 578, 590, 619, 635, 651, 662, 664, 676, 691, 723, 940, 1280, 1326, 1509, 1520, 1638, 1682, 1805, 1833, 1861, 1891, 1900, 1902, 1949, 1967, 1978, 1998, 2006, 2087, 2134, 2165, 2212, 2427, 2475, 2555, 2874, 3067, 3091, 3101, 3146, 3188, 3322, 3353, 3383, 3503, 3523, 3654, 3856, 4150, 4158, 4159, 4174, 4206, 4318, 4417, 4629, 4631, 4875, 5104, 5106, 5111, 5131, 5145, 5146, 5177, 5181, 5246, 5269, 5458, 5474, 5500, 5509, 5579, 5810, 5823, 6058, 6066, 6098, 6411, 6741, 6775, 6932, 7103, 7258, 7303, 7413, 7586, 7591, 7634, 7636, 7655, 7671, 7675, 7756, 7760, 7826, 7931, 7937, 7951, 8017, 8061, 8071, 8117, 8317, 8321, 8353, 8806, 9010, 9237, 9427, 9453, 9469, 9525, 9558, 9574, 9584, 9820, 9973, 10011, 10043, 10064, 10066, 10081, 10136, 10193, 10249, 10511, 10537, 11083, 11350, 11369, 11428, 11622, 11720, 11924, 11974, 11979, 12944, 12945, 13009, 13070, 13110, 13257, 13364, 13370, 13449, 13503, 13514, 13520, 13583, 13593, 13708, 13925, 14192, 14228, 14235, 14279, 14284, 14370, 14393, 14407, 14422, 14471, 14494, 14536, 14617, 14829, 14915, 15094, 15138, 15155, 15170, 15260, 15283, 15435, 15594, 15634, 15810, 16178, 16192, 16196, 16297, 16366, 16498, 16501, 16861, 16966, 17039, 17057, 17240, 17523, 17767, 18094, 18130, 18218, 18344, 18374, 18657, 18679, 18746, 18772, 18779, 18786, 18874, 18884, 18955, 19143, 19497, 19534, 19679, 19729, 19738, 19751, 19910, 19913, 20144, 20188, 20194, 20359, 20490, 20500, 20555, 20594, 20633, 20656, 21099, 21115, 21597, 22139, 22208, 22244, 22530, 22547, 22562, 22567, 22696, 22757, 22798, 22854, 22877, 23068, 23102, 23141, 23154, 23170, 23202, 23368, 23864, 24057, 24215, 24219, 24257, 24271, 24325, 24447, 25137, 25590, 25702, 25706, 25744, 25763, 25811, 25842, 25853, 25954, 26079, 26158, 26285, 26346, 26488, 26598, 26812, 26845, 26852, 26869, 26898, 26909, 26927, 26931, 26946, 26975, 26991, 27039

Appendix I

For T2-Lite, the bit to cell word de-multiplexer shall be used except that, for code-rates 1/3 and 2/5, the parameters shall be used is given in table I.

Table I(1): Parameters for de-multiplexing of bits to sub-streams for code rates 1/3

Modulation format	**QPSK**											
Input bit-number, *di* mod $N_{substreams}$	0	1										
Output bit-number, *e*	0	1										
Modulation format	**16-QAM**											
Input bit-number, *di* mod $N_{substreams}$	0	1	2	3	4	5	6	7				
Output bit-number, *e*	6	0	3	4	5	2	1	7				
Modulation format	**64-QAM**											
Input bit-number, *di* mod $N_{substreams}$	0	1	2	3	4	5	6	7	8	9	10	11
Output bit-number, *e*	4	2	0	5	6	1	3	7	8	9	10	11
Modulation format	**256-QAM**											
Input bit-number, *di* mod $N_{substreams}$	0	1	2	3	4	5	6	7				
Output bit-number, *e*	4	0	1	2	5	3	6	7				

Table I(2): Parameters for de-multiplexing of bits to sub-streams for code rates 2/5

Modulation format	**QPSK**											
Input bit-number, *di* mod $N_{substreams}$	0	1										
Output bit-number, *e*	0	1										
Modulation format	**16-QAM**											
Input bit-number, *di* mod $N_{substreams}$	0	1	2	3	4	5	6	7				
Output bit-number, *e*	7	5	4	0	3	1	2	6				
Modulation format	**64-QAM**											
Input bit-number, *di* mod $N_{substreams}$	0	1	2	3	4	5	6	7	8	9	10	11
Output bit-number, *e*	4	0	1	6	2	3	5	8	7	10	9	11
Modulation format	**256-QAM**											
Input bit-number, *di* mod $N_{substreams}$	0	1	2	3	4	5	6	7				
Output bit-number, *e*	4	0	5	1	2	3	6	7				

Appendix J

Parameters of bits De-multiplexing into sub-streams according to coding rates and modulation modes for DVB-NGH.

Table J(1): Parameters for de-multiplexing of bits to sub-streams for code rates 3/15 and 4/15

Modulation format	**QPSK**							
Input bit-number, di mod $N_{substreams}$	0	1						
Output bit-number, e	0	1						
Modulation format	**16-QAM**							
Input bit-number, di mod $N_{substreams}$	0	1	2	3	4	5	6	7
Output bit-number, e	4	3	2	1	6	5	7	0

Table J(2): Parameters for de-multiplexing of bits to sub-streams for code rates 5/15

Modulation format	**QPSK**											
Input bit-number, di mod $N_{substreams}$	0	1										
Output bit-number, e	0	1										
Modulation format	**16-QAM**											
Input bit-number, di mod $N_{substreams}$	0	1	2	3	4	5	6	7				
Output bit-number, e	6	0	3	4	5	2	1	7				
Modulation format	**64-QAM or NU-64-QAM**											
Input bit-number, di mod $N_{substreams}$	0	1	2	3	4	5	6	7	8	9	10	11
Output bit-number, e	4	2	0	5	6	1	3	7	8	9	10	11
Modulation format	**256-QAM or NU-256-QAM**											
Input bit-number, di mod $N_{substreams}$	0	1	2	3	4	5	6	7				
Output bit-number, e	4	0	1	2	5	3	6	7				

Table J(3): Parameters for de-multiplexing of bits to sub-streams for code rates 6/15

Modulation format	**QPSK**							
Input bit-number, *di* mod $N_{substreams}$	0	1						
Output bit-number, *e*	0	1						
Modulation format	**16-QAM**							
Input bit-number, *di* mod $N_{substreams}$	0	1	2	3	4	5	6	7
Output bit-number, *e*	7	5	4	0	3	1	2	6
Modulation format	**64-QAM or NU-64-QAM**											
Input bit-number, *di* mod $N_{substreams}$	0	1	2	3	4	5	6	7	8	9	10	11
Output bit-number, *e*	4	0	1	6	2	3	5	8	7	10	9	11
Modulation format	**256-QAM or NU-256-QAM**							
Input bit-number, *di* mod $N_{substreams}$	0	1	2	3	4	5	6	7
Output bit-number, *e*	4	0	5	1	2	3	6	7

Table J(4): Parameters for de-multiplexing of bits to sub-streams for code rate 7/15

Modulation format	**QPSK**							
Input bit-number, *di* mod $N_{substreams}$	0	1						
Output bit-number, *e*	0	1						
Modulation format	**16-QAM**							
Input bit-number, *di* mod $N_{substreams}$	0	1	2	3	4	5	6	7
Output bit-number, *e*	0	2	6	3	4	1	5	7
Modulation format	**64-QAM or NU-64-QAM**											
Input bit-number, *di* mod $N_{substreams}$	0	1	2	3	4	5	6	7	8	9	10	11
Output bit-number, *e*	2	0	8	7	1	6	4	3	10	9	5	11
Modulation format	**256-QAM or NU-256-QAM**							
Input bit-number, *di* mod $N_{substreams}$	0	1	2	3	4	5	6	7
Output bit-number, *e*	2	6	0	1	4	5	3	7

Table J(5): Parameters for de-multiplexing of bits to sub-streams for code rate 8/15

Modulation format	**QPSK**							
Input bit-number, *di* mod $N_{substreams}$	0	1						
Output bit-number, *e*	0	1						
Modulation format	**16-QAM**							
Input bit-number, *di* mod $N_{substreams}$	0	1	2	3	4	5	6	7
Output bit-number, *e*	0	4	3	1	2	5	6	7
Modulation format	**64-QAM or NU-64-QAM**							
Input bit-number, *di* mod $N_{substreams}$	0	1	2	3	4	5	6	7
Output bit-number, *e*	2	0	4	1	6	7	8	5
Modulation format	**256-QAM or NU-256-QAM**							
Input bit-number, *di* mod $N_{substreams}$	0	1	2	3	4	5	6	7
Output bit-number, *e*	2	6	1	0	7	5	3	4

Modulation format	**64-QAM or NU-64-QAM**											
Input bit-number, *di* mod $N_{substreams}$	0	1	2	3	4	5	6	7	8	9	10	11
Output bit-number, *e*	10	3	9	11								

Table J(6): Parameters for de-multiplexing of bits to sub-streams for code rate 9/15

Modulation format	**QPSK**							
Input bit-number, *di* mod $N_{substreams}$	0	1						
Output bit-number, *e*	0	1						
Modulation format	**16-QAM**							
Input bit-number, *di* mod $N_{substreams}$	0	1	2	3	4	5	6	7
Output bit-number, *e*	7	1	4	2	5	3	6	0
Modulation format	**64-QAM or NU-64-QAM**							
Input bit-number, *di* mod $N_{substreams}$	0	1	2	3	4	5	6	7
Output bit-number, *e*	11	7	3	10	6	2	9	5
Modulation format	**256-QAM or NU-256-QAM**							
Input bit-number, *di* mod $N_{substreams}$	0	1	2	3	4	5	6	7
Output bit-number, *e*	7	3	1	5	2	6	4	0

Modulation format	**64-QAM or NU-64-QAM**											
Input bit-number, *di* mod $N_{substreams}$	0	1	2	3	4	5	6	7	8	9	10	11
Output bit-number, *e*	1	8	4	0								

Table J(7): Parameters for de-multiplexing of bits to sub-streams for code rates 10/15 and 11/15

Modulation format	**QPSK**	
Input bit-number, $di \bmod N_{substreams}$	0	1
Output bit-number, e	0	1

Modulation format	**16-QAM**							
Input bit-number, $di \bmod N_{substreams}$	0	1	2	3	4	5	6	7
Output bit-number, e	7	1	4	2	5	3	6	0

Modulation format	**64-QAM or NU-64-QAM**											
Input bit-number, $di \bmod N_{substreams}$	0	1	2	3	4	5	6	7	8	9	10	11
Output bit-number, e	11	7	3	10	6	2	9	5	1	8	4	0

Modulation format	**256-QAM or NU-256-QAM**							
Input bit-number, $di \bmod N_{substreams}$	0	1	2	3	4	5	6	7
Output bit-number, e	7	3	1	5	2	6	4	0

Appendix K

1. Carrier Distribution in P1 symbol

The active carriers are distributed using the following algorithm: out of the 853 carriers of the 1K symbol, the 766 carriers from the middle are considered. From these 766 carriers, only 384 carry pilots; the others are set to zero. In order to identify which of the 766 carriers are active, three complementary sequences are concatenated: the length of the two sequences at the ends is 128, while the sequence in the middle is 512 chips long. The last two bits of the third concatenated sequence are zero, resulting in 766 carriers where 384 of them are active carriers.

The resulting carrier distribution is shown in table 68.

Table 68: Distribution of active carriers in the P1 symbol

Modulation Sequence (see clause 9.8.2.2)	Active Carriers in P1 $k_{P1}(0)..k_{P1}(383)$
$k_{P1}(0)..k_{P1}(63)$ CSS_{S1}	44 45 47 51 54 59 62 64 65 66 70 75 78 80 81 82 84 85 87 88 89 90 94 96 97 98 102 107 110 112 113 114 116 117 119 120 121 122 124 125 127 131 132 133 135 136 137 138 142 144 145 146 148 149 151 152 153 154 158 160 161 162 166 171
$k_{P1}(64)..k_{P1}(319)$ CSS_{S2}	172 173 175 179 182 187 190 192 193 194 198 203 206 208 209 210 212 213 215 216 217 218 222 224 225 226 230 235 238 240 241 242 244 245 247 248 249 250 252 253 255 259 260 261 263 264 265 266 270 272 273 274 276 277 279 280 281 282 286 288 289 290 294 299 300 301 303 307 310 315 318 320 321 322 326 331 334 336 337 338 340 341 343 344 345 346 350 352 353 354 358 363 364 365 367 371 374 379 382 384 385 386 390 395 396 397 399 403 406 411 412 413 415 419 420 421 423 424 425 426 428 429 431 435 438 443 446 448 449 450 454 459 462 464 465 466 468 469 471 472 473 474 478 480 481 482 486 491 494 496 497 498 500 501 503 504 505 506 508 509 511 515 516 517 519 520 521 522 526 528 529 530 532 533 535 536 537 538 542 544 545 546 550 555 558 560 561 562 564 565 567 568 569 570 572 573 575 579 580 581 583 584 585 586 588 589 591 595 598 603 604 605 607 611 612 613 615 616 617 618 622 624 625 626 628 629 631 632 633 634 636 637 639 643 644 645 647 648 649 650 654 656 657 658 660 661 663 664 665 666 670 672 673 674 678 683
$k_{P1}(320)..k_{P1}(383)$ CSS_{S1}	684 689 692 696 698 699 701 702 703 704 706 707 708 712 714 715 717 718 719 720 722 723 725 726 727 729 733 734 735 736 738 739 740 744 746 747 748 753 756 760 762 763 765 766 767 768 770 771 772 776 778 779 780 785 788 792 794 795 796 801 805 806 807 809

2. Modulation of the Active Carriers in P1

Active carriers are DBPSK modulated with a modulation pattern. The patterns, described later, encode two signalling fields S1 and S2. Up to 8 values (can encode 3 bits) and 16 values (can encode 4 bits) can be signalled in each field, respectively. Patterns to encode S1 are based on 8 orthogonal sets of 8 complementary sequences of length 8 (total length of each S1 pattern is 64), while patterns to encode S2 are based of 16 orthogonal sets of 16 complementary sequences of length 16 (total length of each S2 pattern is 256).

The two main properties of these patterns are:

a) The sum of the auto-correlations (SoAC) of all the sequences of the set is equal to a Krönecker delta, multiplied by *KN* factor, being *K* the number of the sequences of each set and *N* the length of each sequence. In the case of S1 *K*=*N*=8; in the case of S2, *K*=*N*=16.

b) Each set of sequences are mutually uncorrelated (also called "mates").

The S1 and S2 modulation patterns are shown in table 69.

Table 69: S1 and S2 Modulation patterns

Field	Val	Sequence (Hexadecimal notation)
S1	000	124721741D482E7B
	001	47127421481D7B2E
	010	217412472E7B1D48
	011	742147127B2E481D
	100	1D482E7B12472174
	101	481D7B2E47127421
	110	2E7B1D4821741247
	111	7B2E481D74214712
S2	0000	121D4748212E747B1D1248472E217B7412E247B721D174841DED48B82EDE7B8B
	0001	4748121D747B212E48471D127B742E2147B712E2748421D148B81DED7B8B2EDE
	0010	212E747B121D47482E217B741D12484721D1748412E247B72EDE7B8B1DED48B8
	0011	747B212E4748121D7B742E2148471D12748421D147B712E27B8B2EDE48B81DED
	0100	1D1248472E217B74121D4748212E747B1DED48B82EDE7B8B12E247B721D17484
	0101	48471D127B742E214748121D747B212E48B81DED7B8B2EDE47B712E2748421D1
	0110	2E217B741D124847212E747B121D47482EDE7B8B1DED48B821D1748412E247B7
	0111	7B742E2148471D12747B212E4748121D7B8B2EDE48B81DED748421D147B712E2
	1000	12E247B721D174841DED48B82EDE7B8B121D4748212E747B1D1248472E217B74
	1001	47B712E2748421D148B81DED7B8B2EDE4748121D747B212E48471D127B742E21
	1010	21D1748412E247B72EDE7B8B1DED48B8212E747B121D47482E217B741D124847
	1011	748421D147B712E27B8B2EDE48B81DED747B212E4748121D7B742E2148471D12
	1100	1DED48B82EDE7B8B12E247B721D174841D1248472E217B74121D4748212E747B
	1101	48B81DED7B8B2EDE47B712E2748421D148471D127B742E214748121D747B212E
	1110	2EDE7B8B1DED48B821D1748412E247B72E217B741D124847212E747B121D4748
	1111	7B8B2EDE48B81DED748421D147B712E27B742E2148471D12747B212E4748121D

The bit sequences CSS_{S1} =($CSS_{S1,0}$ … $CSS_{S1,63}$) and CSS_{S2}=($CSS_{S2,0}$ … $CSS_{S2,255}$) for given values of S1 and S2 respectively is obtained by taking the corresponding hexadecimal sequence from left to right and from MSB to LSB, i.e. $CSS_{S1,0}$ is the MSB of the first hexadecimal digit and $CSS_{S1,63}$ is the LSB of the last digit of the S1 sequence.

The final modulation signal is obtained as follows:

1) The Modulation sequence is obtained by concatenating the two CSS_{S1} and CSS_{S2} sequences; the CSS_{S1} sequence is attached at both sides of the CSS_{S2}:

$$\{MSS\_SEQ_0..MSS\_SEQ_{383}\} = \{CSS_{S1}, CSS_{S2}, CSS_{S1}\}$$
$$= \{CSS_{S1,0},..., CSS_{S1,63}, CSS_{S2,0}, ..., CSS_{S2,255}, CSS_{S1,0},..., CSS_{S1,63}\}$$

2) Then, the sequence is modulated using DBPSK:

$$MSS\_DIFF = DBPSK(MSS\_SEQ)$$

The following rule applies for the differential modulation of element *i* of the *MSS_SEQ*:

$$MSS\_DIFF_i = \begin{cases} MSS\_DIFF_{i-1} & MSS\_SEQ_i = 0 \\ -MSS\_DIFF_{i-1} & MSS\_SEQ_i = 1 \end{cases}$$

The differential encoding is started from "dummy" value of +1, i.e. MSS_DIFF_{-1} = +1 by definition. This bit is not applied to any carrier.

3) A scrambling is applied on the MSS_DIFF by bit-by-bit multiplying by a 384-bit scrambler sequence:

$$MSS\_SCR = SCRAMBLING\{MSS\_DIFF\}$$

The scrambler sequence shall be equal to the 384-length sequence of '+1' or '-1' converted from the first 384 bits ($PRBS_0 ... PRBS_{383}$) of the PRBS generator described in clause 5.2.4 with initial state '100111001000110', where a PRBS generator output bit with a value of '0' is converted into '+1' and a PRBS generator output bit with a value of '1' is converted into '-1'.

$$MSS\_SCR_i = MSS\_DIFF_i \times 2\left(\frac{1}{2} - PRBS_i\right)$$

4) The scrambled modulation pattern is applied to the active carriers.

EXAMPLE: If S1=000 and S2=0000, then:

The sequence is:

$$MSS\_SEQ = \{\underbrace{1247...2E7B}_{CSS_{S1}}, \underbrace{121D...7B8B}_{CSS_{S2}}, \underbrace{1247...2E7B}_{CSS_{S1}}\}$$
$$= \{\underbrace{0,0,0,1,...,1,0,1,1}_{CSS_{S1}}, \underbrace{0,0,0,1,...,1,0,1,1}_{CSS_{S2}}, \underbrace{0,0,0,1,...,1,0,1,1}_{CSS_{S1}}\}$$

Then, DBPSK is applied:

$$MSS\_DIFF = \{\underbrace{1,1,1,-1,...,1,1,-1,1}_{CSS_{S1}}, \underbrace{1,1,1,-1,...,1,1,-1,1}_{CSS_{S2}}, \underbrace{1,1,1,-1,...,1,1,-1,1}_{CSS_{S1}}\}$$

The DBPSK output is scrambled by the scrambling sequence, *SCR_SEQ*.

$$SCR\_SEQ = 2(\frac{1}{2} - PRBS_i)$$
$$= \{\underbrace{-1,1,-1,1,...,-1,-1,1,1}_{64}, \underbrace{-1,-1,-1,-1,...,1,-1,-1,1}_{256}, \underbrace{1,1,-1,-1,...,1,1,-1,1}_{64}\}$$

after scrambling:

$$MSS\_SCR = \{\underbrace{-1,1,-1,-1,...,-1,-1,-1,1}_{CSS_{S1}}, \underbrace{-1,-1,-1,1,...,1,-1,1,1}_{CSS_{S2}}, \underbrace{1,1,-1,1,...,1,1,1,1}_{CSS_{S1}}\}$$

The scrambled modulation MSS is mapped to the active carriers, MSB first:

$$c_{44} = -1,\ c_{45} = 1,\ c_{47} = -1,\ c_{51} = -1,...,\ c_{171} = 1$$
$$c_{172} = -1,\ c_{173} = -1,\ c_{175} = -1,...,\ c_{683} = 1$$
$$c_{684} = 1,...,\ c_{805} = 1,\ c_{806} = 1,\ c_{807} = 1,\ c_{809} = 1$$

where c_k is the modulation applied to carrier *k*.

The equation for the modulation of the P1 carriers is given in clause 9.8.2.4.

3. Boosting of the Active Carriers

Taking into account that in a 1K OFDM symbol only 853 carriers are used, and in P1 there are only 384 active carriers, the boosting applied to the P1 active carriers is a voltage ratio of $\sqrt{(853/384)}$ or 3,47 dB, relative to the mean value of all K_{total} of the used carriers of a 1K normal symbol.

4. Generation of the time domain P1 signal

a. Generation of the main part of the P1 signal

The useful part 'A' of the P1 signal is generated from the carrier modulation values, according to the following equation:

$$p_{1A}(t) = \frac{1}{\sqrt{384}} \sum_{i=0}^{383} MSS\_SCR_i \times e^{j2\pi \frac{k_{\mathrm{p1}}(\mathrm{i})-426}{1024T} t}$$

where $k_{\mathrm{p1}}(i)$ for i=0,1,…, 383 are the indices of the 384 active carriers, in increasing order, as defined in clause 9.8.2.1. MSS_SCR_{i} for i=0,1,… , 383 are the modulation values for the active carriers as defined in clause 9.8.2.2, and T is the elementary time period and is defined in table 65.

NOTE: This equation, taken together with the equation in clause 9.5, includes the effect of the boosting described in clause 9.8.2.3, which ensures the power of the P1 symbol is virtually the same as the power of the remaining symbols.

b. Frequency Shifted repetition in Guard Intervals

In order to improve the robustness of the P1, two guard intervals are defined at both sides of the useful part of the symbol. Instead of cyclic continuation like normal OFDM symbols, a frequency shift version of the symbol is used. Thus, denoting P1[C], the first guard interval, P1[A] the main part of the symbol and P1[B] the last guard interval of the symbol, P1[C] carries the frequency shifted version of the first 542T of P1[A], while P1[B] conveys the frequency shifted version of the last 482T of P1[A] (see figure 51).

The frequency shift f_{SH} applied to P1[C] and P1[B] is:

$$f_{SH} = 1/(1\,024T)$$

The time-domain baseband waveform $p_1(t)$ of the P1 symbol is therefore defined as follows:

$$p_1(t) = \begin{cases} p_{1A}(t) e^{j\frac{2\pi}{1024T}t} & 0 \le t < 542T \\ p_{1A}(t - 542T) & 542T \le t < 1\,566T \\ p_{1A}(t - 1\,024T) e^{j\frac{2\pi}{1\,024T}t} & 1\,566 \le t < 2\,048T \\ 0 & \text{otherwise} \end{cases}$$

جمهوريـــة العراق
وزارة التعليم العالي والبحث العلمي
جامعـــــة بابـــل
كليـــة الهندســـة / قسم الهندســـة
الكهربائية

محاكاة وتحليل لمعيار البث الارضي الرقمي لفيديو الجيل الثاني باستخدام سيناريوهات مختلفة

أطروحة

مقدمـــة إلى كليـــة الهندســـة في جامعـــــة بابـــل

وهي جزء من متطلبات نيل درجـــــة الدكتوراه فلسفة

في الهندسة \ الهندسة الكهربائية \ الكترونيـك واتصالات

من قبل

حمزه صبر غايب كريفع

بأشراف

الاستاذ

الدكتور سمير جاسم محمد

١٤٤٣هـ 2022م

الــخــلاصـــــة

يعتبر الجيل الثاني من تقنية البث الارضي الرقمي للفيديو (DVB-T2) من أكثر أنظمة التلفزة الرقمية الأرضية تقدمًا في العالم، حيث يوفر نظام إرسال أرضي عالي الأداء مع موثوقية بث جيدة. و يتمتع هذا المعيار بالقدرة على زيادة سعة القناة عبر مجموعة متنوعة من ظروف الارسال الأرضية، وهو ما يعد تحسينا كبيرًا لهذا النظام. ويقدم نظام (DVB-T2) تحسينات عديدة مقارنة بالجيل الاول منها ما يتعلق بترميز تصحيح الخطأ الأمامي (FEC) ، وأساليب التضمين، وأحجام التحويل الفوريي السريع (FFT)، والأنماط التجريبية الجديدة، وتقنيات الهوائيات المتعددة، ودوران الكوكبة، وتقنيات التأخير الدوري.

في هذه الأطروحة، ينقسم العمل إلى أربعة أهداف رئيسية مع مجموعة من أساليب التضمين، ومعدلات الترميز، وكذلك عدة نماذج من القنوات متعددة المسارات. إلى جانب ذلك، تتم محاكاة وتقييم كل الأجزاء من خلال استخدام برنامج الماتلاب (MATLAB) اصدار(R2020b).حيث يتم في الهدف الأول تقييم نظام (DVB-T2) قبل استخدام تقنية دوران الكوكبة وبعدها. حيث وجد ان تقنية دوران الكوكبة توفر تنوع إضافي يؤدي الى تحسين عمل وحدة ترحيل-تعديل و ترميز البتات (BICM) في بيئات الخبو المختلفة مما يسهم في تحسين الأداء الاجمالي لنظام (DVB-T2).

تم تقييم اداء نظام (DVB-T2) في الهدف الثاني عند تطبيق تقنية الإرسال متعدد الهوائيات (MISO) القائم على أساس مخطط ترميز (Alamouti) المعدل وفي حالة مناطق الشبكات أحادية التردد (SFNs). حيث يتم بعدها مقارنة وضع الإرسال متعدد الهوائيات لنظام (DVB-T2) مع وضع الارسال احادي الهوائي (SISO) للشبكات احادية التردد التقليدية بناءً على مقدار كسب التنوع الناتج. ويوضح الكسب الناتج الفائدة من استخدام تقنية (MISO)، والذي يحسن من جودة الإشارة المستلمة في المناطق احادية التردد.

يتم في الهدف الثالث من الاطروحة محاكاة وتقييم ملف تعريف (T2-Lite). أيضًا، يتم مقارنة أداء نظام (T2-Lite) قبل استخدام تقنية دوران الكوكبة ومخططات التأخير الدوري Q وبعدها. اخيرًا، في الهدف الرابع، يتم اقتراح اعتماد وحدة (BICM) المتطورة من الجيل القادم للبث الرقمي المحمول للفيديو (DVB-NGH) في داخل ملف تعريف (T2-Lite) بدلاً من الوحدة الأصلية. حيث تم استخدام نوعين من تقنيات الدوران مع هذه الوحدة، هما دوران الأبراج ثنائي الأبعاد ورباعي الأبعاد،

بالاعتماد على وضع التضمين المستخدم ومعدلات الترميز. حيث يمكن أن توفر الوحدة المقترحة مكاسب تنوع ممتازة لتحسين متانة نظام (T2-Lite) في بيئات التلاشي.

وتبين النتائج ان مقدار اقصى كسب لتقنية الدوران 3.6 ديسيبل يتحقق عبر قناة الصدى الصفرية (0 dB Echo) ومع أسلوب التضمين QPSK ومعدل ترميز 5/6. وايضا تبين نتائج المحاكاة أن الحد الأقصى لكسب (MISO) هو 3.3 ديسيبل يتحقق من استخدام تظمين QPSK ومعدل ترميز مرتفع يبلغ 5/6 عبر قناة رايليRayleigh MISO . و في الجزء الثالث، يكون كسب التنوع الأقصى الناتج من استخدام دوران الكوكبة بمقدار 2.2 ديسبيل من خلال استخدام أسلوب التضمين QPSKومعدل ترميز 11/15 عبر قناة الصدى الصفرية. بينما تبلغ قيمة الكسب القصوى 3.5 ديسيبل عبر قناة الصدى الصفرية ومع استخدام أسلوب التضمين QPSK ومعدل ترميز عالي 11/15 في حالة استخدام الموديل المقترح.